GREEN AND DIGITAL TRANSFORMATION TOWARDS CIRCULAR ECONOMY IN THE CONSTRUCTION INDUSTRY: UPCYCLING OF CONSTRUCTION AND DEMOLITION WASTES FROM DIVERSE SOURCES AND THEIR INTEGRATION INTO 3D PRINTING TECHNOLOGY

İNŞAAT ENDÜSTRİSİNDE DÖNGÜSEL EKONOMİYE DOĞRU YEŞİL VE DİJİTAL DÖNÜŞÜM: FARKLI KAYNAKLARDAN ELDE EDİLEN İNŞAAT YIKINTI ATIKLARININ İLERİ DÖNÜŞTÜRÜLMESİ VE 3D BASKI TEKNOLOJİSİNE ENTEGRASYONU

ANIL KUL

ASSOC. PROF. GÜRKAN YILDIRIM

Supervisor

Submitted to

Graduate School of Science and Engineering of Hacettepe University

as a Partial Fulfillment to the Requirements

for be Award of the Degree of Doctor of Philosophy

in Civil Engineering

2024

To my beloved wife…

ABSTRACT

GREEN AND DIGITAL TRANSFORMATION TOWARDS CIRCULAR ECONOMY IN THE CONSTRUCTION INDUSTRY: UPCYCLING OF CONSTRUCTION AND DEMOLITION WASTES FROM DIVERSE SOURCES AND THEIR INTEGRATION INTO 3D PRINTING TECHNOLOGY

Anıl KUL

Doctor of Philosophy, Department of Civil Engineering
Supervisor: Assoc. Prof. Gürkan YILDIRIM
March 2024, 156 pages

At the nexus of society, the environment, and urban development, the construction sector constitutes a colossal economy and faces substantial challenges due to the need to accommodate a growing population and displaced individuals from natural disasters, political instability, and other causes. This primary industry is responsible for the largest waste stream, Construction and Demolition Waste (CDW), which accounts for over a third of all waste in the EU. Therefore, urgent action is required to implement feasible and sustainable management strategies to address the challenges associated with its inappropriate management. At this point, 3D concrete printing poses promising potential to address common challenges such as affordable housing, rapid construction and the construction industry's transition to a circular economy by integrating waste-based printable materials.

With a focus on Green and Digital Transformation in the construction sector, this thesis aims to pave the way toward a circular, sustainable, and digital construction industry by generating solutions through the upcycling of CDW and their integration to the 3D concrete printing technology. In this context, the initial focus was on characterizing CDWs from various sources with significantly varying characteristics for use in development of

environment-friendly building materials via geopolymerization technique. The effect of varying chemical contents of CDW from different sources on the mechanical performance of the final product was investigated and optimal conditions were determined based on these variations. Sustainable mortar phases were then developed by incorporating fine recycled concrete aggregates derived from CDW based waste concrete, and the mechanical performance was evaluated considering the influences of the recycled aggregates size and content. In addition, a Life Cycle Assessment (LCA) was conducted to determine the extent of sustainability of each component and its environmental impacts. The final phase entailed the assessment of viability of CDW-based geopolymer concept, extensively investigated in preceding stages, for application to CDW sourced from a distinct geographical region, namely the Netherlands. Moreover, it involves the development of a one-part (just-add-water) CDW-based geopolymer mortar to be integrated into the developed systems for use in a 3D concrete printing technique, facilitating the green and digital transformation of the construction industry in line with the principles of the circular economy.

According to the findings, the mechanical performance of geopolymerized CDW is strongly influenced CDW's intrinsic parameters, which vary depending on source; optimization of related parameters ensures consistent, high performances. LCA analysis demonstrate that, alkaline activators had the highest contribution on environmental impact, followed by CDW treatment; however, impacts could be reduced with mixture design optimization. Furthermore, 62.9% reduction in CO_2 emissions was achieved compared to Portland cement-based systems with similar strength class and embodied energy. The mechanical performance of the one-part geopolymer mixture varied due to the anisotropy; however, these variations could be minimized by optimizing the layer height. Reducing the layer height can minimize the formation of distributed defective regions in the interlayer bonding area caused by the coalescence and expansion of pores, enabling the 3D printed specimens to exhibit fracture behavior as if there were no weak interlayer bond region.

Keywords: Construction and Demolition Wastes, Waste management, Geopolymers, Circular Economy, Green and Digital Transformation, 3D Concrete Printing

ÖZET

İNŞAAT ENDÜSTRİSİNDE DÖNGÜSEL EKONOMİYE DOĞRU YEŞİL VE DİJİTAL DÖNÜŞÜM: FARKLI KAYNAKLARDAN ELDE EDİLEN İNŞAAT YIKINTI ATIKLARININ İLERİ DÖNÜŞTÜRÜLMESİ VE 3D BASKI TEKNOLOJİSİNE ENTEGRASYONU

Anıl KUL

Doktora, İnşaat Mühendisliği Bölümü
Tez Danışmanı: Doç. Dr. Gürkan YILDIRIM
Mart 2024, 156 sayfa

Toplum, çevre ve kentsel gelişimin kesişme noktasında yer alan inşaat sektörü, devasa bir ekonomi oluştururken; artan nüfus, doğal afetler, siyasi istikrarsızlık ve farklı nedenlerle yerinden edilmiş bireylerin barınma ihtiyacı gibi önemli bir zorlukla karşı karşıyadır. Bu temel sektör ayrıca, Avrupa Birliği'nde üretilen tüm atıkların üçte birinden fazlasını oluşturan İnşaat ve Yıkıntı Atıklarından (İYA) sorumludur. Bu nedenle, İYA'nın uygun bir biçimde yönetilmemesinin sebep olacağı zorlukları aşabilmek adına uygulanabilir ve sürdürülebilir yönetim stratejilerinin oluşturulması için ivedi çözümler gerekmektedir. Bu noktada, 3 Boyutlu Beton Baskı, atık bazlı basılabilir malzemeleri entegre ederek uygun fiyatlı konut, hızlı inşaat ve inşaat sektörünün döngüsel ekonomiye geçişi gibi ortak zorlukları ele almak için umut verici bir potansiyel oluşturmaktadır.

İnşaat sektöründe Yeşil ve Dijital Dönüşüme odaklanan bu tez, İYA'nın ileri dönüşümü ve 3 Boyutlu Beton Baskı teknolojisine entegrasyonu adına çözümler üreterek döngüsel, sürdürülebilir ve dijital bir inşaat endüstrisine giden yolu açmayı amaçlamaktadır. Bu bağlamda, tez çalışmalarının ilk aşamasında, jeopolimerizasyon tekniği ile çevre dostu yapı malzemelerinin geliştirilmesinde kullanılmak üzere çeşitli kaynaklardan elde edilmiş

değişken tip ve özelliklere sahip İYA'ların karakterize edilmesine odaklanılmıştır. Farklı kaynaklardan elde edilen İYA'ların değişen kimyasal içeriklerinin nihai ürünün performansı üzerindeki etkisi araştırılmış ve bu varyasyonlara dayalı olarak optimum koşullar belirlenmiştir. Ardından, İYA'nın atık beton fazından elde edilen ince geri dönüştürülmüş beton agregalarının yine İYA esaslı bağlayıcı sisteme dahil edilmesi yoluyla sürdürülebilir harç fazları geliştirilmiş ve geri dönüştürülmüş agrega boyutu ve içeriğinin etkileri dikkate alınarak mekanik performans değerlendirmeleri gerçekleştirilmiştir. Buna ek olarak, her bir bileşenin sürdürülebilirlik derecesini ve çevresel etkilerini belirlemek için bir Yaşam Döngüsü Değerlendirmesi (YDD) yapılmıştır. Son aşama, önceki aşamalarda derinlemesine incelenen İYA bazlı jeopolimer konseptinin tamamen farklı bir coğrafya olan Hollanda'da bulunan İYA'ya uyarlanarak jeopolimer sistemlerin geliştirilmesini ve geliştirilen sistemlerin döngüsel ekonomi konsepti doğrultusunda inşaat sektörünün yeşil ve dijital dönüşümünü sağlamak amacıyla 3 Boyutlu Beton Baskı tekniğine entegre edilmesi için tek bileşenli (sadece su eklenen) İYA bazlı bir jeopolimer harcın geliştirilmesini içermektedir.

Bulgulara göre, İYA esaslı jeopolimerlerin mekanik performansı, İYA'ların tip ve kaynağına bağlı olarak değişkenlik gösteren parametrelerden önemli bir şekilde etkilenmektedir; öte yandan ilgili parametrelerin optimizasyonu tutarlı ve yüksek performanslar elde edilmesine olanak sağlayabilmektedir. YDD analizi, alkali aktivatör fazının en yüksek çevresel etkiye sahip olduğunu ve bunu İYA'ların işlenmesi için gereken işlemlerin izlediğini göstermektedir; ancak bu etkiler karışım tasarımına bağlı olarak azaltılabilmektedir. Ayrıca, İYA-esaslı jeopolimerler benzer mukavemet sınıfındaki ve benzer enerji tüketimine sahip Portland çimentosu bazlı sistemlere kıyasla CO_2 emisyonlarında %62,9'a varan bir azalmaya olanak sağlayabilmektedir. Tek bileşenli jeopolimer karışımının mekanik performansı anizotropi nedeniyle değişiklik göstermiştir; ancak bu değişiklikler yazdırılmış katman yüksekliğinin optimize edilmesiyle en aza indirilebilmektedir. Katman yüksekliğinin azaltılması, katmanlar arası bağlanma alanında bulunan gözeneklerin birleşmesi ve genişlemesinin neden olduğu dağınık kusurlu bölgelerin oluşumunu en aza indirerek 3 Boyutlu baskılanmış numunelerin katmanlar arası zayıf bir bağ bölgeleri yokmuş gibi kırılma davranışı sergilemesini sağlayabilmektedir.

Anahtar Kelimeler: İnşaat ve Yıkıntı Atıkları, Atık Yönetimi, Geopolimerler, Döngüsel Ekonomi, Yeşil ve Dijital Dönüşüm, 3 Boyutlu Beton Baskı

ACKNOWLEDGEMENT

I would like to extend my sincere thanks, first and foremost, to my advisor, Assoc. Prof. Dr. Gürkan YILDIRIM, who provided me with support throughout my thesis work, shared valuable insights, and guided me along the way.

As a special acknowledgment, I owe a debt of gratitude to Assoc. Prof. Dr. Sandra S. Lucas for providing invaluable support during my research at the Technical University of Eindhoven, which enabled me to elevate the quality and scope of my thesis work.

I am deeply thankful to the distinguished members of my thesis committee, Prof. Dr. İlhami DEMİR, Assoc. Prof. Dr. Mustafa Kerem KOÇKAR, and Assoc. Prof. Dr. Özer SEVİM, and Assist. Prof. Hüseyin ULUGÖL for their invaluable insights, critical contributions that have enriched the content and scholarly merit of this work.

I would like to express my gratitude to all my colleagues in the Hacettepe University Civil Engineering Department and the Technical University of Eindhoven Structural Engineering and Design Department 3D Concrete Printing Group, who helped me with my thesis work.

I acknowledge with appreciation the financial support provided by The Scientific and Technological Research Council of Türkiye (TÜBİTAK) under the "2214-A International Research Fellowship Programme for PhD Students", which has facilitated the execution of this research and enabled its completion to the highest standards.

I extend my heartfelt thanks to my family, who raised me and brought me to this day, always encouraged me throughout this journey, and never withheld their love and understanding.

Lastly, and most of all, I would like to extend my deepest appreciation to my beloved wife, whose unwavering love, encouragement, steadfast support, and belief in me have been the foundation of my academic journey and have made this accomplishment possible. I am proud to dedicate this thesis to her, for which she supported me at every stage.

TABLE OF CONTENTS

LIST OF FIGURES

LIST OF TABLES

SYMBOLS AND ABBREVIATIONS

Symbols

CFC	Chlorofluorocarbon
CO_2	Carbon Dioxide
NaOH	Sodium Hydroxide
Na_2SiO_3	Sodium Silicate
NH_x	Nitrogen
NO_x	Nitrogen Oxide
SO_2	Sulfur Dioxide

Abbreviations

3D-AM	Three Dimensional Additive Manufacturing
3DCP	Three Dimensional Concrete Printing
3DPG	Three Dimensional Printable One-part Geopolymer
AASC	Alkali Activated Slag Concrete
ACI	American Concrete Institute
AM	Additive Manufacturing
ANOVA	Analysis of Variance
AP	Acidification Potential
ASTM	American Society for Testing and Materials
C	Concrete
CAH	Calcium Aluminate Hydrates
CASH	Calcium Aluminate Silicate Hydrates
CDW	Construction and Demolition Wastes
CE	Circular Economy
CGM	CDW-based Geopolymer Mortars
CSH	Calcium Silicate Hydrates
Micro-CT	Computed Microtomography
CW	Concrete Waste
DSC	Differential Scanning Calorimetry
DZ	Demolition Zone

ECC	Engineered Cementitious Composite
EDX	Energy-Dispersive X-ray
EGC	Engineered Geopolymer Composite
EP	Eutrophication Potential
EPA	Environmental Protection Agency
EU	European Union
FA	Fly Ash
FFD	Fossil Fuel Depletion
FIEC	European Construction Industry Federation
FTIR	Fourier Transform Infrared Spectrophotometer
G	Glass
GC	Geopolymer Concrete
GGBS	Ground Granulated Blast Furnace Slag
GHG	Greenhouse Gases
GWP	Global Warming Potential
HB	Hollow Brick
IEA	International Energy Agency
ISO	International Organization for Standardization
ITZ	Interfacial Transition Zone
KC	Kaolin Clay
LCA	Life Cycle Assessment
LCI	Life Cycle Inventory
LCIA	Life Cycle Impact Assessment
LOI	Loss on Ignition
LS	Limestone
MSI	Material Sustainability Indicators
NASH	Sodium Aluminosilicate Hydrates
ODP	Ozone Depletion Potential
OECD	Organization for Economic Cooperation and Development
OPC	Ordinary Portland Cement
PC	Portland Cement
PCF	Portland Cement-Fly Ash-based mortar
PDF	Particle Diffraction File
PM	Particulate Matter

RCA	Recycled Concrete Aggregate
RCB	Red Clay Brick
RT	Roof Tile
SCM	Supplementary Cementitious Material
SEM	Scanning Electron Microscopy
SH	Sodium Hydroxide
SHCC	Strain-Hardening Cementitious Composites
SP	Superplasticizer
SS	Sodium Silicate
TG	Thermogravimetry
UHPFRC	Ultra High Performance Fiber Reinforced Concrete
UN	United Nations
US	United States
USA	United States of America
UV	Ultraviolet
UWTT	Ultrasonic Wave Transmission Tests
XRD	X-ray Diffraction
XRF	X-ray Fluorescence

OVERVIEW

The construction sector holds a pivotal position in shaping our built environment, serving as a junction of economic activity and urban development. Within the European Union (EU), it sustains the livelihoods of approximately 400 million urban inhabitants, engages over 3 million enterprises and a workforce of 15 million, and contributes substantially to the annual turnover, amounting to EUR 1,400 billion [1]. Directly aligned with the UN Sustainable Development Goal 11 "Sustainable Cities and Communities" [2], the sector is receiving special attention from EU policy frameworks, notably the strategy for enhancing the sustainable competitiveness of construction industry enterprises [3].

However, the sector faces significant challenges. The widespread use of concrete, the main construction material, has a heavy impact on natural resources and climate while contributing significantly to global CO_2 emissions [4]. Construction and Demolition Waste (CDW) is the largest waste stream by volume, comprising more than one third of all waste generated in the EU [5], posing a huge waste management challenge worldwide. Landfilling of CDW is responsible for ~35% of the deposition area worldwide [6]. Therefore, such large quantities of CDW need to be managed efficiently, feasibly, and innovatively. However, most developing countries fail to properly manage the large quantities of CDW generated, resulting in serious environmental, economic, and social problems.

Due to its fragmented nature, the sector, especially small and medium-sized enterprises, has been slow to adopt innovation and improve production standards in the context of digital transformation. The EU has fully recognized these environmental and technical challenges and has set out a Twin (Green and Digital) Transition strategy [7] that aims to green the construction sector through increased reuse and recycling towards a Circular Economy (CE) [8]. Within this strategy, a digital transformation is also envisaged through the adoption and diffusion of digital manufacturing and additive manufacturing (3D printing, 3D-AM), which will put the construction sector on a sustainable path in terms of production technologies [9]. However, a coherent synthesis of green and digital initiatives has yet to be achieved. Materials science has made fundamental changes possible through significant work to improve the strength and durability of concrete, but there have been no significant advances in the sustainability of concrete and the adaptation of concrete production techniques to technology.

Considering this situation, the current thesis aims to close the existing gap by fulfilling the requirements of Green and Digital Transformation in the construction industry. The main objective of the thesis is to produce fully circular and sustainable solutions to construction applications by utilizing 3D printing technology and transforming CDW into innovative construction materials. The thesis work proceeds through 4 main chapters presented below:

In Chapter 1, *"Sustainable Geopolymerized Construction Materials from Construction and Demolition Waste"*, the current state-of-the-art in waste recycling, a fundamental principle of the circular economy, by integrating CDWs into the geopolymerization technique, which has become increasingly widespread in recent years and is used to produce sustainable and environmental-friendly building materials was presented. Chapter 2 *"Optimizing Mechanical Performance of Geopolymers Produced from Construction and Demolition Waste: A Comparative Study of Materials from Different Origins"* examined the source dependence of CDWs, originating from various sources with vastly variable characteristics, and aimed to minimize this dependency through the upcycling of CDWs obtained from different sources into building materials using the geopolymerization technique alongside a sequential mixture design algorithm. The impact of variations in the chemical content of CDW from different sources on the final product performance was examined, and an optimization based on these variations was developed. In Chapter 3, *"Characterization and Life Cycle Assessment of Geopolymer Mortars with Masonry Units and Recycled Concrete Aggregates Assorted from Construction and Demolition Waste"* the feasibility of incorporating recycled aggregates from the concrete phase of CDW into CDW-based geopolymer binder systems were investigated, with the aim of developing truly sustainable mortar phases encompassing both the binder and aggregate components. In addition to investigating the feasibility of integrating recycled aggregates and influences on the mechanical performance of the final product, a detailed Life Cycle Assessment (LCA) analysis was conducted to evaluate the environmental impacts of the developed mortar mixtures and to compare with Portland cement-based system in terms of sustainability performance. Through LCA analysis, the environmental impacts of geopolymer mortar mixtures were compared to cement-based systems, and the contributions of mixture content to carbon emissions and energy consumption were evaluated. Finally, Chapter 4 *"3D Printable Monolithic Geopolymer Derived from Construction and Demolition Waste: Anisotropy Assessment in Macro- and Micro-Mechanical Perspective"*, based on the concept of sustainable building material production by geopolymerization of CDW-based materials

from different sources based on Chapters 2 and 3, focuses on the development of a one-part (just water added) geopolymer mortar to enable the integration of geopolymer mortar systems produced from CDWs obtained from demolished brick walls in the Netherlands, which has a completely different geography/origin, into the 3D concrete printing technique. To thoroughly examine the compatibility of the developed 3D printable one-part CDW-based geopolymer with the 3D printing technology, a comprehensive investigation was conducted, encompassing both the macro- and micro-mechanical properties of the developed mixture as well as the anisotropic behavior of the structural elements produced by 3D concrete printing technique. It was also investigated how layer height optimization affects mechanical performance, anisotropy and interlayer bond region property in 3D printed specimens produced at different layer heights.

CHAPTER I: SUSTAINABLE GEOPOLYMERIZED CONSTRUCTION MATERIALS FROM CONSTRUCTION AND DEMOLITION WASTE

1.1. Introduction

Construction plays an important role in economic growth in many countries across the world. Its significance is evident in the numerous infrastructure projects being developed, including housing, commercial buildings, transportation, and energy systems. The demand for new construction activities has increased due to population growth, migration, and urbanization, resulting in a significant expansion of the industry. However, the growth of the construction industry has brought about significant environmental challenges. This sector is known for consuming a substantial amount of energy and natural resources, emitting greenhouse gases, and generating significant waste, resulting in a significant negative impact on the environment. In fact, the buildings sector alone accounts for approximately 30% of total global energy consumption [10]. In addition, the building stock is responsible for approximately 27% of the world's carbon dioxide (CO_2) emissions, which result from the day-to-day operation of buildings.

The use of ordinary Portland cement (OPC), the primary binder used in the production of concrete, is a critical factor that contributes to the environmental impact of the industry. The production of OPC is energy intensive. It releases a significant amount of CO_2 into the atmosphere, contributing to global warming. OPC alone is one of the most significant contributors to climate change, accounting for approximately 7-8% of global greenhouse gas emissions [11]. In addition, significant ecological damage, including deforestation, soil erosion and loss of biodiversity, can result from the extraction of raw materials used in cement production [12]. Finding ways to reduce the environmental impact of OPC is therefore critical. One potential solution for reducing energy consumption and greenhouse gas emissions in the production of building materials is the development of environment-friendly alternatives. Geopolymers, also known as alkali activated materials, are promising environmental-friendly solutions that have the potential to be adopted by the construction industry to eliminate burden of OPC on nature. It involves activating aluminosilicate materials with alkali solutions, such as sodium hydroxide or potassium hydroxide, resulting in the formation of geopolymers [13]. Geopolymers have the same properties of OPC, while

requiring less energy to produce, emitting fewer greenhouse gases, and having higher durability and fire resistance [14-17]. Geopolymers can be produced using industrial waste materials such as fly ash, slag and other mining and metallurgical waste, potentially reducing the amount of waste sent to landfills. On the other hand, the construction industry also faces an environmental challenge in waste management. Significant amounts of waste, including concrete, bricks, asphalt, metals, wood and plastics, are generated during construction and demolition activities. Construction and Demolition Wastes (CDW) include not only the types of waste mentioned above, but also hazardous materials such as asbestos and lead, which must be handled with special concern to prevent health risks to workers and the general public. It is estimated that 850 million tons of CDW are generated annually in the European Union, accounting for approximately 25-30% of total waste generation [18]. The construction industry in the USA produces about 570 million tons of CDW annually, which is about 23% of the total waste produced [19]. Improper management of this waste can have serious environmental consequences, including polluting soil, water, and air and destroying habitat. Improper disposal of CDWs in landfills not only consumes valuable land resources, but also leads to the release of harmful gases, including methane, which contributes to climate change. To address this issue, a circular economy approach can be adopted by promoting the reuse and recycling of CDW materials [20]. Recycling a ton of CDW, which includes concrete, brick, and masonry debris, costs approximately $21 per ton, whereas landfilling costs about $136 per ton [21]. Due to its favorable aluminosilicate content, CDW is a promising candidate for alkaline activation in recycling activities [22,23]. However, there is a limited amount of research in this area. For effective waste management, it is necessary to achieve optimal recycling of each component of CDW through proper formulation. In order to achieve this, it is essential to have a comprehensive understanding of the properties and characteristics of each of the components of the CDW. Over the past few years, a growing number of studies have aimed at developing sustainable and efficient recycling methods for various types of CDWs, including concrete, asphalt, wood, and plastics [24-29]. The goal of these studies is the improvement of the utilization of CDW in the construction industry, while at the same time the minimization of its impact on the environment. Overall, promoting practices to manage and recycle CDW will be necessary to advance the circular economy approach in construction and support sustainable development.

To facilitate the active participation of CDW in the circular economy of the construction industry, this chapter aims to review the latest research and applications of alkali activation technology on a wide range of materials, including binders, mortars, concretes, 3D printable composites, engineered geopolymer composites, and insulation materials based on CDW. The work focuses on the analysis of all parameters that can potentially affect the final performance of the materials, and comprehensively evaluates their fresh, mechanical, and durability properties. As CDW is a global issue, in an effort to reduce the carbon footprint of the construction industry, this chapter aims to provide insight into sustainable waste management solutions and the potential use of CDW as a source of feedstock for the production of construction materials.

1.2. Exploring Alternatives to Portland Cement for Sustainable Construction

1.2.1. Ordinary Portland Cement

Concrete is the world's second most used material after water, used in a variety of applications including building, infrastructure, and transportation [30]. However, the production of OPC is an energy-intensive process that causes significant environmental damage. Greenhouse gas emissions, air pollution, and water pollution are among its negative environmental impacts. The calcination process, which releases CO_2 from limestone, is the main source of emissions in cement production. Handling, processing, transporting, and curing raw materials and cement also require significant energy inputs, further increasing emissions. Emissions can cause respiratory and cardiovascular problems for human health by releasing PM, SO_2, and NO_x into the air. In addition, dust and soil contamination can occur during the handling and processing of raw materials and cement. Water contamination may be caused by discharging process water and effluent containing heavy metals and other contaminants.

In 2019, approximately 4.2 billion metric tons of OPC were produced worldwide [31], requiring the energy equivalent of more than 175 nuclear power plants or 5.5 million wind turbines. The production of one metric ton of OPC results in approximately one metric ton of CO_2 emissions, according to the Environmental Protection Agency (EPA) [32]. To put this into perspective, total global CO_2 emissions from all sources in 2019 were approximately 36.4 billion metric tons, and contribution of OPC production was about 4.2

billion metric tons [33]. The lion's share of this contribution, more than 800 million metric tons, came from China (Fig. 1.1), meaning that OPC production accounted for approximately 11.5% of total global CO_2 emissions in 2019. Alternative low-carbon and carbon-neutral cement technologies, as well as improved energy efficiency and best practices in waste management and pollution control, are being advanced to mitigate the environmental impact of cement production. However, to address the negative environmental impacts of cement production on a global scale, significant work remains to be done.

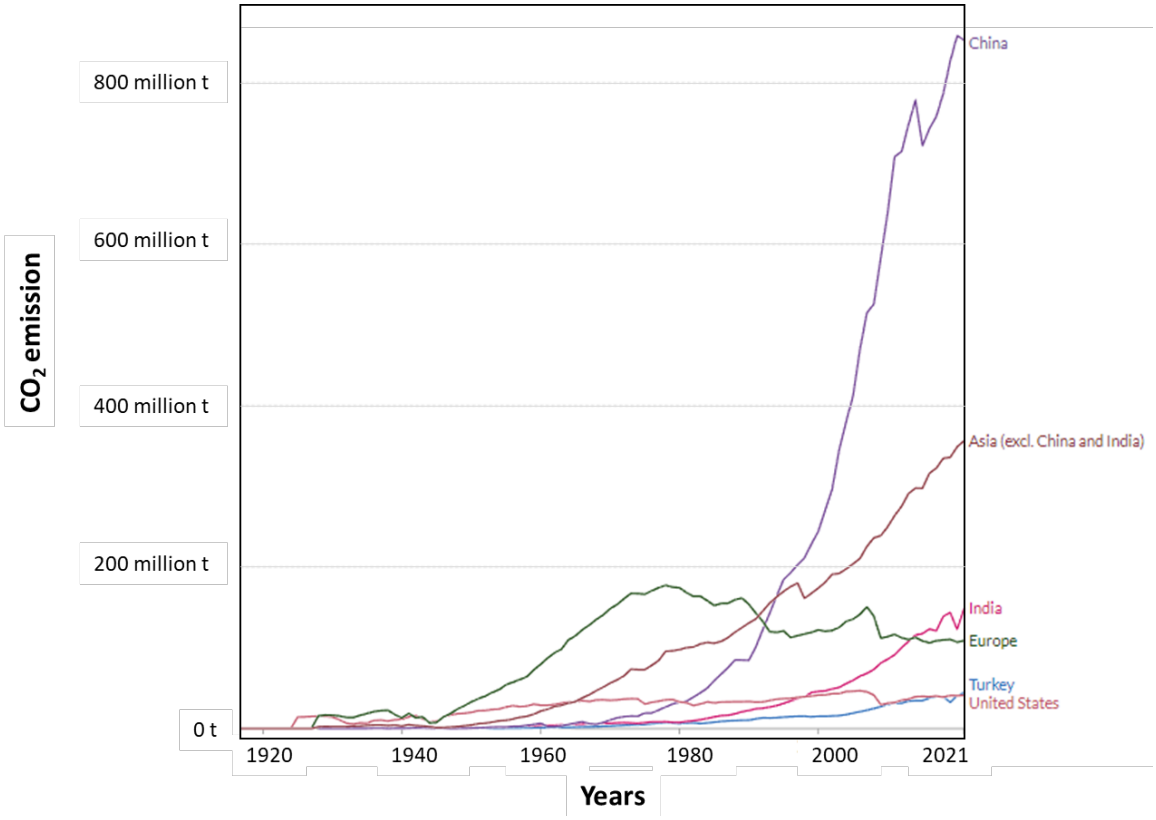

Fig. 1.1. Annual CO_2 emissions from cement [33]

1.2.2. Alternative Materials to Ordinary Portland Cement

The negative environmental impact of OPC production and the depletion of natural resources are driving the need to develop alternative materials in the construction industry. The use of alternative pozzolanic materials reduces or eliminates the need for OPC, thereby greatly reducing the carbon footprint and waste associated with cement manufacture. The pozzolanic reaction refers to the chemical reaction between the amorphous silica and alumina present in pozzolanic materials and the $Ca(OH)_2$ that is produced during the hydration of OPC [34]. The reaction leads to the creation of supplementary calcium silicate

hydrates (CSH) and calcium aluminate hydrates (CAH), contributing to the mechanical performance and durability. The pozzolanic reaction takes place when there is moisture and alkalinity, which activate the pozzolanic material and enable it to react with $Ca(OH)_2$. The reaction is exothermic and occurs slowly, usually taking weeks to months, depending on the type and quantity of pozzolanic material used.

Fly ash, a residue from coal-fired power plants, is widely utilized as an alternative ingredient in cement mixes. Global production figures from 2018 estimated around 780 million tons of fly ash [35]. Its incorporation in cement-based materials has been found to enhance their strength, durability, and reduce permeability. Other materials like slag, rice husk ash, and calcined clay, which are by-products of various industries or agricultural activities, have also been explored for their potential in cement mixtures [36]. Slag originates from steel production, while rice husk ash and calcined clay are agricultural residues. Utilizing these materials in cement mixtures offers several benefits, including increased strength and durability, reduced permeability, and enhanced resistance to chemical and environmental degradation [37-39]. Moreover, their adoption can contribute to lessening the environmental impact of construction by diverting waste from landfills and cutting down energy consumption and carbon emissions associated with Ordinary Portland Cement (OPC) production.

While alternative materials like slag, rice husk ash, and calcined clay hold promise as substitutes for Ordinary Portland Cement (OPC), they present their own challenges. One such issue is the inconsistency of these materials across different sources, which can impact the final product's characteristics. Moreover, some sources might contain pollutants like heavy metals, posing environmental and health risks if not managed properly [40]. Additionally, the availability and cost of these materials can be unpredictable since they originate from industrial processes and may not be consistently produced in large volumes. This variability in supply and pricing can hinder the construction industry's ability to plan and execute projects relying on these materials. Consequently, researchers are exploring alternative aluminosilicate materials, including those derived from Construction and Demolition Waste (CDW) and mining by-products [41]. It is crucial to acknowledge that integrating alternative materials into construction is not flawless, and there may be obstacles and limitations to their widespread adoption. Regulatory barriers or economic constraints, for instance, could impede the use of certain materials in specific regions or applications

[42]. Nevertheless, the growing awareness of the construction sector's environmental impact and the emergence of more sustainable and inventive building materials suggest that the exploration of alternative materials will remain a significant focus of research and development in the years ahead.

1.2.3. Alkali Activation Mechanism to Produce Environment-friendly Binders

In recent years, the use of alternative materials, particularly in the context of geopolymerization and alkali activation processes, as a substitute for OPC has received considerable attention. Alkali activation synthesizes cementitious materials by activating aluminosilicate precursors with strong alkaline solutions. The process of alkali activation comprises a number of series of complicated reactions occurring between the precursor material and the alkaline activator solution, forming amorphous, three-dimensional silicate networks [43]. This is accomplished without the need for the high-temperature calcination that is typically required in the production of OPC, resulting in significant energy savings and a reduced carbon footprint.

The five main phases of alkaline activation are: dissolution, speciation equilibrium, gelation, reorganization, and polymerization and hardening, as depicted in Fig. 1.2 [44]. During the dissolving stage, the alkaline activating solution reacts with the precursor and releases reactive species. Dissolved silica, alumina, and calcium ions can be included in these reactive species, among others. Hydrolysis of the alkaline activator, resulting in the formation of hydroxide (OH^-) ions and/or silicate species, is one of the primary reactions that occurs during the speciation equilibrium phase. Hydroxides and silicates then react with cations released from precursors to form different soluble and insoluble species. For example, calcium ion (Ca^{2+}) released from the precursor reacts with hydroxide ions to form calcium hydroxide ($Ca[OH]_2$), which is a soluble species. The speciated species react to form an amorphous gel-like substance in the gelation phase. This gel-like substance undergoes further structural reorganization in the reorganization phase, resulting in the formation of a stable three-dimensional network containing calcium aluminosilicate (CASH), calcium silicate (CSH) and sodium aluminosilicate (NASH) hydrates. The hardening phase can be prolonged, typically from several days to several weeks, depending on the curing conditions and the composition of the precursor material and alkaline activator used. During this period, the final product continues to undergo structural rearrangement and polymerization,

developing mechanical strength and durability properties similar to that of conventional cementitious materials [45].

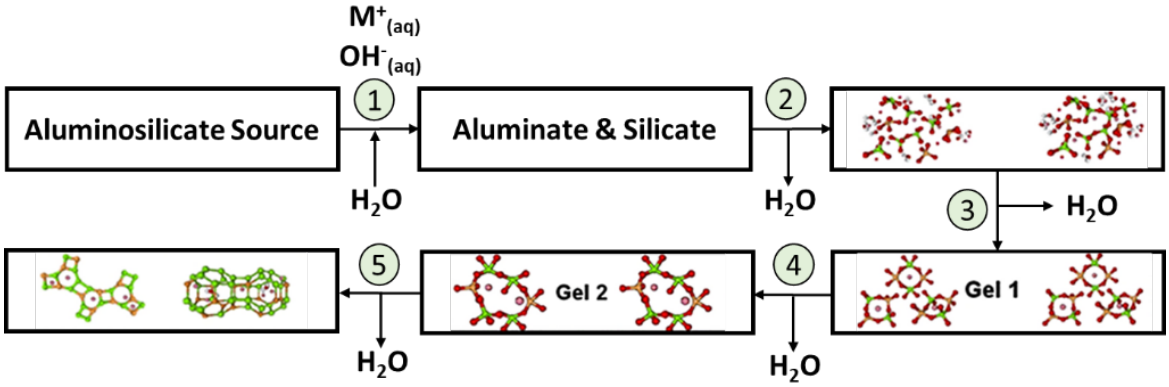

Fig. 1.2. Alkali activation mechanism; (1) dissolution, (2) speciation equilibrium, (3) gelation, (4) reorganization, (5) polymerization and hardening [44]

1.3. Construction and Demolition Wastes as a Promising Alternative in OPC

CDW refers to a diverse mix of waste materials arising from construction, renovation, and demolition activities. It originates from a range of sources including residential, commercial, and industrial buildings, as well as infrastructure projects and other structures. The composition of CDW is subject to numerous influences, such as the nature and features of the structure, the materials utilized, and the construction techniques employed. For instance, CDW from residential properties might include wood, plaster, tiles, bricks, plastics, and metals, whereas CDW from industrial sites could potentially contain hazardous substances like asbestos, lead, and chemicals [46].

The activities leading to the generation of CDW typically result in the accumulation of large quantities of waste. However, data on CDW are often not collected routinely or consistently, so most published figures are estimates that need to be interpreted with caution. These estimates indicate approximately 8.2 billion tons of CDW generated across the EU in 2012 [47], 77 million tons in Japan, 33 million tons in China, and 17 million tons in India in 2010, with nearly 7 million tons each in Dubai in 2011 and Abu Dhabi in 2013, respectively [48]. CDW often constitutes the largest proportion of the overall waste generated, accounting for 34% of urban waste produced in OECD nations. The amount of CDW generated is rapidly

increasing due to the rate of infrastructure development worldwide [48]. The construction industry significantly contributes to CDW generation globally. According to the Global Waste Management Outlook report, the construction and demolition sector generates about 30% of the world's total waste and consumes up to 40% of the world's raw materials [48]. Moreover, CDW generation is expected to rise further due to rapid urbanization, population growth, and economic development in emerging markets. For instance, in China, the construction industry is one of the fastest-growing sectors and a major contributor to CDW generation, accounting for over 50% of the country's total waste [46].

The generation of waste is a common outcome of both human-made construction and demolition activities, as well as natural disasters. The volume and composition of the waste produced vary based on factors such as the type and severity of the disaster and the characteristics of the built environment. Recent natural disasters like the 2023 Türkiye earthquake, the 2015 Nepal earthquake, the 2010 Haiti earthquake, the 2005 Hurricane Katrina, and the 2004 Indian Ocean tsunami resulted in significant amounts of waste, overwhelming existing waste management systems. Debris from these disasters often obstructs rescue and emergency services' efforts to reach survivors. Common materials found in disaster debris include natural aggregates, construction and demolition waste (such as concrete, bricks, timber, and metal), vehicles and boats, and electrical goods and appliances. However, these materials can be recycled and have a significant market in developing countries [49]. They can be repurposed for various uses, such as landfill cover, aggregate for concrete, land reclamation fill, compost for fertilization, and slope stabilization [50]. Additionally, some of these materials can even be utilized to generate energy in a beneficial manner [51,52].

The increase in CDW generation has raised significant concerns regarding its environmental impact, spanning from resource depletion and land use to energy consumption, greenhouse gas emissions, and pollution. Landfills receiving CDW contribute to the depletion of land resources due to their extensive space requirements. Additionally, incinerating CDW releases hazardous air pollutants and greenhouse gases like CO_2 and methane, exacerbating climate change [53]. Moreover, transporting CDW consumes substantial energy and contributes to greenhouse gas emissions. To address the environmental challenges associated with CDW, many countries have implemented regulations and policies for its management. For instance, the European Union has embraced a circular economy approach

to CDW management, aiming for 70% CDW recycling by 2020 [54]. Similarly, in the United States, the Environmental Protection Agency has established guidelines promoting the beneficial use of CDW, advocating for its recycling as a substitute for natural aggregates in construction [55].

Extensive research has been conducted on the utilization of CDW in the concrete industry, but its current application remains largely limited to low-tech methods. Studies indicate that replacing natural aggregates with crushed concrete for structural purposes should be restricted to 25-30% [56,57], while substituting up to 50% of natural sand with CDW-based fine particles is unlikely to significantly affect concrete properties [58]. However, utilizing 100% recycled concrete aggregate (RCA) could diminish the mechanical properties of concrete and increase its absorption capacity compared to standard concrete. Various techniques have been proposed to improve the quality of CDW-based aggregates, such as mechanical grinding, acid soaking, polymer emulsion, and accelerated carbonation. Nevertheless, economic constraints impede the widespread adoption of CDW reuse as a feasible option.

The crushing of CDW generates a substantial amount of fine powder. However, there have been limited studies investigating the use of this powder as a partial replacement for cement. Incorporating concrete waste powders into geopolymer mortar significantly reduces fluidity and compressive strength. It is advisable not to exceed a replacement rate of 15% for Ordinary Portland Cement (OPC) [59]. Using up to 30% CDW powder in conventional concrete instead of OPC can promote hydration and reduce permeability and porosity. However, higher ratios may adversely affect properties such as frost resistance and chloride ion permeability [60]. Utilizing fine powder from recycled concrete as an alternative source for producing Portland cement clinker has been found to be partially viable [61]. In conclusion, CDW can be effectively utilized in concrete production by employing appropriate techniques to enhance its quality while considering its limitations to achieve optimal results.

Using recycled and reused CDW as a source for geopolymer materials can offer a sustainable solution to mitigate ecological impact and reduce the demand for ordinary OPC. Recent studies have demonstrated that CDW can serve as an excellent source of aluminosilicates for geopolymer binders, particularly as demolished structures yield significant quantities of

fine silt particles rich in crystalline aluminosilicates [62-64]. Given the variability of CDW, there is an urgent need for more comprehensive research in developing CDW-based geopolymer materials. Such research would thoroughly explore the effects of CDW's variability on the mechanical, fresh, and structural properties of the final materials.

1.4. Current State-of-art of CDW-based Geopolymers and Future Directions

1.4.1. CDW-based Geopolymerized Binders

In recent years, there has been a noticeable increase in research efforts aimed at developing geopolymers using components derived from CDW, including clay-based masonry (such as red clay bricks, hollow bricks, and roof tiles), concrete and mortar, and waste glass. These materials have shown promise, particularly due to their suitable aluminosilicate nature. Literature suggests that a minimum SiO_2+Al_2O_3+Fe_2O_3 content of over 70% is crucial for achieving successful alkali activation [65], following the ASTM standard related to the pozzolanic activity of coal fly ash and raw or calcined natural pozzolan [66]. It is worth noting that masonry-originated CDW components like red clay bricks, hollow bricks, and roof tiles are considered advantageous due to their chemical composition. In contrast, concrete and glass tend to have weaker aluminosilicate content. In a study, CDW-based roof tiles, red clay bricks, and hollow bricks, activated with 12.5M NaOH and subjected to thermal curing, achieved compressive strengths of approximately 40 MPa. In comparison, glass attained a strength of about 30 MPa. This difference was attributed to the lower Al_2O_3 content of glass (1.27%), and its relatively coarse particle size distribution compared to other materials [67]. Another study illustrated that concrete, with a total SiO_2+ Al_2O_3 content of 36.36%, activated with 19M NaOH and cured at 125°C for 48h, achieved a compressive strength of 34 MPa. Substituting 25% of the concrete with glass increased the compressive strength to 36 MPa. However, the concrete's limited aluminosilicate content was offset by the glass's high SiO_2 content, restricting the concrete's contribution to the compressive strength. Importantly, incorporating bricks and tiles alongside the concrete and glass notably elevated the resulting paste's compressive strength to 54 MPa. In another investigation, glass activated solely with NaOH solutions containing 12% Na achieved a strength of 43 MPa, whereas concrete remained at 9.8 MPa. However, by integrating hollow bricks and roof tiles into the concrete, the compressive strength surged to 59.9 MPa. These findings suggest that the masonry-originated portion of the CDWs demonstrates significant reactivity in the highly

alkaline medium due to the balanced SiO_2 and Al_2O_3 content. Nonetheless, glass and concrete, lacking sufficient Al_2O_3 and SiO_2, respectively, exhibited lower reactivity. Furthermore, combining CDW-based components in alkali activation appears to yield superior performance compared to individual use, as documented in the literature and depicted in Fig. 1.3.

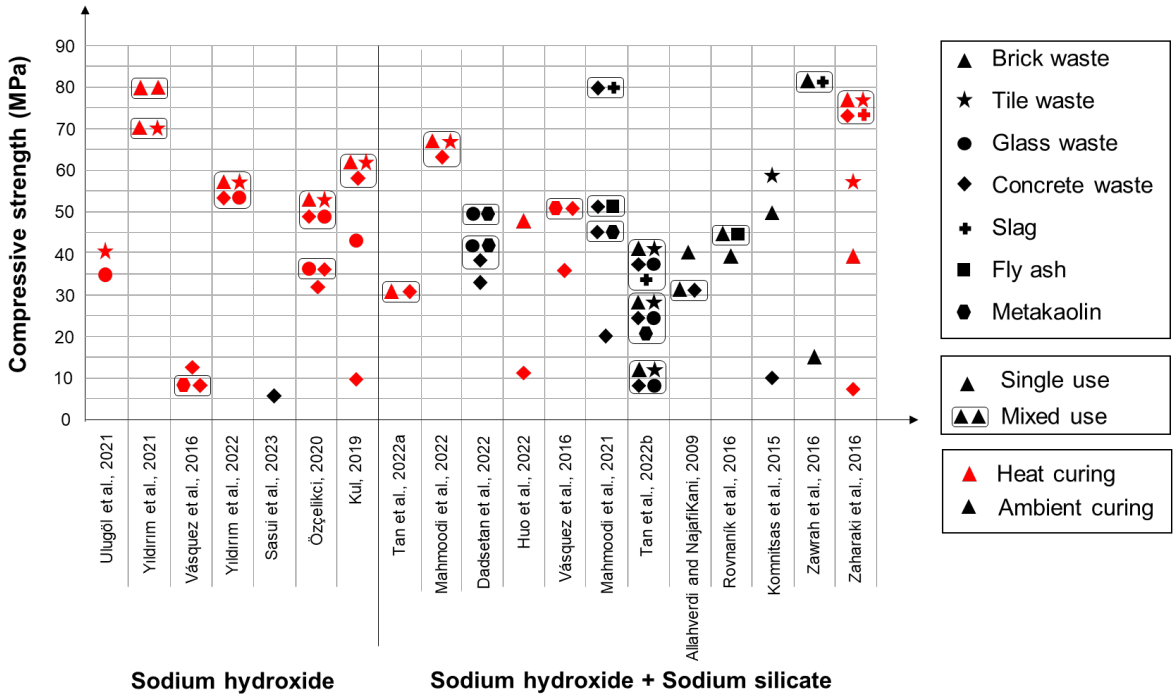

Fig. 1.3. Compressive strength of CDW-based geopolymer binders

Besides the aluminum silicate content, maintaining equilibrium in the Si/Al, Na/Si, and Ca/Si ratios is pivotal for reaction kinetics in alkali activation. According to a recent review, the SiO_2 content of bricks and tiles typically ranges from 53% to 70% and 57% to 70%, respectively, while the Al_2O_3 content ranges from 11% to 20% and 10% to 18%, respectively [23]. When used alone, these materials typically exhibit a Si/Al ratio of around 5, resulting in the formation of NASH type gel structures through alkali activation. However, due to their low Ca content, they lack CSH/CASH type gel structures that could enhance mechanical performance in the system. This deficiency can be addressed by incorporating concrete with a higher CaO content (20% to 31%) into the mixture. However, this may result in a decrease in the Si/Al ratio, which can be compensated for by adding glass with a high SiO_2 content (70% to 75%) to the mixture to achieve ionic balance and higher compressive strengths. For example, in a study where geopolymer was synthesized using brick, ceramic, and concrete waste, it was noted that higher Na/Si ratios, along with Si/Al molar ratios, led to reduced

setting times [70]. This acceleration could be attributed to the enhanced dissolution of aluminosilicates from CDW materials at elevated Na_2O levels, resulting in multiple condensation, compression, and hardening stages. The same study also suggested that achieving maximum compressive strengths may require adjusting the Si/Al ratio, with optimal mechanical performance achieved at well-balanced molar ratios of Si/Al = 10.2 and Na/Si = 0.18. Additionally, it has been observed that a higher Si/Al ratio contributes to enhanced compressive strength in CDW-based geopolymers. The increased Si content strongly influences the formation of alkali aluminosilicate gels, while the presence of Al in the precursor determines the chemical structure and network formation. Since Si-O-Si bonds exhibit greater strength than Al-O-Al and Al-O-Si bonds, an increase in available silica in the alkali activation system can significantly modify the composition and structure of the produced gels, resulting in more polymerized and densely packed reaction products with improved mechanical properties, as depicted in Fig. 1.4 [71]. It has been reported that the Ca/Si ratio also plays a crucial role in determining mechanical performance. An increase in the Ca/Si ratio has been found to positively impact mechanical strength at lower Si/Al ratios (i.e., 4-6). However, at higher Si/Al ratios (i.e., 6-14), the Ca/Si ratio appears to have a threshold value of 1.0-1.5 concerning its influence on compressive strength. Considering the relevant literature on the effects of Si, Al, Ca, and Na oxides' amounts and ratios, it is worth noting that certain thresholds can be identified based on the mechanical properties of geopolymers. However, differences in source materials, alkali activator production techniques, and various calculation methodologies for determining ratios, considering precursor and/or alkali activator individually or collectively, can lead to variations in determining the optimal ingredient quantities.

In recent years, several studies have explored the development of CDW-based geopolymers using different combinations of materials with high pozzolanic activity, like fly ash, metakaolin, and slag, aiming to enhance mechanical performance [72-74]. For instance, one study found that a geopolymer formulated with waste-fired clay bricks achieved a compressive strength of 15 MPa after 90 days of ambient curing. However, replacing 60% of the material with slag led to a significant increase in compressive strength to 83 MPa [72]. This enhancement was attributed to the formation of additional CSH gels in the matrix through hydration reactions of calcium oxide from the slag, which improved mechanical performance alongside the aluminosilicate network in the geopolymer. In a different study, geopolymer binders made solely from concrete waste achieved a compressive strength of 20

MPa within 28 days. This enhancement was attributed to the formation of additional CSH gels in the matrix through hydration reactions of calcium oxide from the slag, which improved mechanical performance alongside the aluminosilicate network in the geopolymer. In a different study, geopolymer binders made solely from concrete waste achieved a compressive strength of 20 MPa within 28 days. However, when 45% of the material was substituted with Class-C fly ash, Class-F fly ash, metakaolin, or slag, the compressive strengths increased to approximately 48, 30, 43, and 82 MPa, respectively [73]. The authors attributed the outstanding performance of slag to its high CaO content, which facilitated the formation of CASH/CSH structures within the matrix. Conversely, other supplementary cementitious materials (SCMs) improved mechanical performance by promoting the formation of CASH/NASH gel structures to varying extents.

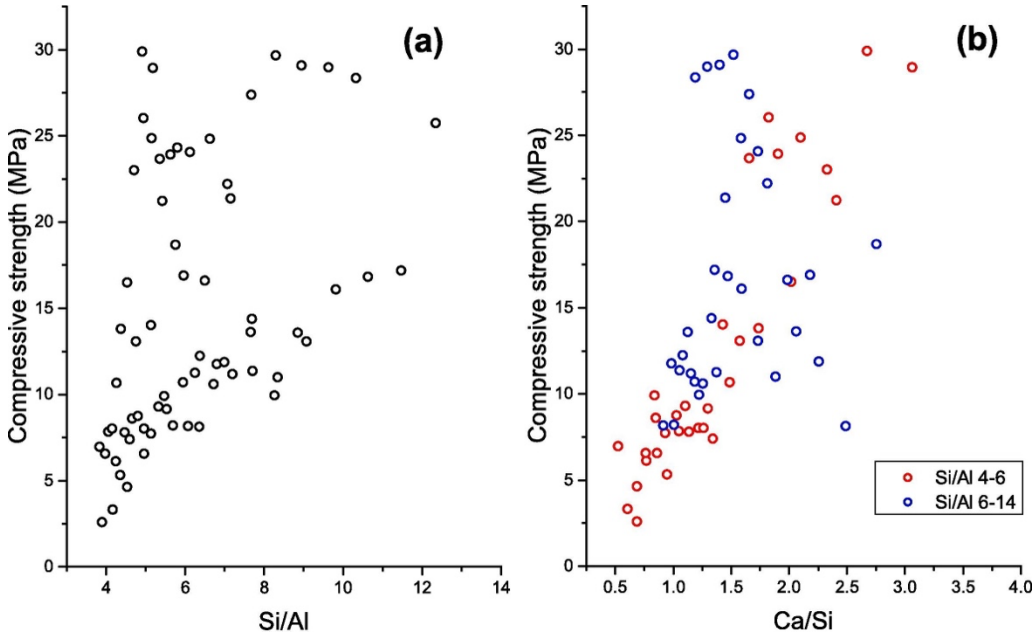

Fig. 1.4. Compressive strength of CDW-based geopolymers with different a) Si/Al, b) Ca/Si ratios [71]

This enhancement was attributed to the formation of additional CSH gels in the matrix through hydration reactions of calcium oxide from the slag, which improved mechanical performance alongside the aluminosilicate network in the geopolymer. In a different study, geopolymer binders made solely from concrete waste achieved a compressive strength of 20 MPa within 28 days. However, when 45% of the material was substituted with Class-C fly ash, Class-F fly ash, metakaolin, or slag, the compressive strengths increased to approximately 48, 30, 43, and 82 MPa, respectively [73]. The authors attributed the

outstanding performance of slag to its high CaO content, which facilitated the formation of CASH/CSH structures within the matrix. Conversely, other supplementary cementitious materials (SCMs) improved mechanical performance by promoting the formation of CASH/NASH gel structures to varying extents. According to Rovnaník et al. [74], geopolymer binders formed by activating brick powder with sodium silicate and sodium hydroxide achieved a compressive strength of 41 MPa after 90 days. However, substituting 25% of the brick powder with fly ash resulted in a roughly 12.5% increase in compressive strength. This enhancement is attributed to fly ash's larger specific surface area, greater pozzolanic activity, and denser microstructure. Overall, integrating SCMs like fly ash, slag, metakaolin, and others significantly enhances the mechanical characteristics of CDW-based geopolymers. The additives encourage the formation of additional CASH/CSH type bonds and gel structures within the matrices, leading to improved compressive strength and denser microstructures.

1.4.2. CDW-based Geopolymerized Mortars and Concretes

The use of different alkali agents in activating CDW-based materials has shown promising progress in producing geopolymers. Recent studies have also focused on creating structural mortar and concrete by incorporating recycled aggregates from CDW-based components. To assess these materials, various long-term durability tests and mechanical tests, such as compressive strength, flexural and tensile strengths, have been conducted. Additionally, tests for drying shrinkage, water absorption, efflorescence, sulfate resistance, and freeze-thaw resistance have been carried out. This section offers a thorough overview of the tests and the relationships between material performance that have been explored in the literature for the development of CDW-based mortars and concretes.

In a recent investigation, the correlation between compressive strength, water absorption, drying shrinkage, and porosity of geopolymer mortars incorporating CDW-based materials with 100% fine recycled aggregate, along with varying ratios of alkali activators and slag substitutions, was examined (see Fig. 1.5) [62]. The study revealed that geopolymer mortars formulated entirely with CDW-based materials achieved a compressive strength of approximately 30 MPa, whereas mixtures with 20% slag substitution attained a compressive strength of around 50 MPa. The results indicated an inverse relationship between compressive strength and water absorption, drying shrinkage, and porosity. Furthermore, a

linear correlation between drying shrinkage and porosity was observed, with a notable increase in drying shrinkage noted when sodium silicate was utilized. Additionally, slag substitution was found to decrease water absorption, porosity, and drying shrinkage, while significantly enhancing compressive strength. In contrast to OPC-based systems, geopolymers exhibit a notable presence of free water within their structures since the mixing water does not directly contribute to gel formation [75]. Consequently, these materials tend to experience significant drying shrinkage over extended periods. This phenomenon is also observed in CDW-based geopolymer systems, where heightened porosity facilitates the continuous leaching of both water and unreacted alkalis from the matrix [76]. This leaching process, known as "efflorescence," occurs when alkalis migrate out of the system and react with CO_2 in the atmosphere, leading to the formation of white crystalline structures like calcite and natrite [76]. While efflorescence primarily poses a visual concern in CDW-based geopolymers, it serves as an indication of internal matrix flaws and an imbalance in the alkali activator. This issue can be effectively mitigated through the use of certain SCMs such as slag. Slag not only enhances pore structure refinement through its self-cementing properties during early stages but also effectively binds alkalis at a high capacity [77].

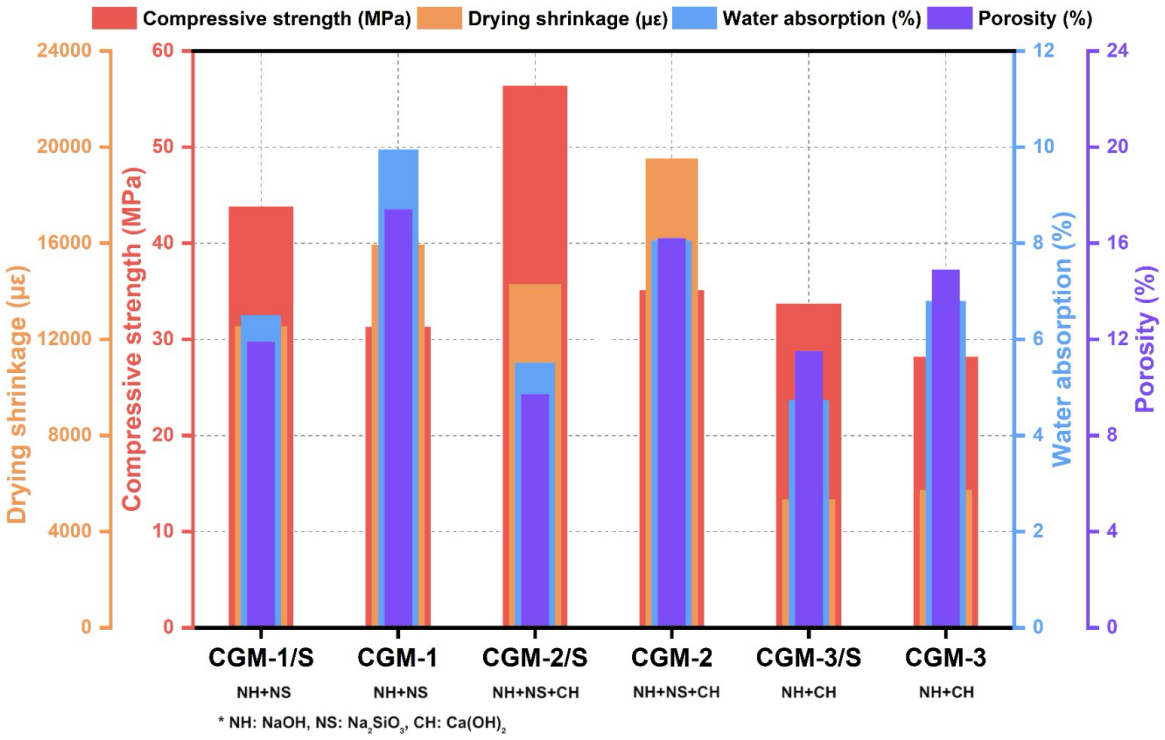

Fig. 1.5. Mechanical and durability properties of CDW-based geopolymer mortars (CGM-1/2/3: 100% CDW based; CGM-1S/2S/3S: 20% slag substituted. Alkaline activator combinations of the mixtures are presented below the mixture names on the horizontal axis) [62]

In research conducted by Yildirim et al. [78], nine variations of geopolymer concrete mixes were prepared, altering alkali activators and incorporating fly ash and slag. Following a 28-day period of curing at room temperature, the highest compressive strength achieved was 40.1 MPa. Notably, the combined use of sodium silicate, calcium hydroxide, and sodium hydroxide, along with the addition of slag, significantly improves mechanical performance. However, increasing the ratio of recycled aggregate/precursor from 1 to 2 resulted in approximately a 29% decline in compressive strength. This drop is attributed to the higher porosity of recycled concrete aggregate compared to regular aggregates, primarily due to the presence of old adhered mortar. This elevated porosity leads to increased water absorption and hinders workability by absorbing some of the mixing water. Additionally, it promotes the formation of weak zones within the matrix due to the coexistence of both old and new interfacial transition zones [79,80]. In another investigation, during the sulfate resistance examination of geopolymer concretes composed entirely of CDW, samples submerged in sulfate solutions displayed an approximate 6.29% decline in compressive strength compared to control samples after 28 days. However, in formulations containing CDW-based materials with 15% slag and 5% Class-F fly ash substitutions, this reduction escalated to approximately 9.13% [81]. Similarly, in the same analysis, subsequent to the rapid chloride permeability assessment, geopolymer concrete specimens crafted solely from CDW exhibited an average chloride ion penetrability of 2670 Coulomb after 28 days of curing. Conversely, in formulations featuring CDW-based components replaced with 15% slag and 5% Class-F fly ash, this value decreased to 2250 Coulomb. While geopolymer concretes derived from CDW showcase promising durability traits, particularly when incorporating specific supplementary cementitious materials (SCMs), further exploration is imperative to ascertain their potential as full replacements for OPC concretes in structural applications.

Recent studies have focused on examining the structural behavior of CDW-based concretes [82-84]. In one of these investigations [82], reinforced beams constructed with CDW-based materials were studied to evaluate their structural performance. The findings revealed that the load and displacement responses of geopolymer concrete beams closely resembled those of OPC concrete beams. However, the incorporation of recycled aggregates led to a decrease of approximately 30% in normalized energy dissipation capacities. Additionally, CDW-based geopolymer concretes exhibited highly ductile behavior in flexural-dominant conditions, with both types of specimens—utilizing normal and recycled concrete aggregates—displaying similar failure patterns. In another study examining the shear

behavior of beams constructed with CDW-based geopolymer concretes [83], it was noted that irrespective of the material composition, all specimens with aspect ratios (a/d) of 0.50 and 1.00 failed in shear, evident from brittle load-deflection and moment-curvature responses. Furthermore, the inclusion of recycled aggregates had minimal impact on the failure mechanism for aspect ratios less than 1.65, corresponding to shear-dominated regions (Fig. 1.6). This was attributed to the observation that the shear-resisting mechanism in reinforced concrete specimens was not significantly reliant on the tensile strength of concrete.

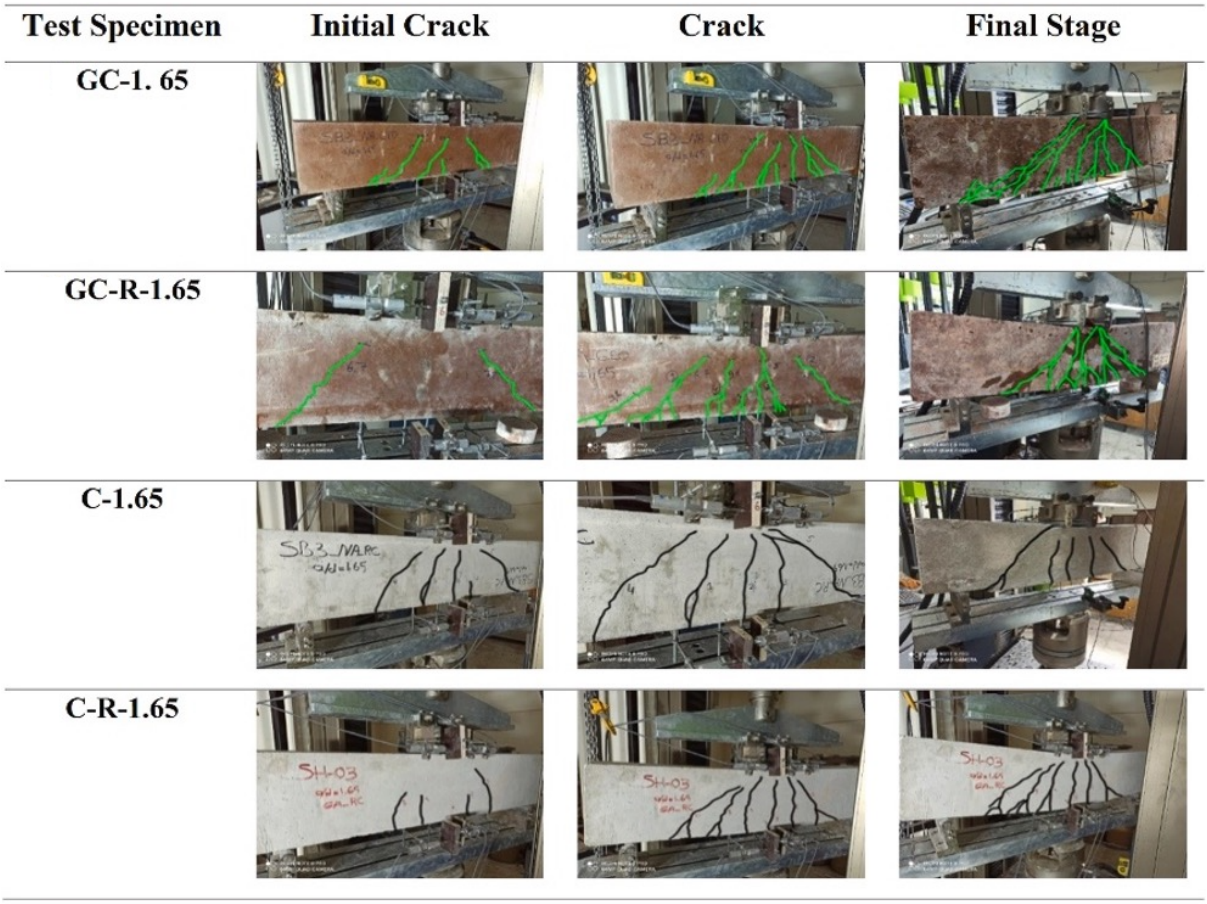

Fig. 1.6. Pattern of crack propagation of CDW-based geopolymer and OPC concrete beams, GC: Geopolymer concrete; GC-R: Geopolymer concrete with recycled concrete aggregates; C: Conventional concrete; C-R: Conventional concrete with recycled concrete aggregates [83]

In another study conducted by Kocaer and Aldemir [84], a novel stress-strain model was devised to accurately assess the flexural capacity of geopolymer structural elements derived from CDW. The main objective of the research was to characterize the distinct mechanical

properties of geopolymer concretes and develop a mathematical framework to broaden the applicability of geopolymer structural elements, which are still undergoing evaluation based on traditional concrete structural element standards. The study began by formulating a unique stress-strain model capable of capturing the compressive behavior of geopolymer concrete, drawing on recent experimental insights into the flexural behavior of geopolymer concrete beam specimens. The subsequent analysis yielded highly promising results, with an absolute mean percentage error of 5.13% across different failure modes. Moreover, the ratios of predicted and experimental ultimate moment capacity demonstrated the superior predictive capability of the developed model compared to the ACI318 Code [85], typically employed for conventional concrete-based systems (Fig. 1.7). This outcome underscores the effectiveness and reliability of the proposed approach, affirming its potential as a robust tool for accurately predicting the flexural capacity of geopolymer structural elements.

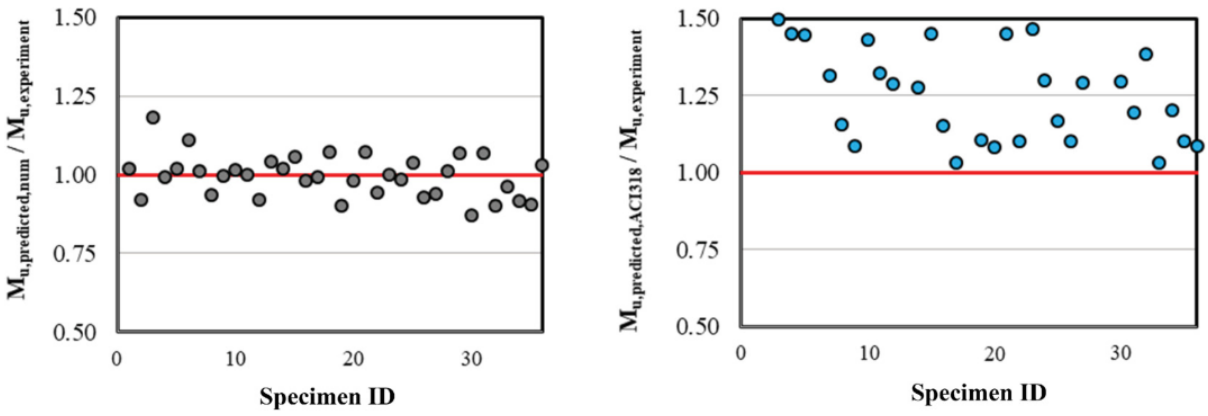

Fig. 1.7. Comparative analysis of estimation performances for the test soft database (Left: Developed model, Right: ACI318 Code) [85]

In today's context, there's a growing imperative to enhance the energy efficiency of buildings within the framework of sustainable practices. This has underscored the significance of developing building materials with enhanced thermal insulation capabilities [86]. Incorporating geopolymer technology into the production of such materials presents a comprehensive solution that addresses both waste recycling and the reduction of building energy consumption. However, it is important to acknowledge that research in this specific domain is still relatively limited. The sole example found in existing literature comes from a study conducted by Kvočka et al. [87], which explored the thermal conductivity characteristics of high-density geopolymer mortars incorporating 50% CDW aggregates

sourced from fired clay, mortar, and concrete rubble. Additionally, the environmental impacts of facade cladding panels produced with these formulations were examined. As an alternative, the study also assessed the thermal performance of a geopolymer containing 40% CDW-based wood particles. The binder phase in these mixtures comprised a blend of metakaolin, ground granulated blast furnace slag, and Class-F fly ash, while the alkali activator phase consisted of potassium silicate for the high-density geopolymer and sodium silicate for the geopolymer with wood waste particles. Results from the investigation indicated that the high-density geopolymer formulation achieved a 28-day thermal resistance of 2.037 (m^2K/W), with an average compressive strength of 37 MPa and a tensile strength of 3 MPa. Furthermore, the apparent density was measured at 1.89 g/cm^3, with an open porosity of approximately 30%. In contrast, the mixture containing waste wood particles exhibited an apparent density of around 1.0 g/cm^3 in dry conditions and an average of 1.15 g/cm^3 in environmental conditions (indoors). Additionally, the flexural strength and elastic modulus measured under three-point bending were approximately 5.6 and 2.02×103 MPa, respectively. Additionally, a "cradle-to-gate" life cycle assessment comparison revealed that prefabricated geopolymeric facade cladding panels represent an environmentally sustainable construction product. In an alternative heat production scenario, the environmental impact of panels crafted from geopolymer mortars was observed to be up to 100% lower across individual impact categories when contrasted with panels composed of natural materials, notably marble, glass, and aluminum (Fig. 1.8). These findings definitively underscore the innate environmental friendliness of geopolymer-based materials, showcasing their superiority over technically competitive alternatives, particularly in the realm of facade panels. Moreover, the design characteristics of these panels, facilitating effortless disassembly and recyclability, hold considerable promise for the development of innovative products integrating a significant proportion of recycled geopolymers, thereby further mitigating environmental burdens. Nonetheless, further research and exploration are imperative to advance the production of CDW-based geopolymer materials that encapsulate these advantageous attributes.

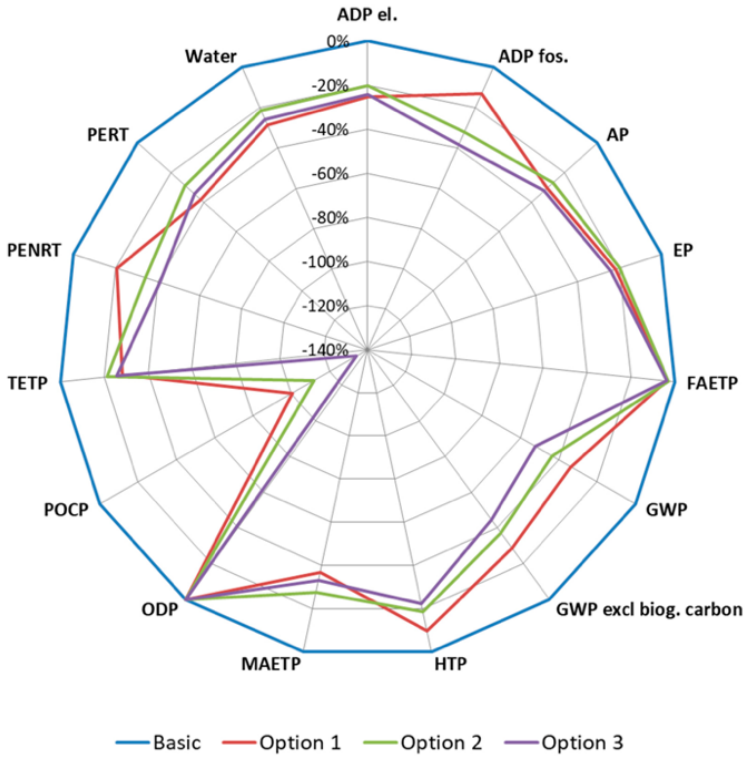

Fig. 1.8. Reduced environmental impact for different heat generation scenarios compared to the basic panel production process [87]

1.5. Multifunctionality of CDW-based Geopolymers

1.5.1. 3D Concrete Printing

Three-dimensional (3D) printing is a cutting-edge manufacturing technology that utilizes computer-controlled systems to fabricate solid objects layer by layer, guided by digital models [88]. In comparison to traditional methods, 3D printing offers enhanced precision and convenience, streamlines production processes, and reduces labor requirements [89]. Additionally, 3D printing holds promise for digitalizing construction practices, a trend gaining traction due to its capacity to address health and security challenges. It is anticipated that 3D printing techniques in construction could substantially cut down on waste and construction time while creating opportunities for technologically advanced employment and mitigating labor shortages in the sector.

The most prevalent form of 3D printing technology in construction is the use of 3D cementitious materials, often involving mortars. Three-dimensional concrete printing

(3DCP) facilitates the creation of cement-based building components or specific architectural features designed digitally and extruded from a 3D printer's nozzle to form tangible objects. By employing 3DCP, the necessity for formwork and temporary structures, which contribute significantly to waste generation, materials consumption, time, and labor costs, can be eliminated [90]. Moreover, 3DCP offers increased architectural flexibility, presenting vast potential to transform the construction industry.

The integration of this innovative technology into the construction sector has garnered significant interest recently, with numerous studies focused on developing 3D printable geopolymer formulations [91-95]. However, research investigating the compatibility of CDW-based geopolymer formulations with the 3D concrete printing (3DCP) technique has been relatively scarce [63,64,96-98]. In a study by Sahin et al. [96], the rheological properties and extrudability performance of CDW-based geopolymers, derived from a combination of CDW-based brick and glass, were examined when activated with alkali activators such as sodium hydroxide (NaOH), sodium silicate (Na_2SiO_3), and calcium hydroxide ($Ca(OH)_2$). NaOH was used individually and in combination with Na_2SiO_3 in ratios of 0.5 and 1, while $Ca(OH)_2$ was added at concentrations ranging from 2% to 10%. The experimental findings revealed that the sole use of NaOH as the alkaline activator had varying effects on the rheological properties of CDW-based geopolymers, depending on the molarity. Flowability increased while buildability and vane shear stress decreased with increasing NaOH molarity from 6.25M to 11.25M. However, flowability decreased after reaching 11.25M due to the formation of sticky gel. The addition of $Ca(OH)_2$ increased viscosity, buildability, and vane shear stress, while Na_2SiO_3 reduced viscosity and enhanced flowability, albeit at the expense of shortened setting/open-time. Geopolymers activated solely with NaOH did not exhibit adequate compressive strength development, whereas the addition of $Ca(OH)_2$ and Na_2SiO_3, especially in ternary combinations, led to enhanced compressive strength. Mixtures containing 6.25M NaOH and 6-10% $Ca(OH)_2$ were identified as suitable for 3D printing applications. Vane shear tests were less sensitive in detecting the effect of $Ca(OH)_2$ compared to ram extruder tests (Fig. 1.9).

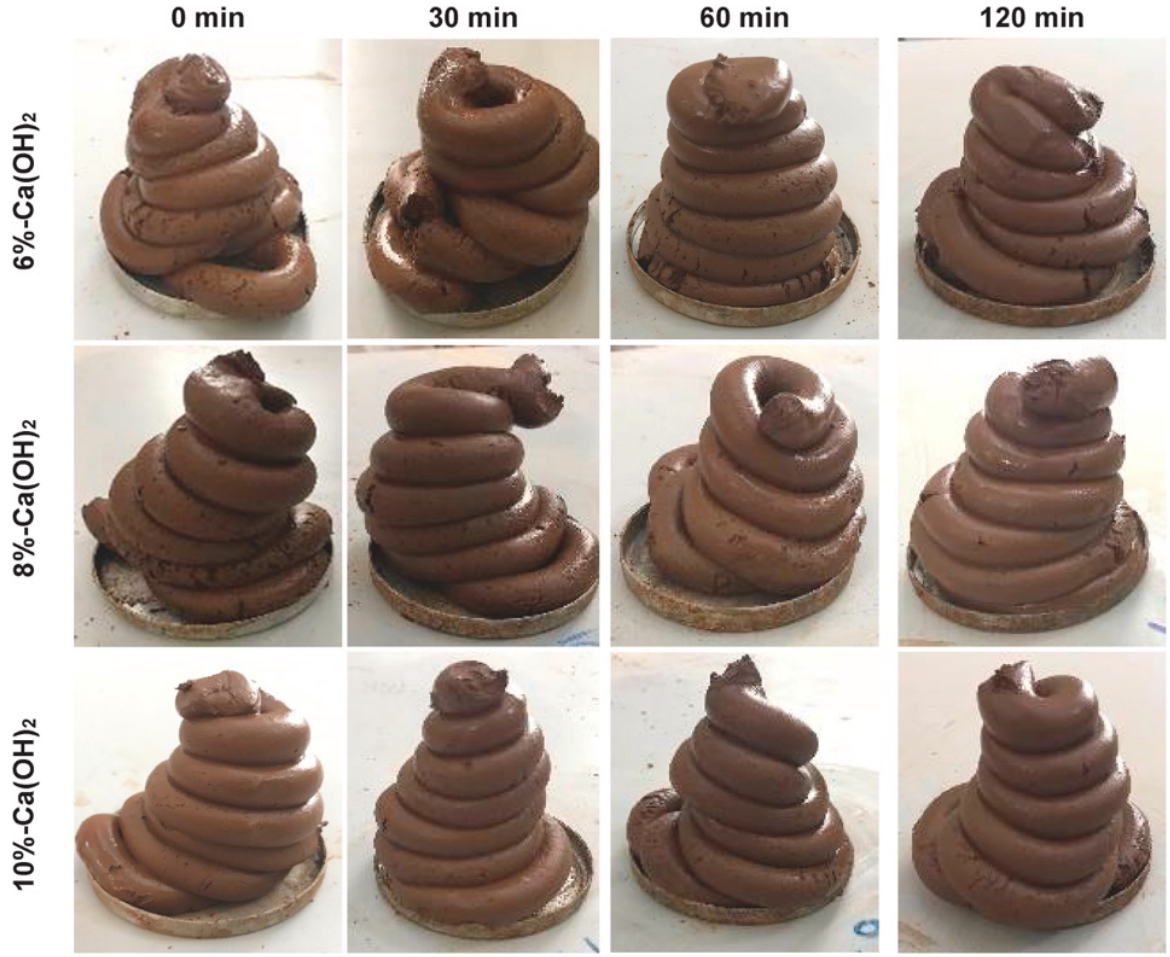

Fig. 1.9. Ram extruded samples of different CDW-based geopolymer mixtures [96]

In the research conducted by [97], the rheological characteristics of geopolymer mortar mixtures entirely derived from CDW were examined using empirical tests like flow table analysis, buildability assessment, and vane shear testing. The aim was to assess the suitability of these mixtures for 3D-Additive Manufacturing (3D-AM) utilizing a laboratory-scale 3D printer. The study revealed that the addition of NaOH significantly influenced the rheological properties, displaying a distinct trend inversion at a specific molarity level. Furthermore, the incorporation of $Ca(OH)_2$ led to increased viscosity, reduced flowability index, and enhanced buildability and vane shear stress. On the other hand, the introduction of Na_2SiO_3 resulted in a decrease in initial yield stress, improved flowability, and accelerated hardening. Interestingly, the study found that the inclusion of recycled concrete aggregates did not affect the rheological properties or compressive strength of the mixtures, indicating their suitability for 3D-AM applications. Performance evaluation was conducted based on various criteria including printability, flowability, viscosity, buildability, extrudability, and open time, with

the mortar mixture exhibiting low viscosity demonstrating precise dimensional conformity in the printed end product (Fig. 1.10).

Fig. 1.10. Visuals of multi-layer specimens of 3D printed geopolymer mixtures. Mixture A is characterized by a low viscosity, whereas Mixture B exhibits a high viscosity profile [97]

Ilcan et al. [64] conducted a study on the rheological properties of geopolymer mortar mixtures suitable for 3D printing, building on previous research. They utilized various testing methods such as flow curve analysis, constant shear rate testing, varied shear rate testing, and three interval thixotropy testing to assess how different types and concentrations of alkali activators affected the mixtures' rheological properties. The research found that increasing NaOH initially decreased static and dynamic flow stresses and plastic viscosity, but beyond a certain point, these parameters began to rise. Conversely, higher $Ca(OH)_2$ content led to a continuous increase in these rheological parameters. In the constant shear rate test, static flow stress was higher than dynamic flow stress, with both decreasing as shear rate increased. The molarity of NaOH affected these stress values, with a reversal observed at a specific threshold, while the inclusion of $Ca(OH)_2$ led to a consistent increase. Thixotropy performance was impacted by NaOH molarity in mixtures activated with NaOH. Additionally, three interval thixotropy testing revealed a positive impact of increasing $Ca(OH)_2$ on thixotropy up to a certain level. The ram extrusion test, assessing extrusion capability and filament quality, aligned with other rheological tests in terms of stress values (Fig. 1.11). Yield stress below 0.55 MPa resulted in continuous flow without defects, while values above 0.70 MPa led to discontinuities and defects. The study also noted various failures during printing, even with prolonged resting times.

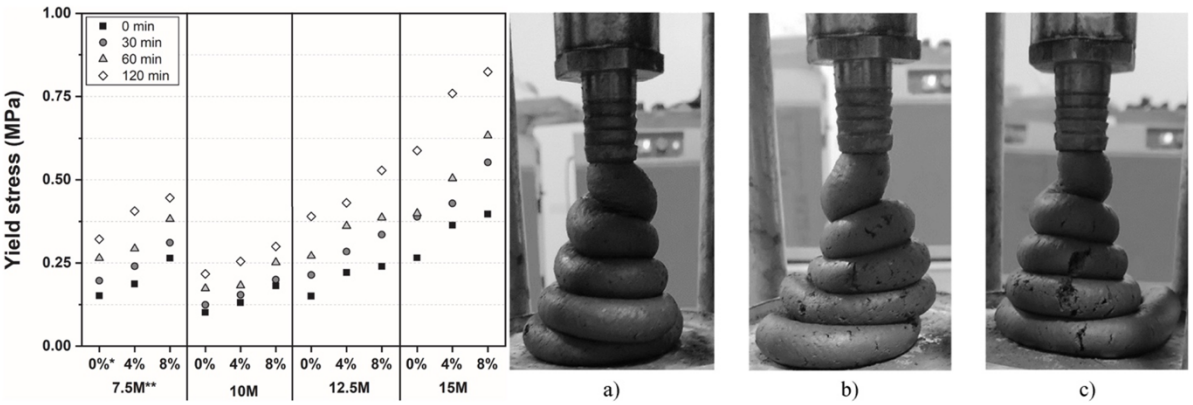

Time-dependent yield stress values of the geopolymer mortar mixtures obtained from ram extrusion tests [*$Ca(OH)_2$ utilization rate, **NaOH molarity]

Representative images of extrusion a) without failure, b) with some flaws and defects, and c) with large splits, flaws and defects.

Fig. 1.11. Quantitative and illustrative results of ram extruder experiments [64]

Demiral et al. [63] examined the anisotropy, or direction-dependency, in the mechanical performance and bonding properties of geopolymer mortars entirely composed of CDW and fabricated through 3D-AM. Their findings indicated a significant influence of alkaline activator content on mechanical properties. Increasing NaOH molarity improved compressive and flexural strengths but decreased splitting and direct tensile strengths of 3D-printed specimens. While adding 4% $Ca(OH)_2$ had a positive effect on mechanical properties, excessive $Ca(OH)_2$ hindered viscosity, offsetting its benefits. Direction-dependent tests revealed anisotropic behavior, though perpendicular-loaded 3D-printed specimens exhibited comparable or slightly superior performance to mold-casted specimens, suggesting minimal influence of the bond zone on perpendicular loading. Anisotropic properties were evident in compressive and flexural strength tests, with variations of up to 20% and 30%, respectively. These variations were linked to the degree of geopolymerization, directly impacting the quality of the interfacial transition zone and porosity in the layer bond zone. The study proposes that enhancing bond adhesion between layers could mitigate anisotropic behavior in printed structures, achievable through optimization of rheological properties and matrix performance. Pasupathy et al. [98], in their study on the impact of brick waste content on 3D printed slag-fly ash based geopolymer mortars, found that incorporating brick waste improved fresh properties such as yield strength and viscosity. However, higher concentrations of brick waste (over 10%) led to diminished hardened properties, particularly in compressive strength and interlayer strength of 3D printed concrete. Additionally, they observed anisotropic behavior in the compressive strength of 3D printed samples, with the highest strength in the printing direction and the lowest strength in the lateral direction.

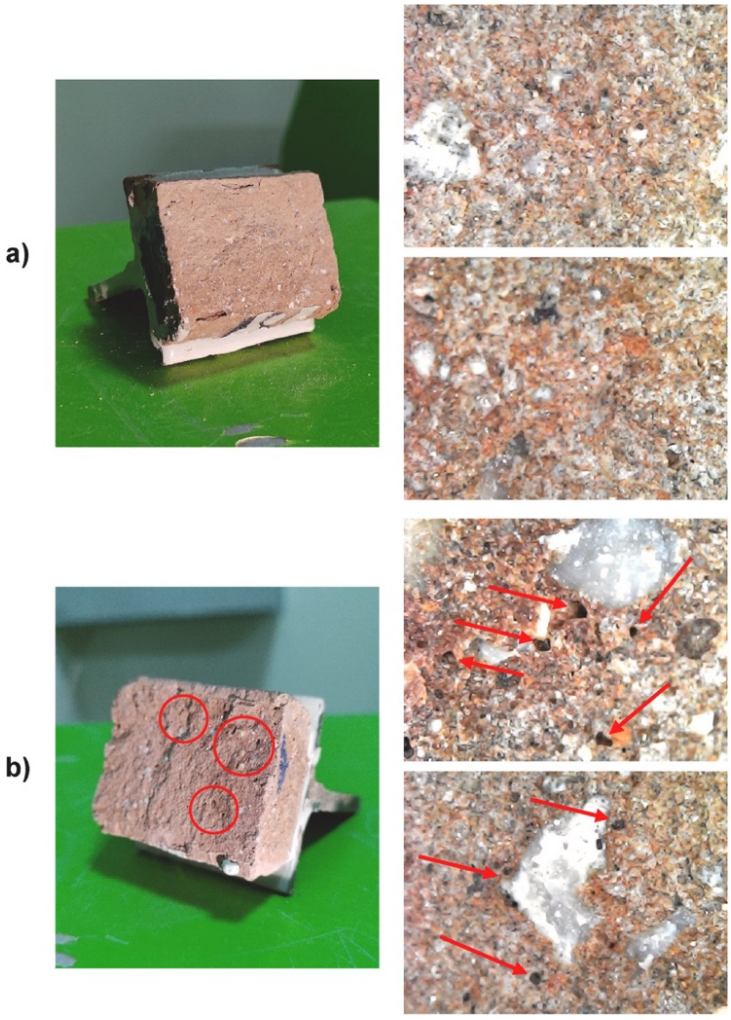

Fig. 1.12. Representative general and close-up views of a) non-porous and b) porous bond zone [63]

Despite advancements in developing 3D printable geopolymer mixtures, understanding the compatibility of CDW-based geopolymer mixtures with 3D-AM techniques remains limited. Further research is needed to explore the rheological behavior of CDW-based geopolymer mixtures and their suitability for 3D-AM. Such investigations can advance the development of sustainable construction materials and innovative construction methods, reducing the construction industry's carbon footprint. Successfully integrating CDW-based geopolymer mixtures into 3D-AM has the potential to yield significant environmental and economic benefits for the construction sector. This approach offers a promising solution to waste disposal and natural resource depletion challenges, emphasizing the importance of ongoing research to ascertain the compatibility of CDW-based geopolymer mixtures with 3D-AM for their sustainable adoption in construction.

1.5.2. Engineered Geopolymer Composites

Concrete structures, often facing challenges due to their vulnerability to cracking under tension, have led to the development of innovative solutions aimed at enhancing resilience, durability, and sustainability [99]. Among these solutions is the emergence of Engineered Cementitious Composites (ECC), also known as Strain-Hardening Cementitious Composites (SHCC). Unlike conventional concrete, ECC exhibits exceptional ductility and tensile elongation capacity exceeding 2% [100]. In contrast to Ultra High Performance Fiber Reinforced Concrete (UHPFRC), which prioritizes particle packing density, ECC adopts a deliberate engineering approach focused on optimizing the interaction between fibers, matrices, and fiber/matrix interfaces to enable multiple cracking mechanisms under tensile loading [100].

The exceptional properties of ECC have enabled its application in a variety of large-scale structures, ranging from impressive bridges to skyscrapers, effectively extending their service life and enhancing functionality [101]. ECC consists of a unique combination of constituents, including Ordinary Portland Cement (OPC), Supplementary Cementitious Materials (SCMs) like fly ash, silica sand, and short fibers [102]. However, despite its evident advantages, ECC faces a notable drawback: its high cement content, which is exacerbated by the absence of coarse aggregates. This increased cement content carries cost implications and contributes to a significant carbon footprint, prompting a concerted effort to explore sustainable alternatives.

In light of the demand outlined above, the emergence of Engineered Geopolymer Composites (EGC) presents a promising opportunity with transformative implications. EGC combines the advantageous properties of ECC to mitigate the inherent brittleness typically associated with geopolymers, offering the potential to reduce the environmental impact linked to conventional building materials [103]. Furthermore, EGC not only matches ECC in terms of sustainability but also demonstrates comparable tensile and flexural properties under static loading conditions, while surpassing ECC in mechanical performance under dynamic loading scenarios [104,105]. These alternative materials are formulated based on the principles of micromechanical design theory, enabling a wide range of customization options, including diverse matrices, fiber reinforcements, and precisely tailored mixing and curing methods. Like other multifunctional advanced construction materials, CDWs show

significant promise for use in EGC matrix development. However, the lack of dedicated studies addressing this specific area highlights a notable research gap that warrants further exploration and investigation. The study conducted by Ulugöl et al. [106] represents the only investigation thus far focusing on unraveling the autogenous self-healing potential of EGCs with entirely CDW-based matrices. These matrices utilized masonry units, concrete, and glass from CDWs in mixed form as precursors, with recycled concrete serving as fine aggregates. To assess the impact of incorporating ground granulated blast furnace slag into CDW-based mixtures, additional formulations were devised with slag substitution while maintaining a consistent Si/Al ratio. Evaluation of self-healing was conducted by observing changes in transport properties (such as electrical impedance and water absorption rate) alongside microstructural characteristics. The findings indicated that the self-healing ability of CDW-based EGCs was linked to the chemical composition of the materials used, particularly the presence of calcium and sodium from raw materials and alkaline activators. Introducing slag to CDW-based EGCs expedited the initial reactions of geopolymeric mixtures, resulting in a slower yet more reliable self-healing process. Detected self-healing products like $CaCO_3$ and Na_2CO_3 in healed microcracks suggested ongoing carbonation and geopolymerization. Furthermore, the self-healing behavior of EGCs exhibited resemblances to OPC-based composites. Another notable outcome was the variability in self-healing characterization results, manifesting inconsistency in water absorption and electrical impedance tests, chiefly due to numerous factors affecting these tests, notably electrical impedance. Conversely, microscopic examinations and microstructural analyses provided clearer indications of self-healing. In light of the collective findings from these investigations, it is strongly recommended to complement existing analyses with additional test methodologies for a comprehensive evaluation of self-healing in EGCs. Employing a wide range of test methods can yield a more holistic understanding of the effectiveness, mechanisms, and complexities underlying the self-healing capabilities showcased by these pioneering construction materials.

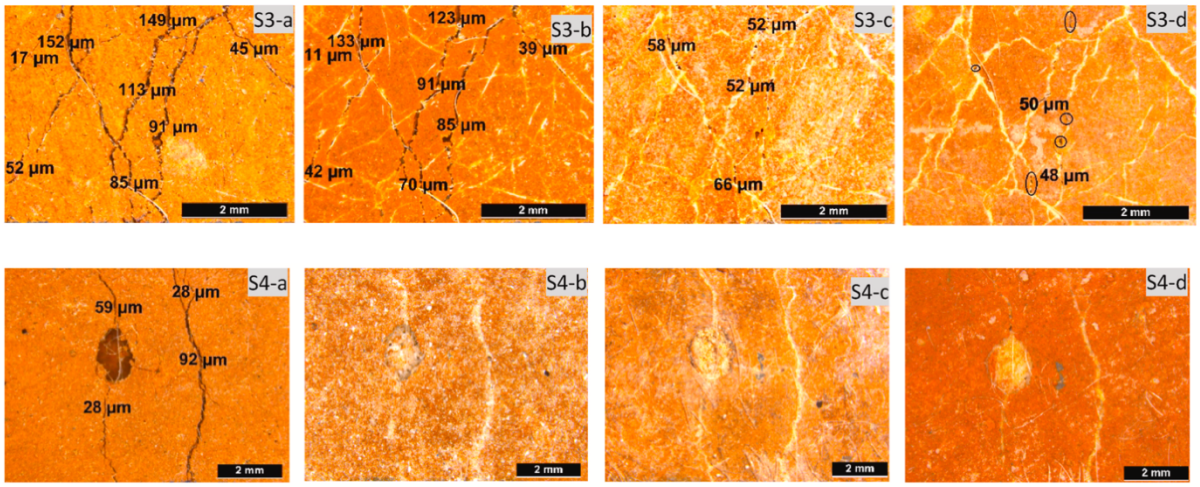

Fig. 1.13. Optical microscopy images of different EGC specimens on the (a) 7th, (b) 28th, (c) 56th, and (d) 90th days showing the effect of self-healing. S3: CDW+SCM-based mixture, S4: Fully CDW-based mixture [106]

1.6. Conclusions

This chapter provides a thorough analysis of the latest research in alkali activation technology, focusing on its application to CDW-based materials. It covers a wide range of materials including binders, mortars, concretes, 3D printable composites, and engineered geopolymer composites. The main goal is to facilitate the integration of CDW into the circular economy, particularly within the construction sector.

- It can be concluded that CDW presents a promising option for the development of geopolymers as a substitute for OPC pastes. Through thermal curing, impressive compressive strengths of approximately 80 MPa can be achieved, while ambient curing still yields noteworthy strengths of around 50 MPa. The addition of supplementary cementitious materials alongside CDWs further enhances strength properties. However, it is essential to acknowledge that CDWs vary in chemical and physical compositions globally. Therefore, thorough characterization and the development of strategies for optimal performance are crucial. Extensive research is needed to explore the effects of CDW utilization in both singular and mixed forms, the choice and concentration of alkali activators, and ideal curing conditions. With dedicated investigation in these areas, CDWs could become a standardized geopolymer binder worldwide.

- The utilization of CDW-based geopolymer binders in mortar and concrete mixtures with the incorporation of recycled aggregates from concrete waste is still at an early stage in the literature. To fully replace conventional OPC-based concrete, extensive long-term durability analyses should be performed, focusing on crucial aspects such as drying shrinkage, water absorption, permeability, freeze-thaw resistance, and resistance to chemical agents in CDW-based mortars and concretes. Furthermore, it is imperative to perform comprehensive characterizations of structural elements like columns, beams, and walls manufactured using CDW-based materials, encompassing evaluations of shear, flexural behavior, creep, crack patterns, and seismic performance. These efforts should be complemented by diverse demonstration activities that attract attention from the construction industry, stakeholders, academia, and governments, thereby facilitating the integration of CDW into the construction sector. Additionally, further research and development endeavors are warranted to overcome remaining challenges, optimize the performance of CDW-based materials, and foster their widespread adoption, thereby contributing to sustainable construction practices.

- Further exploration is necessary to evaluate how well CDW-based geopolymer mixtures align with 3D-AM techniques and to understand their rheological behavior, mechanical properties, and bonding capabilities for application in construction. Successfully incorporating CDW-based geopolymer mixtures into 3D-AM could yield significant environmental and economic advantages by addressing waste disposal and resource depletion issues while promoting circular economy principles in construction. Continuous research into the compatibility of CDW-based geopolymer mixtures with 3D-AM is vital for their sustainable integration into the construction industry, contributing to the advancement of a smarter, more sustainable, and inclusive society.

- Despite the growing interest in CDW-based EGCs, there is a lack of exploration in the current literature, suggesting numerous unexplored opportunities for further investigation. A comprehensive examination of the mechanical, durability, and self-healing properties of CDW-based EGCs has the potential to achieve performance levels similar to those of conventional ECCs and EGCs, albeit with reduced environmental footprints. This research endeavor has the potential to facilitate the widespread adoption of CDW-based EGCs, highlighting their capacity to deliver reduced environmental

impacts while maintaining performance standards comparable to ECCs and traditional EGCs utilizing widely-used SCMs.

- The utilization of geopolymers derived from CDW presents a promising opportunity for enhancing the energy efficiency of buildings. This innovative approach, characterized by its low embodied energy, recycling capabilities, and reduced resource consumption, has gained recognition for sustainable construction methods. However, despite its considerable promise, the full realization of this technology remains a challenge due to a notable research gap and insufficient exploration in this area.

CHAPTER II: OPTIMIZING MECHANICAL PERFORMANCE OF GEOPOLYMERS PRODUCED FROM CONSTRUCTION AND DEMOLITION WASTE: A COMPARATIVE STUDY OF MATERIALS FROM DIFFERENT ORIGINS

2.1. Introduction

Concrete is an indispensable material in the construction industry due to the great benefits it provides and is therefore the most consumed material in the world after water [170]; on the other hand, it has harmful environmental impacts that cannot be neglected. For every 1.0 ton of clinker production, 1.5 tons of natural resources are consumed as raw materials, contributing to the release of 0.8–1.0 tons of CO_2 into the atmosphere [108]. This high amount of CO_2 emission comes from the combustion of fuels to provide the needed exorbitant energy (about 4.5 GJ) [109,110]. Such environmental devastation/energy consumption seems to increase exponentially, as concrete production is expected to reach 6 billion tons by the end of 2050 [111]. Therefore, it is mandatory to hold redundant concrete production within certain limits and/or develop more environment-friendly building materials alternatively.

At this point, geopolymers, have a great potential as a candidate to replace PC due to superior performances in strength- and durability-related parameters [112,113]. In addition to these performance-based advantages, geopolymer is very economical as obtained from waste-originated precursors. From a sustainability perspective, recycling/reusing wastes with geopolymerization reduces concerns related to finding available disposal areas and prevents these hazardous materials from penetrating the clean/rich underground resources. To date, numerous studies demonstrated that geopolymer binders, mortars, and composites can achieve results comparable to PC-based counterparts [114-117]. However, the main focus in published literature was developing the geopolymeric binder phase by utilizing main-stream wastes such as fly ash, ground granulated blast furnace slag, and metakaolin either individually or together. Since these wastes were considered problematic in the past, the idea of recycling/reusing them through geopolymerization was a reasonable solution. Nowadays, these wastes are no longer considered troublesome in the construction industry, besides, they are highly demanded and even sold at almost comparable prices to PC. Hence, the new trend

is recycling less-demanded and more problematic wastes in present conditions through geopolymerization technology.

Construction and demolition waste (CDW) is one of the most challenging wastes that are difficult to cope with due to its extensive generation worldwide. These wastes are mainly emerging by the consequences of the infrastructural operations, urban transformation projects, or other processes that contain demolition/maintenance/repair and pose a challenge for advanced and developing countries. For instance, more than one-third of the entire building stock is expected to be demolished due to planned infrastructural operations in Türkiye [106]. At this point, geopolymerization is an up to date/practical/effective solution for CDW, which has rich alumina and silica content. In parallel with this, previous studies showed that CDW-based geopolymers could achieve satisfactory results, which were suitable for many standard construction applications [26,82-84,118,119]. However, some shortcomings restrict the widespread use of CDW in geopolymer production. One of such shortcomings limiting the use of CDW in geopolymer production is the vast difference in properties of even the same type of waste. Possible diversities among CDW-based materials can result in the reluctance of value chain stakeholders, particularly manufacturers and building companies to use these materials in the development of new generation environmental-friendly building materials. For instance, despite the basic brick manufacturing process being fairly uniform, individual manufacturing plants modify their production to fit particular raw materials and operations [120]. Moreover, since brick manufacturing is a multi-phase process, the interferences in each step can play a significant role in the final product, in addition to the properties of locally available clay. Similar concerns also exist in concrete production, which constitutes a substantial part of CDW.

Likewise, conflicting results were also reported by different literature studies. For instance, [121] examined the alkali activation potentials of concrete, tile, and brick separately at varying NaOH molarities and different curing temperatures. As a result of the 7-day curing, tile-based geopolymers exhibited the best compressive strength performance (57.8 MPa) under optimum synthesis conditions (10M NaOH, curing temperature 80 °C), while concrete achieved only 13 MPa with 90 °C curing temperature and 14 M NaOH concentration. Additionally, the maximum compressive strength acquired by brick-based geopolymers was 49.5 MPa for 8M NaOH concentration and 90 °C. Zaharaki et al. [122] investigated the usability of slag, brick, tile, concrete, and red mud in the alkali activation process. Among control mixtures, which were activated with 10M NaOH solution and cured at 80 °C for 24h,

specimens produced with slag reached the highest compressive strength, while the concrete reached the lowest result. Besides, tile-based geopolymers exhibited better mechanical performance than brick-based ones. In another study, Ulugöl et al. [67] investigated the sole use of roof tile (RT), hollow brick (HB), red clay brick (RCB), and glass waste (G) by considering the optimum Na concentration (10, 12, and 15%) and curing temperature (50 to 125 °C). The results showed that HB-based geopolymer paste activated with 12% Na solution and cured at 115 °C for 24h reached the greatest compressive strength. At the same production and curing conditions, RT and RCB exhibited relatively lower performance than HB. On the other hand, G-based geopolymer pastes achieved the lowest compressive strength compared to brick/tile waste-based geopolymers. Mahmoodi et al. [123] developed binary systems of brick and concrete wastes in ambient environment. In this study, the highest compressive strength result was 34.6 MPa and achieved by geopolymer paste containing 60% brick and 40% concrete in the binder phase with Si/Al=8.4 and Na_2O/SiO_2=0.18 at 28-day. In general, geopolymer systems with more brick exhibited better performance compared to concrete. However, it was also reported that geopolymer with more concrete could achieve a higher compressive strength under certain conditions (Si/Al=9.3 and Na_2O/SiO_2=0.21).

The source-dependent variations mentioned above continue to be a limiting factor for the utilization and widespread adoption of CDW in geopolymer synthesis. Therefore, it is crucial to prioritize the type and origin of CDW in geopolymer production and capitalize on the additional diversity of CDW through a collective approach. In light of this context, this chapter of the thesis presents a fresh perspective. For the first time in literature, variations in the properties of identical CDW species intricately linked to their origins were collectively and comprehensively explored. These differences play a direct role in influencing the performance of geopolymer systems. In the current chapter of the thesis, the following issues were focused on: (i) investigating/characterizing the properties of CDW-based precursors obtained from different demolition zones; (ii) utilizing many discarded parts of CDW to provide complete valorization without further separation; (iii) assessing the mechanical performances of geopolymer paste mixtures containing different wastes in varying proportions. Based on these, the authors aimed to present a method addressing key considerations in the geopolymerization process when utilizing CDW. This approach explores the impact of waste variations on compressive strength, offering insights into the intricate relationship between CDW characteristics and geopolymer performance. Here, roof

tile (RT), hollow brick (HB), red clay brick (RCB), concrete (C), and glass (G) wastes were collected from five different demolition zones and used as precursors in geopolymer production. X-ray fluorescence (XRF) and X-ray diffraction (XRD) analyses were performed on the CDW-based precursors for the microstructural characterization. Moreover, the laser diffraction particle sizing method was used to determine the particle size distributions of precursors. At this point, it should be noted that the same crushing/grinding procedures were applied to all CDWs. Consequently, it was planned to characterize these CDWs through the above-listed tests within a holistic approach. A total of seven mixtures were designed for the geopolymer paste phases consisting of CDWs collected from different regions to achieve maximum performance. This design process included the following steps: (i) to examine the effect of C and G; (ii) to compare the individual effect of clayey CDWs (HB, RCB, and RT) and (iii) to examine the effect of the amount of clayey CDWs.

2.2. Materials and Methodology

2.2.1. Materials

CDW-based materials were sorted into five different classes including hollow brick (HB), red clay brick (RCB), roof tile (RT), concrete (C), and glass (G). These materials were collected from different urban transformation and demolition zones (DZ) in Türkiye. Fig. 2.1 represents the HB, RCB, RT, C, and G after pre-treatment. Pre-treatment stage was a non-complex, two-step, crushing-grinding process (each material was crushed with a jaw opening of 2 mm and ground for one hour in ball mill) to acquire sufficient fineness for geopolymer production. It should also be noted that crushing-grinding processes were applied with the same parameters for all materials; in other words, no special attention was given to bringing all materials to the same fineness level. The same grinding procedures resulted in precursors in different particle size distributions because of CDWs' different grindability performances, even if they were the same type of waste (obtained from different sources). In this way, it is possible to investigate the effect of fineness on the geopolymerization, and less energy and labor are required in large-scale applications when the crushing-grinding of materials is combined with the same process. Detailed analysis results of CDW-based materials were presented in the following sections.

Fig. 2.1. Powderized CDW-based materials (left to right: RT, RCB, HB, C, and G)

In the production of geopolymer paste, sodium hydroxide (NaOH) was used as the alkali activator. It was known that aluminosilicate materials such as CDWs first need to be dissolved in an alkaline environment to be used in geopolymer production [124]. NaOH, used in mixtures as alkali activator, was solid in white flake form with at least 98% purity, and the water for preparing NaOH solution was tap water.

2.2.2. Methodology

Within the scope of this chapter of the thesis, CDW-based materials were characterized in terms of their chemical composition, particle size distribution, crystalline nature, and compressive strength of the geopolymers produced with the combination of these materials. To determine their chemical composition, X-ray fluorescence (XRF) test was applied to the powdered CDW-based materials. The particle size distribution of the CDW-based materials prepared under the same crushing and grinding process was analyzed using the laser diffraction particle size analysis method. In order to determine the crystalline nature, X-ray diffraction (XRD) test was performed by applying a scan range of $5° \leq 2\theta \leq 55°$, 2θ step length of 0.033°, a scanning step time of 30.48 s, and a wavelength Kα1 of copper (λ=1.5406Å). Afterward, geopolymer paste mixtures were produced using NaOH as an alkali activator and CDW-based materials as precursors to determine the effect of CDW and source diversity on mechanical performance. In this context, three groups of mixture combinations were designated with the following process: i) to examine the effect of C and G, ii) to examine the effect of HB, RCB, and RT, iii) to examine the effect of the amount of clayey waste materials. Mixture designs of CDW-based materials are demonstrated, and the mixture design sequences for the DZ I are provided as an example with bold dashes in Fig. 2.2 to provide a clear explanation of algorithm. To provide a clearer explanation of the example presented for DZ I, in Phase I, the mass distribution of clayey CDW content is evenly distributed to achieve a total of 60% (20% each) while determining the effects of glass waste

and concrete waste. For this purpose, Mix 1 (containing 30% glass waste) and Mix 2 (containing 30% concrete waste) were produced. Since Mix 1, which contains a high amount of glass waste, exhibited higher compressive strength, the base mixture ratio for Phase II was determined based on this mixture. In this base mixture, the mass distributions of clayey CDW were modified for each brick waste in a ratio of 2:1:1, and Phase II was completed. The option with the highest strength (Mix 3 containing 30% HB) was selected to proceed to Phase III. In Phase III, which examines the influence of the increasing share of clayey waste combination with a mass share of 60% in Phases I and II on the mechanical properties, the glass waste/concrete waste ratio was fixed at 3, and the total clayey waste content was increased to 70% (Mix 6) and 80% (Mix 7), respectively, for the mixture with the best mass distribution determined in Phase II. As a result of all these stages, the mixture that exhibited the highest strength in Phase III was selected, and the same procedure was repeated for other DZs.

All mixtures were produced with a water-to-solid ratio of 0.30 and activated with a 15 M NaOH solution. Six cubic specimens with 50×50×50 mm dimensions were produced for each mixture and subjected to heat curing at 115 °C for 48h immediately after casting. These curing parameters were chosen based on the optimum results of the authors' previous studies [26,67]. By the end of curing time, specimens were subjected to compressive strength testing at a loading rate of 0.9 kN/s, and the compressive strength of the geopolymers was determined by averaging the result of six test samples. To examine the microstructure and determine the geopolymers' short-range structural order, Scanning Electron Microscopy/Energy-Dispersive X-ray (SEM/EDX) and Fourier Transform Infrared Spectrophotometer (FTIR) analyses were performed, respectively.

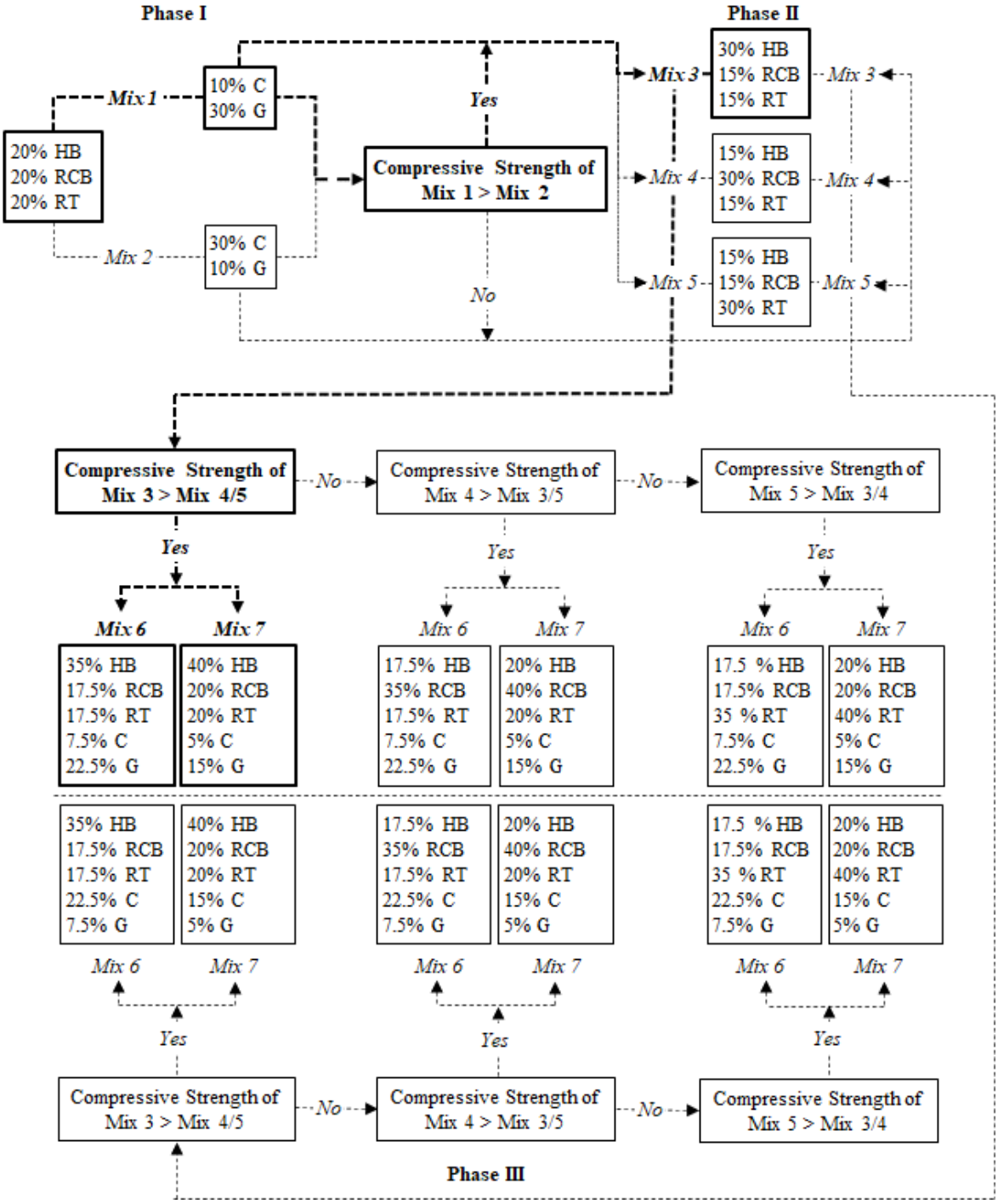

Fig. 2.2. Sequential algorithmic mix design

2.3. Experimental Results and Discussion

2.3.1. Chemical compositions of CDWs

Chemical compositions of CDW-based materials collected from five different demolition zones are presented in Table 2.1. It has been frequently reported in the literature that chemical composition, especially SiO_2 and Al_2O_3 content of the precursors, is one of the most determinative parameters on the mechanical and chemical properties of ultimate geopolymer products [125-127]. Even if other parameters are kept constant, changes in the chemical composition of precursor materials often significantly affect the properties of the final product. In particular, since materials utilized in geopolymer production have a wide range of SiO_2 and Al_2O_3 content, it is crucial to determine the chemical properties and analyze their relationship with the final product. On the other hand, although CDW-based materials are expected to have similar chemical content regardless of wherever they are obtained, they can inevitably be affected and differentiated by different factors including the raw materials, the production process, the burning-cooling method, and the environmental influences they are exposed to during their service life.

According to Table 2.1, it was observed that the diversity in the chemical composition of CDW-based materials collected from different demolition zones was at the non-negligible level. In this context, clayey wastes (i.e., HB, RCB, RT) had SiO_2 content in the 42.1-59.9% range and Al_2O_3 content in the 12.6-18.3% range. Chemical composition analysis results demonstrated that all CDW-based clayey materials are rich in alumina-silica content, making them suitable for geopolymer production or partial substitution of CDW blended Portland cement mixtures [128]. Furthermore, the chemical composition of the CDW-based clayey materials is comparable to that of the Class F fly ash, which is commonly employed in manufacturing geopolymers in previous research [129]. However, contrary to the spherical grain structure of fly ash, brick and tile wastes have an irregular angular shape with a rough surface, and it is expected that different crystalline structures, particle-size and -morphology will affect the properties of the final geopolymer product [130]. Besides the alumina-silicate content, it is well known that the Si/Al ratios of the materials also play an essential role in the geopolymerization kinetics. The rate and efficiency of the geopolymerization reactions are highly dependent on the amount of soluble Si and Al species in the medium and the Si/Al balance. While it was necessary to acquire the optimum Si/Al ratio for producing geopolymer products with high mechanical performance, lower Si/Al ratios yield the lower

strength geopolymer products due to the formation of Na-Al-Si structures in the grains phase rather than an amorphous phase [127]. In the following sections regarding the micro- and macro-mechanical examinations, a comprehensive analysis was provided on how the Si/Al ratios of precursors, formed through the combination of different CDW-based materials, affect the performance of the resulting geopolymer materials.

Table 2.1. Chemical composition of the materials

Region	Material	Chemical composition (%)								
		SiO_2	Al_2O_3	Fe_2O_3	CaO	MgO	K_2O	Na_2O	SO_3	LoI
DZ I	**HB**	48.9	13.7	11.0	7.44	4.82	2.07	0.37	1.47	3.02
	RCB	52.6	14.8	8.31	4.64	2.78	2.45	0.69	0.95	2.92
	RT	50.8	14.4	10.5	7.09	4.55	2.28	0.46	0.83	2.13
	C	56.9	8.76	4.01	11.8	1.50	1.53	1.16	0.85	9.76
DZ II	**HB**	52.5	14.9	8.59	4.06	2.65	2.74	0.44	0.52	1.99
	RCB	57.6	14.4	8.28	4.70	2.53	2.14	0.77	1.93	1.45
	RT	55.3	14.8	8.28	6.69	4.72	2.11	1.04	1.16	1.45
	C	56.0	8.88	4.23	11.8	1.51	1.51	1.03	0.72	8.84
DZ III	**HB**	57.7	14.7	7.90	3.97	2.24	2.43	-	0.42	3.15
	RCB	59.9	13.6	7.40	5.20	2.27	2.02	0.93	2.31	1.30
	RT	54.7	13.2	9.28	6.90	4.01	1.92	0.68	0.54	2.20
	C	54.7	9.76	4.22	11.5	1.52	1.53	2.02	0.80	8.94
DZ IV	**HB**	56.8	15.8	8.24	3.13	2.41	2.88	0.32	1.48	0.77
	RCB	59.2	18.3	7.72	2.78	2.35	2.77	0.42	1.41	0.73
	RT	53.4	16.3	9.49	5.27	3.64	2.78	0.39	1.61	1.67
	C	37.4	10.7	3.82	21.2	1.29	2.22	1.96	0.54	19.7
DZ V	**HB**	42.1	13.8	11.8	6.42	6.45	1.55	1.45	1.46	1.43
	RCB	45.8	13.5	11.9	7.81	5.55	1.88	0.98	1.88	3.90
	RT	46.2	12.6	12.1	9.88	5.41	1.16	1.13	0.40	2.59
	C	34.8	4.36	3.45	27.2	4.46	0.79	0.19	1.32	22.0
	G	65.4	0.98	0.54	8.97	3.73	0.14	12.0	0.65	1.60

DZ: Demolition zone, HB: Hollow brick, RCB: Red clay brick, RT: Roof tile, C: Concrete, G: Glass, LoI: Loss on ignition

The chemical compositions of C collected from DZ I, DZ II, and DZ III were quite similar to each other, with SiO_2, Al_2O_3, and CaO ranges between 54.7-56.9%, 8.76-9.76%, and 11.5%-11.8% respectively. On the other hand, C collected from DZ IV and DZ V was relatively different compared to other zones with SiO_2, Al_2O_3, and CaO contents of 34.8-37.4%, 4.36-10.7%, and 21.2%-27.2%, respectively. This situation is thought to be caused by the variation in the origin of aggregate that constitutes a large part of the concrete volume; smaller fractions blend with the cement phase of the concrete in the crushing stage. To this end, this might be related to the fact that C collected from DZ I, DZ II, and DZ III contain

silica-based aggregates, having major phases as quartz and albite [131,132], whereas C collected from DZ IV and DZ V might be produced with limestone aggregate with higher calcium content [133]. Besides the aggregate type, these differences observed in the chemical content of C can be attributed to the type of cement used, admixtures, and transported chemicals such as sulfate and chloride to which the concrete is exposed during its service life. Loss on ignition (LoI) values displayed a significant variation per DZ, with values ranging from 8.84 to 22.0. The main reason behind this situation was thought to be the carbonation and hydrated cement content of the of concrete [134].

G was obtained from a single source since its availability in demolition regions is restricted and the same glass type (flat glass) is commonly utilized in the Türkiye's construction industry [135]. According to Table 2.1, G had an abundant SiO_2 content of 65.4% and a Na_2O content of 12.0%. Contrary to its high SiO_2 content, having an Al_2O_3 content of 0.98% causes G to be a relatively poor aluminosilicate source in geopolymer production due to an excessive Si/Al ratio. Therefore, the common focus of research has been concentrated on the use of G in the manufacture of sodium silicate, which is employed as an alkali activator in the development of geopolymers, via energy-intensive processes such as fusion and hydrothermal [136,137]. Nevertheless, as reported in the literature, it is also utilized in geopolymerization by mixing with other precursor materials in binary or other forms, since it contributes to the increase in the Si/Al ratio of the mixtures [106,119,138-140].

2.3.2. Particle size distributions of CDWs

Particle size distributions of CDWs collected from different demolition zones after being subjected to the same crushing and grinding processes are given in Fig. 2.3. Besides, their related d(0.1), d(0.5), and d(0.9) characteristic particle diameters and span values were presented in Table 2.2. A threshold at 15 μm was defined to assess differences in particle size (Fig. 2.3), which could reflect the reactivity of CDW elements since the mechanical performance was found to be enhanced for the geopolymers where the majority of the particle size distribution of the precursors was below this limit [121,128,141]. Considering the particle size distributions of HB, RCB, and RT, it was observed that all clayey CDWs had varied particle size distributions. At least 50% of the clayey materials were found to be smaller than 15 μm, except for DZ I – RCB (43.5%). The coefficient of variation [CoV=(standard deviation/mean)*100] for the particle sizes corresponding to the 15 μm

threshold was determined as 25.81, 13.49, 13.02, 6.58, and 4.39% for DZ I to DZ V, respectively, indicating differences in the particle size distributions of the CDWs per DZ.

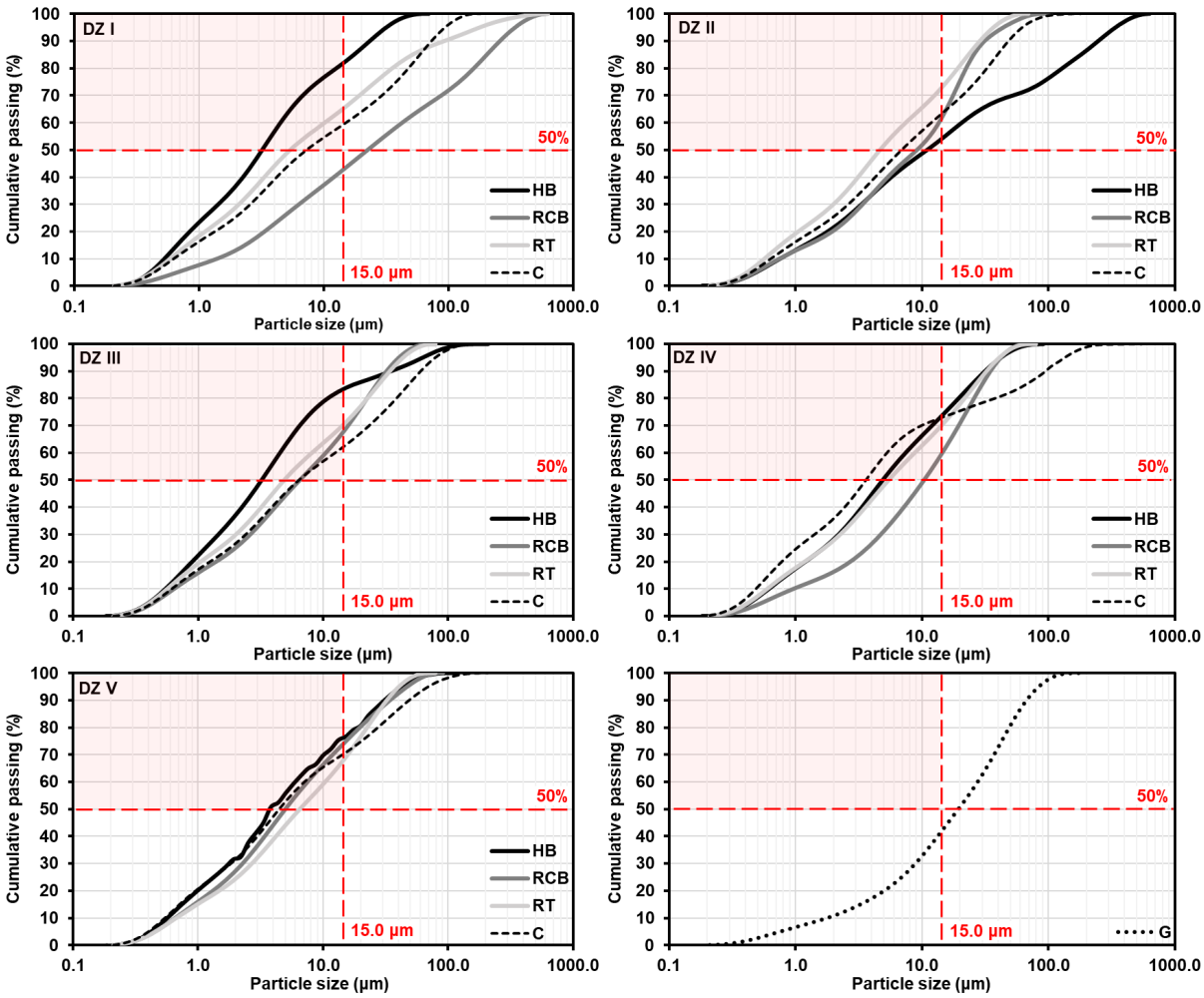

Fig. 2.3. Particle size distributions of CDWs (Highlighted region represents the particles that passed from 15 µm with a minimum of 50%)

Since there was no definite relationship between chemical composition and particle size, these discrepancies could be explained by the variable degrees of brittleness and morphological imperfections in each collected sample. Material properties such as strength and nature, brittleness, hardness, smoothness, stickiness, and moisture content have significant impacts on grindability and thereby particle size distribution [142]. On the other hand, the presence of phases such as quartz in different amounts and intensities may affect the grindability performance of CDWs [143]. Pereira-de-Oliveira et al. [144] reported that differences in average powder size in brick and tiles might result from the fabrication process

of the materials since the brick manufacture temperature is generally lower than the tile manufacture temperature.

Table 2.2. Characteristic particle diameters of the materials

Region	Material	Characteristic particle diameters (μm)			
		d(0.1)	d(0.5)	d(0.9)	Span*
DZ I	HB	0.519	3.181	23.25	7.15
	RCB	1.403	22.65	260.2	11.4
	RT	0.587	5.399	93.41	17.2
	C	0.626	7.292	73.25	9.96
DZ II	HB	0.754	10.99	247.4	22.4
	RCB	0.740	9.122	31.26	3.35
	RT	0.566	4.641	28.54	6.03
	C	0.635	6.908	48.42	6.92
DZ III	HB	0.543	3.206	34.64	10.6
	RCB	0.634	6.481	32.04	4.85
	RT	0.559	4.853	34.03	6.90
	C	0.610	6.358	60.08	9.35
DZ IV	HB	0.612	4.879	31.39	6.31
	RCB	0.951	10.34	34.59	3.25
	RT	0.592	5.412	32.14	5.83
	C	0.486	3.596	95.01	26.3
DZ V	HB	0.557	4.192	31.15	7.30
	RCB	0.651	4.965	34.22	6.76
	RT	0.663	6.494	32.25	4.86
	C	0.536	4.425	48.56	10.9
	G	1.748	19.41	67.22	3.37

DZ: Demolition zone, HB: Hollow brick, RCB: Red clay brick, RT: Roof tile, C: Concrete, G: Glass
*Span values were calculated according to the formula:
$\text{Span} = [\text{d}(0.9) - \text{d}(0.1)]/\text{d}(0.5)$

Concrete wastes (C) collected from different demolition zones were found to be finer than 15 μm with a minimum of 50%; and showed similar particle size distribution except for C of DZ IV. Factors such as the variability of the materials used in its production, the type of aggregate, the water-to-binder ratio, the moisture content, and the agents it is exposed to during its service life have a serious effect on the grindability of C. Regarding the type of aggregate, the siliceous or limestone originated aggregates used in the concrete production, as well as their various Mohs hardness indexes, results in a varying particle size distribution of different concrete wastes after the same crushing and grinding process. Therefore, the possible agglomeration behavior of limestone particles during grinding might be another reason for the variation noted for DZ IV [145]. It should also be noted that the grindability

index of waste concrete is mainly depended on the strength properties and these properties were the combination of compressive strength and plastic deformation under the external load [146].

Waste glass (G) showed coarser particle size distribution (40% finer than 15 μm) generally after the same crushing and grinding processes compared to other CDWs. The amorphous crystalline nature of G might be one of the major reasons for its coarser particle size distribution. The brittle and amorphous property of glass causes it to have a sharp-edged grain morphology leading to a higher tendency of agglomeration during grinding; thereby degrading the grindability performance [147].

According to span values presented in Table 2.2, a varied distribution among the CDW elements was noted for DZ I, DZ II, and DZ IV. Especially, DZ I – RT, DZ II – HB, and DZ IV – C had relatively higher spans, indicating a relatively non-uniform granularity and a non-consistent particle size distribution. However, the point that needs to be focused on here is to reach the particle size distribution that will provide the highest compressive strength, instead of highlighting the variability in grindability of bricks and tiles collected from different demolition zones due to their different nature. To reach the highest compressive strength, grinding all the materials separately, with different grinding durations to obtain the optimum fineness of each material would not be practical in terms of both energy consumption and cost. Therefore, it would be more feasible for different types of CDWs to grind all together to better represent the real-time cases of CDW in the actual field conditions where different types of mixed CDW are present collectively. Within this context, the effects of particle size distributions on the final properties are detailed in the following sections, aiming to reveal the performance properties of all CDW elements when subjected to the same pre-treatment.

2.3.3. Crystalline natures of CDWs

The crystalline natures of CDWs collected from different demolition zones assessed by applying XRD analyses are presented in Fig. 2.4. The types, PDF numbers, and chemical formulas of crystalline phases observed in CDW-based materials are presented in Table 2.3. According to the findings, clayey CDWs exhibited a semi-crystalline structure with major peaks detected at approximately 21° and 26° corresponding to quartz. In addition to quartz,

structures such as mullite, akermanite, diopside, and cristobalite, which consist of silica, alumina, and calcium-based components, were also detected as minor peaks. As is known, quartz, which constitutes a significant component of the crystalline structure of clayey materials, is mostly unreactive and undergoes almost no change in intensity after interaction with the alkalis [148]. However, with the calcination of these materials, in their manufacturing, by heat treatment up to 800-1000 °C, their crystallinity can be disrupted, resulting in the development of amorphous alumina and silica favorably contributing to their reactivity in the presence of alkalis [149,150]. On the other hand, beyond the calcination temperature of 900 °C, the formation of thermodynamically stable structures such as mullite and tridymite begins due to the recrystallization and reorganization of alumina and silica, which weaken the reactivity of such materials [151-153]. Literature studies have shown that the calcination of clay can increase the material's reactivity and ensure the development of geopolymers with higher mechanical properties [154,155]. Hence, the variations observed in the crystalline nature of the clayey CDWs highly depend on the calcination process as well as the source of raw materials used in their production. Although applying a further thermal treatment on the clayey CDWs can result in higher performance geopolymers produced with them, it is non-negligible that the extra calcination processes are highly inefficient in terms of cost, energy, and application practice. Therefore, it is of great importance to identify these materials accurately to be applied in the most suitable and cost-effective manner, especially when the circular economy is of focus. Considering all of the above statements and the satisfying mechanical performances declared by the authors in the previous studies [26,62,63,67,96,97,106], clayey CDWs were revealed to have high reactivity in an alkaline environment, yielding excellent polymerization and gel formation.

Table 2.3. Types, PDF numbers, and chemical formulas of crystalline phases observed in CDW-based materials

Crystalline phase	Symbol	PDF number	Chemical formula
Quartz	Q	96-101-1160	SiO_2
Crystobalite	Cr	96-900-8230	SiO_2
Diopside	D	96-900-5280	$Al_{0.6}CaMg_{0.7}O_6Si_{1.7}$
Mullite	M	96-900-5502	Al_2O_5Si
Akermanite	A	96-900-6115	$AlCa_2Mg_{0.4}O_7Si_{1.5}$
Calcite	Cc	96-900-0968	$CaCO_3$
Albite	Al	96-154-0705	Ca_3O_5Si

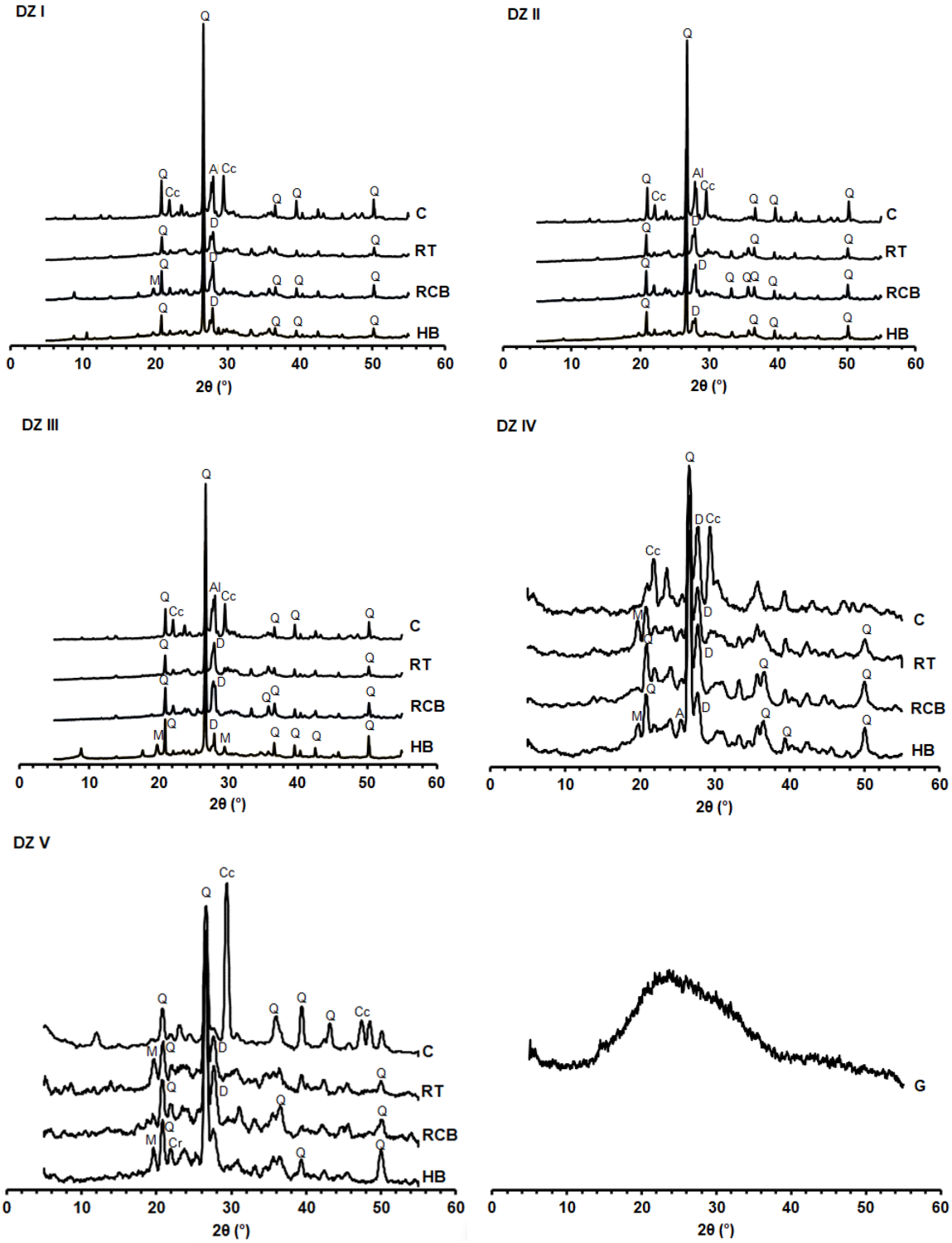

Fig. 2.4. Crystalline nature of the materials collected from different demolition zones

Considering the XRD analysis results of C, it was detected that C is mainly composed of crystals such as quartz, calcite, and albite. Unlike clayey CDWs, significant differences were registered in the crystalline natures of Cs obtained from different demolition zones. In this context, while quartz peaks were found at approximately 26° in DZ I, DZ II, and DZ III,

calcite peaks around 29° were accompanied by quartz peaks at 26° with similar intensities in DZ IV and DZ V. These differences were also found to be compatible with the chemical compositions of C. According to their crystalline structures, it can be presumed that C collected from DZ I, DZ II, and DZ III was most likely produced with silicious aggregates; conversely, C collected from DZ IV and DZ V might be produced with mixed silicious-calcareous aggregates [156]. On the other hand, calcite peaks can also be related to the carbonation of the portlandite content of concrete samples [157].

According to the crystalline nature of G, it was detected that G had a completely amorphous nature. As is well known, the amorphousness of the materials influences their reactiveness in the presence of alkalis [67]. However, the complete amorphousness of a material does not ensure that it will have excellent geopolymerization performance because this property is also highly dependent on the particle size distribution and chemical composition.

2.3.4. Compressive strengths of CDW-based geopolymers

The compressive strength results of CDW-based geopolymers containing CDWs from different origins are presented in this section. To determine the influence of the phases of the mixture design algorithm, Si/Al ratios of the mixtures, and the characteristic particle size, individual evaluation was performed for each demolition zone.

According to the results in Fig. 2.5, for Phase I, DZ I-1 coded mixture showed 45.0 MPa compressive strength, while DZ I-2 coded mixture had 41.8 MPa. Although DZ I-1 had a coarser particle size distribution compared to DZ I-2, it can be stated that the factor that may have caused this situation is the amorphous crystalline structure and higher SiO_2 content of the G. As is well known, in the presence of an alkaline solution, the amorphous phase of the precursor employed in the synthesis of geopolymer is more prone to dissolve quickly; thus, has more determinative role in geopolymerization [44,158]. These characteristics of G were found to be more predominant than the potential contribution of C on the mechanical performance, providing the formation of extra calcium-based gels (i.e., (N,C)ASH) [70]. Another reason for this output, therefore, might be the relatively low calcium content (11.8%) of C obtained from the DZ I, contributing inefficiently to gel formation responsible for strength development. In Phase II, compressive strengths of the DZ I-3, DZ I-4, DZ I-5 coded mixtures, which were produced by keeping the G/C ratio constant at 3 and to examine

the performance of HB, RCB and RT, were found to be 45.9, 34.7, and 42.2 MPa, respectively. The effect of fineness on the geopolymerization mechanism was demonstrated herein by the fact that under the same Si/Al ratio, DZ I-3 and DZ I-5 exhibited higher compressive strengths due to their characteristic particle diameters significantly lower than DZ I-4. The increased fineness of the precursor results in a larger surface area, leading to an increase in geopolymerization and, thus, an improvement in mechanical performance [121, 159].

At last, for Phase III, indicating the impact of the increased clayey CDW content based on the mixture with the highest mechanical performance in Phase II, the compressive strength results of DZ I-6 and DZ I-7 coded mixtures were found to be 54.0 and 56.9 MPa, respectively. From Phase II to III, the Si/Al ratio of the mixtures showed a decreasing trend (from 9.72 to 8.05 on average) with the increase of clayey CDWs; in other words, the decreasing amount of G significantly reduced the amount of SiO_2 (from 65.4% to 50.8% on average) in the mixtures. In the given situation, the enhancement in the compressive strength in Phase III should be related to the fact that CDW-based bricks and tile have a more balanced SiO_2 and Al_2O_3 content than concrete and glass [160]. Increasing the amount of Al^{3+} ions (meanwhile decreasing the Si/Al) leads to greater ionic balance in geopolymeric systems that causes an enhancement in the mechanical performance [161,162]. Another important point indicated by the findings was that for mixtures with similar characteristic particle diameters, the mixture containing more clayey CDW exhibited higher strength due to the higher amount of balanced SiO_2 and Al_2O_3.

According to the compressive strength results of geopolymer pastes produced with CDWs collected from DZ II, G was found to be more effective than C in terms of geopolymerization efficiency (Fig. 2.6). The similarities in C of DZ I and DZ II, in terms of chemical content, particle size distribution, and crystalline structure, caused similar mechanical performance trends of both materials after geopolymerization. On the other hand, the compressive strengths of Phase I mixtures were slightly higher than the DZ I due to the lower characteristic particle diameters. The most important outcome of these results is that close mechanical performances can be obtained when the CDWs have similar nature and bring similar fineness regardless of where CDWs were collected.

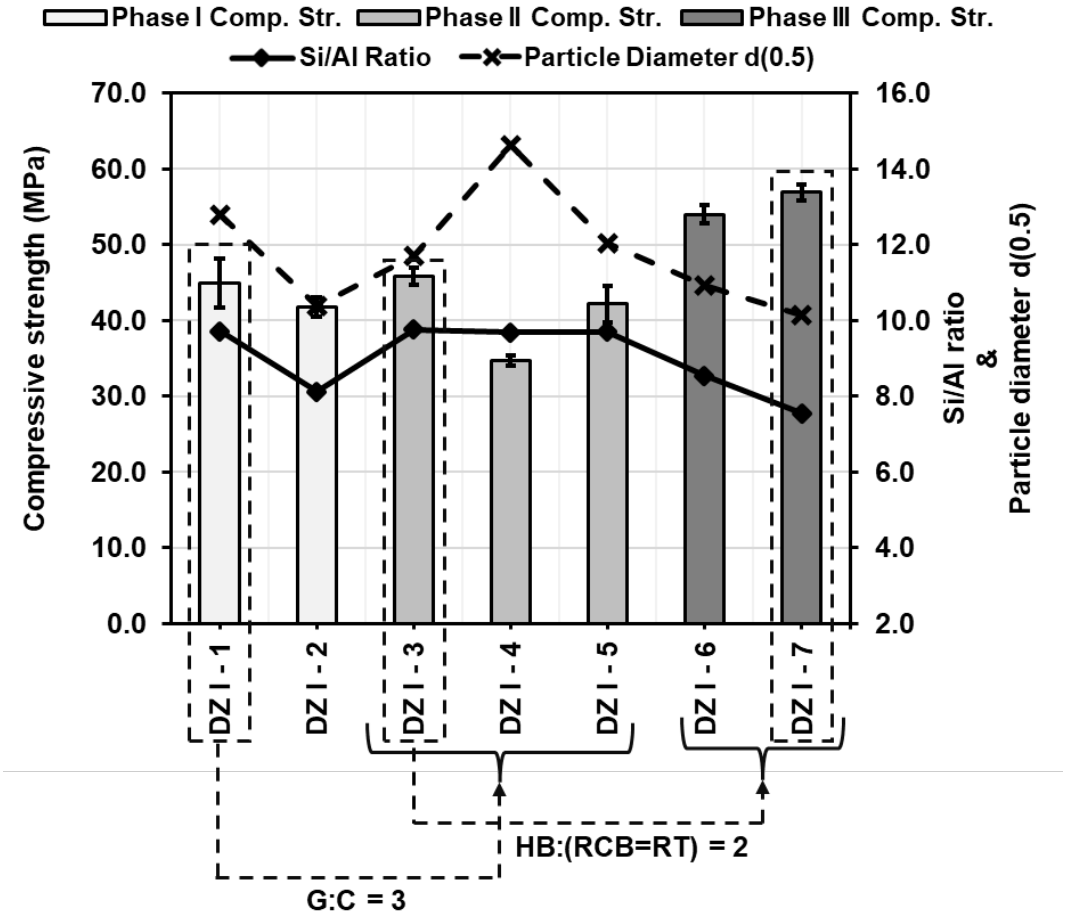

Fig. 2.5. Compressive strength results of geopolymers produced with CDWs collected from Demolition Zone I

In the Phase II, in which the effect of CDW-based clayey materials was investigated, DZ II-3, DZ II-4 and DZ II-5 coded mixtures exhibited compressive strength values of 51.6, 50.3 and 55.2 MPa, respectively. Obviously, for the close Si/Al ratios, the particle size distribution was more dominant for the mechanical performance of the geopolymers. The highest performances for Phase II were noted for the mixtures that contain finer clayey CDW elements, e.g., HB for DZ I and RT for DZ II. For the Phase III, the compressive strengths of DZ II-6 and DZ II-7 coded mixtures, which were generated considering the mixture with highest mechanical performance in Phase II, were found to be 58.9 and 60.3 MPa, respectively. Similar to the results obtained from DZ I, the compressive strength of the mixtures was found to have an increasing trend with decreasing Si/Al ratios, i.e., an increasing amount of balanced Si/Al of clayey CDWs.

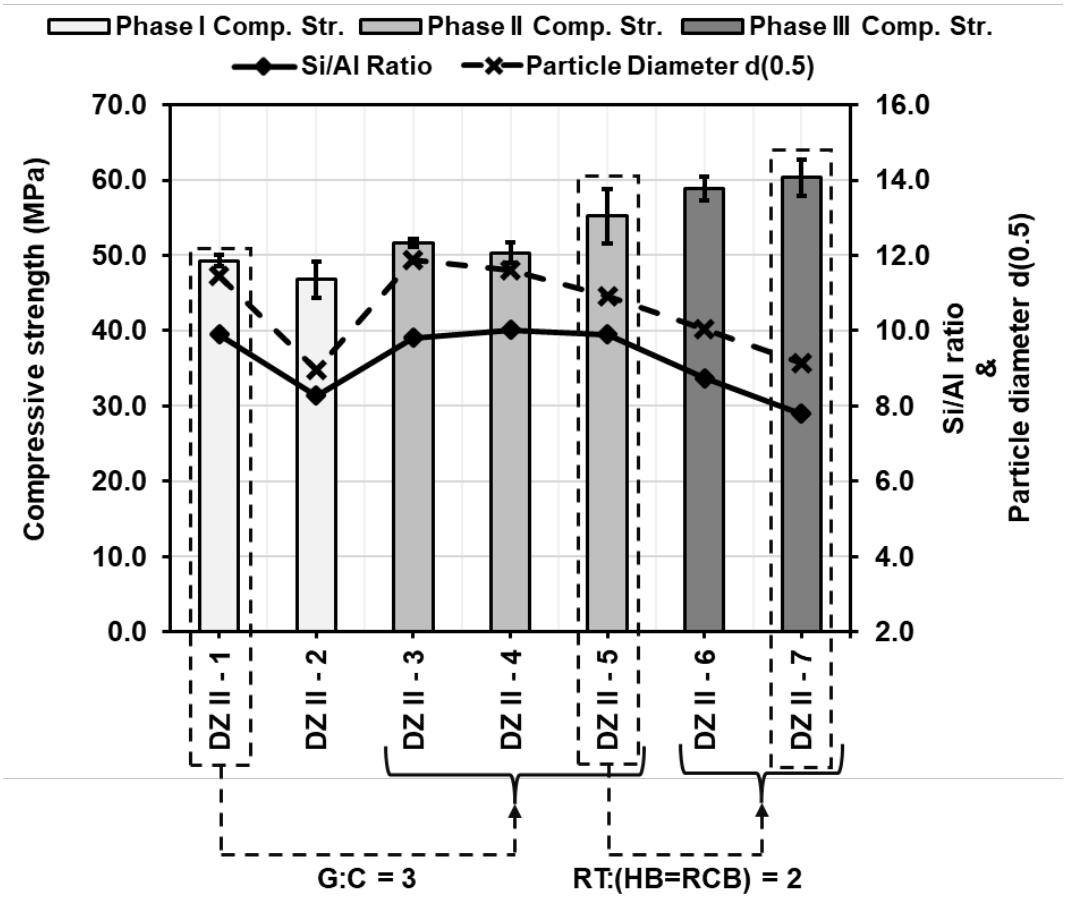

Fig. 2.6. Compressive strength results of geopolymers produced with CDWs collected from Demolition Zone II

Geopolymer mixtures produced with CDWs derived from DZ III exhibited higher mechanical performance than previous DZs, with a higher Si/Al ratio and lower characteristic particle diameter than other DZs; the latter was significantly lower, while the former was slightly higher (Fig. 2.7). In Phase I, DZ III-1 coded mixture exhibited 58.3 MPa of compressive strength, while DZ III-2 showed 54.0 MPa, which demonstrated that the G was better than C in terms of mechanical performance. Additionally, it was found that mixtures (Phase II: DZ III- 3, DZ III-4, and DZ III-5) containing various amounts of HB, RCB, and RT showed similar mechanical performance; however, the mixture with lower characteristic particle diameter distinguished by its higher compressive strength. After optimizing precursor design (Phase III), a maximum of 68 MPa compressive strength result were obtained in DZ III-7 coded mixture. Similar to the previously discussed DZs, it was found that increasing the share of the clayey CDWs in the mixture led to an increase in compressive strength. These results indicated that clayey CDWs are more promising source for the production of geopolymers with higher strength by having balanced Si/Al, efficient

particle size distribution and lower characteristic particle diameter compared to G and C. As is known, alkalinity and curing conditions might be insufficient to provide complete dissolution for the grains of coarser materials. This is most likely to result in reaction products that have less cohesive and less binding capability in the medium, thus, lower mechanical properties [67]. On the other hand, a greater and balanced amount of SiO_2 and Al_2O_3 in clayey CDWs enhances the formation of Si-O-Al bonds which is mainly responsible for mechanical performance [121,160]. However, this was thought to be related to the significantly lower characteristic particle diameter of DZ III-7 than that of the DZ III-6.

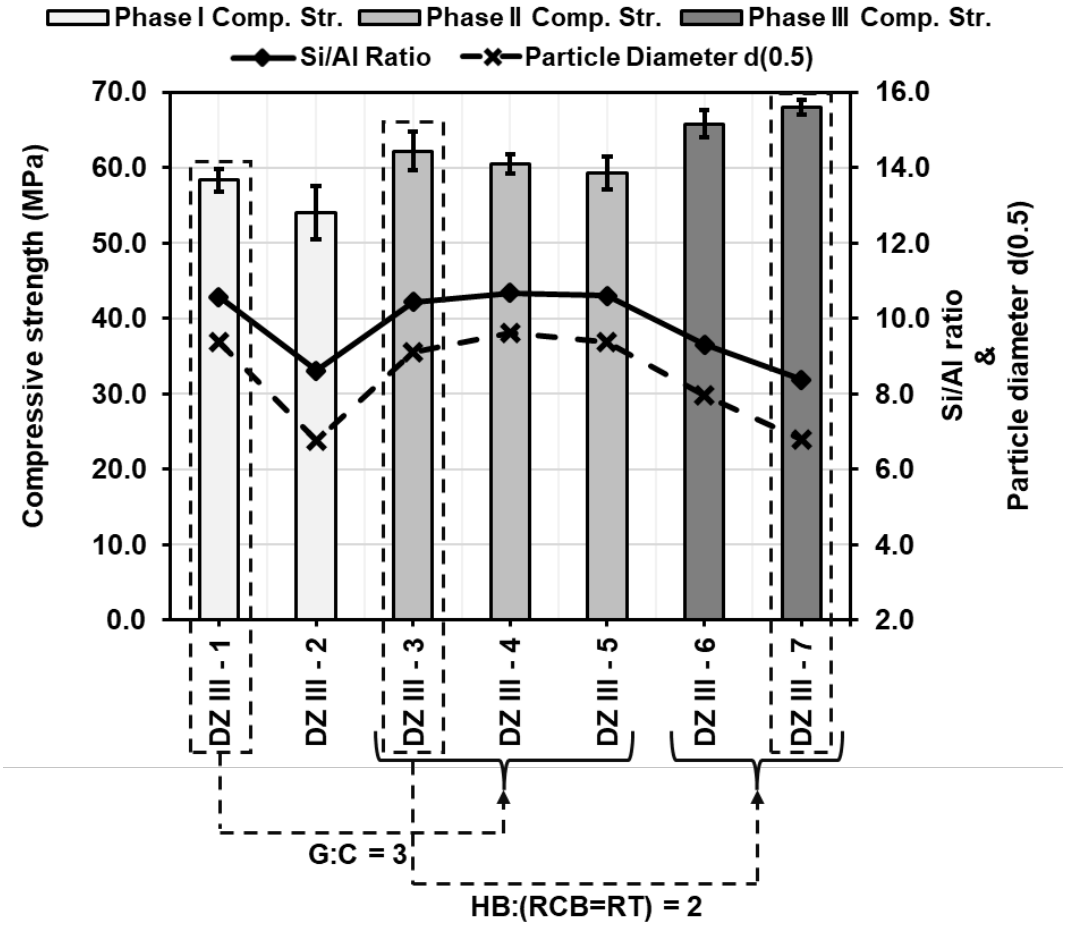

Fig. 2.7. Compressive strength results of geopolymers produced with CDWs collected from Demolition Zone III

For the DZ IV, contrary to other demolition zones, C exhibited higher performance than G (Fig. 2.8). The main reason behind this circumstance was that the CaO content of DZ IV-C was approximately twice that of the CaO content of C discussed in the previously mentioned

demolition zones. As is known, in the presence of high CaO in the medium, NASH gels tend to transform into CASH gels and result in the formation of (C,N)ASH 3D aluminosilicate networks [123,163], which causes an increase in the mechanical properties of the geopolymer product. In Phase II, although the Si/Al ratios of DZ IV-3, DZ IV-4, and DZ IV-5 coded mixtures were quite similar, differences in their compressive strengths were in the range of 49.4-58.1 MPa, which can be related to the non-uniform distribution of C with a span value of 26.3 (Table 2.2), and likely to result in a less densely packed and non-homogenous matrix with a higher amount of voids or pores. The reactivity of the raw materials might be less efficient due to fewer reactive sites available, causing variations in the gel production responsible for strength. However, it can be argued that the possible drawbacks expected to arise from the lower Si/Al ratios and large span value of C might be compensated by the significantly smaller characteristic particle diameter of Phase II mixtures, which distinguished them from the DZs mentioned above. On the other hand, for the DZ IV-3, although HB of the DZ IV is neither the finest material nor the highest SiO_2+Al_2O_3 content among clayey CDWs, it likely exhibited comparable compressive strengths thanks to the akermanite peak as observed by XRD analysis. There are several studies in the literature reporting that akermanite somehow improves the mechanical strength thanks to its filler effect and its ability to control volume expansion [164,165]. In Phase III, for DZ IV-6 and DZ IV-7, the maximum compressive strength result of 63.6 MPa was obtained for the mixture consisting of 80% clayey CDWs, while 62.2 MPa for 70% clayey waste content. Similar to Phase II, the higher compressive strength of the DZ IV-7 can be attributed to the mixture's significantly smaller characteristic particle size than the mixtures of previous DZs.

In final stage, the DZ V-1 coded mixture containing 30% G showed a compressive strength result of 40.4 MPa, while the DZ V-2 coded mixture containing 30% C showed a compressive strength result of 45.4 MPa (Fig. 2.9). DZ V-C with the highest CaO content of 27.2% among other C was found to be more efficient compared to G. This situation can be associated with the fact that high CaO content contributes to the compressive strength by providing extra CASH gel formation to the system, as mentioned before. As is well known, similar impacts were also reported for slag and class C fly ash, both of which have a high CaO concentration and are commonly utilized in geopolymer manufacture, having a similar influence [67,123].

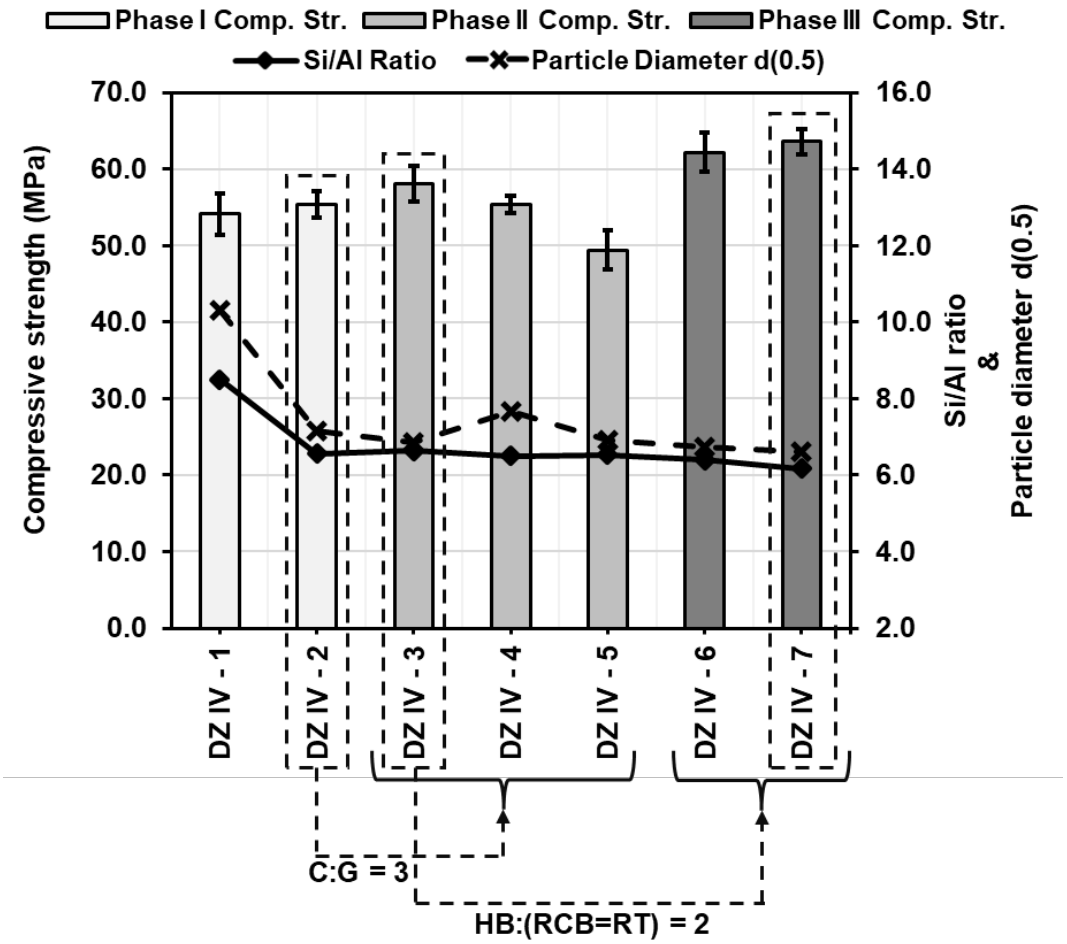

Fig. 2.8. Compressive strength results of geopolymers produced with CDWs collected from Demolition Zone IV

Following the determination of the C/G ratio, in Phase II, the DZ V-3 coded mixture in which HB was utilized at the maximum rate showed the highest performance among the three mixtures with a compressive strength of 52.2 MPa. Although XRF revealed that HB had poorer aluminosilicate content than RCB and RT, the relatively finer particle size distribution of HB might have caused better mechanical performance. On the other hand, DZ V-6 and DZ V-7 coded mixtures exhibited compressive strength values of 54.5 MPa and 50.2 MPa, respectively (Phase III). For the first time in all series, it was observed that increasing the ratio of clayey CDWs to 80% caused a decrease in compressive strength. Although a balanced Si/Al ratio is one of the most determining factors in geopolymerization reactions, it can be clearly stated that factors such as material dissolubility and, thus, polycondensation rate play a more critical role in most cases, which can reflect a lower dissolubility for DZ V-7 [166,167]. Besides, the factor that may cause this situation is most

likely associated with the slightly lower SiO_2+Al_2O_3 content of DZ V-7, reducing the potential for further gel formation (Table 2.1).

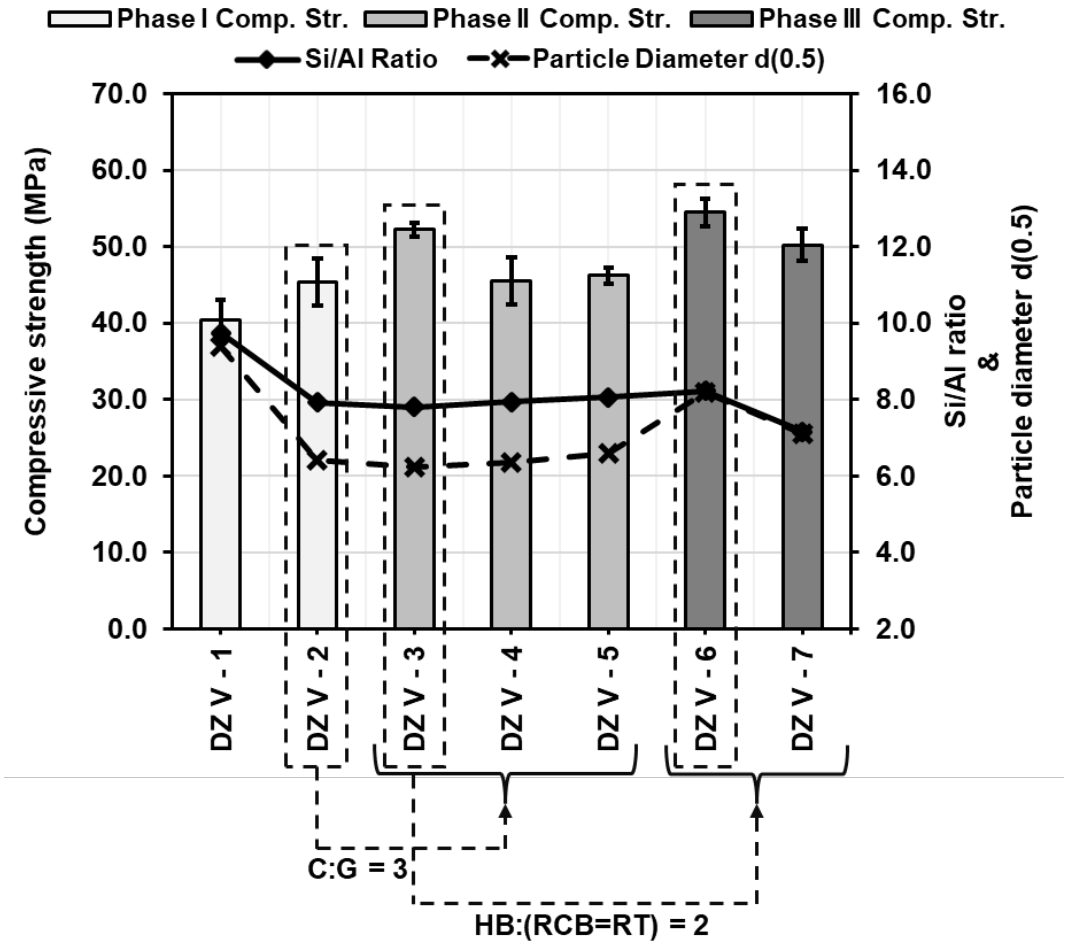

Fig. 2.9. Compressive strength results of geopolymers produced with CDWs collected from Demolition Zone V

The relationship of mechanical, physical, and chemical features of mixtures for different demolition zones is presented in Fig. 2.10. To understand the impact of these features, compressive strengths, Si/Al ratios, particle diameters, and aluminosiliceous (SiO_2+Al_2O_3) contents of the mixtures with the highest mechanical performance for each DZ were evaluated. At first glance, it can be stated that decrease in the characteristic particle diameter led to an enhancement in a strength. On the other hand, from DZ I to DZ III, the Si/Al ratio and aluminosiliceous content increased, which can be considered as the other parameter behind the strength improvement. Considering the fact that DZ IV has the lowest Si/Al ratio and lower aluminosiliceous content than DZ II, the higher mechanical performance of DZ IV can reveal the significance of the fineness of the material. A general statement, therefore, can be established as the Si/Al ratio and aluminosiliceous content deterministic parameters

on the mechanical performance; however, these parameters should be evaluated with the significant influence of the material fineness. In other words, further grinding for CDWs can provide strength improvement to a degree, but remarkable strength improvement can only be ensured by the balanced ratio and adequate amount of Si and Al. In conclusion, based on the chemical composition, particle size distribution, and crystal structure of CDWs, optimizing the mix designs resulted in maximum compressive strengths ranging from 54.5 MPa to 68 MPa for varying DZs. This demonstrated that even though collected CDWs from different demolition zones vary in origin, chemistry, brittleness, and crystalline structures, similar geopolymers with high strength can be successfully developed by optimizing mixture designs.

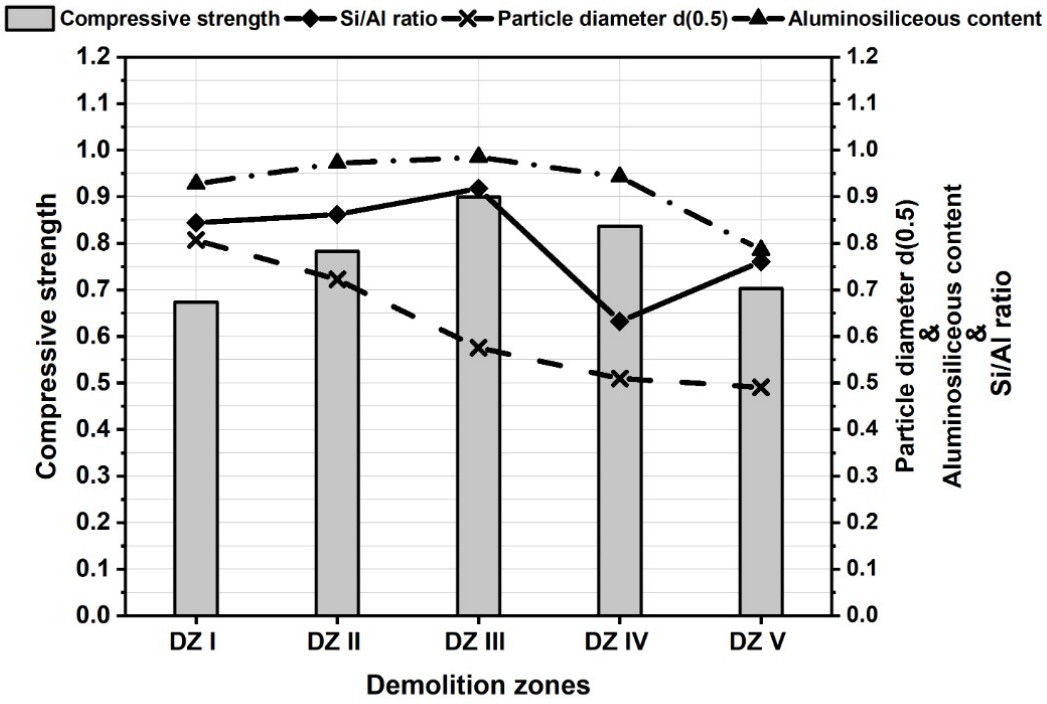

Fig. 2.10. Relationship of mechanical, physical, and chemical features (axes were normalized)

Multiple regression analysis was used to statistically investigate the effects of Si/Al ratio, particle diameter d(0.5), and aluminosilicate content (SiO_2+Al_2O_3) on the compressive strength of selected geopolymer pastes (Table 2.4). According to the regression statistics that present the information regarding the model's overall fit, the Multiple R value of 0.988 showed the correlation between the observed values of the dependent variable, compressive strength, and the predicted values based on the model [168]. A value close to 1 suggests a

strong positive relationship between the predicted and observed values. The R-Square value of 0.976 indicates that the independent variables (Si/Al ratio, characteristic particle diameter, and aluminosilicate contents) can explain 97.6% of the variance in compressive strength [169]. The adjusted R-Square value of 0.903, which considers the number of predictors in the model, also indicates a good fit [170]. The standard error value of 0.024 represents the average distance between the observed values of compressive strength and the regression line [169], with a small standard error indicating a good fit. Overall, the results suggested that the model was a good fit for the data, and the independent variables accurately predicted compressive strength.

Table 2.4. Multiple regression analysis of CDW-based geopolymer binders

Regression Statistics		**ANOVA**					
Multiple R	0.988	**Source**	**df**	**SS**	**MS**	**F**	**Significance F**
R-square	0.976	**Regression**	3	0.024	0.008	13.409	0.197
Adjusted R-square	0.903	**Residual**	1	0.001	0.001		
Standard error	0.024	**Total**	4	0.025			

Statistics of Independent Variables				
	Coefficients	**Standard error**	**t Stat**	**P-value**
Intercept	0.155	0.250	0.620	0.647
Si/Al ratio	0.210	0.158	1.334	0.410
Particle diameter d(0.5)	-0.368	0.126	-2.918	0.210
Aluminosilicate content	0.842	0.187	4.514	0.139

The Analysis of Variance (ANOVA) results summarize the significance of the regression model by breaking down the variability in the data into two components: regression and residual [171]. The regression component explains the amount of variability in the dependent variable that is attributed to the independent variables, while the residual component represents the unexplained variability. The ANOVA revealed that the regression model had a good fit for the data, with a significant F-value of 13.409 and a corresponding p-value of 0.197. The residual MS was 0.001, indicating the average amount of unexplained variability in the dependent variable, while the total SS was 0.025, representing the total variability in the dependent variable. Overall, the ANOVA suggested that Si/Al ratio, particle diameter d(0.5), and aluminosilicate content significantly affected the compressive strength of the material being studied.

The coefficients provide direction and strength information about the relationship between independent variables and the dependent variable in the multiple regression model. It can be used to identify which independent variables are statistically significant predictors of the dependent variable. According to the findings, the Si/Al ratio and aluminosilicate content had the positive impact on the dependent variable, with coefficients of 0.210 (t=1.334, p=0.410) and 0.842 (t=4.514, p=0.139), respectively; besides, the latter had the highest impact among all parameters. Conversely, the coefficient for particle diameter was -0.368 (t=-2.918, p=0.210), implying that a one-unit increase in diameter was associated with a -0.368-unit decrease in the dependent variable, holding other variables constant. The standard errors of the estimates were relatively low, ranging from 0.158 to 0.250, indicating that the model had a good fit for the data.

These results suggest that the Si/Al ratio and aluminosilicate content positively contributed to the compressive strength of geopolymer pastes, while particle diameter d(0.5) had a negative impact. Si/Al ratio had a positive effect on compressive strength because an increase in Si/Al ratio indicates an increase in the number of aluminum atoms per silicon atom in the zeolite framework [172]. This results in a higher positive charge in the framework, which attracts more counter ions, such as Na^+ or H^+, leading to a higher compressive strength of the geopolymers. The particle diameter d(0.5) has a negative effect on compressive strength because larger particles have a lower surface area to volume ratio, resulting in fewer ion-exchange sites available for counter ions. As a result, the compressive strength decreases as the particle size increases. Aluminosilicate content has a positive effect on compressive strength because a higher aluminosilicate content means there are more aluminum and silicon atoms in the zeolite framework. This leads to a higher positive charge in the framework and attracts more counter ions, which results in a higher compressive strength.

2.3.5. Scanning electron microscopy/Energy-dispersive X-ray (SEM/EDX) Analysis

SEM/EDX analysis was conducted on the selected geopolymer pastes in order to examine in-depth microstructural characteristics and elemental distribution (Fig. 2.11). The selection was done according to: (i) the mixture with the highest mechanical performance (DZ III-7) among all mixtures; (ii) the mixtures with the highest G (DZ III-1) and (iii) the highest C (DZ III-2) content among the mixtures produced with CDWs collected from the same region (DZ III); (iv) the mixture with the highest mechanical performance (DZ IV-7) among other demolition zones (in other words, except DZ III); (v) and the mixture with the lowest performance (DZ I-4) among all demolition zones. According to the SEM micrographs, similar structures were observed for varied mixtures due to the similar ingredients. However, the diversity of CDWs resulted in a heterogeneous matrix composed of different types of geopolymeric gel formations. At this point, the ultimate gel structure responsible for strength is directly related to the aluminosilicate and calcium content of the precursor and the pH level of medium; accordingly, gel structures such as NASH, CASH, and (N,C)ASH can be formed [62,173,174]. For instance, regional EDX results demonstrated that Na- and Ca-based gel structures were detected for all mixtures with varying densities according to their dominant CDW-based ingredient.

For all mixtures, the co-existence of Na and Ca ions in elemental count indicated the formation of Na- and Ca-based gels intertwined to form (N,C)ASH. Besides, the elemental counts of the DZ III-2 mixture containing the highest C amount can be attributed to the extensive formation of Ca-dominated gels, whereas the formation of Na-dominated gels was observed for other mixtures. Based on the visual inspections on SEM micrographs, in accordance with the compressive strengths, the DZ III-7 and DZ IV-7 had a dense structure with fewer unreacted particles, whereas the DZ III-1 and DZ III-2 had relatively less dense structures with higher amounts of unreacted particles. For DZ I-4, which had the lowest strength result, the quantity of unreacted particles was higher than the other mixtures.

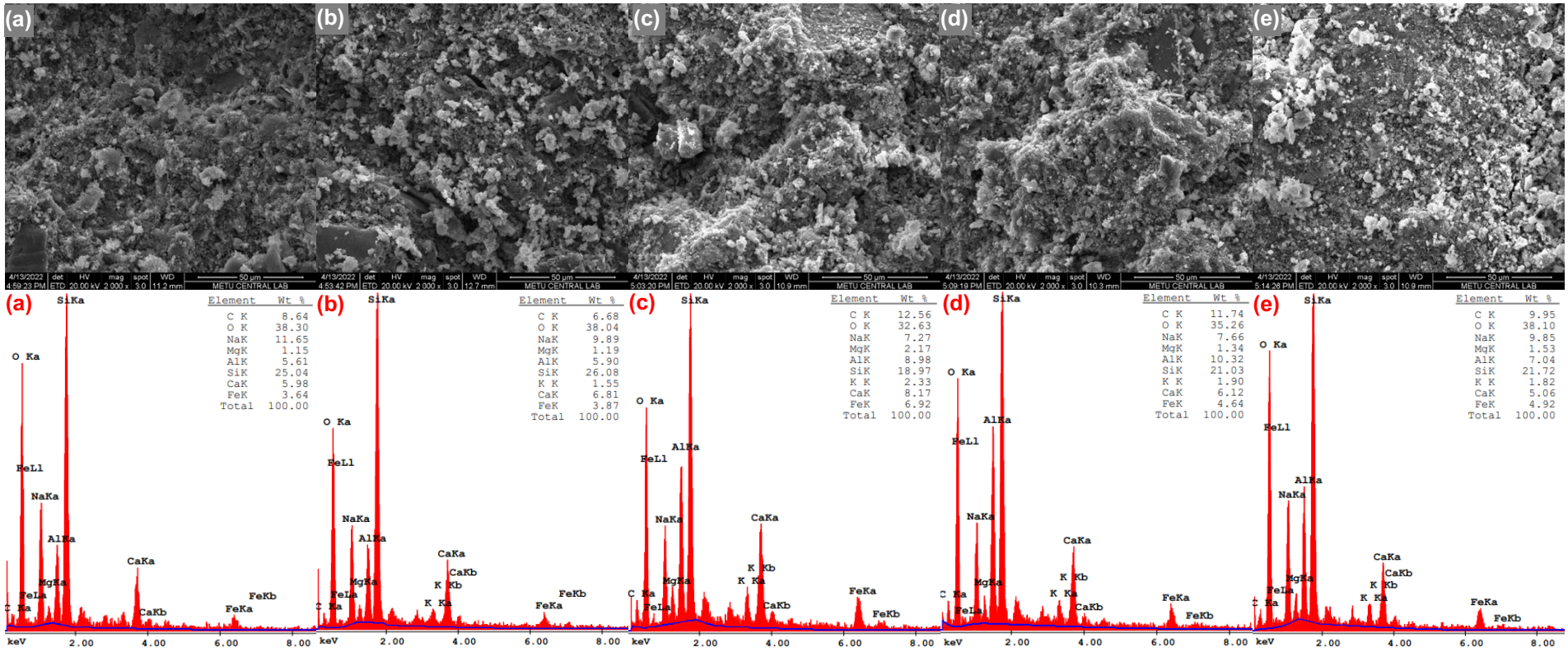

Fig. 2.11. SEM/EDX analysis of CDW-based geopolymers (a) DZ III-7, (b) DZ III-1, (c) DZ III-2, (d) DZ IV-7, (e) DZ I-4

2.3.6. Fourier Transform Infrared Spectrophotometer (FTIR) Analysis

The short-range structural order of the selected geopolymer paste mixtures (same as the selection criteria mentioned in the SEM analysis) was examined in detail by Fourier Transform Infrared Spectrophotometer (FTIR) analysis. According to the results presented in Fig. 2.12, the absorption band observed in all selected samples around 977-982 cm^{-1} of wavenumbers is associated with the formation of the Si-O-T (T= Si or Al) band formed as a result of geopolymerization [175-177]. This absorption band represents the formation of amorphous aluminosilicate gels as a result of the interaction of CDW-based materials with sodium hydroxide [121]. In addition, although FTIR analysis was not performed on raw CDW-based materials in this study, it has been reported in the literature that the peaks occurring in this region partially shift to the lower wavenumbers in geopolymer samples compared to raw CDW-based materials, causing a considerable increase in intensity [121]. On the other hand, small absorption bands were also observed approximately between 1462-1469 cm^{-1} for all geopolymer samples. The band observed between 1462-1469 cm^{-1} indicates the presence of carbonation products (i.e., calcite, natrite) that occur as a result of the reaction of alkali cations in the matrix with CO_2 in the atmosphere [178,179]. Another point that should be mentioned here is that the stronger absorption band in this region was observed in the DZ IV-7, which contains higher C than the other mixtures used in the FTIR analyses. This might be explained by the fact that the carbonation products in this mixture were greater due to the presence of calcite in the C, as revealed by the XRD analysis. In addition, the observed small asymmetric stretching bands at the wavenumber of ~700 cm^{-1} are assigned to pseudolattice vibrations of small aluminosilicate rings [180].

In general, no clear differences were registered between the selected geopolymer pastes according to the FTIR analysis. As mentioned before, this demonstrated that regardless of where CDWs are collected, their atomic bond structures were found to be remarkably similar as a result of geopolymerization. Nevertheless, it was observed that CDWs collected from different demolition zones may have very small differences in absorption intensities in general due to their slightly different chemical composition, crystal structure and degree of geopolymerization.

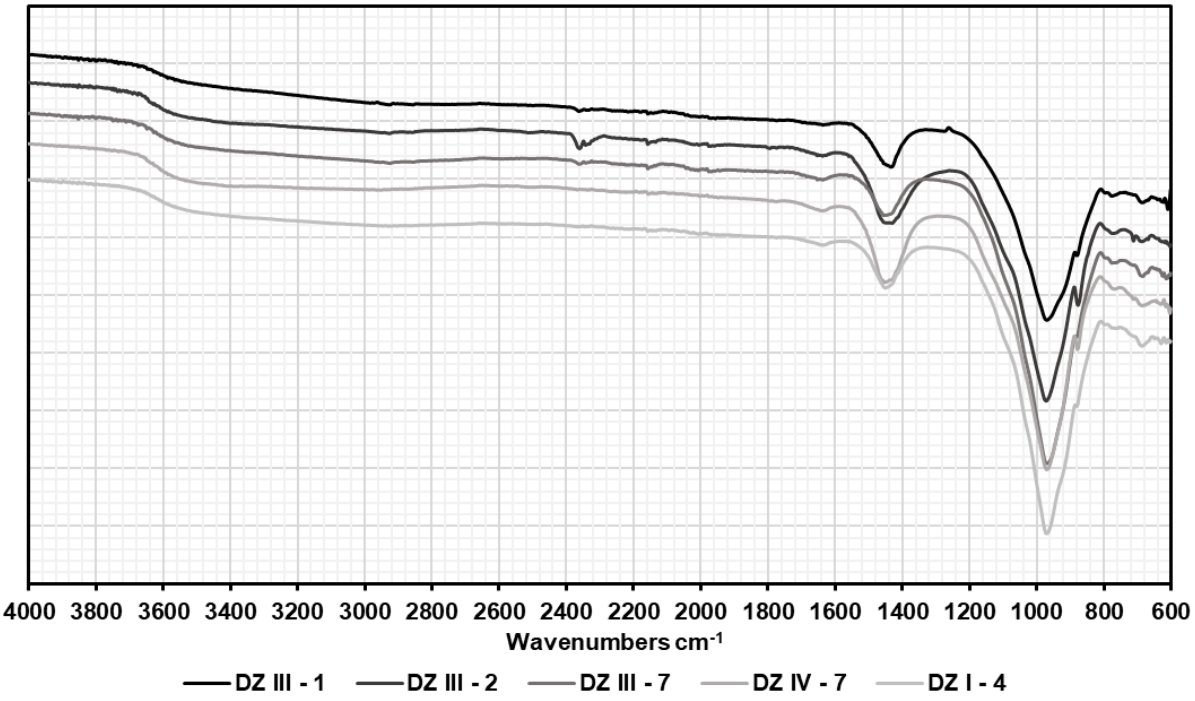

Fig. 2.12. FTIR spectra of selected geopolymer pastes

2.4. Conclusions

The present chapter of the thesis investigates the influence of the origin of construction and demolition waste (CDW) (obtained from different demolition zones) on their geopolymerization performance in terms of microstructural analyses and compressive strength tests. In this context, the effect of physical and chemical properties on the mechanical properties of CDWs including roof tile (RT), hollow brick (HB), red clay brick (RCB), concrete (C), and glass (G) from five different demolition zones (except glass) was investigated. According to the findings of the studies conducted in this chapter, the following conclusions were drawn:

- Compressive strengths of CDW-based geopolymer mixtures were found to be in the range of 34.7 to 68.0 MPa, indicating a significant influence of the CDW characteristics on the mechanical performance. However, through precursor-based optimization, it was possible to achieve consistent mechanical performance ranging from 54.5 to 68 MPa, regardless of the origin of the CDW. Additionally, when optimizing the mixture designs using CDWs collected from the same source, a noteworthy increase in compressive strength of up to 64% was observed.

- HB, RCB and RT forming the clayey phase of CDW were the most suitable candidates for geopolymerization with balanced and high aluminosilicate content. The increase of the clayey phase in the binder phase improved the mechanical performances; the high CaO content of the concrete waste increased the strength, while the relatively high SiO_2/Al_2O_3 and low grain size were more advantageous for the glass waste.

- The Si/Al ratio and aluminosilicate content represented critical determinants of the compressive strength of materials. Nonetheless, it was crucial to acknowledge that the material's fineness also exerted a notable influence on its compressive strength. While further grinding may offer some benefits in terms of strength enhancement, substantial improvements can solely be attained by ensuring a balanced Si/Al ratio and the overall quantity of these constituents.

- The SEM micrographs revealed that the mixtures exhibited similar structures, which is likely attributable to the comparable ingredients utilized. However, the heterogeneous nature of the CDWs led to the formation of distinct geopolymeric gel structures within the matrix. The ultimate gel structure, which plays a crucial role in determining the strength of the material, is heavily influenced by factors such as the aluminosilicate and calcium content of the precursor and the pH level of the medium. This can result in the formation of various gel structures, including NASH, CASH, and (N,C)ASH.

- The FTIR analysis revealed the presence of similar geopolymeric gel structures and carbonated products in the matrix of each mixture. Notably, no significant differences in the selected geopolymer pastes were observed. These results suggest that the atomic bond structures of CDWs subjected to geopolymerization are largely consistent, regardless of their origin. However, minor variations in absorption intensities were detected in the CDWs collected from different demolition zones, potentially attributed to subtle differences in their chemical composition, crystal structure, and degree of geopolymerization.

Overall, the compressive strength of geopolymerized CDW is heavily influenced by the chemical composition, crystal structure, and fineness of the CDW, which may vary based on their origin. Nonetheless, optimization of these parameters on a precursor basis can lead to

consistent and high compressive strength of CDW-based geopolymers irrespective of the CDW source. These findings underline the necessity of comprehensively assessing the aforementioned parameters when seeking to optimize the compressive strength of materials.

In the light of the data obtained in this chapter of the thesis, hollow brick (HB), red clay brick (RCB) and roof tile (RT) clayey CDWs, which, despite having variable contents, make it possible to consistently achieve above a certain mechanical performance, have been selected as the main precursor phase of CDW-based geopolymers to be produced in the following chapters of the study as a result of these promising results.

CHAPTER III: CHARACTERIZATION AND LIFE CYCLE ASSESSMENT OF GEOPOLYMER MORTARS WITH MASONRY UNITS AND RECYCLED CONCRETE AGGREGATES ASSORTED FROM CONSTRUCTION AND DEMOLITION WASTE

3.1. Introduction

Geopolymeric binders offer a promising alternative to reduce carbon emissions from cement production by utilizing industrial by-products as precursors [181,182]. The properties of the geopolymeric binders are influenced by precursor characteristics such as source, composition, and particle size [183]; therefore, fly ash and ground granulated blast furnace slag, whose characteristics and performance are already totally known, are commonly used precursors in geopolymer production. Main reason behind that is their suitable SiO_2 and Al_2O_3 content; however, they are no longer considered waste and are widely used as pozzolans in the construction industry [23,183,184]. Moreover, they have currently been in great demand and can be sold at comparable prices even with PC. Therefore, current research in geopolymer technology focuses on utilizing more challenging and locally available waste materials as precursors.

Typically disposed of in landfills or discarded without recycling, CDWs lead to the depletion of valuable land resources and threaten sustainable development [185]. Urgent measures are needed to explore innovative and efficient approaches for the recycling and reuse of CDW. Fortunately, masonry-based CDW with its high aluminosilicate content has great potential for geopolymerization technique, as revealed in the previous chapter of the thesis. Besides, a former study performed by the author of the thesis on CDW-based geopolymers investigating the use of CDW elements as precursor phases in binary combinations rather than in single variation [26] demonstrated that the CDW-based masonry precursors can be combined to produce geopolymer binders, eliminating the need for selective demolishing and individual separation. The compressive strength of these binders was found to be increased with higher curing temperatures, longer curing periods, higher NaOH molarity, and increased amounts of HB in the precursor combination. Optimal results were obtained at a curing temperature/period of 115°C/48h and NaOH concentration of 15M, achieving compressive strengths of up to 80 MPa. In another recent study [62], the mechanical and durability properties of geopolymer matrices incorporating CDW-based materials with

100% recycled aggregate and various alkali activator ratios and slag substitutions were investigated. Geopolymers made solely from CDW-based products achieved 30 MPa compressive strength, while slag substituted mixtures reached 50 MPa. Considering the fact that the diversity in CDW leads to significant variations in the aluminosilicate content (SiO_2 and Al_2O_3), higher Si/Al ratio enhanced the compressive strength of CDW-based geopolymers by influencing the formation of alkali aluminosilicate gels [71]. Increasing the available silica in the alkali activation system significantly alters the composition and structure of the gels, resulting in polymerized and densely packed reaction products with improved mechanical properties. Moreover, the Ca/Si ratio is an important factor in mechanical performance, with a positive effect at low Si/Al ratios and a threshold value at high Si/Al ratios. While researchers have directed their efforts toward investigating CDW-based geopolymers, there is a pressing need for comprehensive and inclusive studies to optimize the diverse range of chemical and morphological characteristics of these waste materials to utilize all CDW components effectively considering their quality and/or quantity.

Concrete waste (CW), which has the lion's share among CDW components in most countries [186], is widely used as recycled concrete aggregate (RCA) in practical applications. However, the RCA production is still limited considering the amount of RCA generated in the EU is approximately 9.4 percent of total aggregate demand [187]. Parthiban et al. [188], who investigated the influence of RCA on the mechanical and durability properties of ambient-cured alkali activated slag concrete (AASC), stated that all AASC mixtures exhibited superior mechanical performance than PC-based concrete and the highest strength was achieved with a 50% RCA content. Koushkbaghi et al. [189] found that replacing 30% of RCA in metakaolin geopolymer concrete decreased compressive strength by 28%. Adhesion of old mortar to RCA weakened the aggregate-paste interface but overlapping hydration products enhanced geopolymer paste formation. In another study, Rahman and Khattak [190], who developed roller-compacted geopolymer concrete using 100% RCA, stated that RCA-based concrete exhibited satisfactory compressive strength (7.53-27.6 MPa), flexural strength (2.1-3.8 MPa), and elastic modulus (15.97-46.77 GPa), making it suitable for robust base pavement. Although the studies mentioned above have shown the feasibility of using RCA in geopolymer-based systems, the potential advantages and shortcomings of including RCA in CDW-based geopolymer mortars are still unclear. In the previous studies of the authors [83,97,106], the RCA was used successfully in CDW-based

geopolymer systems, while the effects of aggregate-related properties such as size and amount were not discussed in detail. Additionally, the ITZ properties of RCA used in CDW-based geopolymer matrix have remained unclarified.

Notwithstanding the fact that geopolymers are considered an environment-friendly alternative to cement since the binder phases consist of industrial by-products, it is critical to precisely identify their environmental impacts. At this point, the Life Cycle Assessment (LCA) analysis method, a sustainable development tool used to measure and compare the environmental impacts of products and services throughout the entire life cycle, can be lifesaving [191]. In this context, many studies have been conducted to evaluate the environmental effects of geopolymer binders. At first glance, it was reported that geopolymer binders caused 27-64% less greenhouse gas emissions compared to conventional cement-based binders [192-197]. However, related assessments are subject to variation because the contents of the examined materials are different and the database, inventory, assumptions, and boundaries employed differ; hence, making a direct comparison may not stand on a sound basis. Although the number of LCA studies for conventional geopolymer systems has reached a certain level, it is severely limited for CDW-based geopolymers. Investigating the energy consumption and carbon dioxide emissions of the geopolymers produced with the brick-PC combination, Fořt et al. [198], reported that increasing the brick content could reduce the carbon footprints and energy consumption of the mixtures by 63% and 81%, respectively. In addition, the geopolymer mixture (3:7-PC:brick) exhibited mechanical performance comparable to the completely PC-containing mixture, reduced energy consumption and Greenhouse Gases (GHG) emissions by 45% and 72%, respectively. A study [199] analyzed the environmental impact of geopolymer mixtures produced from recycled brick and ceramic tile. The results showed that the mixture containing fly ash had the lowest impact on environmental impact categories, including Ozone Depletion Potential (ODP), Global Warming Potential (GWP), Acidification Potential (AP), Eutrophication Potential (EP), and Fossil Fuel Depletion. The use of alkali activators was found to have a greater impact than the manufacturing process. The thermal curing process had a low impact, the highest difference was noted for GWP with about 10 kg.CO_2.eq. In another study [139], the environmental impact of CDW-based engineered geopolymer composites was investigated and the negative effects of alkali activator use were confirmed. However, it was revealed that the optimization of the mixture design and the use

of renewable energy sources in the production of alkaline activators could bring serious positive results.

It is vital to produce a fast, easy-to-apply, economical, and environment-friendly solution for the re-utilization of the enormous level of CDWs generated due to the activities of the construction industry and natural disasters such as earthquakes and floods. In this context, the current chapter of the thesis focuses on the production of a holistic solution in recycling CDW to the construction materials for construction and housing in developing economies and disaster-prone regions, which can meet the structural performance criteria in a few days with accelerated curing. Besides, based on the literature framework presented above, it can be stated that the mechanical and environmental characteristics of geopolymer mortars comprising 100% CDW as both aggregate and binder phases are still limited and unclear. Especially the comprehensive life cycle assessment of CDW-based geopolymer mortars by following the cradle-to-gate approach to reveal their environmental impacts is still in its infancy. Although the emphasis that geopolymers are more advantageous than cementitious systems in environmental terms is frequently made superficial in the literature, it is believed that quantifying these aspects by conducting LCA analysis will further raise interest and awareness in recycling CDW through geopolymerization. Accordingly, the current chapter of the thesis aims to fill this knowledge gap by investigating the ITZ properties in heat-cured masonry-based geopolymer mortars containing fine RCA (<5 mm) and addressing the key parameters affecting mechanical performance, such as RCA-related properties, curing temperature, and molar concentration of sodium hydroxide and the environmental impacts of geopolymers with a comprehensive LCA analysis.

3.2. Experimental Program

3.2.1. Materials

Construction demolition waste-based materials such as hollow brick (HB), red clay brick (RCB), and roof tile (RT) were used as precursors in the production of geopolymer mortars. The CDW-based materials were collected from an urban transformation area after being categorized. A two-step crushing-grinding process was used to pulverize each CDW-based material. In the first step, materials were crushed and downsized using a laboratory-type jaw

crusher with a 1 mm jaw opening. Later, crushed materials were placed into a laboratory-type mill with steel balls and ground for an hour in the second step.

The digital images of the original, ground CDW-based precursors and their SEM images are shown in Fig. 3.1. The particle size distributions and characteristic particle diameters are demonstrated in Fig. 3.2 and Table 3.1, respectively. As seen, at least 90% of all precursors passed through 50 μm, which can be considered satisfactory. According to Komnitsas et al. [121], the mechanical performance of geopolymers can be significantly enhanced using precursors with particle size fractions of 50% that pass through a 15 μm sieve (d(0.5) < 15 μm). Correspondingly, d(0.5) values are 5.39 μm, 8.50 μm, and 4.75 μm for HB, RCB, and RT, respectively.

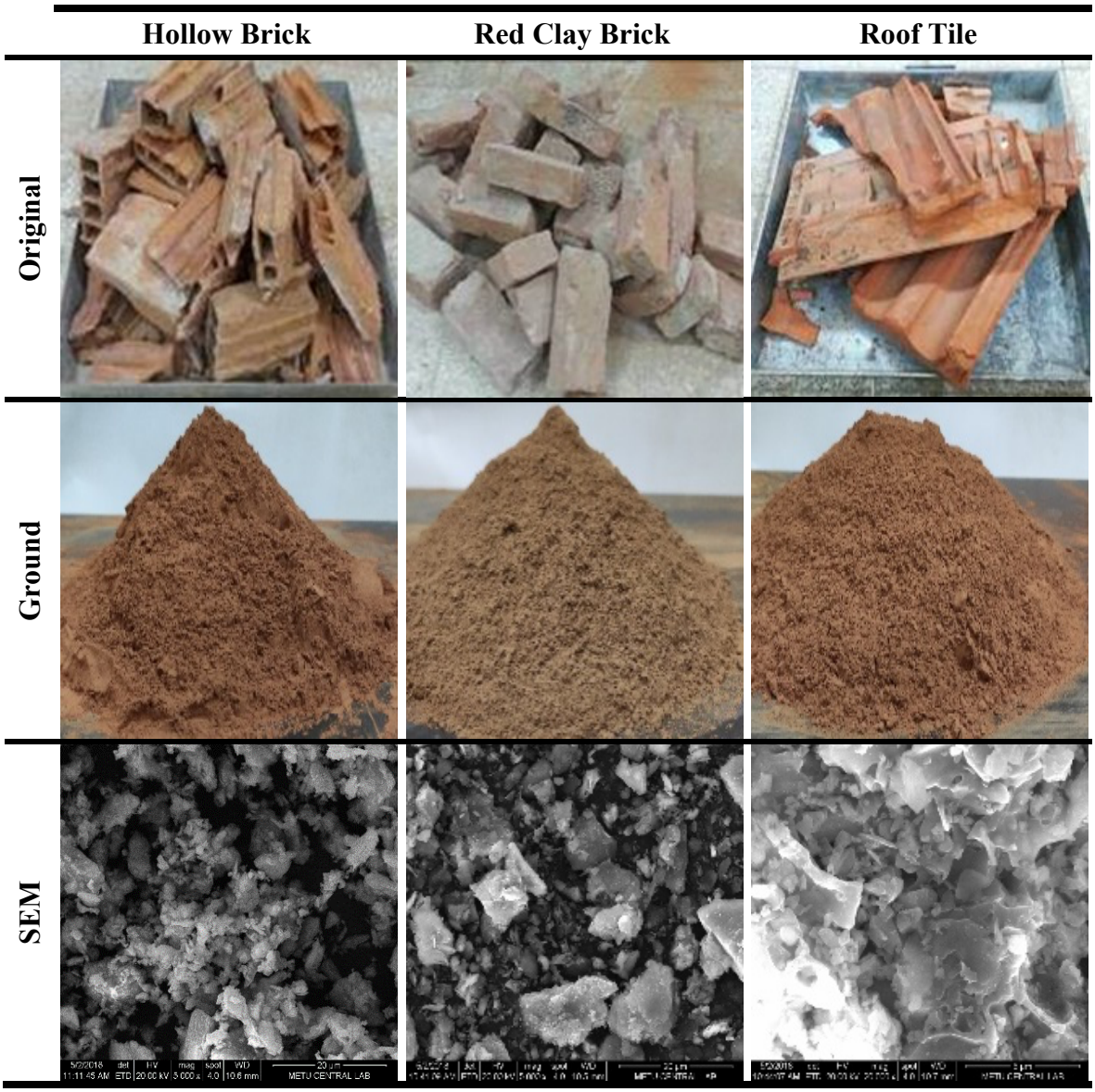

Fig. 3.1. Representative original, ground, and SEM views of CDW-based precursors

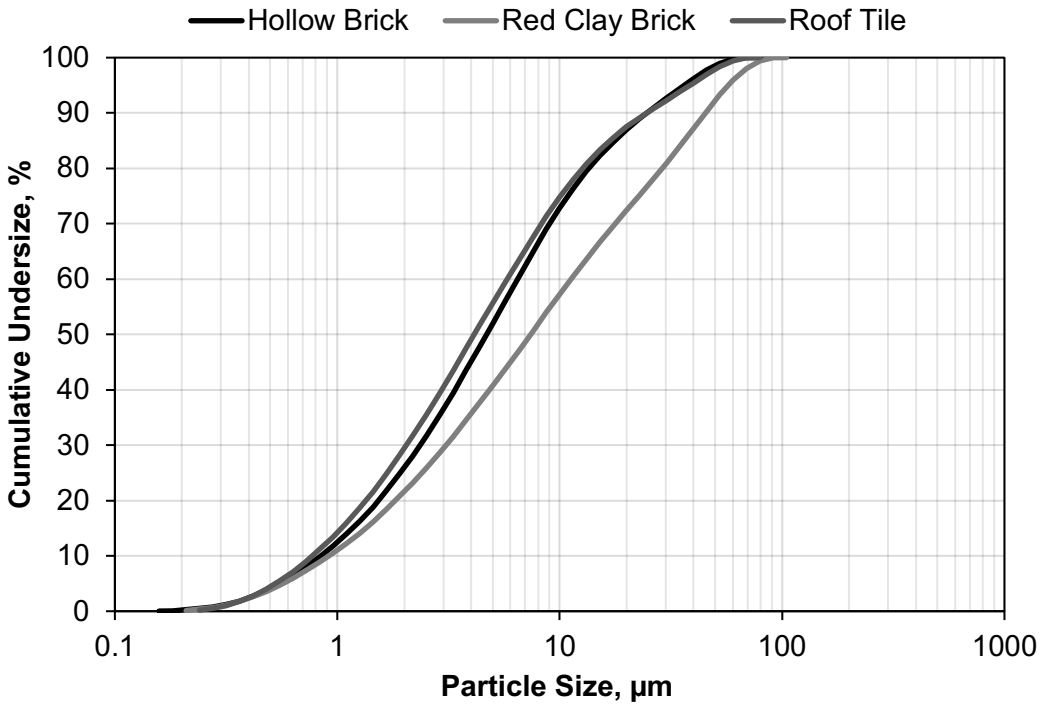

Fig. 3.2. Particle size distributions of CDW-based precursors

Table 3.1. Characteristic particle diameters of CDW-based precursors (units in μm)

Properties	Hollow Brick	Red Clay Brick	Roof Tile
Surface-weighted mean diameter D[3.2]	2.45	2.89	2.32
Volume-weighted mean diameter D[4.3]	10.45	18.00	10.26
d(0.1)	0.97	1.06	0.89
d(0.5)	5.39	8.50	4.75
d(0.9)	28.42	51.85	28.38

The chemical compositions of CDW-based precursors as determined by X-ray fluorescence (XRF) analysis are presented in Table 3.2. As discussed earlier, the CDW-based precursors are very suitable materials for geopolymerization due to their high SiO_2 and Al_2O_3 contents. Accordingly, the total SiO_2 and Al_2O_3 contents of HB, RCB, and RT are around 70±3%.

Table 3.2. Chemical compositions of CDW-based precursors

Chemical Composition, %	Hollow Brick	Red Clay Brick	Roof Tile
Loss on ignition	4.91	4.68	6.64
SiO_2	53.5	52.4	49.3
Al_2O_3	19.3	19.9	20.0
Fe_2O_3	7.45	7.92	8.16
CaO	4.21	4.18	5.16
MgO	2.61	2.84	3.29
SO_3	1.46	0.95	0.79
Na_2O	1.50	1.58	1.23
K_2O	3.58	3.72	3.67
TiO_2	0.92	1.06	1.08

X-ray diffraction (XRD) analysis of the precursors is displayed in Fig. 3.3. Also, the powder diffraction file (PDF) numbers with chemical formulas of crystal phases are listed in Table 3.3. The RT, RCB, and HB precursors were semi-crystalline structures with slight discrepancies and comparable XRD patterns. As expected, apparent Quartz peaks were found at 26.5° in all CDW-based precursors. The observed quartz mineral is a tetrahedral structure created between silicon atoms and oxygen that crystallizes in the hexagonal system and has beneficial impacts on the mechanical characteristics of geopolymers due to its ability to provide barriers for crack propagation [200]. Apart from quartz, the major peaks were detected as cristobalite, tridymite, diopside, and lazurite crystals for CDW-based precursors. The tridymite and cristobalite phases are open-structured silica polymorphs that can dissolve twice as fast as quartz in an alkaline environment [201]. These phases arise from the sintering of masonry units at 800–1000 °C, which causes changes in crystalline clay networks [151].

Table 3.3. Crystalline phases of the precursors as determined by the XRD analyses

Crystalline phase	Symbol	PDF number	Chemical formula
Quartz	Q	96-901-1494	SiO_2
Cristobalite	Cr	96-900-1581	SiO_2
Tridymite	T	96-901-3394	SiO_2
Diopside	D	96-900-1333	$Al_{0.06}\,Ca_{0.91}\,Fe_{0.1}\,Mg_{0.91}\,Na_{0.05}\,O_6\,Si_{1.97}$
Lazurite	L	96-901-1357	$Al_{2.91}\,Ca_{0.6}\,Na_{3.48}\,O_{11.52}\,Si_{3.09}$

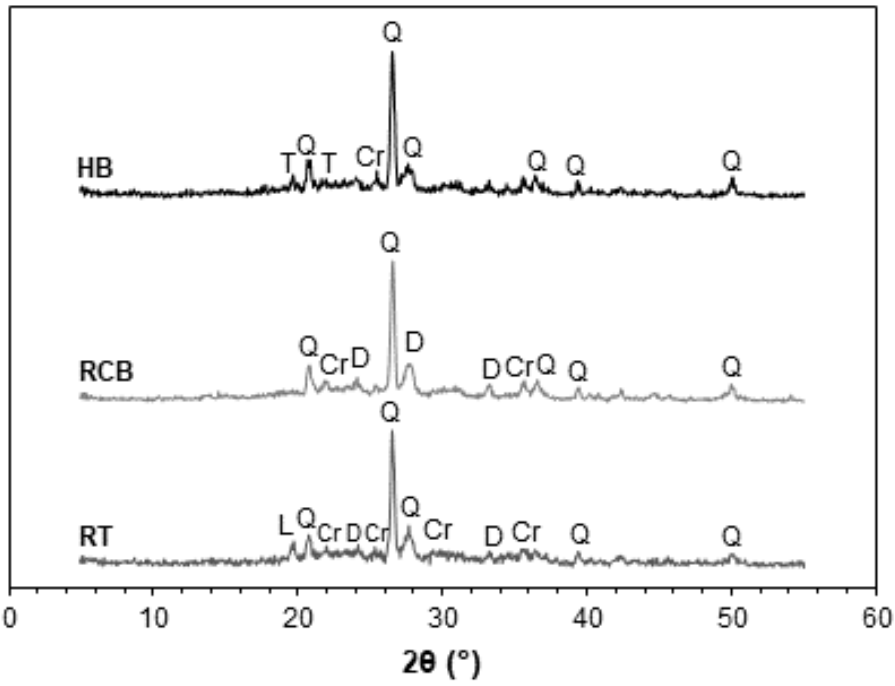

Fig. 3.3. X-ray diffractograms of CDW-based precursors

Recycled concrete aggregate (RCA), finer than 5 mm, was obtained from concrete waste (CW) collected from the urban transformation area, with unknown properties. Firstly, CW was crushed with the help of a hammer drill, and then fed into a jaw crusher to reduce the particle size. In this stage, jaw opening of the crusher was set to 5 mm, 2 mm, and 1 mm to ensure obtaining RCA with different sizes. Afterward, obtained RCA was passed through sieves having 4.75-2.00-0.85-0.10 mm openings, respectively. Lastly, it was assorted into three different size ranges 4.75-2.00 mm, 2.00-0.85 mm, and 0.85-0.10 mm. The views and physical properties of RCA are illustrated in Fig. 3.4 and Table 3.4, respectively.

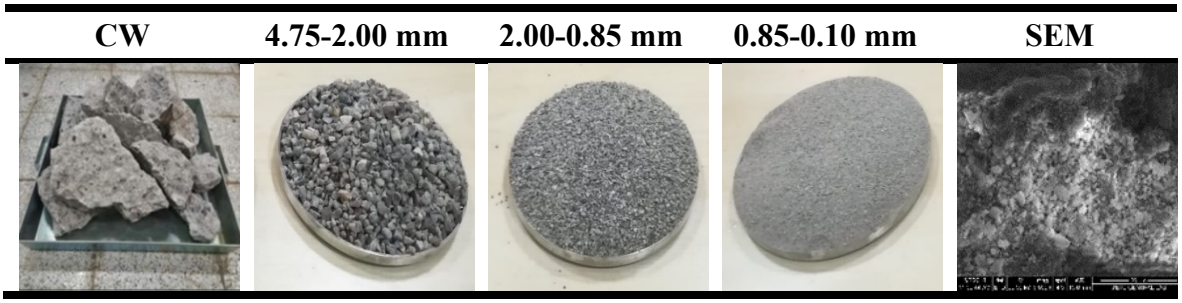

Fig. 3.4. Digital images of CW with original, 4.75-2.00 mm, 2.00-0.85 mm and 0.85-0.10 mm particle size ranges, and its SEM image

Table 3.4. Physical properties of RCA according to particle size ranges

Properties	4.75-2.00 mm	2.00-0.85 mm	0.85-0.10 mm
Compacted bulk density, kg/m^3	1395.8	1338.9	1346.4
Loose bulk density, kg/m^3	1261.5	1198.2	1251.3
Specific gravity	2.44	2.32	2.11
Water absorption, %	4.07	6.81	13.09
Porosity, %	9.48	14.76	24.42

For an alkaline activation, commercially available sodium hydroxide with a minimum of 98% sodium hydroxide, a maximum of 0.4% sodium carbonate, 0.1% sodium chloride, and a maximum of 15 ppm iron was used in a flake form.

3.2.2. Mixture Design

In the scope of the experimental program, a total of 81 mixtures (27 different combinations for each precursor type) were prepared depending on the precursor type (HB, RCB, and RT), molar concentration of sodium hydroxide solution (10M, 15M, and 19M), aggregate size (4.75-2.00 mm, 2.00-0.85 mm, 0.85-0.10 mm), and aggregate/binder ratio (0.36, 0.45, and 0.55) parameters. Additionally, these mixtures were subjected to three different curing temperatures of 105°C, 115°C, and 125°C for 72-hour. Accordingly, the mixture proportions of the CDW-based geopolymer mortars are given in Table 3.5.

The mixtures were coded in this order: precursor type-aggregate size-molarity of sodium hydroxide solution-aggregate/binder ratio. However, for the sake of simplicity, the mixtures were collectively presented under the CDW title instead of listing the precursors separately in Table 3.5. Additionally, aggregate sizes were abbreviated for simplicity as 4.75-2.00 mm [A], 2.00-0.85 mm [B], and 0.85-0.10 mm [C]. For instance, HB-C-19-0.55 coded mixture corresponds to hollow brick-based geopolymer mortar containing 0.85-0.10 mm RCA activated with 19M sodium hydroxide solution and 0.55 aggregate/binder ratio.

Table 3.5. Mixture proportions

Precursor, 1000gr	Mixture ID.	RCA/binder	RCA, gr	Molarity	NaOH, gr	RCA size, mm
CDW (HB, RCB or RT)	**CDW-A-10-0.36**	0.36	360	10	139.09	4.75-2.00
	CDW-A-15-0.36			15	208.73	
	CDW-A-19-0.36			19	260.91	
	CDW-A-10-0.45	0.45	450	10	139.09	
	CDW-A-15-0.45			15	208.73	
	CDW-A-19-0.45			19	260.91	
	CDW-A-10-0.55	0.55	550	10	139.09	
	CDW-A-15-0.55			15	208.73	
	CDW-A-19-0.55			19	260.91	
	CDW-B-10-0.36	0.36	360	10	139.09	2.00-0.85
	CDW-B-15-0.36			15	208.73	
	CDW-B-19-0.36			19	260.91	
	CDW-B-10-0.45	0.45	450	10	139.09	
	CDW-B-15-0.45			15	208.73	
	CDW-B-19-0.45			19	260.91	
	CDW-B-10-0.55	0.55	550	10	139.09	
	CDW-B-15-0.55			15	208.73	
	CDW-B-19-0.55			19	260.91	
	CDW-C-10-0.36	0.36	360	10	139.09	0.85-0.10
	CDW-C-15-0.36			15	208.73	
	CDW-C-19-0.36			19	260.91	
	CDW-C-10-0.45	0.45	450	10	139.09	
	CDW-C-15-0.45			15	208.73	
	CDW-C-19-0.45			19	260.91	
	CDW-C-10-0.55	0.55	550	10	139.09	
	CDW-C-15-0.55			15	208.73	
	CDW-C-19-0.55			19	260.91	

3.2.3. Casting, Curing, and Testing Details

The production procedure of the CDW-based geopolymer mortars began with the preparation of sodium hydroxide solutions. NaOH pellets were dissolved in tap water at different concentrations corresponding to 10M, 15M, and 19M and allowed to cool in the laboratory until room temperature was attained. In the mixing stage, the CDW-based precursors and RCA were put into a mortar mixer at 100 rpm for 60 seconds. Then, NaOH solution was slowly added to the mixture for 30 seconds, and mixing was continued for 210 seconds. In the last stage, the mortar was allowed to mix for an additional 60 seconds at 150 rpm before the end of mixing. Eventually, the fresh mortars were cast into pre-oiled cubic

molds having dimensions of 50×50×50 mm and placed immediately into the oven for 72-hour heat cure. The water/binder ratio was kept constant for all mixtures at 0.35. Following the heat curing, the CDW-based geopolymer mortars were immediately removed and demolded. The views of cubic specimens in the fresh state, after curing, and hardened state are shown in Fig. 3.5.

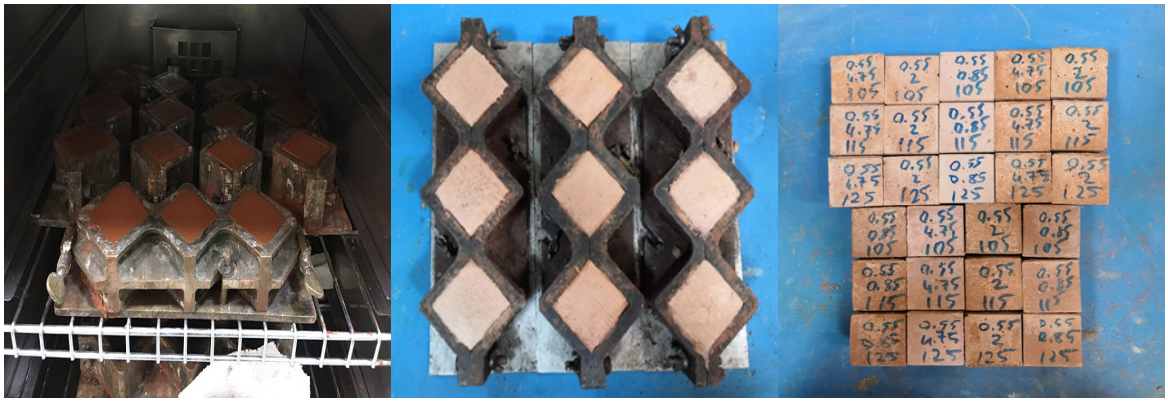

Fig. 3.5. Views of cubic specimens in the fresh state, after curing, and in the hardened state (left to right)

The mechanical performance characterization was made through a compressive strength test, widely accepted in practical applications, according to ASTM C109 [202]. The tests were performed using cubic specimens with 50×50×50 mm dimensions at a 100-ton capacity loading device. Besides, the compressive strength results of CDW-based geopolymer mortars were evaluated by Pearson Correlation to determine statistically which parameter was more effective on strength. The Pearson's correlation coefficient is a tool used to determine how much a relationship exists between two variables. It can have a value between -1 and 1, with -1 indicating a strong inverse relationship, 0 indicating no relationship and 1 indicating a strong direct relationship [203]. Along with the compressive strength test, line mapping analysis through a scanning electron microscope was made to reveal the aggregate, paste, and ITZ structures in CDW-based geopolymer mortars containing RCA with different sizes. The process involves scanning a small sample area with an electron beam in a linear pattern, and then determining the composition and distribution of elements on the sample's surface.

3.3. Macro- and Micro-mechanical Test Results and Discussions

3.3.1. Compression Strength Results

In Fig. 3.6, the compressive strength results of CDW-based geopolymer mortars are illustrated. The results are presented as the average compressive strength results of six cubic specimens. Among all mortars, the strength results ranged between 66.2 and 23.1 MPa with a maximum deviation of ±6 MPa. Additionally, in Table 3.6, the correlation coefficients of the CDW-based mortar strength for aggregate size, curing temperature, sodium hydroxide, and aggregate/binder ratio are provided to evaluate which parameter contributed more to the compressive strength. In parallel, the highest correlation coefficients, the indicators of improved compressive strength, were achieved by aggregate size as -0.679, -0.555, and -0.676 for HB, RCB, and RT precursors, respectively. Here, the minus sign indicates that the relationship is inverse, which means the strength increases with the decrease in aggregate size. On the other hand, the aggregate/binder ratio was the least effective parameter considering the lowest correlation coefficients. Detailed discussions of the compressive strength results are given in the following sections.

Table 3.6. Pearson Correlation for the strength results of the geopolymer mortars strength with aggregate size, curing temperature, sodium hydroxide molarity, and aggregate/binder ratio

Precursor		Aggregate size	Molarity	Temperature	Aggregate/binder
HB	Pearson Correlation	-0.679	0.261	-0.198	-0.001
	Sig. (2-tailed)	0.000	0.019	0.076	0.991
	N	81	81	81	81
RCB	Pearson Correlation	-0.555	0.462	-0.243	0.048
	Sig. (2-tailed)	0.000	0.000	0.029	0.669
	N	81	81	81	81
RT	Pearson Correlation	-0.676	0.357	-0.144	0.052
	Sig. (2-tailed)	0.000	0.001	0.198	0.644
	N	81	81	81	81

Note: Sig. (2-tailed): Significance level, should be under 0.05 (%).

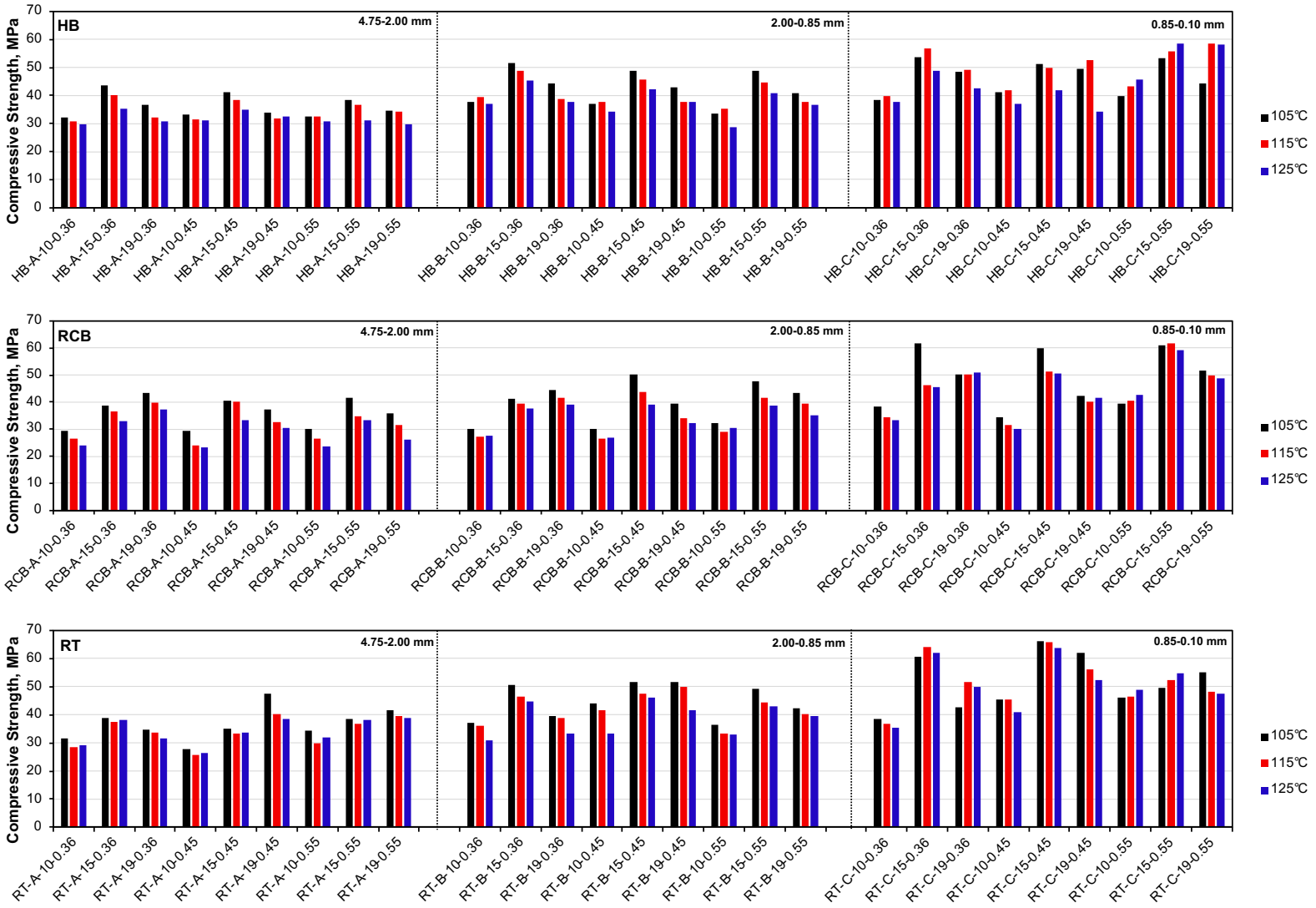

Fig. 3.6. Compressive strength results of CDW-based geopolymer mortars

3.3.2. Effect of Precursor Type

Considering CDW-based precursor types, the RT-based geopolymer mortars achieved the highest average compressive strength, followed by HB- and RCB-based geopolymer mortars, respectively. Among all mixtures, the maximum compressive strength was 66.2 MPa, achieved by the RT-C-15-0.45 coded mixture. As discussed in earlier sections, the mechanical performance can be remarkably enhanced when the d(0.5) value is smaller than 15 μm [121]. Accordingly, d(0.5) values of precursors were 5.39 μm, 8.50 μm, and 4.75 μm for HB, RCB, and RT, respectively. Finer particles may have better reactivity and stronger geopolymerization, leading to an improved paste with a denser microstructure. This is primarily due to the increased specific surface area, which increases the reaction rate since the dissolution phase proceeds faster, resulting in an accelerated setting and rapid strength development [23].

Another key parameter affecting the strength is the precursors' chemical compositions, which are crucial for promoting geopolymerization [204]. However, the total amount of siliceous and aluminous oxides of HB, RCB, and RT precursors is 72.8%, 72.3%, and 69.3%, which can be accepted as almost identical despite the minor deviations. In summary, it was confirmed that any masonry-based waste could be successfully used as a precursor in geopolymer synthesis regardless of the origin if it was finely ground enough.

3.3.3. Effect of Aggregate Size

A significant amount of fine powder is generated during the crushing process of RCA, accounting for around 15-20% of total waste concrete [205]. Therefore, it is crucial for the sustainability of the construction industry to focus on increasing the replacement level of RCA, rather than avoiding its use. However, aggregate size plays a critical role in the mechanical properties of geopolymers, similar to cementitious materials. Moreover, fine RCA usage has more impact than natural sand due to the parameters related to old adhered mortar, such as ITZ characteristics and high water absorption capacity [206]. Accordingly, regardless of all other parameters except aggregate size, the average compressive strengths of CDW-based geopolymer mortars with the use of 4.75-2.00 mm, 2.00-0.85 mm, and 0.85-0.10 mm sized RCA were found to be 33.9 MPa, 39.6 MPa, and 48.3 MPa, respectively.

As expected, aggregate size was found to be the most dominant parameter of the mechanical performance, which can be easily concluded from the Pearson correlation coefficients given in Table 3.6. These coefficients were -0.679, -0.555, and -0.676, which were the indicators of a strong relationship between strength and aggregate size for HB, RCB, and RT precursors, respectively. The mechanical properties were significantly improved as the aggregate size decreased. The main reason for increased strength is the particle packing effect of smaller-sized aggregates, resulting in a denser matrix [207]. Another reason is the improvement in ITZ characteristics, which is directly linked with mechanical performance, as the aggregate size reduces [208]. This improvement will be detailed in the following sections.

3.3.4. Effect of Concentration of Sodium Hydroxide Solution

In this thesis, sodium hydroxide solutions with three different concentrations (10M, 15M, and 19M) were used to understand the effect of different molarities on the compressive strengths of geopolymer mortars. Regarding the results listed in Fig. 3.6, the CDW-based geopolymer mortars prepared with 15M NaOH solution reached the highest strength result. Regardless of the other parameters, CDW-based geopolymer mortars activated with 10M, 15M, and 19M sodium hydroxide solutions yielded 34.2 MPa, 46.0 MPa, and 41.6 MPa average compressive strength results, respectively.

As a general trend, it was observed that the compressive strength sharply increased in the transition from 10M to 15M, while there was a slight decrease in 19M. For instance, considering the RT-C-10-0.45, RT-C-15-0.45, and RT-C-19-0.45 specimens cured at 115 °C, the compressive strength results were found to be 45.5, 66.2, and 61.9 MPa, respectively. Besides, most mixtures followed this trend, as seen in Fig. 3.6. Indeed, the mechanical characteristics of geopolymers strengthen with increasing hydroxide concentration in solution. However, this enhancement is not constant; rather, there is an optimum alkali concentration range, which allows for a higher level of silica and alumina leaching [209]. If the molarity of the hydroxide solution exceeds the optimum alkali concentration range, the mechanical properties decline due to the increased viscosity, which makes the leaching of Si and Al atoms difficult [23].

On the contrary, using sodium hydroxide solution with a low concentration causes poorer geopolymerization because of inadequate alkalinity, which reduces the dissolution rate of Si and Al. As the concentration of hydroxide solution approaches the optimum range, the rate of dissolution rises, resulting in higher strength due to the increased amount of OH^- ions [121].

Consequently, sodium hydroxide solution with a 15M concentration yielded higher strengths and was found to be the optimum molarity. However, the impact of an alkali solution differs by precursor. For instance, as listed in Table 3.6, RCB had the highest Pearson Correlation coefficient of 0.462, while this corresponded to 0.261 and 0.357 for HB and RT, respectively. This showed that the relation between the strength and molarity of hydroxide solution was more prominent in RCB compared to other precursors. Since the particle fractions of RCB were coarser than others, it can be concluded that the effect of fineness on compressive strength differs depending on the molarity of sodium hydroxide.

3.3.5. Effect of Curing Temperature

Curing temperature is one of the most critical factors affecting the mechanical properties of geopolymers due to its role in controlling reaction rate [210]. As a result of the experimental studies, the optimum curing temperature was 105 °C since the average compressive strength of specimens cured at this temperature became 42.7 MPa. The results reduced to 40.7 MPa and 38.4 MPa for specimens cured at 115 °C and 125 °C, respectively. According to the obtained results, the general tendency is that the compressive strength decreases as the temperature increases for the tested temperature intervals in this thesis study. However, the predetermined curing temperatures also have great importance in the confirmation of this statement. For instance, at lower curing temperatures, the increase in temperature (up to 110 °C) mostly improves the mechanical properties of CDW-based geopolymer materials [26,62,211]. Therefore, there is an optimum range of temperature for strong geopolymerization rather than a linear relationship, similar to alkaline solutions. When the curing temperature exceeds this threshold, the compressive strength gradually decreases due to the deterioration of reaction products at higher temperatures [211], formation of cracks and drying shrinkage [212], or loss of humidity required for polymerization [213]. Conversely, the dissolution of silica and alumina decelerates at low curing temperatures or ambient conditions, resulting in slower poly-condensation with weak paste properties [23].

3.3.6. Effect of Aggregate/Binder Ratio

Three different aggregate/binder ratios (0.36, 0.45, and 0.55) were selected to investigate the effect of aggregate/binder ratio on the compressive strength of the CDW-based geopolymer mortars. The results showed that the average compressive strengths of the mortars designed with 0.36, 0.45, and 0.55 aggregate/binder ratios were determined as 40.2 MPa, 40.6 MPa, and 42.2 MPa, respectively. Although the mortars containing highest amount of aggregate (0.55 aggregate/binder ratio) exhibited slightly better mechanical performance, it can be negligible since the differences between the results were very low.

As also shown in Table 3.6, the aggregate/binder ratio, which had the smallest Pearson Correlation coefficient among all parameters, was found to be the least effective parameter on the compressive strength. Although the replacement ratio of RCA significantly affects the mechanical properties of geopolymer-based materials [214], it was found ineffective in CDW-based geopolymer mortars, considering the replacement ratios used in the study. However, RCA is mostly substituted with natural aggregate at certain ratios rather than a full replacement.

On the contrary, in this study, since the RCA had already been fully replaced in all mixtures, there were no significant changes in mechanical properties depending on the aggregate/binder ratio. Another point is that the effect of RCA replacement is directly linked to the targeted strength of the material [215]. For instance, in high-strength concrete, mechanical performance is sharply reduced with increasing RCA replacement due to failure in weaker adhered old mortar. This may not be observed in concretes with low strength since their ultimate strength depends predominantly on paste properties [215].

According to the results, the CDW-based geopolymer mortars produced in the scope of the thesis study can be accepted as moderate-strength mortars (average strength was around 40 MPa). Therefore, this caused the precursor, molar concentration, curing temperature, and aggregate size to gain more importance in strength than the replacement ratio of the RCA.

3.3.7. Interfacial Transition Zone (ITZ)

It is a well-known fact that the ITZ properties have a significant impact on compressive strength [216,217]. Therefore, in this section, ITZ regions were deeply inspected through line mapping analysis. Fig. 3.7 presents the sectional view of RCA obtained from the RCB-B-15-0.55 specimen cured at 115 ºC. This specimen was selected due to exhibiting average compressive strength performance (41.7 MPa), which could provide general information about ITZ in CDW-based geopolymer mortars. In contrast with natural aggregates, the interface properties of RCA with the geopolymer matrix are more complicated [218].

There are two ITZs in the geopolymer matrix when RCA is substituted: the former is the old ITZ between adhered old mortar and original natural aggregates (ITZ_1) and the latter is the new ITZ between new mortar and old mortar connected to the surface of RCAs (ITZ_2). This additional ITZ increases the likelihood of fracture and reduces the bond strength [219]. Therefore, deep prospecting is necessary to investigate the microstructure of the matrix in the case of RCA inclusion.

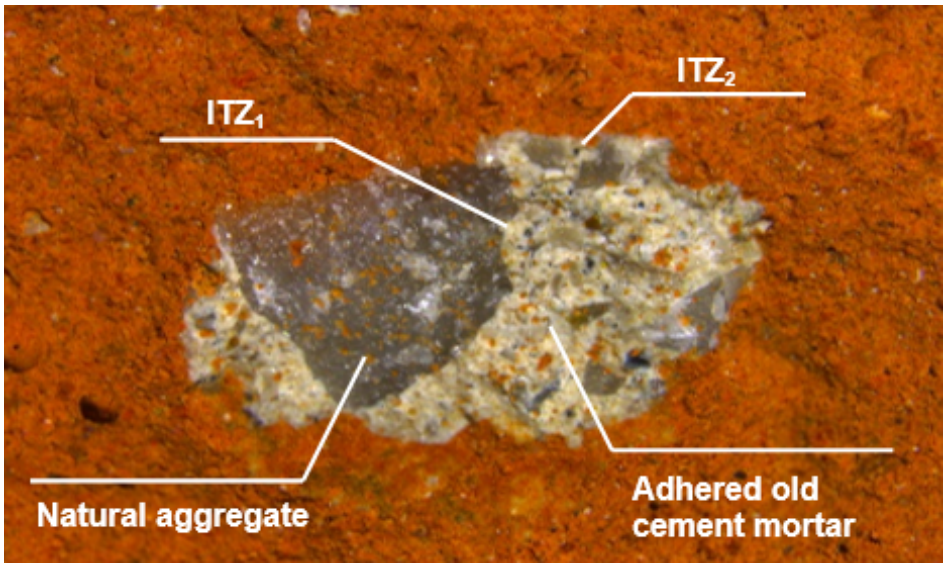

Fig. 3.7. The sectional view of RCA obtained from RCB-B-15-0.55 mixture

In Fig. 3.8 and Fig. 3.9, the line mapping analyses with SEM images of the aggregate-paste connection of RCB-B-15-0.55 coded mixture are displayed. While the former focuses on the RCA with a 1 mm diameter, the latter is obtained from the RCA having a 2 mm. The reason for that is to investigate the effect of aggregate size, which was found to be the main parameter affecting the compressive strengths of mortars, on ITZ properties. As clearly

observed, the ITZ in Fig. 3.8 is narrower and shallower, which confirms the improvement in compressive strength with smaller aggregates, compared to the ITZ shown in Fig. 3.9. The narrowing of ITZ when the use of smaller aggregate was also stated in previous studies [220,221].

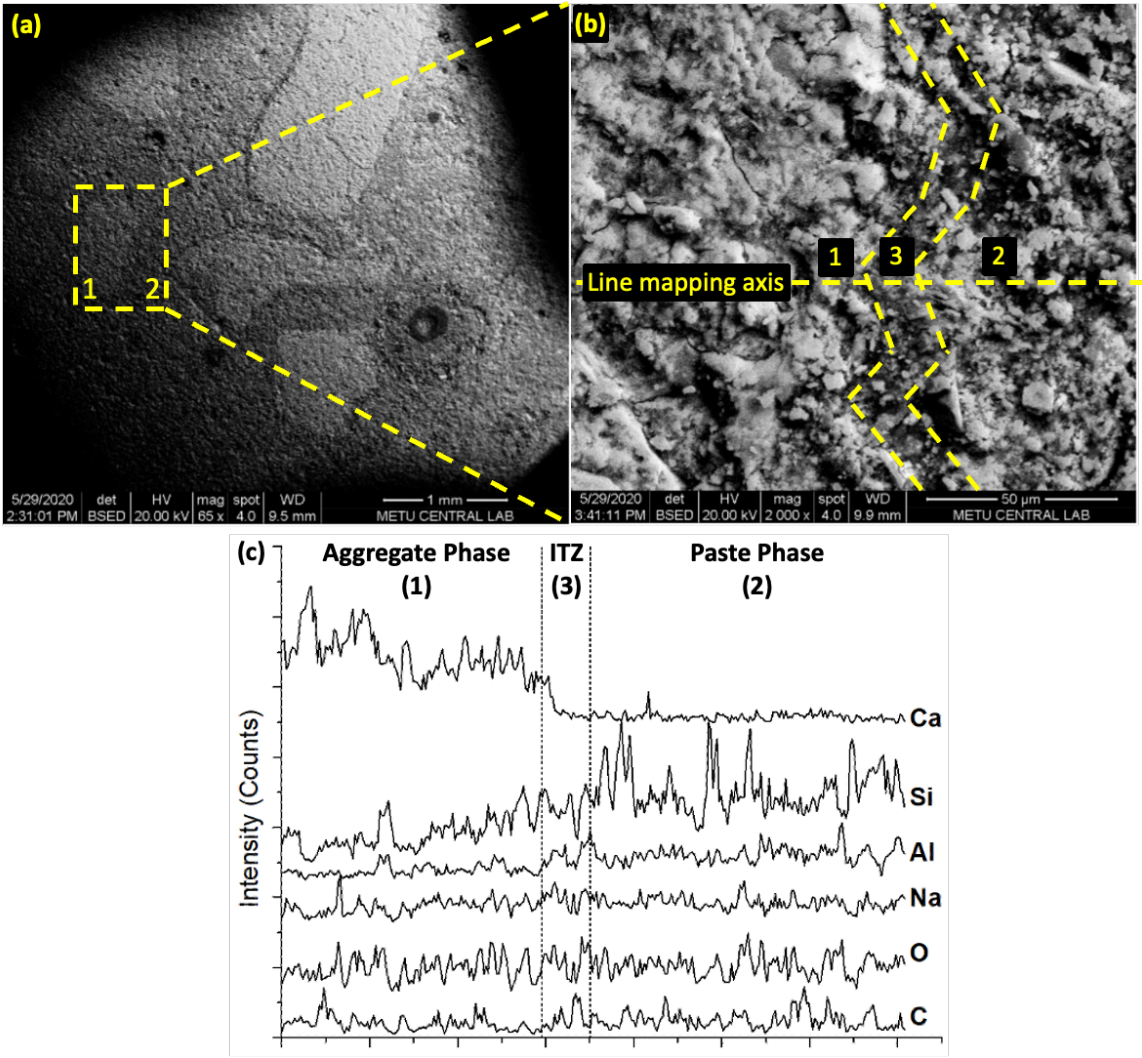

Fig. 3.8. SEM images of aggregate (1mm) paste connection (a) an area [65×] containing both aggregate (1) and geopolymer paste (2), (b) zoomed view [2000×] of yellow dotted area plotted in a (arrows point out the ITZ), (c) mapping analysis of line through aggregate, ITZ, and paste

Another striking point is the difference in the sharpness of changes in ITZ regions between the aggregate and paste. In line with mapping analyses given in Fig. 3.8-c, the changes in Ca and Si intensities at ITZ regions are less gradual, which is an indicator of soft transition and similarity between structures. On the other hand, the intensities of Ca and Si are sharply

changing, as shown in Fig. 3.9. The sharp changes in Fig. 3.9 show that the interface properties of the aggregate and paste phases are significantly different, and the indicator of low bonding strength leads to a decrease in compressive strength. On the other hand, the thinner ITZ in the smaller aggregate explains the higher compressive strength.

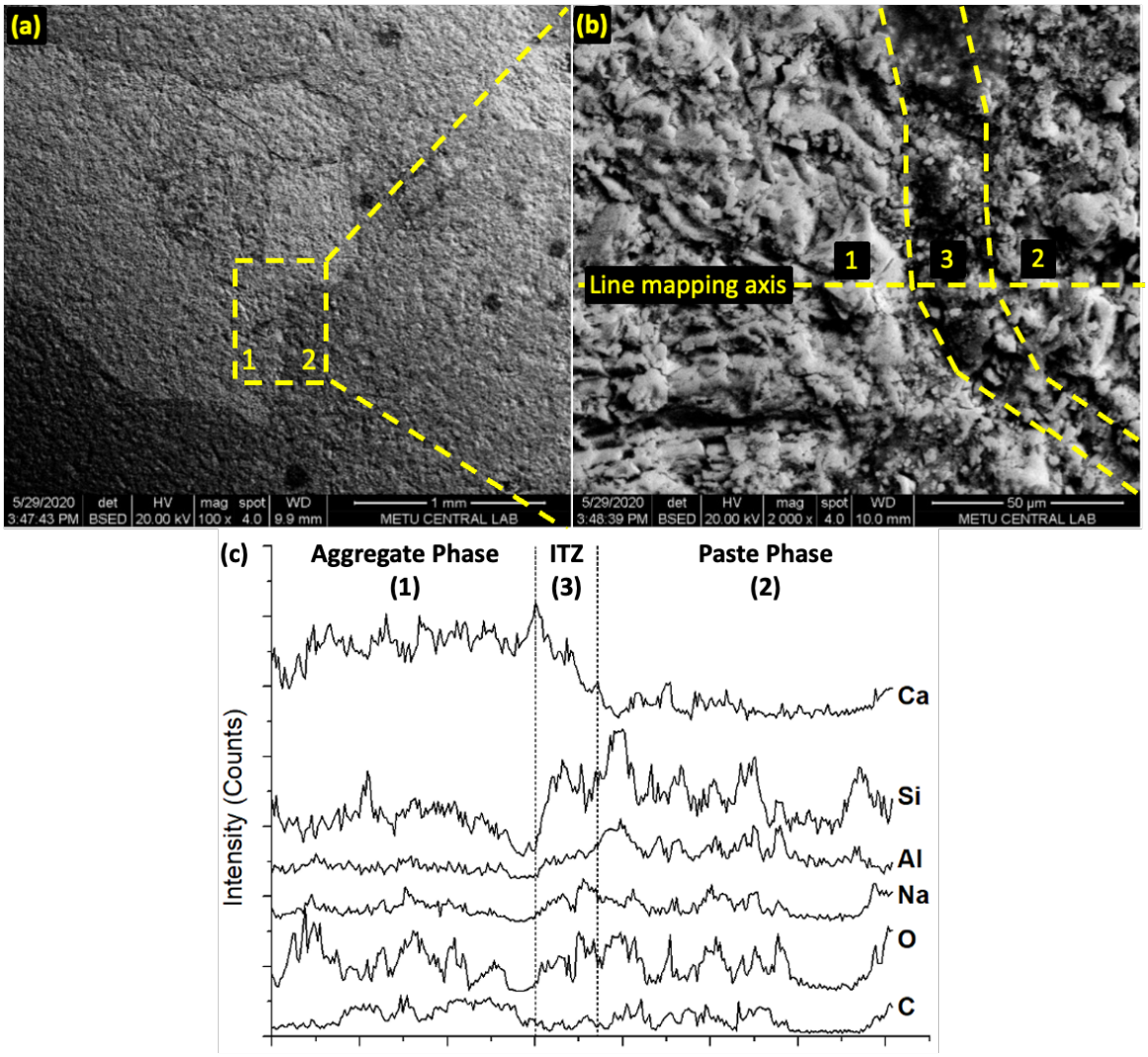

Fig. 3.9. SEM images of aggregate (2mm) paste connection (a) an area [100×] containing both aggregate (1) and geopolymer paste (2), (b) zoomed view [2000×] of yellow dotted area plotted in a (arrows point out the ITZ), (c) mapping analysis of line through aggregate, ITZ, and paste

3.4. Life Cycle Assessment of CDW-based Geopolymer Mortars

3.4.1. Description of the System for LCA

The LCA analysis framework was divided into 3 main stages according to the ISO 14040 and ISO 14044 standards [222,223]. The goal and scope of the study, system boundaries, and functional unit were determined in the first stage. In the second stage, which included the creation of the inventory analysis, the material-energy consumptions and waste-emission productions were defined. In the last stage, the environmental impacts of geopolymer mortars were identified according to the various impact categories. The stages of LCA are detailed in the following sections.

3.4.2. Goal and scope of the study

The current LCA study was performed to highlight the environmental impact of the CDW-based geopolymer mortars and reveal their pros and cons against the PC-based conventional systems. For this purpose, a base mixture from CDW-based geopolymer mortar mixtures, which were produced to investigate mechanical properties, was selected, and a Portland cement-fly ash-based mortar (PCF) mixture with the similar compressive strength class (with an average compressive strength of 47.4 MPa at 28 days) was produced to enable comparison. The reasons behind selecting such kind of mortar for the comparison are the fly ash content, which allows the comparison of a by-product's environmental impact, and the similarity in both mechanical performances and aggregate content. Since the developed geopolymer mortars will be used in developing geopolymer composites in further studies, the design parameters were determined to be similar to a conventional PCF mortar. Fig. 3.10 represents the mixtures that were subjected to LCA analysis. The selection methodology of the mixtures was carried out according to the following steps:

(i) RT-C-10-0.45 was chosen as the base mixture with an average compressive strength of 44.0 MPa for different curing temperatures in RT-C, the group with the highest average compressive strength independent of all parameters.
(ii) In order to examine the environmental impacts of molarity, versions of the base mixture with different molarities (RT-C-15-0.45 and RT-C-19-0.45) were selected.

(iii) Impacts of the binder phase were investigated by the versions of the base mixture prepared with different binder types with the same mixing ratios (HB-C-10-0.45 and RCB-C-10-0.45).

(iv) Versions of the base mix with different aggregate/binder contents (RT-C-10-0.36 and RT-B-10-0.45) were included in the analysis to evaluate the impact of aggregate content, while versions containing the different sizes of aggregate were chosen to compare the particle size impact of aggregate (RT-A-10-0.45 and RT-B-10-0.45).

(v) To reveal the environmental impacts of thermal curing, the versions of the base mixture conducted thermal curing at different heats (105°C, 115°C, and 125°C) were selected.

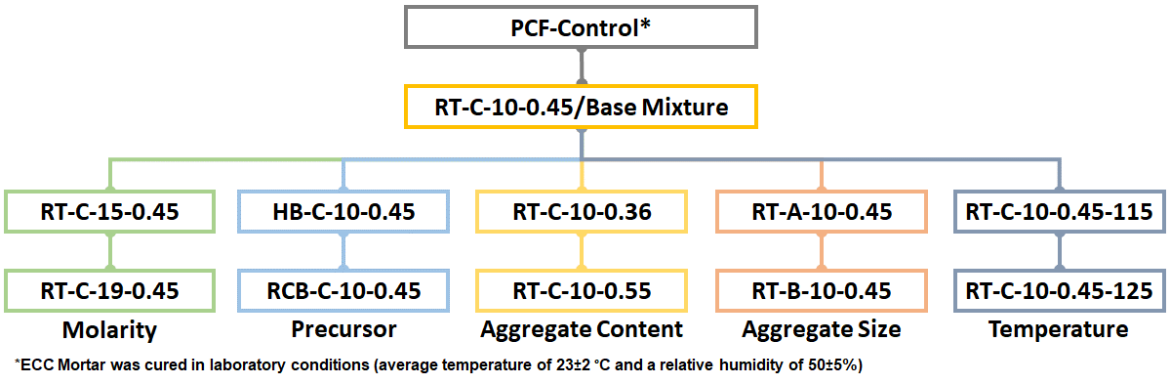

Fig. 3.10. Selected PC-Fly ash-based mortar and CDW-based Geopolymer Mortars for LCA

A system boundary was determined for the production of CDW-based geopolymer mortar, covering transporting, processing, mixing, and curing. The functional unit of the analysis performed with the cradle-to-gate approach was determined to be "1m^3 of CDW-based geopolymer mortar". Fig. 3.11 depicts the system boundary of the CDW-based geopolymer mortar production. The system boundary was determined according to the cradle-to-gate approach; thus, the initiation of the system was the transportation of the CDW elements to the laboratory. Thereafter, the processing of brick-based precursors and waste concrete-based RCA, including the crushing, and grinding/sieving stages (grinding for bricks and sieving for waste concrete), were followed. The alkali activator's components, sodium hydroxide and water were included at the mixing stage of the system. After the mixing stage, the thermal curing process was included. Finally, the system boundary was completed by performing the energy consumption-waste/emissions assignments. For the production of PCF mortar, all ingredients were purchased from suppliers at different locations, and a system boundary was not defined in detail due to a lack of the production details of

ingredients. Therefore, only the transportation and production (mixing stage) data of PCF mortar was integrated into the calculations.

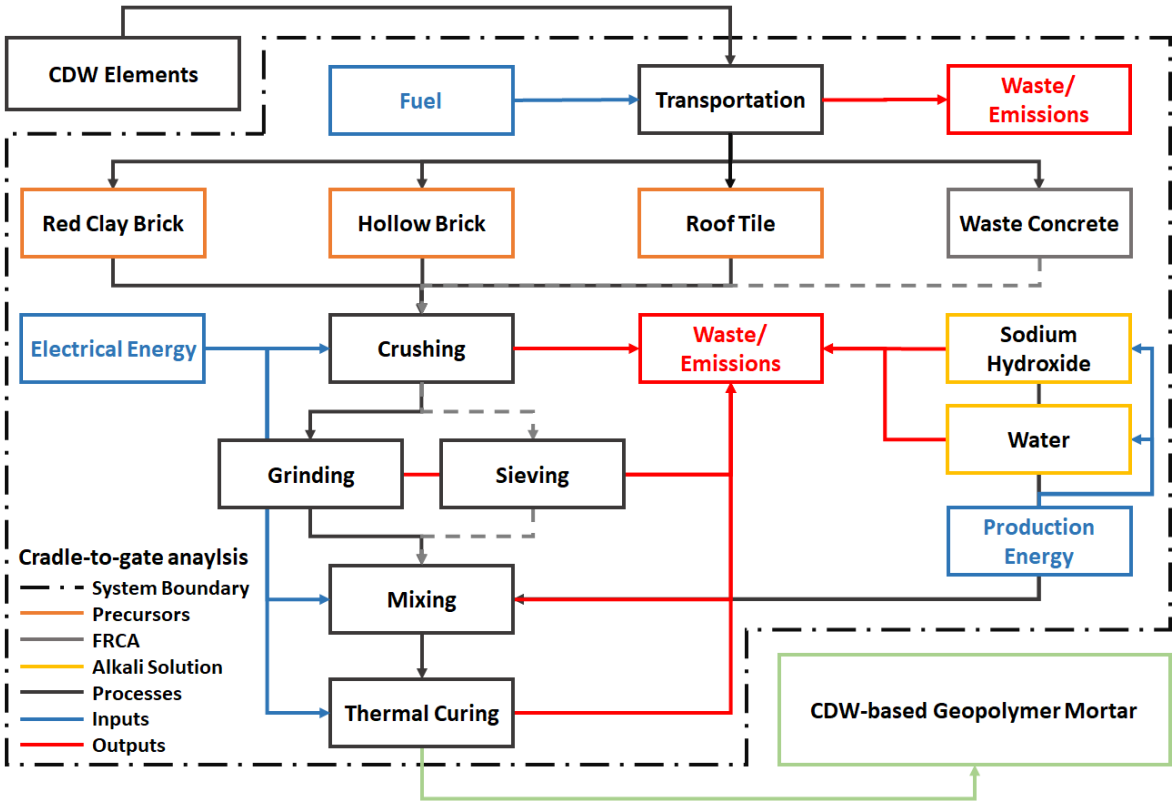

Fig. 3.11. System Boundary to produce 1m^3 of CDW-based geopolymer mortars

3.4.3. Life Cycle Inventory (LCI)

LCI of CDW-based geopolymer mortar mixtures was adopted from experimental studies on a lab scale. To enable a realistic comparison with PCF mortar, the related data was scaled up to an industrial scale using industrial-scale versions of the equipment used for processing the geopolymers in the lab. The main reason behind this approach is that the existing database of cement and silica sand, which are the components of PCF, is based on industrial-scale production procedures, and data on the processing of CDW elements is not available. The transportation and material flows of CDW-based geopolymer mortars are detailed in Table 3.7 and Table 3.8, respectively. Transportation distances were determined by using Google Maps. Depending on the quantity of each material, different types of freight are calculated in tkm, as seen in Table 3.7. The CDW-based precursors were transported from different demolition sites in Ankara, Türkiye, while the Portland cement and silica sand were purchased from a supplier 15.2 km from the laboratory, and the alkaline activator was purchased from a supplier 13.4 km away.

Table 3.7. Transportation inventory for CDW-based geopolymer mortars

Material	Distance (km)	Freight (tkm)*
Portland Cement	15.20	1.12
Fly Ash	553.8	49.1
Silica Sand	15.20	0.89
Superplasticizer	14.20	0.01
Roof Tile	10.90	1.47
Red Clay Brick	9.400	1.27
Hollow Brick	10.90	1.48
Concrete Waste	12.10	0.73
Sodium Hydroxide	13.40	0.28

*Calculated according to the criteria of "amount of material in tonne transported over a specified distance".

Table 3.8 presents the material quantities required for the production of 1 m^3 CDW-based and PCF mortar. To produce the PCF mortar, ordinary Portland cement with a strength class of 42.5 was employed, and silica sand was used as the fine aggregate phase. Since the SimaPro databases do not contain country-specific data for Türkiye on material and energy consumption or emissions caused by these materials throughout their life cycles, the existing data on cement and silica sand were taken into consideration. In this respect, the averaged transformation and market data for different regions were factored into the equation, considering the fact that the data available for cement and silica sand in the databases varied according to the regions.

In addition, the fact that construction and demolition wastes are easily accessible in every region globally is another main reason for the holistic approach to PCF mortar, which is executed by using the average data obtained from different regions in the databases. The data used for the analysis were determined according to transformation data of Switzerland, Europe without Switzerland, the United States, Canada-Quebec, and the Rest of the World for cement, and based on Global, and the Rest of the World for silica sand.

There is no data in the databases on behalf of the production process for the waste bricks that form the precursor phase of CDW-based geopolymer mortars. Because of this, the energy input for the precursor phase was only determined using the energy consumption data of the equipment employed in the pre-processing (crushing & grinding) that was carried out to prepare the materials for alkaline activation. Similar to that, the inputs for the recycling

aggregate were determined by taking the pre-processing into account (crushing & sieving). Since there is no country-specific data for the sodium hydroxide used in the alkali activator phase, Sodium Hyroxide-Rest of the World data in SimaPro was included in the calculations. Tap water, Rest of the World (production with underground water without treatment) data was used for water, the other component of the alkali activator phase.

Table 3.8. Inventory input material flows for PCF and CDW-based geopolymer mortars

PCF Mortar Ingredients (kg/m^3)						
Mixture ID	**PC[1]**	**FA[1]**	**SS[1]**	**SP[1]**	**W[1]**	**Total**
PCF-Control	554.3	665.2	439.0	4.3	329.3	1992.2
Specific Gravity (g/cm^3)	3.06	2.10	2.60	1.10	1.00	

Geopolymer Mortar Ingredients (kg/m^3)								
Comparison Parameters	**Mixture ID**	**RT[1]**	**RCB[1]**	**HB[1]**	**CW[1]**	**SH[1]**	**W[1]**	**Total**
Molarity	**RT-C-10-0.45**	1014.5	-	-	456.5	141.1	355.1	1967.2
	RT-C-15-0.45	981.9	-	-	441.9	205	343.7	1972.4
	RT-C-19-0.45	958.9	-	-	431.5	250.2	335.6	1976.1
Precursor	**RT-C-10-0.45**	1014.5	-	-	456.5	141.1	355.1	1967.2
	HB-C-10-0.45	-	-	1019.7	458.9	141.8	356.9	1977.3
	RCB-C-10-0.45	-	1013.2	-	455.9	140.9	354.6	1964.6
Aggregate Content	**RT-C-10-0.36**	1060.4	-	-	381.7	147.5	371.1	1960.7
	RT-C-10-0.45	1014.5	-	-	456.5	141.1	355.1	1967.2
	RT-C-10-0.55	968	-	-	532.4	134.6	338.8	1973.7
Aggregate Size	**RT-A-10-0.45**	1045.1	-	-	470.3	145.4	365.8	2026.5
	RT-B-10-0.45	1034.8	-	-	465.6	143.9	362.2	2006.5
	RT-C-10-0.45	1014.5	-	-	456.5	141.1	355.1	1967.2
Thermal Curing	**RT-C-10-0.45**	1014.5	-	-	456.5	141.1	355.1	1967.2
	RT-C-10-0.45[2]	1014.5	-	-	456.5	141.1	355.1	1967.2
	RT-C-10-0.45[3]	1014.5	-	-	456.5	141.1	355.1	1967.2
Specific Gravity (g/cm^3)		2.80	2.79	2.84	2.29[4]	2.13	1.00	

[1]PC: Portland Cement, FA: Fly Ash, SS: Silica Sand, SP: Superplasticizer, RT: Roof Tile, RCB: Red Clay Brick, HB: Hollow Brick, CW: Concrete Waste, SH: NaOH, W: Water;
[2]Related mixture was conducted to thermal curing at 115°C;
[3]Related mixture was conducted to thermal curing at 125°C;
[4]Average value for RCAs (RCA-A: 2.440; RCA-B: 2.320; RCA-C: 2.10)

Table 3.9 presents input energy flow data for mixtures. Only the mixing operation that was carried out to prepare the mixture was considered to be the energy consumption input for the PCF mortar; no additional input was allocated for the curing phase due to the ambient curing of the mixture. In addition to the energy inputs for the pre-treatments and mixing procedure for preparing the precursor and recycling aggregate described above, the energy input for the applied thermal curing was also included in the analysis for CDW-based geopolymer mortar mixtures. The total electrical energy consumed during the working period was computed, based on the hourly electricity consumption information, to determine the energy input for the equipment. Relevant calculations have been scaled-up by using capacity and consumption data of industrial-scale versions of the equipment used in the production process performed in a laboratory. For example, the pre-crushing process to make CDW ready for grinding was performed by a lab-scale jaw crusher with a power consumption of 1.5 kW; 3.5 kg of raw CDW was crushed in 5 minutes and loaded into a ball mill with a power consumption of 1.5 kW for 1 hour to perform the grinding process. Since this process requires a large number of iterations for the production of 1 m^3 CDW-based geopolymer mortar and does not realistically reflect the energy consumption caused by the material's life cycle, the energy consumption calculations were based on the production capacity and power consumption of the industrial-scale versions of the equipment. In this context, the power consumption values for the selected industrial scale ball mill, crusher, sieve, and mixer were 280 kW, 15 kW, 7.4 kW, and 190 kW, respectively. Working capacity was 20 tons for the ball mill and crusher, 10 tons for the sieve, and 120 m^3 for the mixer. For the thermal curing process, a 180 kW industrial walk-in oven with a volume of 21.7 m^3 was chosen. Electricity data for the types of equipment were modeled on the basis of the Türkiye grid mix in the SimaPro database [140].

Table 3.9. Inventory input energy flows for CDW-based geopolymer and PCF mortars

Comparison Parameters	#Mixture ID*	Energy Consumption (MJ)									
		Precursor Preparation		RCA Preparation				Production & Curing (°C)			
		C	G	RCA-A	RCA-B	RCA-C	S	M	105	115	125
	PCF-Control	-	-	-	-	-	-	5.7	-	-	-
Molarity	**RT-C-10-0.45**	2.7	51.1	-	-	1.5	2.5	5.5	17.2	-	-
	RT-C-15-0.45	2.7	49.5	-	-	1.4	2.4	5.6	17.3	-	-
	RT-C-19-0.45	2.6	48.3	-	-	1.4	2.3	5.6	17.3	-	-
Precursor	**RT-C-10-0.45**	2.7	51.1	-	-	1.5	2.5	5.5	17.2	-	-
	HB-C-10-0.45	2.8	51.4	-	-	1.5	2.5	5.6	17.3	-	-
	RCB-C-10-0.45	2.7	51.1	-	-	1.5	2.5	5.5	17.2	-	-
Aggregate Content	**RT-C-10-0.36**	2.9	53.4	-	-	1.2	2.1	5.5	17.2	-	-
	RT-C-10-0.45	2.7	51.1	-	-	1.5	2.5	5.5	17.2	-	-
	RT-C-10-0.55	2.6	48.8	-	-	1.7	2.9	5.6	17.3	-	-
Aggregate Size	**RT-A-10-0.45**	2.8	52.7	1.3	-	-	2.5	5.7	17.7	-	-
	RT-B-10-0.45	2.8	52.2	-	1.4	-	2.5	5.6	17.6	-	-
	RT-C-10-0.45	2.7	51.1	-	-	1.5	2.5	5.5	17.2	-	-
Thermal Curing	**RT-C-10-0.45**	2.7	51.1	-	-	1.5	2.5	5.5	17.2	-	-
	RT-C-10-0.45**	2.7	51.1	-	-	1.5	2.5	5.5	-	17.7	-
	RT-C-10-0.45***	2.7	51.1	-	-	1.5	2.5	5.5	-	-	18.3

*C: Crushing, G: Grinding, RCA: Recycled Aggregate, RCA-A, B, C: Recycled Aggregate Particle Size (A:4.75-2.00 mm, B: 2.00-0.85 mm, C: 0.85-0.10 mm), S: Sieving, M: Mixing; **Related mixture was conducted to thermal curing at 115°C; ***Related mixture was conducted to thermal curing at 125°C

3.4.4. Environmental Impact Assessment

Depending on the LCI analysis, the environmental impacts of CDW-based geopolymer and PCF mortars were determined with SimaPro 9.0 and the Ecoinvent 3.0 embedded database. For the environmental assessment, the TRACI 2.1 V1.05/US 2008 (Tool for Reduction and Assessment of Chemicals and Other Environmental Impacts) Method was used [224]. Environmental impacts selected to be analyzed were Global Warming Potential (GWP), Ozone Depletion Potential (ODP), Acidification Potential (AP), Eutrophication Potential

(EP), and Fossil Fuel Depletion (FFD). The GWP, which reflects the ability to retain heat relative to CO_2 over a hundred-year period, is a reference indicator of the greenhouse impact causing global warming [225]. The ODP is the amount of ozone destroyed by a vapor emission over its entire atmospheric lifetime in comparison to the same mass of CFC-11 (Chlorofluorocarbon) emission [226]. As a consequence of the increased ultraviolet (UV) radiation due to the stratospheric ozone layer depletion [224], ecosystems and human life may be impacted [227]. Acidification, which can affect humans, animals, ecosystems, soil, and ground-surface waters, is caused by Sulfur dioxide (SO_2), nitrous oxides (NO_x), and reduced nitrogen (NH_x) generated by fossil fuel combustion [224]. The AP indicates the total amount of acidic pollutants, including SO_2, NO_x, and NH_x, that have contaminated soil, groundwater, surface water, ecosystems, and other materials [228]. Eutrophication is a phenomenon that causes an overabundance of algae and plants due to the enrichment of nutrients, especially nitrogen and phosphorus, from polluted emissions, wastewater, and fertilizers [229]. In this context, EP represents the total nitrogen emissions from overfertilization that have an adverse effect on the terrestrial and aquatic ecosystems [230]. While this phenomenon reduces the oxygen and solar energy rates in aquatic eutrophication, it causes pollution of plants and groundwater in terrestrial eutrophication [229]. FFD is the TRACI methodology's energy usage indicator with the megajoule (MJ) surplus unit, which reflects how much more energy will be required in the future to extract one unit of fossil fuel [231].

3.4.5. Life Cycle Impact Assessment (LCIA)

The environmental impact assessment results of PCF and CDW-based geopolymer mortars are presented in Table 3.10 and illustrated in Fig. 3.12. At first sight, the promising impact results of CDW-based geopolymer mortars in all categories can be recognized, obviously, except for the ODP and EP. GWP, the most critical and highly weighted impact category according to the European Commission [232] was found to be significantly lower for all geopolymer mortars compared to the PCF control mixture. The AP values were also significantly lower than the PCF mortar for all geopolymer mortars; while the FFD values were found to be similar to PCF mortar except for mixtures produced with high-alkali activator content (RT-C-15-0.45 and RT-C-19-0.45). Reflecting the benefits of recycling waste on environmental impacts to a large extent, geopolymer mortars had 65.9% less GWP, and 34.3% less AP compared to the PCF. Besides, the geopolymerization technique ensured

an 8.2% lower FFD than the PCF, demonstrating that the FFD could be reduced with further optimization. For ODP and EP values, the PCF mortar exhibited the lowest environmental impact compared to the geopolymer mortars. ODP related outputs mainly resulted from the chlor-alkali process in the sodium hydroxide production, which covers the usage of carbon tetrachloride to recover chlorine from gas streams [233,234].

Table 3.10. Environmental impact assessment result mixtures

Comparison Parameters	Impact category	Ozone depletion potential (ODP)	Global warming potential (GWP)	Acidification potential (AP)	Eutrophication potential (EP)	Fossil fuel depletion (FFD)
	Unit	**kg CFC-11 eq**	**kg CO_2 eq**	**kg SO_2 eq**	**kg N eq**	**MJ surplus**
	PCF-Control	2.04E-05	501.1	1.37	0.564	194.2
Molarity	**RT-C-10-0.45**	11.5E-05	178.7	0.941	1.188	186.1
	RT-C-15-0.45	16.7E-05	251.4	1.330	1.679	260.1
	RT-C-19-0.45	20.3E-05	302.8	1.605	2.025	312.5
Precursor	**RT-C-10-0.45**	11.5E-05	178.7	0.941	1.188	186.1
	HB-C-10-0.45	11.6E-05	179.6	0.946	1.194	187.1
	RCB-C-10-0.45	11.5E-05	178.3	0.940	1.187	185.5
Aggregate Content	**RT-C-10-0.36**	12.0E-05	186.3	0.982	1.240	193.9
	RT-C-10-0.45	11.5E-05	178.7	0.941	1.188	186.1
	RT-C-10-0.55	11.0E-05	171.0	0.900	1.136	178.2
Aggregate Size	**RT-A-10-0.45**	11.9E-05	184.0	0.969	1.224	191.6
	RT-B-10-0.45	11.8E-05	182.2	0.960	1.212	189.7
	RT-C-10-0.45	11.5E-05	178.7	0.941	1.188	186.1
Thermal Curing	**RT-C-10-0.45**	11.5E-05	178.7	0.941	1.188	186.1
	RT-C-10-0.45**	11.5E-05	178.8	0.942	1.189	186.2
	RT-C-10-0.45***	11.5E-05	178.9	0.942	1.190	186.3

**Related mixture was conducted to thermal curing at 115°C; ***Related mixture was conducted to thermal curing at 125°C

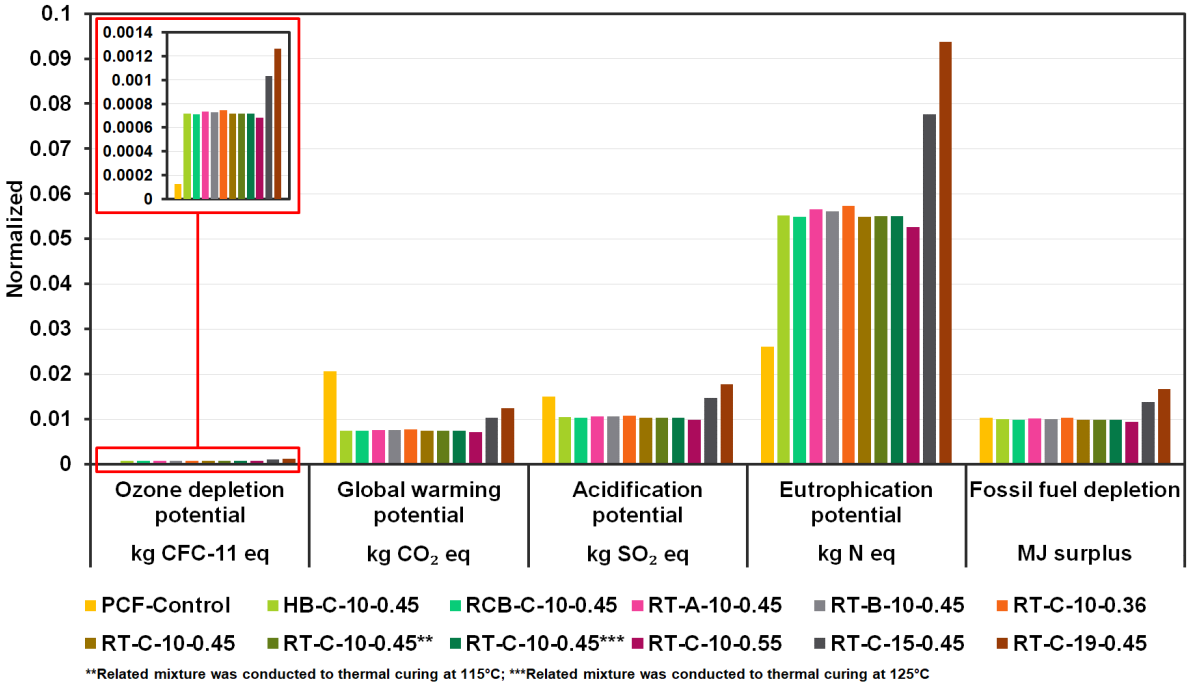

Fig. 3.12. Normalized environmental impact assessment results of PCF and CDW-based geopolymer mortars

3.4.6. Contribution Analysis

At this stage, besides the assessment of the environmental impacts of the selected mixtures discussed above, contribution analysis was performed to evaluate the contribution of each component to the environmental impact categories, individually. As can be inferred from Fig. 3.13, the Portland cement was found to be responsible for approximately 63.7% of the FFD for the PCF-control mixture, whereas this ratio increased up to 93.2% for other environmental impacts. This contribution was followed by the Fly Ash, with a contribution rate varied between 4.5-28.1%, while highest contributions were noted for the ODP and FFD. Considering that only transportation data was included for the Fly Ash, this result was expected since the transportation process directly requires the diesel used in lorries which is responsible for the execrations of fossil and higher CO_2 emissions and eventually makes ODP and FFD more sensitive compared to other environmental impact categories [235].

On the other hand, in the RT-C-10-0.45 coded geopolymer base-mixture, it was observed that sodium hydroxide was responsible for at least 88.18% of the calculated environmental impact values considering all categories. Moreover, the contribution of sodium hydroxide to ODP is calculated as 98.78% and this situation is associated with the release of tetra-chloro methane into the atmosphere, which may damage the ozone layer, due to the electrolysis

process during the production of sodium hydroxide [234]. While the highest impact in the AP, EP, GWP, and FFD categories after sodium hydroxide was found to be driven by the grinding process with values ranging from 4.8 to 5.2%, its impact on the ODP was not noteworthy. Apart from these parameters, thermal curing, which causes environmental effects to be responsible only for electricity consumption, showed a similar proportional distribution but lesser impact than grinding.

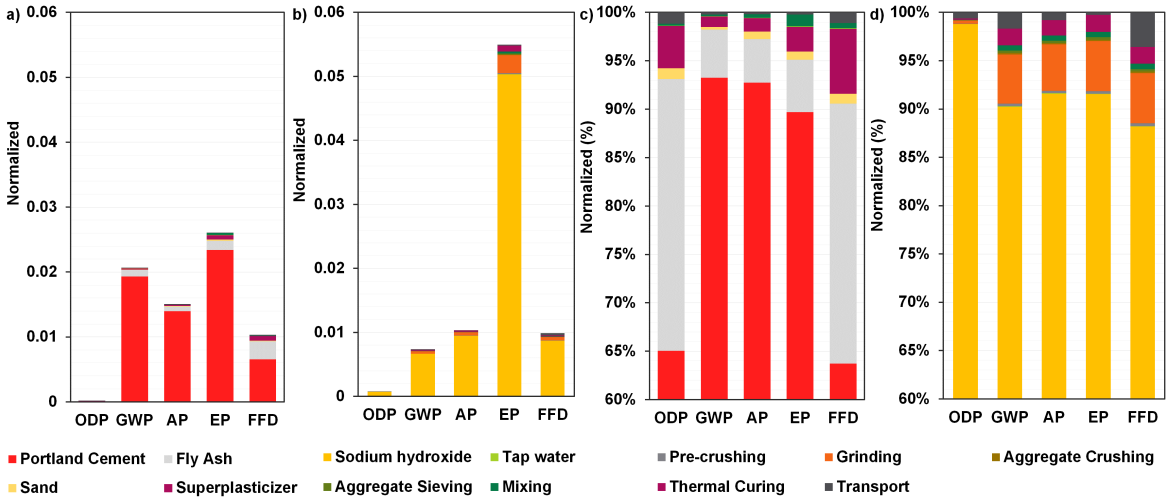

Fig. 3.13. Environmental impacts of PCF-Control and RT-C-10-0.45 (a) Normalized results of PCF-Control (b) Normalized results of RT-C-10-0.45 (c) Contribution of materials and production processes for PCF-Control (d) Contribution of materials and production processes for RT-C-10-0.45

In the following section, the environmental impacts of the differentiation in the parameters such as precursor types, alkali activator content, recycled aggregate content/size, and thermal curing are presented in Fig. 3.14 to 3.18, respectively. In each figure, examined material or process was highlighted with dashed lines. According to Fig. 3.14, considering that RT, HB, and RCB were subjected to the same crushing-grinding processes and all other remaining parameters (i.e., alkali activator, thermal curing, recycled aggregates, etc.) were applied at the same rate and type, it can be stated that different values obtained in the environmental impact categories may be attributed only to the specific gravity of different types of precursors (Table 3.8) and, accordingly, the different weights of the mixtures to be produced in the same volume. For instance, according to Table 3.8, it was seen that a total of 1977.3 kg of material was used in the RCB-based mixture, 1967.2 kg in the RT-based mixture, and 1964.6 kg in the HB-based mixture to produce 1 m^3 of geopolymer, and these values were

completely in the same trend with the values calculated for all environmental impact categories.

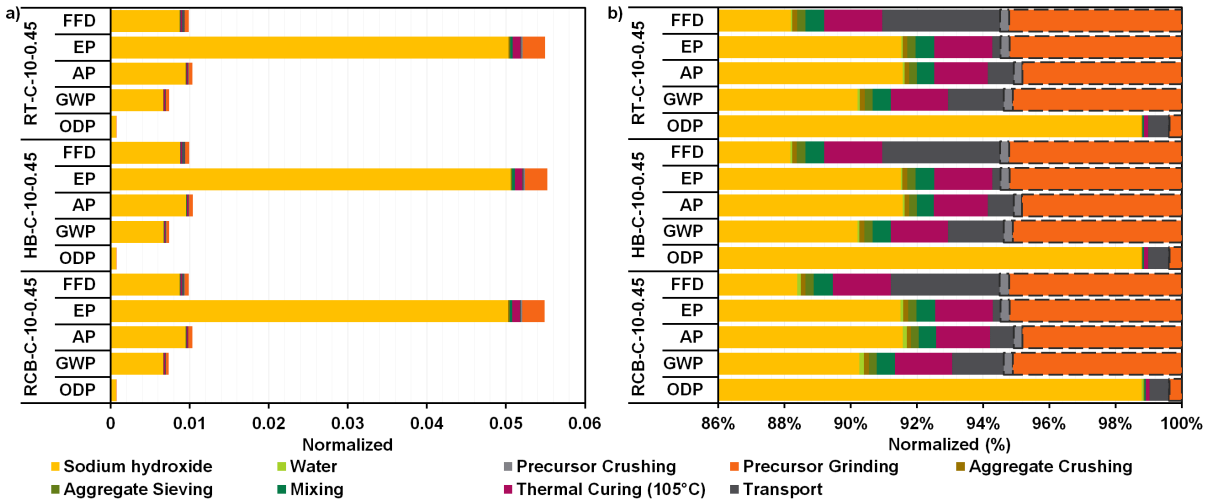

Fig. 3.14. Environmental impacts of precursor type (a) Normalized results (b) Contribution of materials and production processes

Fig. 3.15 depicts the contribution of materials and processes to environmental impacts from a molarity-related point of view. According to Fig. 3.15a, it can be stated that the molarity concentration had a dominant influence on the environmental impacts of geopolymers for all impact categories. At this point, the impact factors for 15M had increased by 39.8–44.7% compared to the 10M concentration, and the increment rates for the transition from 15M to 19M ranged from 20.1-21.9%. The ODP was the category most affected by alkaline activator molarity, with at least 98.8% contribution to environmental impacts, while FFD was the least affected category, with at least 88.2% contribution.

According to Fig. 3.16, an increase in the usage rate of the RCA in geopolymer mortars led to a decrease in environmental burden for all impact categories. However, since the contribution of the RCA usage was significantly lower, the positive impact of the RCA content remained restricted (Fig. 3.16b). For instance, as the RCA content increased up to 0.45 from 0.36, a reduction in environmental impact, regardless of the category, was noted in the range of 4.0-4.3%.

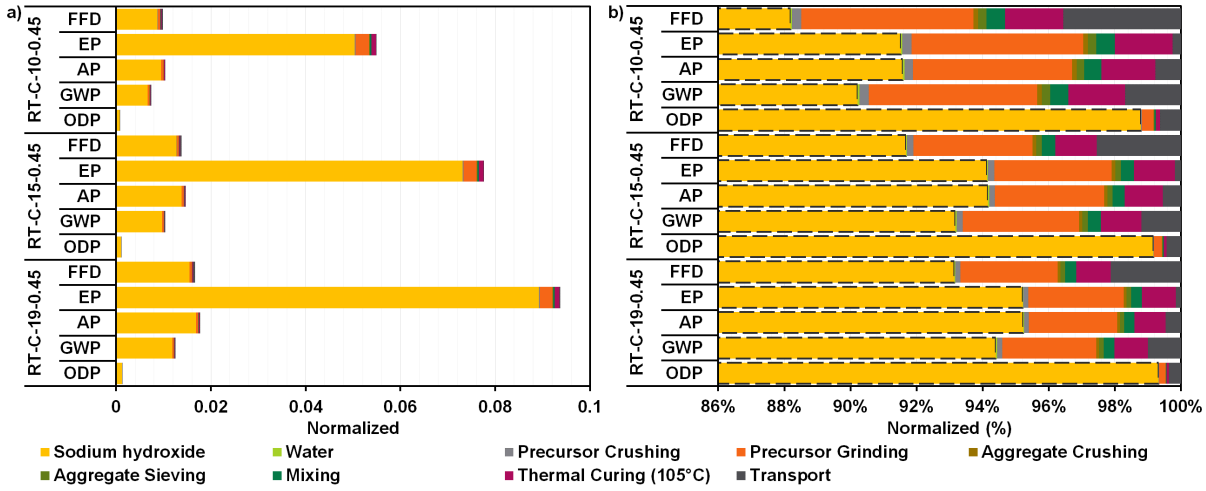

Fig. 3.15. Environmental impacts of alkali activator content (a) Normalized results (b) Contribution of materials and production processes

Similarly, an increase in the RCA content from 0.45 to 0.55 resulted in a decrease in environmental impacts between 4.2-4.6%. In general, it can be stated that the usage of RCA can assist in reducing the environmental burden of geopolymer mortars; however, since the RCA had the lowest contribution, possible advantages would be restricted, and the contribution share of other ingredients and processes would tend to be same with other mixture options.

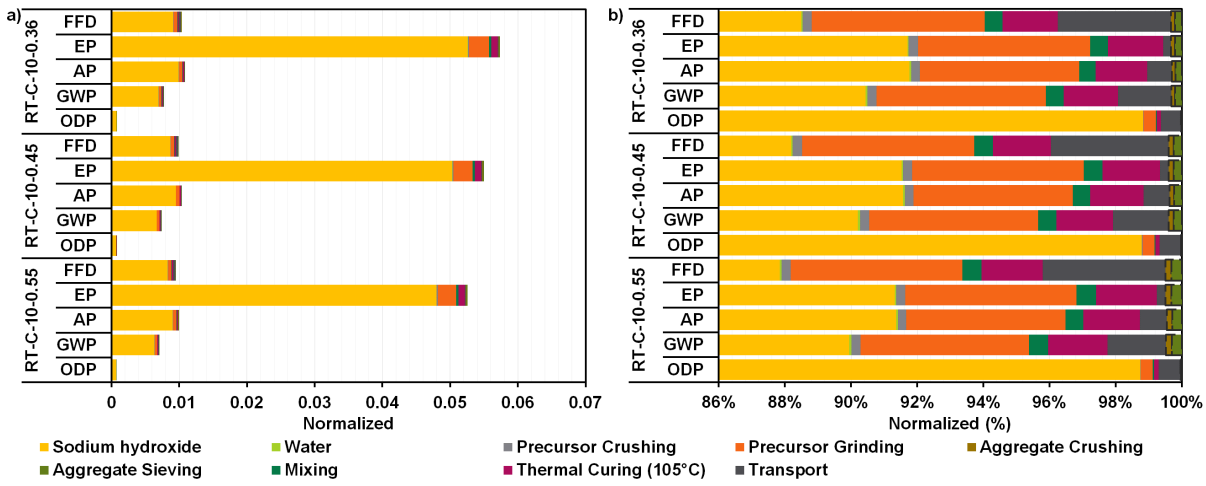

Fig. 3.16. Environmental impacts of recycled aggregate content (a) Normalized results (b) Contribution of materials and production processes

Fig. 3.17 demonstrates the contribution of aggregate size to the environmental impacts of CDW-based geopolymer mortars. It was expected that using the RCA would cause a

reduction in the environmental burden of geopolymer mortar; however, compared to the base mixture (RT-C-10-0.45), the expected behavior was not observed with the increase in aggregate size. To obtain the RCA with different particle sizes, three aggregate crushing processes were performed with different jaw crusher openings, which caused increased energy consumption with the reduction of the aggregate size desired to be produced (Table 3.9). On the other hand, due to the decrease in aggregate density with the reduction in aggregate size, the amount of material required to produce 1m^3 of CDW-based geopolymer mortar was decreased, thus reducing the energy requirement and environmental impacts. Therefore, considering the impacts of aggregate content and size on the environment and the mechanical performances, the findings revealed that the optimization of RCA content and size could be made possible to produce environment-friendly geopolymer mixtures with high mechanical performances (RT-C-10-0.55 coded mixture with an average compressive strength of 46.3 MPa).

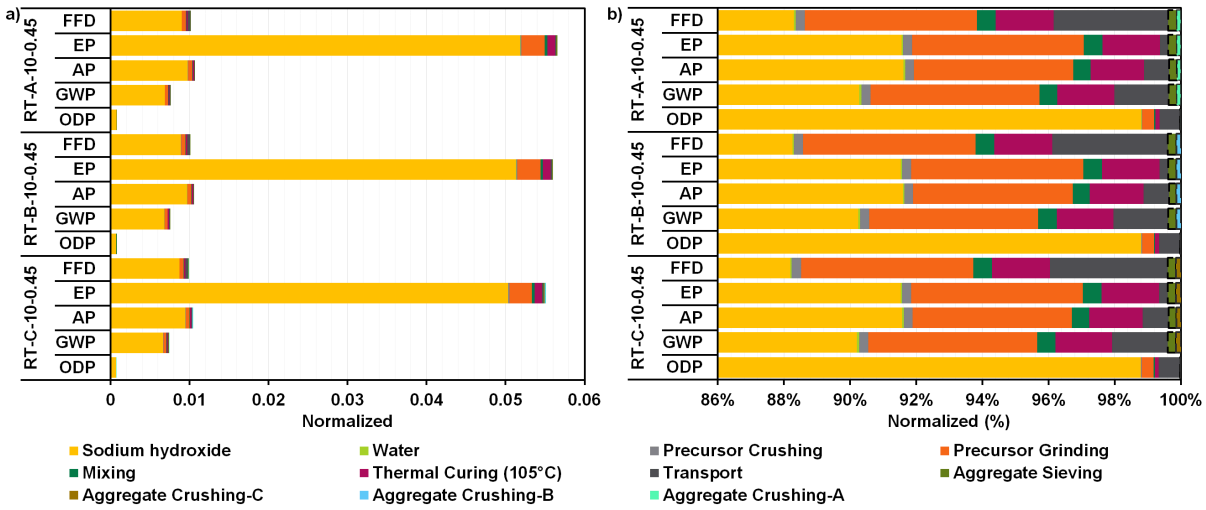

Fig. 3.17. Environmental impacts of recycled aggregate size (a) Normalized results (b) Contribution of materials and production processes

Fig. 3.18 demonstrates the impact of thermal curing under various temperatures. According to Fig. 3.18a, it can be stated that the impact of elevated temperature between 105-125 °C slightly changed with negligible increases, as expected considering the energy consumption values (Table 3.9). Notwithstanding that the change was inconsiderable, thermal curing ranked 3rd or 4th in contributing to environmental impact due to the high energy consumption demand in the process (Fig. 3.18b). On the other hand, significantly lower environmental impacts compared to PCF mortar make the CDW-based geopolymer mortars a promising

building material due to their high mechanical performance gained in short curing times. Therefore, it is believed that further optimizations for lower cure temperatures and durations can significantly increase the environmental advantages of CDW-based geopolymer mortars.

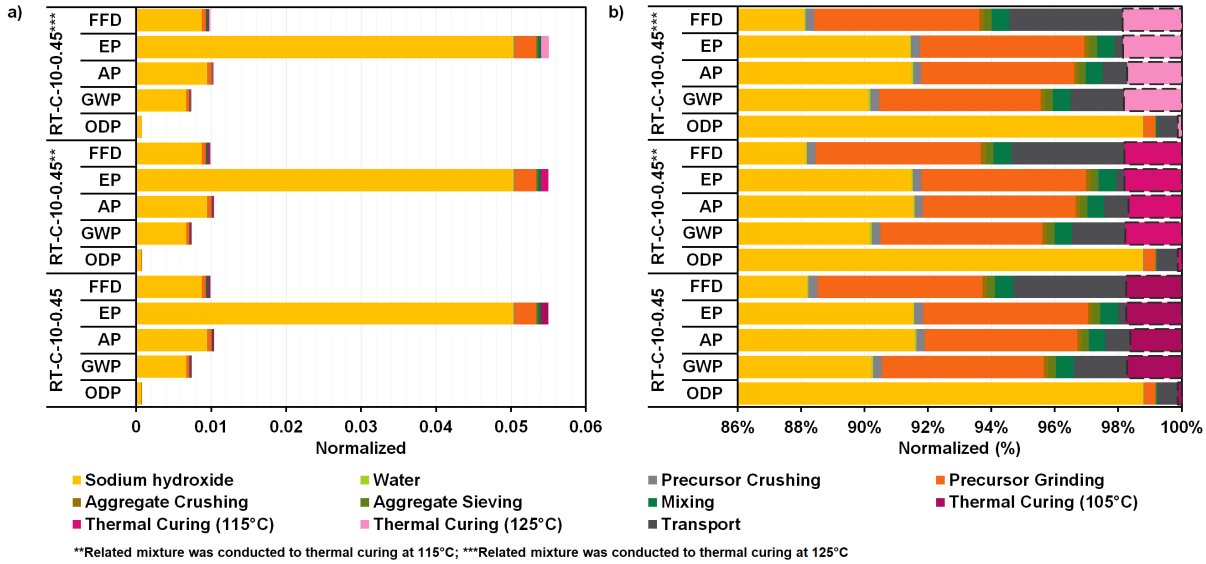

Fig. 3.18. Environmental impacts of thermal curing (a) Normalized results (b) Contribution of materials and production processes

3.4.7. Material Sustainability Indicators

CDW-based geopolymer and PCF mortars' Material Sustainability Indicators (MSI), a fundamental and easily applicable approach to determine the sustainability degree of materials depending on the amount of carbon and embodied energy of the material per strength development [236], are presented in Fig. 3.19. In the determination of MSI values, geopolymer mortars were classified in five different cases, similar to LCA analysis, according to the strength responsible parameters, including molarity, precursor type, aggregate content and size, and temperature. The findings revealed that PCF-Control contained a drastically high level of embodied carbon per MPa compared to all geopolymers. Compared to the cement-based PCF mortar, the geopolymer base mixture (RT-C-10-0.45), which had the similar strength level as PCF-Control, caused 62.9% less carbon emissions per strength development with a similar energy consumption. According to the parameter related results, the influence of the molarity change became more prominent for 19M, while for 10M and 15M differed slightly, indicating that the environmental impact of the alkali activator can be taken under control to a certain degree; thus, the further optimization of

alkali content would be beneficial for geopolymers. The influence of precursor type on the amount of embedded energy and carbon showed an increasing linear trend in the order RT, HB, and RCB. Considering that the environmental impact of precursor type was highly similar in LCIA, the exhibited trend was correlated to the compressive strength development, which was noted as 45.5, 41.3, and 34.4 MPa for RT, HB, and RCB, respectively. The influence of aggregate amount on MSI was manifested with an inverse relationship between the increase in the aggregate amount and embodied energy-carbon. Up to 0.55 of aggregate/binder ratio, embodied energy-carbon significantly decreased due to the decrease in alkali-activator and precursor amount; in particular, the first was responsible for the highest level of environmental impact. For the aggregate size influence, the MSI values declined as the aggregate size increased because the dry density of the aggregate reduced, which led to a decrease in the weights of the other ingredients required to produce 1 m^3 of geopolymer mortar. The elevated temperature did not significantly affect the MSI values for up to 115 °C, whereas at 125 °C embodied energy-carbon level increased due to the increase in electricity usage. Considering the average compressive strength results of geopolymer mortars, which were 45.5, 45.6, and 41.1 MPa at 105 °C, 115 °C, and 125 °C, respectively, it was revealed that the production of geopolymers with desired mechanical performance and lower environmental impact would be possible by optimizing the curing temperature.

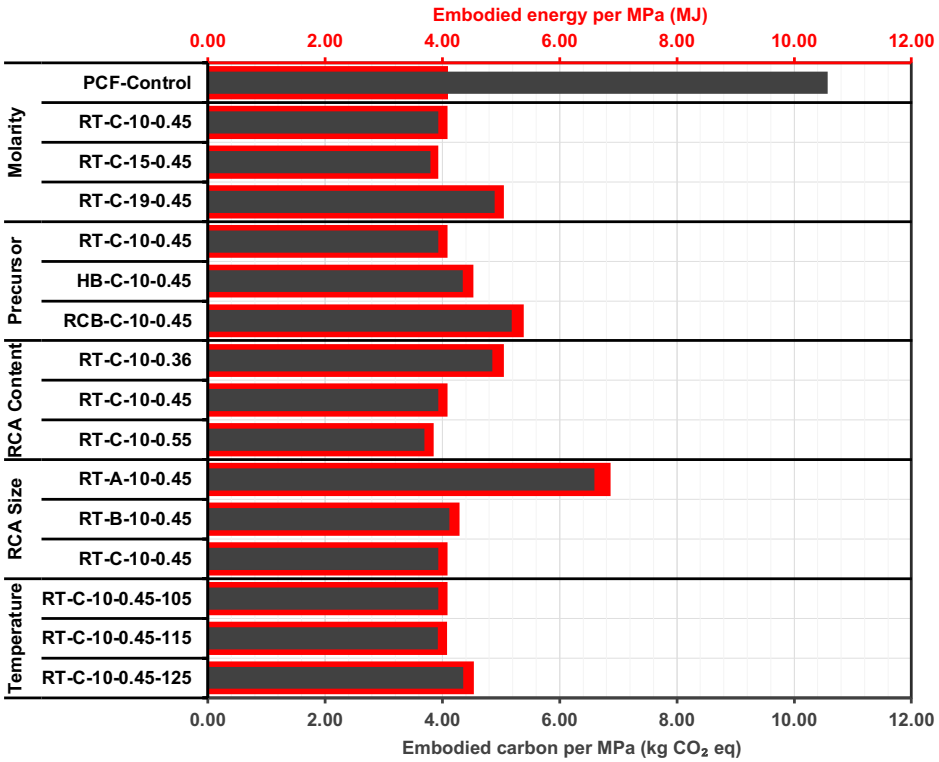

Fig. 3.19. Embodied energy and carbon per MPa of PCF and CDW-based geopolymer mortars

3.5. Conclusions

The current chapter of the thesis investigated the single-use of HB, RCB, and RT as precursors and the feasibility of full inclusion of RCA (<5 mm) in the production of CDW-based geopolymer mortars subjected to heat-curing. Precursor type, the molar concentration of sodium hydroxide, RCA size, RCA/binder ratio, and curing temperature parameters were applied at three levels, and the ITZ properties of 1 mm and 2 mm sized RCAs with geopolymer paste were investigated by line mapping analyses through a scanning electron microscope in addition to compressive strength test. According to the given results previously, the following conclusions can be drawn:

- The 100% CDW-based geopolymer mortar achieved a remarkable compressive strength of 66.2 MPa after 72-hour heat-curing. The significant influence of RCA size on compressive strength was confirmed through Pearson correlation, with smaller RCA (0.85-0.10 mm) in CDW-based geopolymer mortars demonstrating higher strength attributed to improved particle packing.

- On microstructural scale, smaller-sized RCAs (1 mm) exhibited a thinner ITZ in comparison to larger RCAs (2 mm). The alterations in Ca and Si at the ITZ around the larger RCAs resulted in the apparent separation and increased vulnerability to fracture. Besides, the influence of the RCA/binder ratio on compressive strength was found to be negligible.

- RT-based geopolymer mortars showed higher compressive strength compared to HB- and RCB-based mortars due to finer particle fractions, in the case chemical compositions of the precursors were almost identical.

- For the molar concentration, one of the most critical parameters on mechanical performance, activating mixtures with 15M NaOH solution generally improved mechanical performance, but excessive concentration led to non-homogeneous microstructure formation, while lower molarity caused limited geopolymerization.

- Among the curing temperatures tested, 105 °C was optimal, temperatures beyond this adversely affected compressive strength due to final product instability and excessive water loss, leading to drying shrinkage and crack susceptibility.

- In the LCA analyses, sodium hydroxide had the largest share of environmental impact, followed by the grinding of CDW-based precursors. In addition, transportation and thermal curing had the largest impact after sodium hydroxide and precursor grinding, depending on the impact category. Optimizing the mixture design allowed a reduction in GWP and AP by 65.9% and 34.3%, respectively. Additionally, the geopolymerization method guaranteed an FFD potential 8.2% lower than the PCF. On the contrary, regarding the ODP and EP values, the PCF mortar had the lowest negative burden on the environment.

- For the Portland cement-based mortar with same strength category, the highest contribution was noted for the Portland cement. The geopolymer base mixture (RT-C-10-0.45), which has a similar strength level as the Portland cement-based control mortar, emitted 62.9% less CO_2 per strength development with similar energy consumption.

CHAPTER IV: 3D PRINTABLE ONE-PART GEOPOLYMER DERIVED FROM CONSTRUCTION AND DEMOLITION WASTE: ANISOTROPY ASSESSMENT IN MACRO- AND MICRO-MECHANICAL PERSPECTIVE

4.1. Introduction

The global population is expected to grow by approximately 80 million people each year, reaching almost 10 billion by 2050 [237], and demanding the construction of an average of 20 million new homes per year [238]. This rapid growth is driving not only the demand for housing but also the massive amounts of construction and demolition waste (CDW) generated by the construction industry [239]. On the other hand, natural disasters, and wars around the world cause numerous people to become homeless or to migrate en masse and require new accommodation. With housing demand on the rise, governments around the world are faced with the challenge of providing adequate housing. The urgency to accommodate the growing population and the masses of displaced people is therefore leading to a focus on rapid construction methods and recycled construction materials that take into account the principles of the circular economy.

In the construction industry, 3D concrete printing emerges as a promising solution for meeting the demand for efficient and rapid construction. This innovative technology facilitates the rapid and precise construction of structures layer by layer, leading to a substantial reduction in both construction time and costs. The term, 3D printing, encompasses various methods wherein material is systematically deposited, connected, or solidified under computer control to craft a three-dimensional object. This process involves the layer-by-layer placement of different material types [240], possessing significant potential to minimize construction waste and improve the design flexibility of created structures. Previous literature indicates that the application of 3D printing in construction can lead to a reduction in fabrication waste by 30–60%, a decrease in labor costs by 50–80%, and a shortened production time by 50–70% [241]. Combining these advantages, 3D concrete printing becomes a powerful tool to find solutions for the joint challenges of affordable housing for more people, rapid construction, and transition of construction industry to the circular economy.

The development of 3D-printable mortar or concrete requires a fine-tuned balance of properties, presenting a unique set of characteristics, in comparison to traditional mortar or concrete. Specifically, the material must exhibit extrudability, denoting low viscosity, to enable continuous flow through the print nozzle [242]. Simultaneously, it necessitates high buildability, characterized by substantial yield stress, to ensure the structural integrity and stability of the printed layers. This coexistence of requirements poses a particular challenge in achieving a balance of these characteristics, which are inherently contradictory. To make this possible, special mixture designs should be developed that take into consideration both the material characteristics and the limitations of the 3D printer system. Approximately 15-45% of the total mixture fraction in the majority of 3D-printed concretes consists of Ordinary Portland Cement (OPC) [243,244], which poses a significant environmental burden due to high CO_2 emissions and the energy-intensive processes involved in its production [245]. At this point, geopolymers, also known as geopolymer binders, constitute an important OPC alternative by enabling the utilization of different precursor materials with or without pozzolanic properties.

Besides their sustainable and environment-friendly properties [246,247], geopolymers enable control of rheology, one of the most critical parameters for 3D concrete printing, without requiring additional viscosity modifier chemicals. The combination and concentration of precursors and alkaline activators used allow direct control of rheological properties and give geopolymers high thixotropic properties, making them an excellent candidate for 3D printing [96,97,248]. Studies exploring the adaptation of geopolymers to 3D printing technology have been gaining increasing interest in recent years. In one of these studies, Panda et al. [249] investigated the application of fly ash-based geopolymer in 3D printing for construction, with a focus on sustainable large-scale concrete printing using extrusion methods. The geopolymer mixture was developed using a mix of fly ash (FA), ground granulated blast furnace slag (GGBS), silica fume as the precursor, fine river sand as aggregate, potassium silicate as alkaline activator solution and actigel-cellulose mixture for rheology control. Through mechanical tests such as compression, flexural, and tensile bond strength, conducted on both printed and casted geopolymers, it was found that the 3D printed materials' mechanical properties varied according to the direction of the load, a result of the anisotropic nature of the printing process. By taking world coordinates to define loading directions, the 3D printed specimens demonstrated approximately 2% higher strength than the casted specimens in the Y direction; conversely, exhibited 5% lower strength in the X

and Z directions. Zhang et al. [91], who investigated the rheological properties of 3D printable geopolymers, activated their precursor phase consisting of a mixture of granulated blast furnace slag and steel slag using sodium hydroxide and sodium silicate. They aimed to enhance the stability and shape retention capabilities of the mixtures by incorporating defoamer, superplasticizer, and redispersible latex additives. Their findings indicated that the stability of the printed structure increased with an improvement in structural rebuilding ability and yield stress. It was noted that reducing the Si/Na ratio in the alkaline activator phase contributed to the enhancement of these parameters. In another study by Panda et al. [250], fly ash-based geopolymer mixtures activated with sodium silicate and sodium hydroxide solution were examined for their rheological and mechanical properties with the substitution of GGBS and silica fume. It was reported that while the effect of GGBS substitution on rheological properties was low, it increased early-age strength. On the other hand, the substitution of silica fume significantly improved the thixotropic performance and structural build-up level. Additionally, it was noted that the 3D printed samples had slightly higher mechanical performance compared to mold-casted ones. Alghamdi et al. [251] aimed to control the rheological and mechanical properties of fly ash-based geopolymers by substituting different amounts and combinations of slag, Portland cement, and limestone. They activated these precursor combinations using sodium hydroxide, sodium silicate solution, or sodium sulfate. According to the results, the yield stress was influenced by particle sizes and packing, and the presence of alkaline activators increased tack force and adhesive energy compared to traditional cement-based binders. While the compressive and flexural strength tests generally yielded mechanical properties similar to conventionally cast specimens, there were instances of strength reduction due to microcracking (especially in heat-cured mixtures) and weak layer bonding in mixtures containing Portland cement. Investigating the impact of a heating process on the rheological control of 3D printable geopolymers, Souza et al. [252] activated metakaolin precursors using various combinations of sodium hydroxide and sodium silicate. They highlighted the significant influence of the activators' Si/Al ratio and water content on rheological properties. Additionally, applying a preheating treatment at 50°C was found to substantially enhance the buildability performance of the system. By utilizing a heating device attached to the printer head, they indicated the potential for achieving highly flowable and easily pumpable binders with significant structuration.

The 3D printable geopolymers found in the literature are generally developed using a two-component production technique based on the activation of precursor phases with alkaline

activator solutions. However, the use of these highly alkaline and corrosive activator solutions [253], while enabling controlled and successful experimental work at the laboratory scale, is unfortunately not practical or controllable for large-scale applications. To address this issue, Panda et al. [254] developed a 3D printable one-part geopolymer mixture by activating the dry mixture phase consisting of fly ash, ground granulated blast furnace slag, and fine silver sand with a mixture of potassium silicate powder and potassium hydroxide powder. Their rheological studies revealed that the mixtures exhibited successful thixotropic behavior, and the use of GGBS enhanced thixotropy and compressive strength performance due to its angular texture and amorphous phases. The effects of anisotropy were reflected in the compressive strength results, and while samples in different loading directions showed some variations, they were not significantly different. In another study, Bong et al. [255] focused on investigating the rheological and mechanical properties of geopolymer mixtures produced with slag and fly ash as precursor phases, a mixture of sodium metasilicate-sodium silicate powders as the alkali activator phases, and sucrose powder as retarder admixture. It was reported that the content and combination of alkali activators directly affected the rheological properties and the printable open-time, with the possibility of extending the open-time up to 65 minutes through control of these parameters. While the compressive strengths of 3D printed samples were lower compared to mold-casted ones, the flexural strengths in the Y and Z directions (loaded perpendicular to the plane of the interlayers) were higher in the 3D printed samples compared to the mold-casted ones. Muthukrishnan et al. [256], focused on the rheological characteristics of 3D printable one-part geopolymers, constituting GGBS and fly ash as precursor, sodium metasilicate as alkaline activator, magnesium aluminosilicate as thixotropy enhancer additive and sucrose as retarder. While emphasizing the necessity of exceeding a certain threshold for the mixing duration to ensure the complete dissolution of solid activators, it has been reported that the mixture's open-time can be extended beyond 90 minutes through re-mixing. According to the mechanical performance tests, the influences of anisotropy were clearly observed. The compressive and flexural strengths were significantly higher in the axial and horizontal directions depending on the printing direction, while the strengths in the direction perpendicular to the printing direction exhibited relatively lower performance.

For the adaptation of geopolymer binders to 3D printing, which is considered to be environment-friendly and sustainable alternatives to OPC, the majority of the research conducted so far has focused on the use of industrial by-products such as fly ash, ground granulated blast furnace slag, which are widely used in the cement industry in so many

applications. At this point, the development of construction materials tailored for 3D printing has reached a saturation point. However, one of the crucial factors in facilitating the widespread adoption of 3D printing is the expansion of the spectrum of printable building materials that are easily accessible and economically viable printable building materials with environmentally sustainable properties. Besides, for 3D printable materials, and in line with the goals of the circular economy, which prioritize waste reduction and resource efficiency maximization, it should also be provided and supported through the recycling of materials that have reached the end of their service life. With these objectives in consideration, the current chapter of thesis focuses on the development of a 3D printable one-part geopolymer (3DPG) suitable for the integration of CDW-based materials derived from a completely different source, brick masonry waste from the Netherlands, and the validation of the concept of geopolymerization of CDW-based materials based on the results of Chapters 2 and 3. The matrix was designed to be used in precursor and filler phases of brick masonry wastes, and it was aimed to support/regulate the mechanical and rheological properties with the addition of materials such as ground granulated blast furnace slag, kaolin clay and limestone. The macromechanical properties of the developed 3DPG mixture were investigated by compressive strength, flexural strength, split tensile and direct tensile tests to investigate the development of geopolymerization and the effect of anisotropy. The micromechanical properties were analyzed by X-ray fluorescence spectrometry (XRF), X-ray diffraction (XRD), Fourier transform infrared (FTIR), Thermogravimetry (TG) and Differential Scanning Calorimetry (DSC), Scanning electron microscopy and energy dispersive X-ray spectroscopy (SEM/EDX) and computed microtomography (Micro-CT) tests were performed.

4.2. Materials and Methodology

4.2.1. Basic Properties of Precursors

In this chapter of the thesis, ground granulated blast furnace slag (GGBS), limestone (LS) and kaolin clay (KC) were utilized as part of the precursor materials. Since it was obtained from crushed demolished brick walls stored in landfill areas in the Netherlands, construction and demolition waste (CDW) had a composition of approximately 85% of brick waste and 15% of concrete mortar waste. The fine fractions of CDW (below 100μm) were considered as the precursor phase in the mixtures, while the relatively coarse fractions (between 100-1000μm) were considered as fillers. Commercially available sodium hydroxide (NaOH) and

sodium silicate (Na_2SiO_3) (28wt% SiO_2, 29.25wt% Na_2O, 42.75wt% H_2O) were utilized as alkali activators. Chemical compositions of the materials are listed in Table 4.1, as determined by X-ray fluorescence spectrometry (XRF). The literature frequently states that the chemical composition, in particular the SiO_2 and Al_2O_3 content of the precursors, is one of the most important parameters in determining the mechanical and chemical properties of the final geopolymer products [127]. In this context, CDW and kaolin clay, due to their high SiO_2 and Al_2O_3 contents, are suitable candidates for geopolymerization, while precursors with a high CaO concentration such as GGBS and limestone can support the mechanical performances by enabling the formation of calcium-based strength-giving gel products [67].

Table 4.1. Chemical composition of precursors

Oxides (%)	CDW	GGBS	Limestone	Kaolin Clay
SiO_2	59.5	27.9	7.2	54.5
CaO	17.4	49.4	86.9	-
Al_2O_3	9.2	9.6	0.7	35.3
Na_2O	2.9	2.5	2.7	3.7
Fe_2O_3	5.9	0.5	1.4	0.7
K_2O	2.5	0.4	-	4.6
MgO	1.3	6.7	0.6	-
SO_3	-	1.1	-	-
LOI	2.9	2.5	2.7	3.7

Particle size distributions (Fig. 4.1) and average particle sizes, d(0.5), were determined via laser particle size analyzer; related parameters of CDW, GGBS, LS and KC were measured as, 26.55 mm, 14.12 mm, 15.40 mm and 15.92 mm, respectively. Considering the particle size threshold of 15 μm, which reflects the reactivity of the precursors in geopolymerization alongside their chemical composition [121,141], it was observed that more than 50% of all precursors were below this threshold, while CDW-powder remained relatively coarse with 35%. On the other hand, CDW-filler with a good gradation is expected to improve packing density by causing smaller void space volume formation [257].

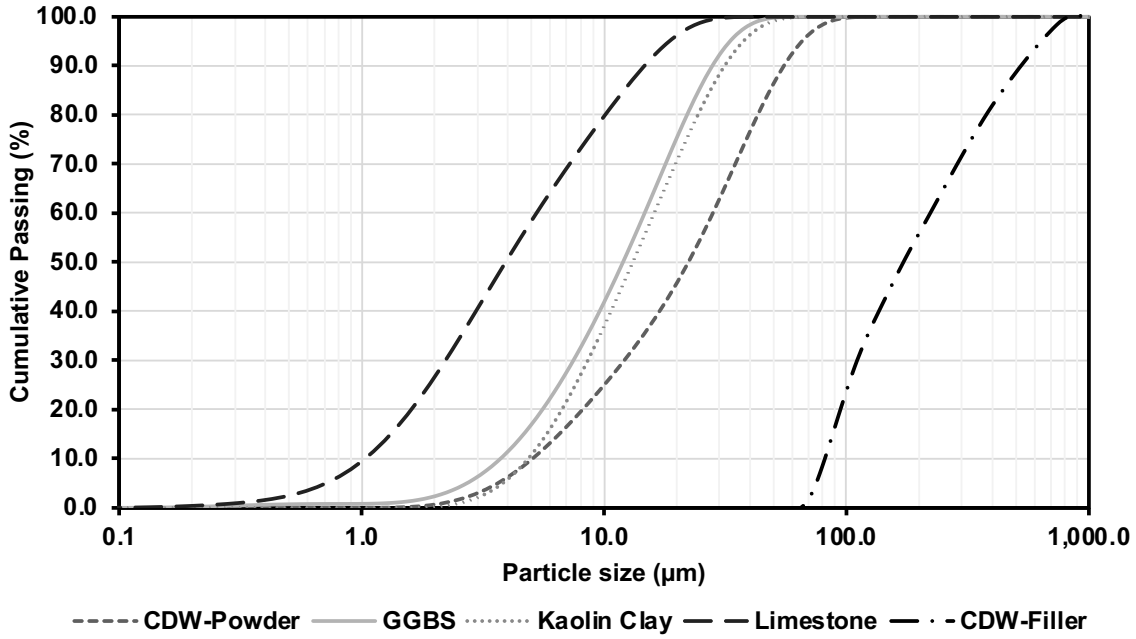

Fig. 4.1. Particle size distribution of precursors and filler

4.2.2. Methodology of Rheological, Macro- and Micromechanical Characterization

The flowability and buildability tests, which are simple empirical tests that make it possible to understand the suitability of the fresh state properties of the developed mixtures for 3D printing, were measured at 0, 30, 60 and 90 minutes, starting immediately after the completion of the mixing procedure (initial test at 5 min, considered as 0 min). The flowability test was performed following the ASTM C1437 [258] standard and the flowability index values were calculated by considering the relative change in the amount of spread along different horizontal directions. The buildability test was carried out using the flowability test setup with a mini-slump test procedure under a certain load (600 g) and the buildability performances were determined by calculating the vertical deformations of the mixtures. In addition to empirical rheology tests, the rheological performance of the 3D printable mixture was also investigated by means of methods that could enable more precise evaluations. To this end, a rotational rheometer was used to evaluate the static yield strength, viscosity, and associated thixotropic performance of the developed mixture. A three-stage shearing protocol was conducted to assess thixotropy. In the first stage, shear was applied to the sample at a rate of $0.01s^{-1}$, followed by an increase in shear rate to $0.3\ s^{-1}$, and finally, the shear rate was reduced back to $0.01s^{-1}$ in the last stage. This protocol was established to simulate the resting of material in the pump hopper, its transfer from the hopper to the nozzle via the pump, and the initiation of the curing process for the printed material, respectively.

Ultrasonic wave transmission tests (UWTT) were carried out following the ASTM C597 [259] standard in order to monitor the densification and thus the stiffening of the matrix due to the progressive geopolymerization. The P-wave velocities of the ultrasonic pulse transmitted every minute for a period of one hour were calculated. In order to analyze the mechanical properties of 3D printed specimens depending on the layer thickness and loading orientation, all of the mechanical tests presented below were carried out by means of specimens extracted from printed samples with two different layer thicknesses (8 and 10 mm). The anisotropic performances were analyzed by loading the specimens in 3 different orientations (Fig. 4.2). Mechanical performances of ambient cured geopolymer mixtures were evaluated by applying different mechanical tests at different ages (7, 28, 90-days) on both mold-casted and 3D printed specimens. Compressive strength tests were performed on 40 mm cubic specimens at a loading rate of 2400 N/s, while 3-point flexural strength tests were performed using 40x40x160 mm prismatic specimens at a loading rate of 50N/s. Splitting and direct tension tests were performed using 40 mm cubic specimens at loading rates of 50N/s and 1mm/min respectively. In particular, the direct tension test was performed only on 3D printed samples, and a compressive load of 100 N was applied during the 30-minute adhesive drying period to prevent tensile stresses in the sample due to the shrinkage of the adhesive after the adhesive was applied to the loading planes from the upper and lower surfaces of the samples.

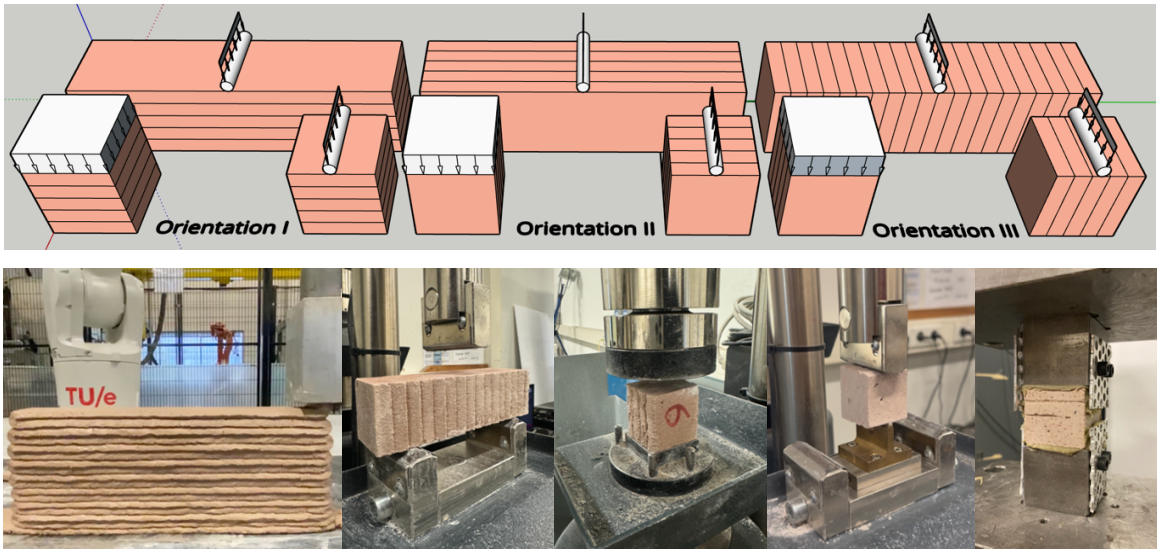

Fig. 4.2. Loading orientations and representative visuals of mechanical tests (Left to right: Printed wall segment, flexural strength, compressive strength, splitting tensile and direct tension tests)

X-ray diffraction (XRD) analysis to determine the crystalline phases of precursors and geopolymer mixture was performed with a 2-theta range of 10 to 60º, a 2-theta step of 0.02° and a time per step of 0.2 seconds. Fourier transform infrared (FTIR) spectroscopy was conducted in the wavelength range of 400-4000 cm^{-1} to determine the molecular and bond structure of the precursors and geopolymer mixture. Thermogravimetry (TG) and Differential Scanning Calorimetry (DSC) analyses were conducted to determine the degradation temperatures of the precursors and geopolymer mixture at temperatures ranging from 25 to 1000 °C with an incremental rate of 10 °C/min. The thermograms generated were used to assess the degradation temperatures and degrees of the chemically/physically bound water and/or bond structure. Besides, in-depth microstructural analyses were carried out on the mortar specimens; microstructure, reaction products and elemental distribution were investigated by scanning electron microscopy and energy dispersive X-ray spectroscopy (SEM/EDX) analysis. To investigate interlayer bond properties according to the pore size distribution, Micro-CT analyses were performed on 35 mm cubic samples extracted from the printed specimens with a voltage of 40–100 kV and a voxel size of 0.45 μm.

4.3. Development of 3D Printable One-Part Geopolymer Mortar

4.3.1. Mixture Design Methodology

Preliminary studies conducted for the development of "3D Printable One-Part Geopolymer Mortar" involved examining the fresh-state properties such as early-age mechanical properties, flowability, and buildability of mixtures developed using different precursor materials. Additionally, the impact of these properties on mixtures based on molar ratios of SiO_2-Al_2O_3-Na_2O-CaO was investigated.

In the initial stage, the focus was placed on activating the precursor and filler materials derived from construction CDW. Following that, various combinations of kaolin clay, limestone, and ground granulated blast furnace slag (GGBS) were introduced into the mixtures to leverage their potential benefits in terms of mechanical and rheological properties. When kaolin clay (KC) is activated with alkali suspensions, it demonstrates notable shear-thinning behavior and low viscosities, thereby facilitating seamless passage through suspension nozzles while enhancing thixotropic performance [260]. Besides, they are widely accessible and have been utilized across various industries due to their particle

size, surface chemistry, and physical properties [261]. Another widely available, cost-effective source material, limestone (LS) [262], enhances the reactivity of geopolymers by improving nucleation sites [263], while also contributing to the development of rheological properties and open time [264]. It is expected that GGBS, a commonly used precursor in geopolymerization, will support the buildability, which is one of the most critical parameters for 3D printing, by enhancing rigidity due to the formation of gel structures such as CSH and CASH, thereby increasing their ultimate mechanical performance [265]. Considering the advantages of the mentioned precursors, Table 4.2 presents the mixture designs and molar ratios of the one-part geopolymer mixtures formulated to leverage these benefits.

Table 4.2. Mixture designs of produced geopolymer mixtures

Ingredients	Mixtures (kg/m^3)							
	M1	**M2**	**M3**	**M4**	**M5**	**M6**	**M7**	**M8**
CDW-P	617.5	465.3	317.1	191.7	195.6	198.8	200.6	202.5
CDW-F	926.3	930.6	951.2	958.7	977.8	994.0	1003.2	1012.6
LS	-	-	158.5	149.1	152.1	154.6	156.1	157.5
GGBS	-	-	-	149.1	152.1	154.6	156.1	157.5
KC	-	155.1	158.5	149.1	152.1	154.6	156.1	157.5
SH	65.9	66.2	67.6	68.2	69.5	35.3	26.8	18.0
SS	65.9	66.2	67.6	68.2	34.8	35.3	26.8	18.0
Water	370.5	372.3	380.5	383.5	391.1	397.6	401.3	405.1
Molar Ratios								
SiO_2/Na_2O	8.60	8.43	7.71	7.38	7.39	10.49	11.72	13.28
SiO_2/Al_2O_3	10.98	8.48	8.33	7.99	7.99	7.99	7.99	7.99
CaO/SiO_2	0.40	0.36	0.57	0.67	0.67	0.67	0.67	0.67

Note: CDW-P and CDW-F: Construction and demolition waste-based precursor and filler, LS: Limestone, GGBS: Ground granulated blast furnace slag, KC: Kaolin clay, SH: Sodium hydroxide, SS: Sodium silicate

4.3.2. Early Age Fresh State and Mechanical Investigations

The molar ratios of the developed mixtures, early-age compressive strengths (3 days), and flowability-buildability (5 minutes) test results are presented in Fig. 4.3. The findings indicate that a reduction in SiO_2/Al_2O_3, (i.e., a more balanced SiO_2/Al_2O_3 content) significantly improved compressive strength due to enhancement in the formation of Si-O-Al bonds, which is mainly responsible for mechanical performance [121], without significantly affecting fresh-state properties. Regarding mechanical properties, the same situation occurred for CaO/SiO_2; increasing the CaO/SiO_2 ratio through LS and GGBS substitution significantly increased the compressive strength; however, in particular, the

substitution of GGBS decreased the flowability values while increasing the buildability (M4). The observed behavior can be explained by the high reactivity of CaO in GGBS, which accelerates the formation of Ca-based gel structures [94]. This, in turn, increases the stiffness of the matrix and the yield stress [92]. The significant increase in the SiO_2/Na_2O ratio, which was the most determining molar ratio for mechanical performance alongside CaO/SiO_2, notably positively affected the mechanical properties due to the stimulation of geopolymerization by the increase of available soluble reactive silica in the matrix [266]. Besides, increasing SiO_2/Na_2O caused a slight change in flowability and enhanced buildability due to improved shape-retention ability [267]. However, as an observation to these positive outcomes, beyond a certain point, the increase in SiO_2/Na_2O ratio led to a loss in mechanical properties, indicating the presence of a threshold (M8). The main reason for this threshold was the predominance of precursor and filler phases in the increase of SiO_2/Na_2O, rather than soluble silicates (M5 to M8). The amount of soluble silicate in the system decreased, but the increase in the SiO_2/Na_2O ratio of the system efficiently supported gel formation up to a certain point.

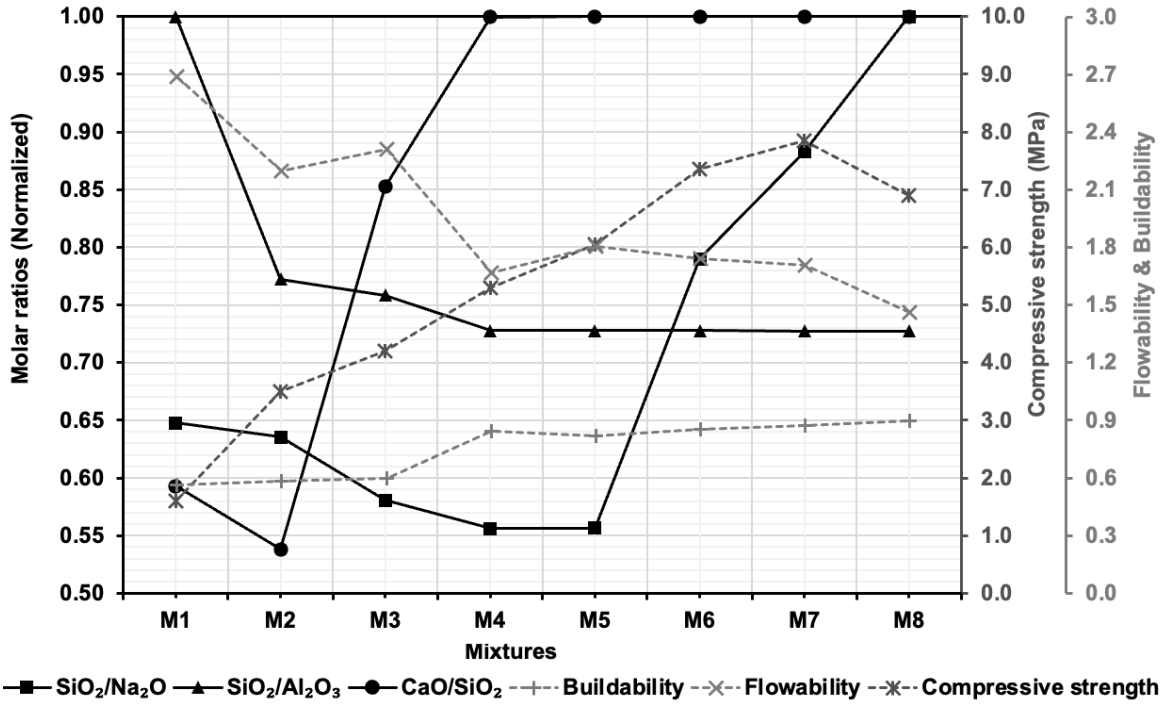

Fig. 4.3. Relationships among molar ratios, early age compressive strength and fresh properties

The time-dependent flowability and buildability indexes of the developed mixtures are presented in Fig. 4.4a, while their compressive strengths are depicted in Fig. 4.4b. The findings obviously demonstrated the inverse relationship between flowability and buildability index. This is a natural outcome of the ongoing polycondensation process. The 3D polymeric framework is formed by monosilicate chains and cyclic trimers through geopolymerization [268].

The stiffness of the matrix increases gradually due to the gel structures, resulting in a decrease in the flowability of the system and an improvement in the buildability performance. At later ages (7, 14 and 28 days) geopolymerization continued further, resulting in a consistent increase in compressive strengths. The trend observed in the influences of mixture content on compressive strengths at early ages was sustained at later ages.

Based on the overall results, the mixture with the optimum flowability, buildability, and compressive strength values for lower alkali activator content (M7) was determined as the mixture to be used in 3D printer operations in the later stages of the study.

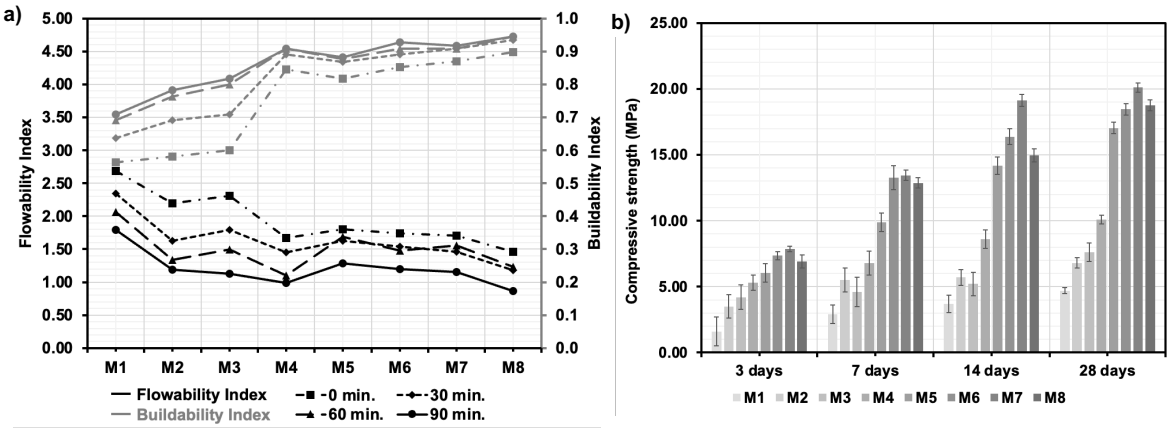

Fig. 4.4. Basic properties of geopolymer mixtures a) Time-dependent flowability and buildability indices, b) Mechanical performances as a function of curing duration

Thixotropy, a vital parameter for 3D printing, refers to the reversible change in a material's viscosity caused by flocculation and de-flocculation processes when at rest and after being sheared, respectively [269]. During the extrusion phase, the material undergoes shearing either by the pump or by the nozzle walls, resulting in a decrease in the mixture's viscosity.

After deposition, to prevent the layer from flowing and to maintain its shape, it is essential that the layer reflocculates rapidly. Evidence of thixotropic behavior was clearly seen in the tests performed using M7 mix (Fig. 4.5a). At all test ages, the viscosity decreased significantly under high shear rate. However, upon removal of the shearing effect, the initial visco-elastic structure returned. This indicates that the material has the necessary shape retention and buildability required for printing layers on top of each other after extruding from the nozzle. Although the initial viscosity values increased with time due to progressive geopolymerization, the high rate of thixotropic behavior revealed the extended open time of the material. The thixotropic recovery rate had considerably high values between 82.2-84.1% depending on time, with an increment by increased testing duration.

This time-dependent change was also valid for the initial yield stress values, but the dynamic yield strength values gradually converged after the high shear force was applied (Fig. 4.5b). The increase in ultrasonic pulse velocity values due to progressive geopolymerization was consistent with the improvement of the static yield strength over time (Fig. 4.5c). After 60 minutes, the speed (approx. 300 m/s) was significantly lower than 1400 m/s, which was considered to be the speed at which the initial setting started [270-272].

To validate the thixotropic property, an ultrasonic wave transmission test was performed on the sample that remained in the mixer hopper after the 30-second mixing procedure was completed every 15 minutes. The results showed that the pulse velocity increased with curing time, but the increase was limited due to the shear force applied at intervals, indicating thixotropic recovery (Fig. 4.5d).

This situation reveals that the fresh state properties of the developed 3D printable one-part geopolymeric mortar can be maintained only by remixing at certain intervals for printer types where mortar mixtures are prepared first and then placed in the 3D printer pump. It will also make it possible to reintegrate the waste mortar that may arise from faulty production into the system.

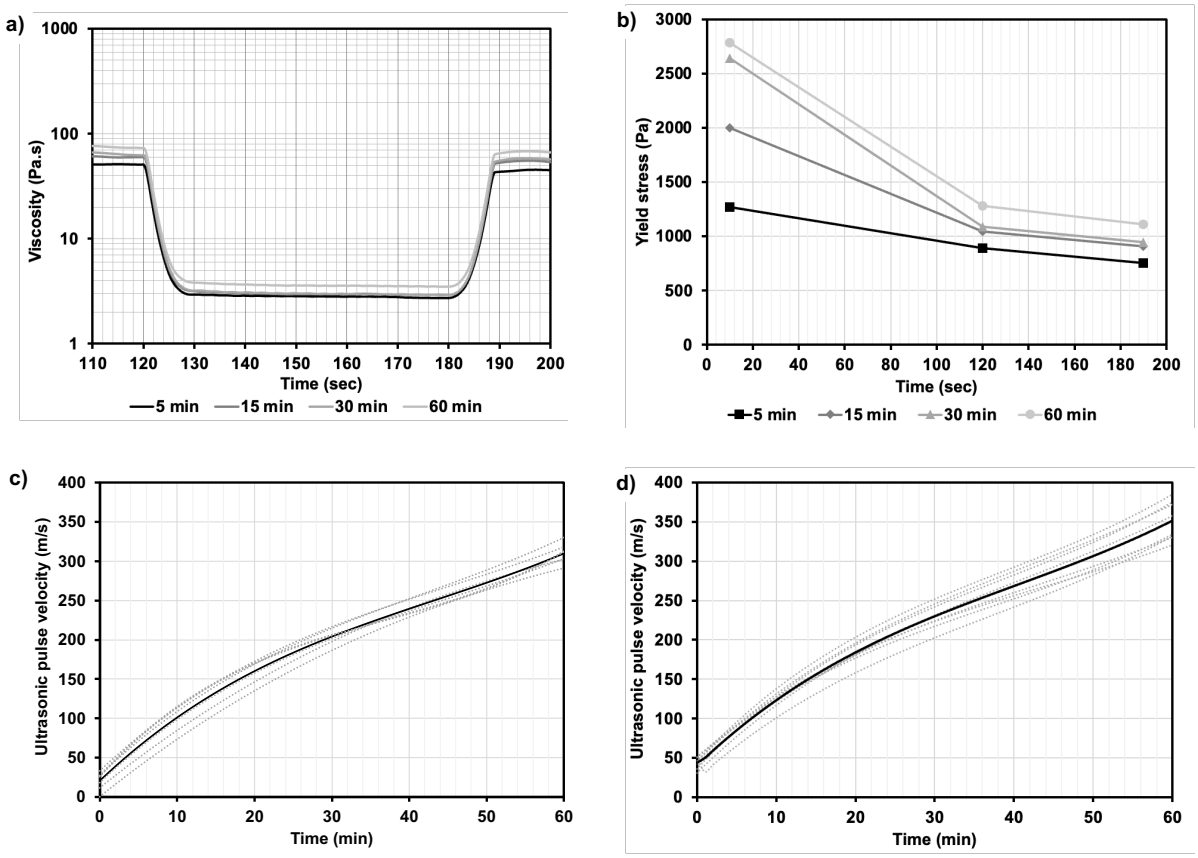

Fig. 4.5. Rheological analysis of 3D printable geopolymer a)Viscosity recovery, b)Yield stress and c) ultrasonic pulse velocity d) ultrasonic pulse velocity of remixed mixture (for c and d, the dashed lines represent all test results, and the continuous line represents the average result)

4.4. Microstructural Examinations of 3DPG

A series of analyses were carried out to determine the microstructural crystal phases, molecular structure and bond structures, and thermal decomposition of the developed 3D printable one-part geopolymer (3DPG) before and after geopolymerization. Fig. 4.6 and Table 4.3 present the particle diffraction file (PDF) numbers and chemical formulas obtained as a result of the XRD analyses performed to observe the crystal structures. In general, a major Quartz phase was detected at 31 degrees of 2θ for all precursors. In the precursor phase, major Kaolinite and Calcite phases were observed, which are characteristic phases for kaolin and limestone; on the other hand, for GGBS an amorphous structure was detected. In CDW, the major phases were Quartz and Albite, the latter being a suitable phase for geopolymerization, especially with its Na-Al-Si based structure [273]. In the 3DPG, the intensities of the peaks decreased significantly and/or turned into almost completely different

peaks compared to XRD patterns of precursors (Fig. 4.6), indicating the occurrence of geopolymerization reactions [265]. Given that the elemental composition of the identified phases corresponds to the gel and nanoscale crystals present in geopolymer matrices, the identification of the Calcium Aluminosilicate ($CaAl_2Si_2O_8$) crystal phase in 3DPG indicates the presence of phases associated with the formation of the CASH gel structure within the system.

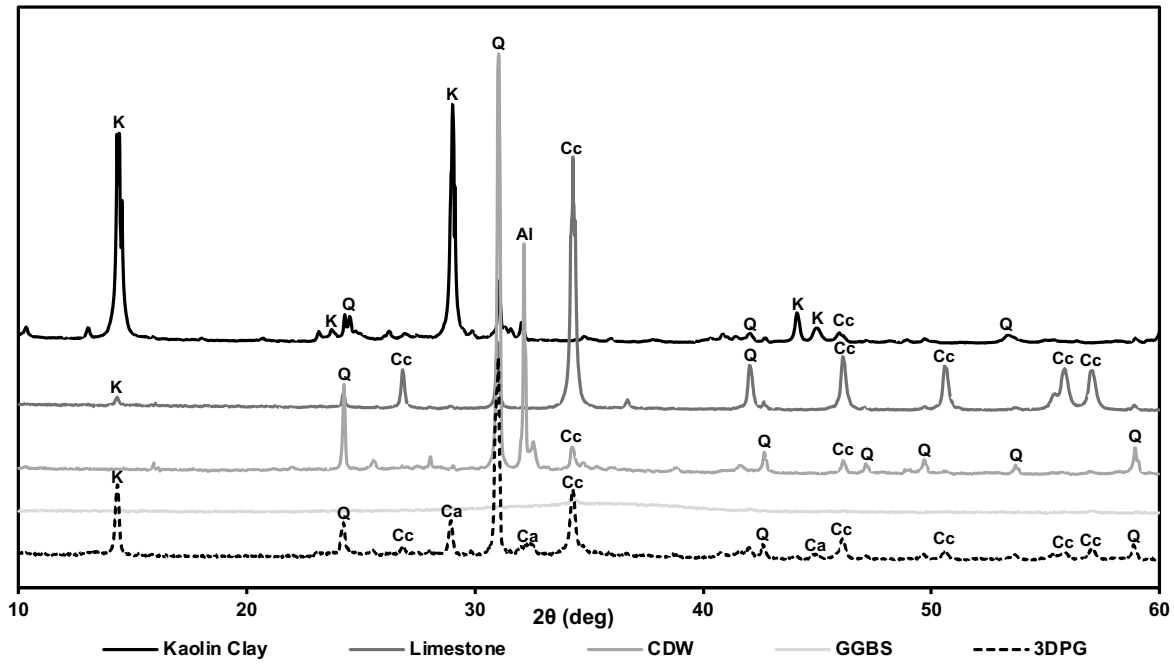

Fig. 4.6. X-ray diffractograms of the precursors and 3DPG

Table 4.3. Crystalline phases of the precursors as determined by the XRD analyses

Crystalline phase	Symbol	PDF number	Chemical formula
Quartz	Q	96-901-0145	SiO_2
Calcite	Cc	96-210-0190	$CaCO_3$
Kaolinite	K	96-901-7768	$Al_2Si_2O_5(OH)_4$
Albite	Al	96-900-0530	$NaAlSi_3O_8$
Calcium Aluminosilicate	Ca	96-153-0000	$CaAl_2Si_2O_8$

FTIR spectroscopy was used to characterize the short-range structural order of precursors and 3DPG (Fig. 4.7). The minor peaks observed in the regions between 3100-2800 cm^{-1} are attributed to the stretching vibrations of hydroxyl groups (-OH) and water (H-O-H) [274]. These peaks were observed in all precursors except limestone. Besides, for region between

2400-1800 cm^{-1}, bending vibration peaks of H-O-H were detected for all precursors and 3DPG. The absorption bands in the 1600-1300 cm^{-1} range, observed in all precursors except limestone, were attributed to the stretching vibrations of O-C-O bonds formed due to atmospheric carbonation [275]. Peaks and peaks indicating T-O-Si (T=Si, Al) bonds detected in the 1100-900 cm^{-1} region (extending up to 800 cm^{-1} for GGBS) are generally attributed to the geopolymer structure for the final product [276,277]. The CDW precursor exhibited similar peak structure to 3DPG due to its dominant content in the system. On the other hand, the fact that the final product shifts to relatively higher wavelengths as a result of geopolymerization compared to these bonds [148,159], which are represented by a large bump at lower wavelengths for GGBS, indicates that it contributes to the formation of Calcium Aluminosilicate phases detected in XRD analysis. For lower wavelengths (between 800-600 cm^{-1}), Si-O-Si bonds representing quartz phases were detected in the region [275], which contains a high intensity peak especially for kaolin clay and low peaks for other materials.

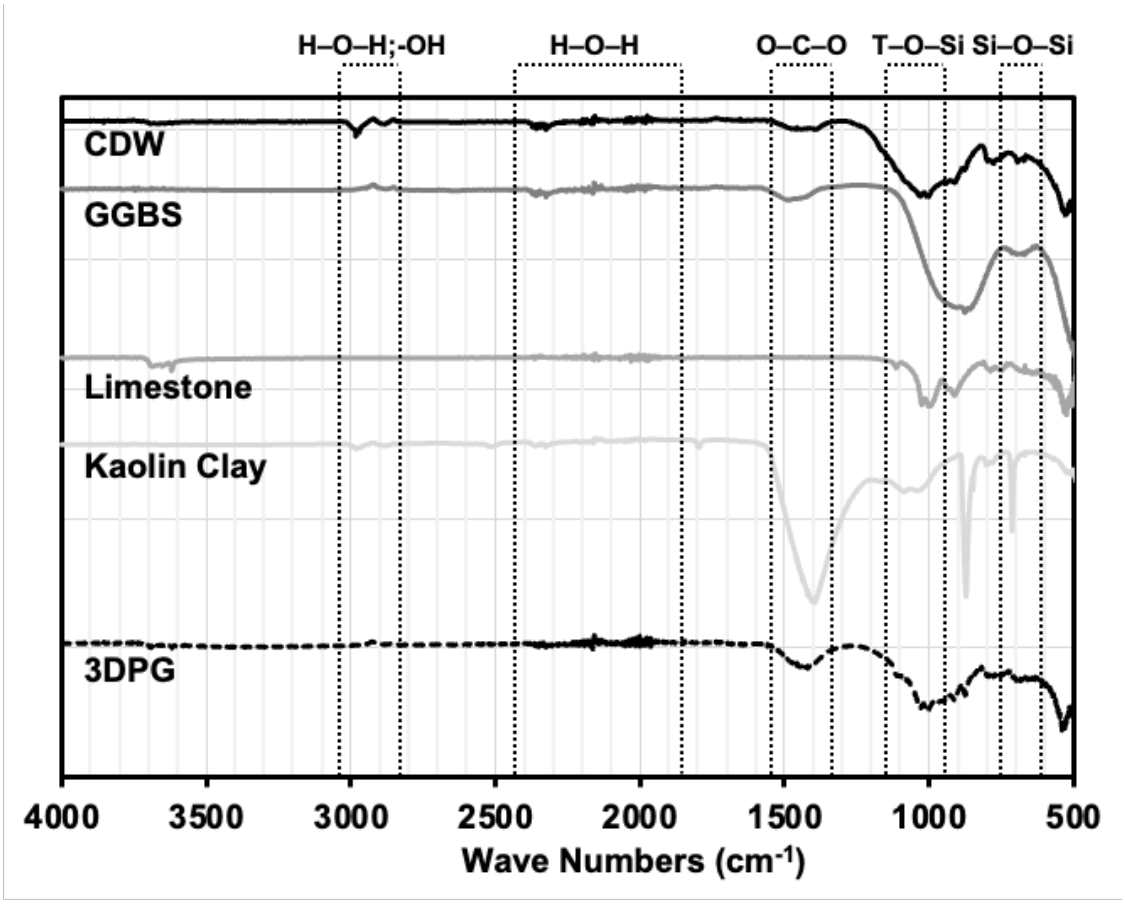

Fig. 4.7. Fourier-transform infrared spectroscopy results of precursors and 3D Printable Geopolymer (3DPG)

The findings of Thermogravimetry (TG) and Differential Scanning Calorimetry (DSC) analyses performed to characterize the thermal properties of Precursors and 3DPG are presented in Fig. 4.8. In the TG thermogram, in the temperature range of 0-300 °C, the mass loss seen in the precursors and 3DPG is associated with the dehydration of physically and chemically bound water [278,279]. The dehydration of physically bound water occurs up to the temperature range of 100-120 °C [280], while the dehydration of chemically bound water occurs beyond this temperature range [281].

The TG analysis of CDW indicated a low level of mass loss at low temperatures, while the DSC analysis showed a weak endothermic peak detected in the range of 700-800°C, indicating the presence of $CaCO_3$ with different crystallinity [282]. The observed thermal stability of CDW is likely due to the treatment of the brick phase at 800-1000°C during production [62], as the composition of CDW is approximately 85% brick waste and 15% concrete mortar waste.
The $CaCO_3$ phase, on the other hand, is thought to result from atmospheric carbonation of the low amount of concrete phase. TG analysis of GGBS demonstrated the thermal stability of the material by showing a relatively low mass loss in the low temperature range, which was confirmed by the absence of a pronounced endothermic or exothermic peak in the DSC analysis at low temperatures. However, at higher temperatures (around 600-700°C), a slight decrease in mass loss and an exothermic peak starting from 800°C were observed. This is related to the decarbonation of calcium carbonate and sodium carbonate, which are present in different crystalline forms [280,283].

However, the TG analysis of Kaolin Clay indicated the dehydration of adsorbed free water with an initial slight decrease and a more pronounced mass loss, followed by the thermal decomposition of hydroxyl groups, which occurred around 600°C, confirming the transformation of kaolinite to metakaolinite with a large endothermic peak in DSC [284].

The TG analysis of limestone indicated significant mass loss associated with the thermal decomposition of calcium carbonate, while the DSC showed this decomposition as a significant endothermic response, indicating that the material absorbs energy, which is used to initiate the decomposition reaction [285,286].

The analysis of 3DPG showed that the high level of mass loss from relatively low to average temperatures was due to the dehydration of the bound water of the geopolymeric gel structure [281]. The endothermic peak detected in the DSC around 700°C was caused by the decomposition of atmospheric carbonation products, which were also observed in the precursors [287]. The fact that the peak in question had a lower intensity at lower temperatures compared to the peak detected in limestone was associated with the well-crystallized structure of $CaCO_3$ in limestone [288] and its incorporation into the geopolymer gel structure after geopolymerization. This also explains the low intensity calcite peaks detected in 3DPG in XRD analysis.

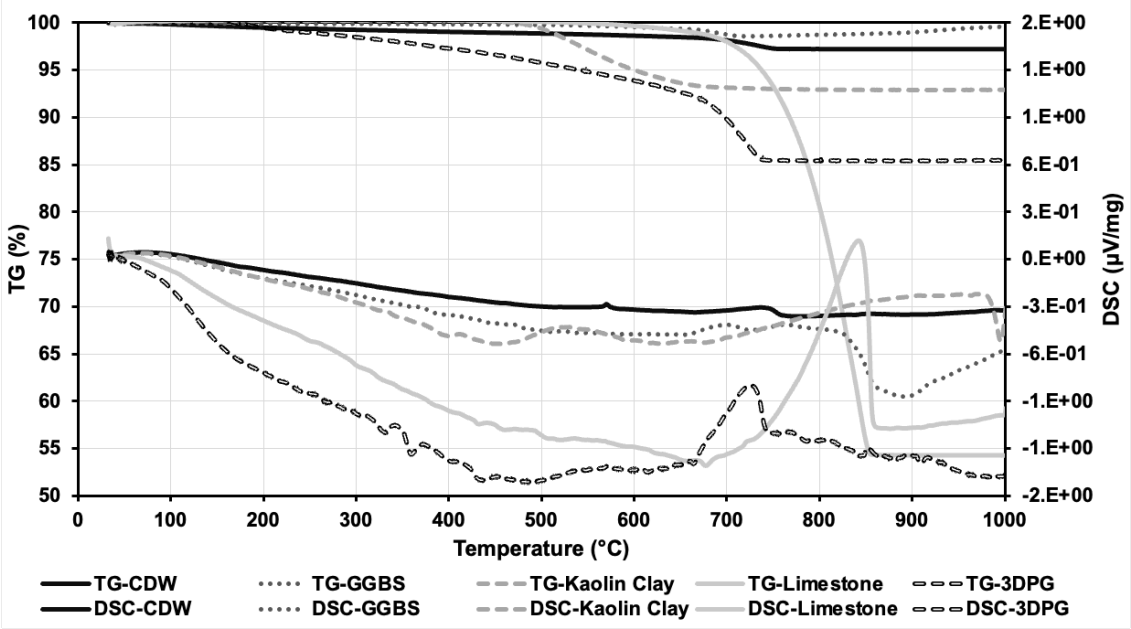

Fig. 4.8. Thermogravimetry (TG) and Differential Scanning Calorimetry (DSC) results of precursors and 3D Printable Geopolymer (3DPG)

Scanning electron microscopy and energy dispersive X-ray spectroscopy (SEM/EDX) micrographs of 3DPG are presented in Fig. 4.9. The average measurements obtained as a result of spot EDX analysis (Fig. 4.9a) are given in Table 4.4. The SEM analysis revealed the dense structure formed as a result of geopolymerization, while the spot EDX analysis showed the presence of CASH gel structures containing predominantly Calcium-Aluminium-Silicon elements. The regional EDX analysis confirmed the results obtained in the spot analyses. In general terms, the dominant CASH structure detected supports the Calcium Aluminosilicate ($CaAl_2Si_2O_8$) phase detected in XRD analysis and the transformations of peaks representing T-O-Si bonds observed in FTIR analysis.

Table 4.4. Detected elements and their atomic-weight concentrations

Element name	Atomic concentration (%)	Weight concentration (%)
Carbon	5.15	2.93
Oxygen	51.72	37.91
Sodium	1.60	1.66
Magnesium	0.76	0.80
Aluminum	12.63	15.37
Silicon	16.35	20.51
Potassium	2.34	3.86
Calcium	10.05	17.66

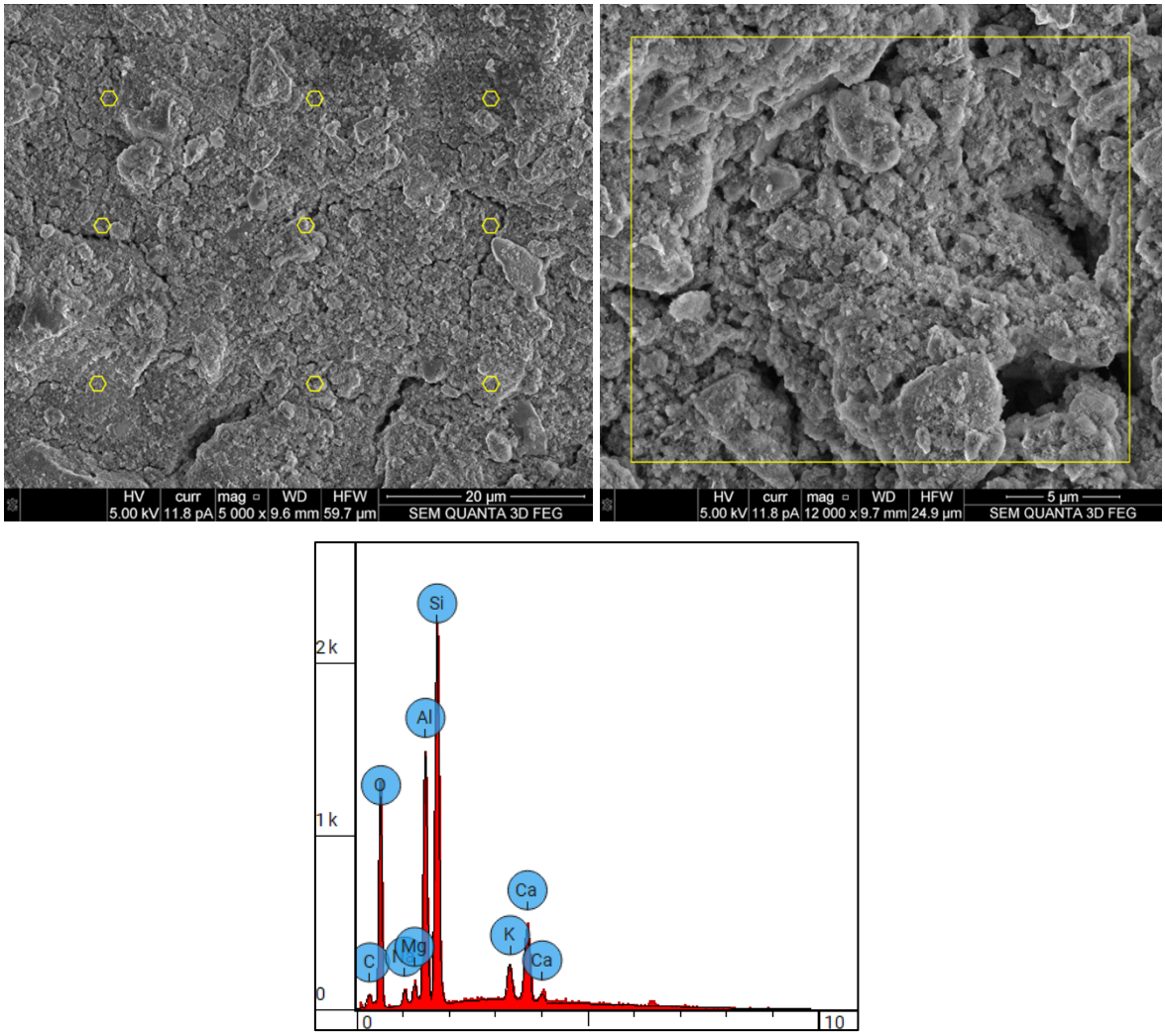

Fig. 4.9. Scanning electron microscopy and energy dispersive X-ray spectroscopy (SEM/EDX) analyses a) Spot EDX analysis, b) Regional EDX analysis, c) Measurements related to regional analysis

4.5. Anisotropic Performance of 3D Printable One-Part Geopolymer Mortar

3D printed specimens' macro-mechanical test results (Fig. 4.10) show that the mechanical properties increase with age, indicating that geopolymerization promoted the formation of strength-giving gels [63,265]. However, the rate of increase in mechanical performance decreased over time. Anisotropy, an unavoidable condition for the 3D printing production technique, was observed for all test types and ages. Additionally, layer height was found to be an important factor influencing mechanical performance. The effect of layer height was found to be independent of loading orientation and age, while it was clear that reduction in layer height made it possible to achieve relatively higher mechanical performances. The main reason behind this can be attributed to the fact that for the same material volume discharged per unit time when printing with lower layer height, the layers become more and more compressed and the interlayer bonding zone contains less void volume. A positive impact on anisotropy can be observed with lower layer height, particularly for flexural and splitting tensile strength, due to elimination of macro-defects caused by pores, voids, and flaws in the matrix [289,290]. However, although optimization of the layer height has positive effects, these effects can only contribute up to a certain level. Considering all the tests, the positive effect of layer height on anisotropy for different orientations could be improved by at most 15% on average. When the mechanical performances were examined according to the loading orientation, slightly lower strengths were generally obtained for compressive strength results compared to mold-casted specimens (except for Orientation-I), however, degree of anisotropy was not significant. On the other hand, the compressive strength results for Orientation-I were slightly higher compared to the mold-casted specimens. The main reason for this is the compression of the material transferred from the chamber of the 3D printer to the nozzle as it passes through the auger of the pump, thus decreasing the water/binder ratio of the matrix and increasing the strength as a result of the conversion to a denser structure [291]. In the specimens loaded in Orientation-III direction, where the effect of increasing height on the strength of the printed wall element was examined, the compressive strength of the specimen taken from the lower zone of the wall was found to be higher compared to the specimen taken from the upper zone of the wall. This can be attributed to the fact that with the increase in the number of printed layers in a wall segment, the dead-load carried by the lower layers gradually increases and creates a compression effect, thus relatively eliminating possible macro-defects that would affect the mechanical properties. In examining the flexural strength results, similar or slightly higher

strengths were obtained for Orientation-I as for the mold cast specimens, while the anisotropy was relatively high for specimens with higher layer height. For Orientation-II and -III, high and low strengths were obtained respectively compared to mold-casted specimens. At this point, the flexural strength performance is governed by the direction of the tensile stress at the mid-span relative to the interlayer interface bond region, which is the region with the lowest bond strength in the specimens. In this context, the significant loss of flexural strength found for Orientation-III can be directly related to the fact that the tensile stress occurs perpendicular to the interlayer bond plane. On the other hand, a significant strength increase was obtained for Orientation-II. Unlike Orientation-I, the tensile stress plane and the bond plane are in a linear intersection rather than a planar intersection. In other words, the area of influence of the weak bond region where the tensile stress causes damage is lower. Therefore, the specimens were able to withstand higher tensile stress. Similar behavior has been frequently observed in the literature, where it has been reported that although the laminated structure weakens the strength of the printed specimens, the bond and loading plane relationship can reverse the effect [291-293].

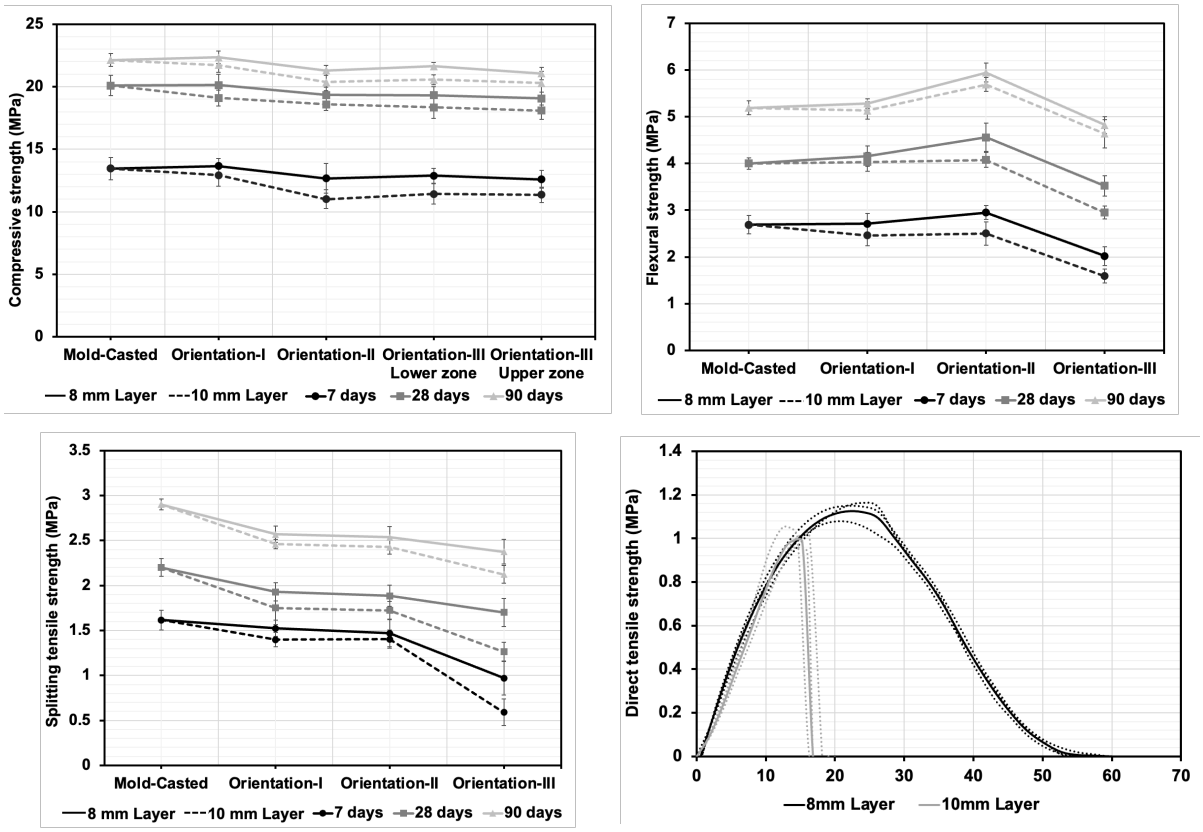

Fig. 4.10. Mechanical response of 3DPG under compressive, flexural, splitting, and direct tensile loading in different orientations

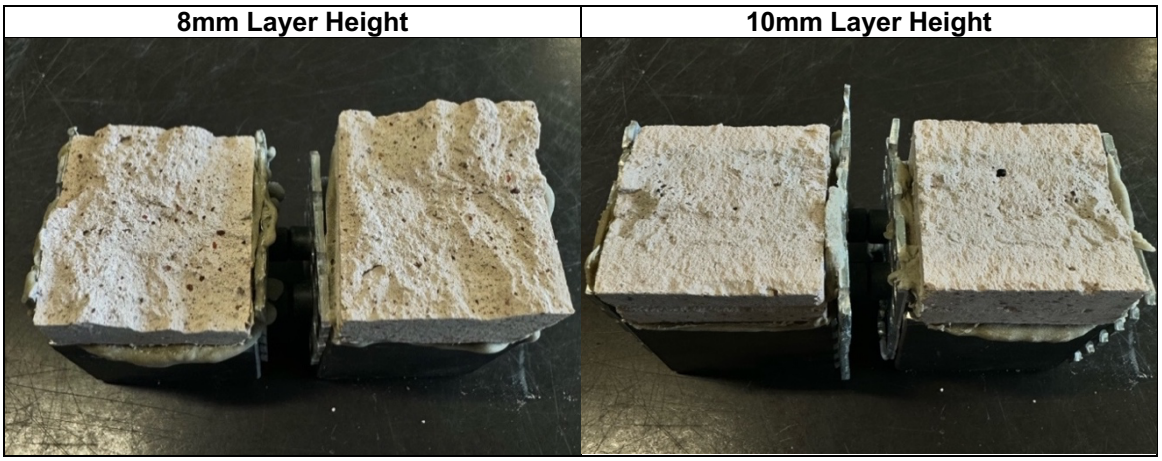

Fig. 4.11. Fractured specimens after direct tensile test

In the splitting tensile test, the effect of anisotropy was highly visible and 3D printed samples exhibited low strength properties compared to mold-casted samples. Although decreasing the layer height increased the strength, this was only possible up to a certain level. While the strengths for Orientation-I and -II were quite close to each other, in Orientation III the strength decreased significantly due to the tension stress being in a direction perpendicular to the interlayer bond plane.

Direct tensile tests carried out on 90-day-old specimens clearly showed that optimizing layer height had a significant effect on interlayer bond strength. A reduction in layer height of 20% increased the direct tensile strength by 15%. Due to the reduction in layer height, macro-defects in the interface bond region were eliminated; thus, the tensile stress could be transferred to the layers instead of being localized in the bond region, acting as if the interface region did not exist (Fig. 4.11).

The results obtained from Micro-CT tests performed to investigate how layer height affects the pore properties of the matrix, especially in the bond region, are presented in Fig. 4.12. Reduction of layer height resulted in a significant decrease in pore content, which supports the enhancement of mechanical properties by compression effect at optimized layer height. The total pore ratio was around 2.92% in the sample with a layer height of 8 mm, whereas 5.45% in the sample with a layer height of 10 mm. The pore content, which was lower in the layer region, increased in the interlayer bond region and decreased when passing to the next layer. Especially in the interlayer bond region, these pores would merge and cause the formation of a distributed defect zone. However, the reduction in layer thickness

disconnected these pores and kept them as localized defects, thus contributing to the strengthening of the mechanical properties [294].

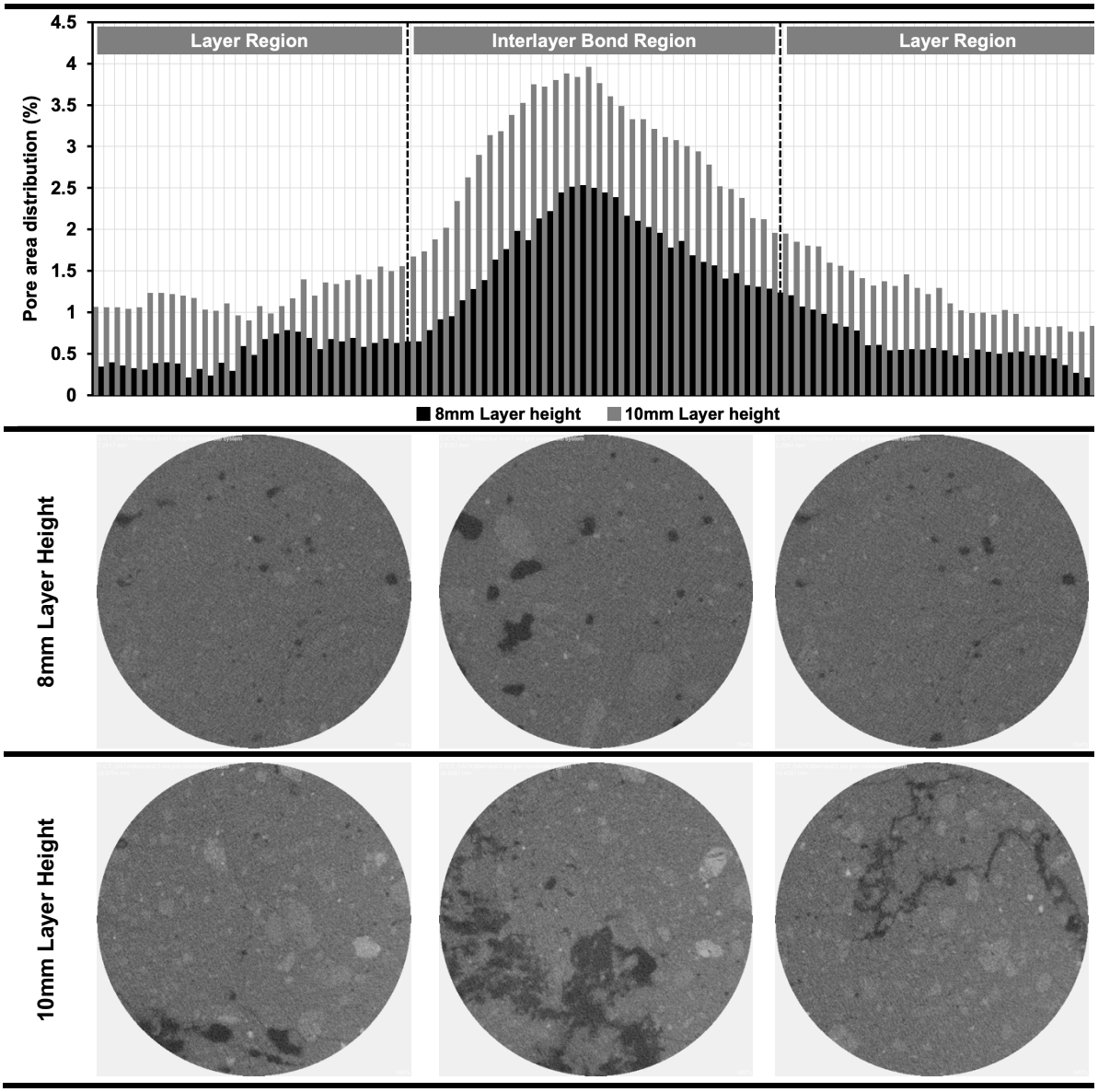

Fig. 4.12. Pore area distribution and Micro-CT images for layer and interlayer bond region (Shades of gray are the matrix, black regions are the pores)

4.6. Conclusions

The current chapter of thesis focuses on the development of CDW-based one-part 3D printable geopolymer (3DPG) to merge the focal points of the construction industry's digitalization, the reutilization of waste materials, and the development of sustainable building materials in order to provide a rapid, sustainable, and circular economy-compliant solution to the increasing housing demand worldwide due to factors such as natural disasters,

rising population, and irregular migration. To this end, a system was developed in which 70% of dry content constituted brick masonry wastes as in precursor and filler phases. Moreover, with the objective of enhancing/regulating mechanical and rheological properties, materials such as ground granulated blast furnace slag (GGBS), limestone (LS) and, kaolin clay (KC) were incorporated into systems. The mechanical properties of the 3DPG mixture were evaluated through compressive strength, flexural strength, split tensile, and direct tensile testing to assess the progress of geopolymerization and the impact of anisotropy. The findings obtained from this chapter of thesis are outlined as follows:

- Optimization of the SiO_2/Al_2O_3 ratio in the mixtures improved compressive strength by promoting the formation of Si-O-Al bonds, which are critical for mechanical performance and buildability performance. Additionally, increasing the CaO/SiO_2 ratio, particularly through GGBS substitution, significantly improved compressive strength while slightly affecting flowability but improving workability through the formation of Ca-based gel structures. The mechanical performance of the geopolymer was positively impacted by the SiO_2/Na_2O ratio up to a certain threshold, beyond which further increase led to a decrease in mechanical strength due to the predominance of precursor and filler phases.

- The inverse correlation between flowability and buildability indexes was attributed to ongoing polycondensation, leading to the formation of a 3D polymeric framework primarily comprising monosilicate chains and cyclic trimers through geopolymerization. Due to the high thixotropic performance (reaching 82.2-84.1% depending on time), 3DPG exhibited a significant decrease in viscosity under high shear rates, coupled with the restoration of its initial viscoelastic structure upon shear rate removal, ensuring adequate shape retention and buildability for layer-by-layer printing. Besides, the pulse velocity increased with curing time, but the increase could be restricted, i.e., open-time could be prolonged by applying shear force through remixing at intervals.

- Given that the elemental composition of the identified phases corresponds to the gel and nanoscale crystals present in geopolymer matrices, the identification of the Calcium Aluminosilicate ($CaAl_2Si_2O_8$) crystal phase in 3DPG indicated the presence of phases associated with the formation of the CASH gel structure within the system. Formation of CASH gel structure was also validated in SEM/EDX analyses. The shift of the T-O-Si bonds detected for GGBS to relatively higher wavelengths in the final product due to the

geopolymerization indicated that GGBS contributed to the formation of these Calcium Aluminosilicate phases detected in the XRD analysis. In TG and DSC analyses, the decrease and transformation of the high-density and well-crystallized $CaCO_3$ peaks detected for limestone in the final product indicated that this structure was incorporated into calcium-based geopolymeric gel structures.

- Mechanical tests revealed the presence of anisotropy, but the compression effect caused by reducing the layer height reduced the degree of anisotropy to some extent. The main factor controlling anisotropy was the relative positioning of the interlayer bond plane and the loading plane. Strength losses were higher in orientations where the loading plane was parallel to the bond plane or perpendicular to the tensile stress. In the opposite orientations, effects that favored mechanical performance were obtained. The positive effects of reducing the layer height were more pronounced in tensile tests. The pores in the interlayer bonding region merged, resulting in the formation of a distributed defect region. However, decreasing the layer height caused the pores in this region to be compressed, minimized and localized. Moreover, this positive effect was also validated by the fact that samples with low layer height fractured unevenly under direct tension, rather than flatly from interlayer bond region.

CONCLUDING REMARKS

The construction industry, one of the largest industries worldwide, imposes a significant burden on society and nature due to its linear economic structure and material flow that leads to intensive energy-carbon consumption. Aligned with the UN Sustainable Development Goal 11 of "Sustainable Cities and Communities", EU policy frameworks are focused on enhancing the sustainable competitiveness of construction industry enterprises. Furthermore, the EU's Green and Digital Transition strategy aims to increase sustainability, promote reuse, and facilitate a transition towards a circular economy within the construction industry. Achieving these objectives and strategies is only possible through the implementation of circular economy principles and the establishment of a sustainable structure for all components of the sector's value chain. In this context, it is crucial for the sector to recycle its own waste, innovate manufacturing and construction techniques with advanced and digital approaches. The recycling of Construction and Demolition Waste (CDW), which constitutes the largest waste stream and comprises over one-third of all waste produced in the EU, is of significant importance to enable a circular economy in the construction industry. Additionally, integrating digital manufacturing techniques such as 3D printing or 3D-Additive Manufacturing is necessary to revolutionize production technologies and break the sector's energy-waste-intensive linear economic structure.

In order to implement those goals and strategies sustainably and effectively, the current thesis aims to generate solutions for different components of the construction industry's value chain. The primary objective is to develop circular and sustainable solutions for construction applications by using 3D printing technology and transforming Construction and Demolition Waste (CDW) into innovative construction materials. In this context, the thesis initially focused on characterizing a variety of CDW with highly variable types and properties sourced from different origins to be used in the development of environment-friendly building materials using geopolymerization technique. Subsequently, sustainable mortar phases were developed through the use of recycled concrete aggregates obtained from the waste concrete phase of CDW, and a Life Cycle Assessment (LCA) was conducted to determine the sustainability level and environmental impacts of each component of mortar mixtures. The final stage involved adapting the geopolymer concept based on CDW to a completely different geographical area, the Netherlands, by developing geopolymer systems and integrating them into the 3D Concrete Printing technique to ensure the green and digital

transformation of the construction sector in line with the circular economy concept. This included the development of a single-component (or water-added only) geopolymer mortar based on CDW, which was integrated into the 3D Concrete Printing technique to enable circular economy-oriented geopolymer systems in the construction sector. The findings obtained within the scope of the thesis study are presented below:

CDW provides a promising option for developing geopolymeric binders, serving as a substitute for OPC pastes. However, it is vital to recognize the global variability in CDW's chemical and physical compositions. Thus, thorough characterization and strategic developments of mixture designs are imperative for optimal performance. To make this optimization possible CDWs from different origins were utilized to produce geopolymer pastes and their mechanical performances were evaluated in relation to their individual parameters. CDW-based geopolymer pastes exhibited compressive strengths ranging from 34.7 to 68.0 MPa, showing the significant impact of CDW type and origin on mechanical performance. Through precursor-based optimization, consistent mechanical performance from 54.5 to 68 MPa was achieved, regardless of CDW origin. Optimizing mixtures from the same source notably increased compressive strength by up to 64%. hollow brick, red clay brick, and roof tile, forming the clayey phase of CDW, were ideal for geopolymerization due to their balanced aluminosilicate content. Increasing the clayey phase improved mechanical performance, with high CaO content boosting strength and glass waste's SiO_2/Al_2O_3 ratio proving advantageous. The SiO_2/Al_2O_3 ratio and aluminosilicate content determined compressive strength, while material fineness also played a significant role. Maintaining a balanced Si/Al ratio and overall constituent quantity led to substantial improvements. The heterogeneous nature of CDWs produced distinct geopolymeric gel structures within the matrix, influencing material strength through factors like precursor composition and medium pH, resulting in various gel structures like NASH, CASH, and (N,C)ASH.

CDWs offer advantages in both paste and mortar production for green building materials. The integration of recycled concrete aggregate (RCA) from CDWs into geopolymer mortar systems resulted in high-strength and stable phases. Specifically, the 100% CDW-based geopolymer mortar achieved compressive strength of 66.2 MPa after 72-hour heat-curing, emphasizing the influence of RCA size; smaller RCAs (0.85-0.10 mm) in CDW-based geopolymer mortars exhibited higher strength due to improved particle packing. On a microstructural scale, smaller-sized RCAs (1 mm) had a thinner ITZ, increasing

vulnerability to fracture around larger RCAs due to Ca and Si alterations at the ITZ. However, the RCA/binder ratio had negligible impact on compressive strength. Molar concentration was crucial; activating mixtures with a 15M NaOH solution improved mechanical performance, but excessive concentration led to non-homogeneous microstructure formation, while lower molarity limited geopolymerization. Optimal curing at 105 °C was essential to prevent loss in compressive strength due to final product instability, excessive water loss, and drying shrinkage. In LCA analyses comparing CDW-based geopolymer mortars to Portland cement-based conventional systems, sodium hydroxide and treatment of CDW-based precursors had significant environmental impacts. Optimizing mixture design reduced Global Warming Potential and Acidification Potential by 65.9% and 34.3%, respectively, with geopolymerization ensuring a lower Fossil Fuel Depletion potential than Portland cement-based mortar. However, Portland cement-based mortar had the least negative environmental impact concerning Ozone Depletion Potential and Eutrophication Potential values. Additionally, the CDW-based geopolymer mortar emitted 62.9% less CO_2 per strength development with similar energy consumption compared to the Portland cement-based mortar, in the same strength class.

In addition to their sustainable and environment-friendly properties, geopolymers provide a high degree of compatibility with 3D concrete printing, which is the technique that will build the future of the construction industry, thanks to the direct control of rheological properties with the combination and concentration of precursors and alkaline activators. Optimizing the SiO_2/Al_2O_3 ratio in mixtures played a pivotal role in enhancing compressive strength by facilitating the formation of crucial Si-O-Al bonds, essential for both mechanical and buildability performance. Furthermore, increasing the CaO/SiO_2 ratio, especially through GGBS substitution, significantly boosted compressive strength while marginally impacting flowability. This increase in CaO/SiO_2 ratio also improved workability by forming Ca-based gel structures. However, the mechanical performance of the geopolymer was positively affected by the SiO_2/Na_2O ratio only up to a certain threshold; exceeding this threshold led to decreased mechanical strength due to the dominance of precursor and filler phases. This high thixotropic performance, reaching 82.2-84.1% depending on time, allowed 3DPG to significantly decrease viscosity under high shear rates, ensuring adequate shape retention and buildability for layer-by-layer printing. Additionally, stiffening over time could be controlled by applying shear force through remixing at intervals, thereby extending the open-time. Mechanical tests unveiled anisotropy, albeit reducing layer height mitigated its degree

to some extent by compressing pores in the interlayer bonding region and preventing the forming of a distributed defect region. The main factor influencing anisotropy was the relative positioning of the interlayer bond plane and the loading plane; in some orientations, relatively higher mechanical performance was achieved compared to mold-cast specimens. Decreasing layer height not only compressed and localized pores in the interlayer bonding region but also led to uneven fractures under direct tension, as if there is no weak bond region, contrasting with flat fractures from the interlayer bond region seen in samples with higher layer height.

FUTURE RECOMMENDATIONS

Geopolymers derived from CDWs offer a more environment-friendly alternative compared to Portland cement-based systems. While the chemical and physical compositions of CDWs vary from local to global scales, it is generally possible to obtain similar final products by recycling them through the geopolymerization technique. In this context, there are no significant barriers preventing these wastes from being widely used in the production of construction materials. The findings demonstrating the feasibility of recycling these materials through geopolymerization with waste from various sources/geographies within the scope of thesis studies are believed to provide valuable guidance for further research aimed at expanding such studies. With dedicated research in these areas, CDW-based geopolymers have the potential to become a standardized construction material worldwide.

Further research into the durability and long-term performance of CDW-based geopolymers is essential. These studies should evaluate factors such as structural stability, load-bearing capacity, and resistance to environmental conditions to determine whether these materials are a reliable option for long-life construction projects. Research is critical to establishing industry standards and promoting wider acceptance of CDW-based geopolymers in the construction industry.

Further exploration is necessary to evaluate the compatibility of CDW-based geopolymer mixtures with 3D concrete printing technique and to understand their rheological behavior, mechanical properties, and bonding capabilities for application in construction. Continuous research into the compatibility of CDW-based geopolymer mixtures with 3D-AM is vital for their sustainable integration into the construction industry, contributing to the advancement of a smarter, more sustainable, and inclusive society by promoting circular economy principles in construction, addressing waste disposal and resource depletion issues, and providing significant environmental and economic advantages.

Despite the potential sustainability benefits, 3D printable concrete designs are generally cement-based and the carbon footprint associated with their production remains a concern. In this context, it is of great importance to develop cement-free, truly environment-friendly mixtures suitable for 3D printing concrete. Comprehensive research should be carried out in

order to comprehensively evaluate the environmental and economic impacts of the 3D printable materials and 3D concrete printing technique.

3D concrete printing represents a promising tool for optimizing and enhancing critical parameters within the construction industry, including material consumption, construction speed, labor requirements, energy usage, and carbon emissions. Despite being in the nascent stages of its life cycle, concerted global efforts could expedite its widespread adoption in a relatively brief timeframe. Additionally, the development of suitable construction materials tailored to this technology, particularly with an emphasis on utilizing locally sourced materials, stands to further accelerate the integration of this technique.

The use of specialized equipment increases the cost of implementing 3D concrete printing due to the costs of chemical additives of the materials developed. In this context, the current thesis creates advantages in terms of cost due to the use of waste and the lack of rheology modifying chemicals compared to cement-based systems. However, extensive studies are required to reduce the costs of the materials and the technique to enable widespread adoption of the technique.

Considering the current state of 3D concrete printing, there is a need for studies that will enable faster production at high standards by improving printing processes, refining nozzle design, improving layer bonding and optimizing curing methods for higher speed without compromising quality. Innovations in automation, robotics, artificial intelligence, design-manufacturing and real-time monitoring systems can be integrated into 3D concrete printing systems to significantly improve printing efficiency and precision.

REFERENCES

[1] FIEC, (2017). European Construction Industry Federation–Annual Report 2017.

[2] United Nations, (2015). Transforming our world: The 2030 agenda for sustainable development. Resolution adopted by the General Assembly.

[3] European Union, (2012). Strategy for the sustainable competitiveness of the construction sector and its enterprises. COM/2012/0433 final.

[4] Scrivener et al., (2016). Eco-efficient cements: Potential, economically viable solutions for a low-CO2, Cement Based Materials Industry, Paris.

[5] Gálvez-Martos, J. L., Styles, D., Schoenberger, H., & Zeschmar-Lahl, B. (2018). Construction and demolition waste best management practice in Europe. Resources, Conservation and Recycling, 136, 166-178.

[6] Yazdani, M., Kabirifar, K., Frimpong, B. E., Shariati, M., Mirmozaffari, M., & Boskabadi, A. (2021). Improving construction and demolition waste collection service in an urban area using a simheuristic approach: A case study in Sydney, Australia. Journal of Cleaner Production, 280, 124138.

[7] Muench, S., Stoermer, E., Jensen, K., Asikainen, T., Salvi, M., & Scapolo, F. (2022). Towards a Green and Digital Future: Key Requirements for Successful Twin Transitions in the European Union. Luxembourg: Publications Office of the European Union.

[8] EU Commission COM/2020/98 final - A New Circular Economy Action Plan for a Cleaner and More Competitive Europe.

[9] EU Commission, (2016). Report on 3D-printing: Current and future application areas, existing industrial value chains and missing competences in the EU.

[10] International Energy Agency, IEA, 2022. Tracking Buildings 2022. Paris: International Energy Agency. Available at: https://www.iea.org/reports/tracking-buildings-2021.

[11] Amran, M., Makul, N., Fediuk, R., Lee, Y. H., Vatin, N. I., Lee, Y. Y., & Mohammed, K. (2022). Global carbon recoverability experiences from the cement industry. Case Studies in Construction Materials, 17, e01439.

[12] Hossain, M. U., Poon, C. S., Lo, I. M., & Cheng, J. C. (2017). Comparative LCA on using waste materials in the cement industry: A Hong Kong case study. Resources, Conservation and Recycling, 120, 199-208.

[13] Zhang, Z., Provis, J. L., Reid, A., & Wang, H. (2014). Geopolymer foam concrete: An emerging material for sustainable construction. Construction and Building Materials, 56, 113-127.

[14] Bernal, S., Gutiérrez, R., & Rodríguez, E. (2013). Alkali-activated materials: cementing a sustainable future. https://doi.org/10.25100/IYC.V15I2.2608.G3434.

[15] Neupane, K., Chalmers, D., & Kidd, P. (2018). High-strength geopolymer concrete-properties, advantages and challenges. Advances in Materials, 7(2), 15-25.

[16] Pouhet, R., & Cyr, M. (2015). Alkali–silica reaction in metakaolin-based geopolymer mortar. Materials and Structures, 48, 571-583.

[17] Jiang, X., Xiao, R., Zhang, M., Hu, W., Bai, Y., & Huang, B. (2020). A laboratory investigation of steel to fly ash-based geopolymer paste bonding behavior after exposure to elevated temperatures. Construction and Building Materials, 254, 119267.

[18] Eurostat, 2018. Eurostat Statistics for Waste Flow Generation 2016. http://epp.eurostat.ec.europa.eu/portal/page/portal/eurostat/home/

[19] US Environmental Protection Agency, 2020. Advancing sustainable materials management

[20] Zhang, C., Hu, M., Di Maio, F., Sprecher, B., Yang, X., & Tukker, A. (2022). An overview of the waste hierarchy framework for analyzing the circularity in construction and demolition waste management in Europe. Science of the Total Environment, 803, 149892.

[21] Lennon, M. (2005). Recycling construction and demolition wastes: a guide for architects and contractors (pp. 1-38). Boston: Commonwealth of Massachusetts, Department of Environmental Protection.

[22] Robayo-Salazar, R. A., Valencia-Saavedra, W., & Mejía de Gutiérrez, R. (2020). Construction and demolition waste (CDW) recycling—As both binder and aggregates—In alkali-activated materials: A novel re-use concept. Sustainability, 12(14), 5775.

[23] Alhawat, M., Ashour, A., Yildirim, G., Aldemir, A., & Sahmaran, M. (2022). Properties of geopolymers sourced from construction and demolition waste: A review. Journal of Building Engineering, 50, 104104.

[24] Xiao, J., Ma, Z., Sui, T., Akbarnezhad, A., & Duan, Z. (2018). Mechanical properties of concrete mixed with recycled powder produced from construction and demolition waste. Journal of Cleaner Production, 188, 720-731.

[25] Choudhary, J., Kumar, B., & Gupta, A. (2020). Utilization of solid waste materials as alternative fillers in asphalt mixes: A review. Construction and Building Materials, 234, 117271.

[26] Yıldırım, G., Kul, A., Özçelikci, E., Şahmaran, M., Aldemir, A., Figueira, D., & Ashour, A. (2021). Development of alkali-activated binders from recycled mixed masonry-originated waste. Journal of Building Engineering, 33, 101690.

[27] Tuğluca, M. S., Özdoğru, E., İlcan, H., Özçelikci, E., Ulugöl, H., & Şahmaran, M. (2023). Characterization of chemically treated waste wood fiber and its potential

application in cementitious composites. Cement and Concrete Composites, 137, 104938.

[28] Sevim, O., Demir, I., Alakara, E. H., & Bayer, İ. R. (2023). Experimental Evaluation of New Geopolymer Composite with Inclusion of Slag and Construction Waste Firebrick at Elevated Temperatures. Polymers, 15(9), 2127.

[29] Sevim, O., Alakara, E. H., Demir, I., & Bayer, I. R. (2023). Effect of magnetic water on properties of slag-based geopolymer composites incorporating ceramic tile waste from construction and demolition waste. Archives of Civil and Mechanical Engineering, 23(2), 107.

[30] Vijayan, D. S., Arvindan, S., & Janarthanan, T. S. (2020). Evaluation of ferrock: A greener substitute to cement. Materials Today: Proceedings, 22, 781-787.

[31] Garside, M. (2020). Major countries in worldwide cement production 2015–2019. Statista International.

[32] EPA, U., 2020. Inventory of US Greenhouse Gas Emissions and Sinks: 1990-2019. United States Environmental Protection Agency. Retrieved from https://www.epa.gov/ghgemissions/inventory-us-greenhouse-gas-emissions-and-sinks-1990-2019

[33] Friedlingstein, P., O'sullivan, M., Jones, M. W., Andrew, R. M., Gregor, L., Hauck, J., ... & Zheng, B. (2022). Global Carbon Budget 2022. Earth System Science Data, 14 (11), 4811–4900.

[34] Shi, C., & Day, R. L. (2000). Pozzolanic reaction in the presence of chemical activators: Part II—Reaction products and mechanism. Cement and Concrete Research, 30(4), 607-613.

[35] Singh, N., Kumar, P., & Goyal, P. (2019). Reviewing the behaviour of high volume fly ash based self-compacting concrete. Journal of Building Engineering, 26, 100882.

[36] Malhotra, V. M., & Mehta, P. K. (2004). Pozzolanic and cementitious materials. Crc Press.

[37] Juenger, M. C., & Siddique, R. (2015). Recent advances in understanding the role of supplementary cementitious materials in concrete. Cement and Concrete Research, 78, 71-80.

[38] Hossain, M. M., Karim, M. R., Hasan, M., Hossain, M. K., & Zain, M. F. M. (2016). Durability of mortar and concrete made up of pozzolans as a partial replacement of cement: A review. Construction and Building Materials, 116, 128-140.

[39] Juenger, M. C., Snellings, R., & Bernal, S. A. (2019). Supplementary cementitious materials: New sources, characterization, and performance insights. Cement and Concrete Research, 122, 257-273.

[40] Cinquepalmi, M. A., Mangialardi, T., Panei, L., Paolini, A. E., & Piga, L. (2008). Reuse of cement-solidified municipal incinerator fly ash in cement mortars:

Physico-mechanical and leaching characteristics. Journal of Hazardous materials, 151(2-3), 585-593.

[41] Simão, F. V., Chambart, H., Vandemeulebroeke, L., Nielsen, P., Adrianto, L. R., Pfister, S., & Cappuyns, V. (2022). Mine waste as a sustainable resource for facing bricks. Journal of Cleaner Production, 368, 133118.

[42] Habert, G., De Lacaillerie, J. D. E., & Roussel, N. (2011). An environmental evaluation of geopolymer based concrete production: reviewing current research trends. Journal of Cleaner Production, 19(11), 1229-1238.

[43] Palomo, A., Grutzeck, M. W., & Blanco, M. T. (1999). Alkali-activated fly ashes: A cement for the future. Cement and concrete research, 29(8), 1323-1329.

[44] Duxson, P., Fernández-Jiménez, A., Provis, J. L., Lukey, G. C., Palomo, A., & van Deventer, J. S. (2007). Geopolymer technology: the current state of the art. Journal of Materials Science, 42, 2917-2933.

[45] Bernal, S. A., De Gutiérrez, R. M., & Provis, J. L. (2012). Engineering and durability properties of concretes based on alkali-activated granulated blast furnace slag/metakaolin blends. Construction and Building Materials, 33, 99-108.

[46] Huang, B., Wang, X., Kua, H., Geng, Y., Bleischwitz, R., & Ren, J. (2018). Construction and demolition waste management in China through the 3R principle. Resources, Conservation and Recycling, 129, 36-44.

[47] Eurostat, 2015. Waste statistics. https://ec.europa.eu/eurostat/statistics-explained/index.php?title=Waste_statistics

[48] UNEP, 2015. Global Waste Management Outlook. https://www.unep.org/resources/report/global-waste-management-outlook

[49] World Bank & United Nations, 2010. Natural hazards, unnatural disasters: the economics of effective prevention. Washington, DC: The International Bank for Reconstruction and Development/The World Bank.

[50] Channell, M. G., Graves, M. R., Medina, V. F., Morrow, A. B., Brandon, D. L., & Nestler, C. C. (2009). Enhanced tools and techniques to support debris management in disaster response missions. US Army Corps of Engineers. Vicksburg, MS: Environmental Laboratory US Army Engineer Research and Development Center.

[51] Yepsen, R. (2008). Generating biomass fuel from disaster debris. Biocycle, 49(7) 51.

[52] USEPA, 2008. Planning for natural disaster debris. Washington: Office of Solid Waste and Emergency Response, Office of Solid Waste, USEPA.

[53] Liikanen, M., Grönman, K., Deviatkin, I., Havukainen, J., Hyvärinen, M., Kärki, T. & Horttanainen, M. (2019). Construction and demolition waste as a raw material for wood polymer composites–Assessment of environmental impacts. Journal of Cleaner Production, 225, 716-727.

[54] European Commission, 2021. Circular economy action plan. https://environment.ec.europa.eu/strategy/circular-economy-action-plan_en

[55] Environmental Protection Agency, 2022. Sustainable Management of Construction and Demolition Materials. Retrieved from https://www.epa.gov/smm/sustainable-management-construction-and-demolition-materials

[56] Etxeberria, M., Vázquez, E., Marí, A., & Barra, M. (2007). Influence of amount of recycled coarse aggregates and production process on properties of recycled aggregate concrete. Cement and Concrete Research, 37(5), 735-742.

[57] Ali, A. A. M., Zidan, R. S., & Ahmed, T. W. (2020). Evaluation of high-strength concrete made with recycled aggregate under effect of well water. Case Studies in Construction Materials, 12, e00338.

[58] Halicka, A., Ogrodnik, P., & Zegardlo, B. (2013). Using ceramic sanitary ware waste as concrete aggregate. Construction and Building Materials, 48, 295-305.

[59] Kim, Y. J., & Choi, Y. W. (2012). Utilization of waste concrete powder as a substitution material for cement. Construction and Building Materials, 30, 500-504.

[60] Ma, Z., Li, W., Wu, H., & Cao, C. (2019). Chloride permeability of concrete mixed with activity recycled powder obtained from C&D waste. Construction and Building Materials, 199, 652-663.

[61] Schoon, J., De Buysser, K., Van Driessche, I., & De Belie, N. (2015). Fines extracted from recycled concrete as alternative raw material for Portland cement clinker production. Cement and Concrete Composites, 58, 70-80.

[62] Ozcelikci, E., Kul, A., Gunal, M. F., Ozel, B. F., Yildirim, G., Ashour, A., & Sahmaran, M. (2023). A comprehensive study on the compressive strength, durability-related parameters and microstructure of geopolymer mortars based on mixed construction and demolition waste. Journal of Cleaner Production, 396, 136522.

[63] Demiral, N. C., Ekinci, M. O., Sahin, O., Ilcan, H., Kul, A., Yildirim, G., & Sahmaran, M. (2022). Mechanical anisotropy evaluation and bonding properties of 3D-printable construction and demolition waste-based geopolymer mortars. Cement and Concrete Composites, 134, 104814.

[64] Ilcan, H., Sahin, O., Kul, A., Ozcelikci, E., & Sahmaran, M. (2023). Rheological property and extrudability performance assessment of construction and demolition waste-based geopolymer mortars with varied testing protocols. Cement and Concrete Composites, 136, 104891.

[65] Leroy, M. N. L., Dupont, F. M. C., & Elie, K. (2019). Valorization of wood ashes as partial replacement of Portland cement: mechanical performance and durability. European Journal of Scientific Research, 151(4), 468-478.

[66] ASTM C618-19 (2019) Standard specification for coal fly ash and raw or calcined natural pozzolan for use in concrete. ASTM International, West Conshohocken, PA.

[67] Ulugöl, H., Kul, A., Yıldırım, G., Şahmaran, M., Aldemir, A., Figueira, D., & Ashour, A. (2021). Mechanical and microstructural characterization of geopolymers from assorted construction and demolition waste-based masonry and glass. Journal of Cleaner Production, 280, 124358.

[68] Özçelikci, E., (2020). Development of Geopolymer Concretes with Construction Demolition Waste.

[69] Kul, A. (2019). New Generation Geopolymer Binders Incorporating Construction Demolition Wastes.

[70] Mahmoodi, O., Siad, H., Lachemi, M., Dadsetan, S., & Şahmaran, M. (2022). Optimized application of ternary brick, ceramic and concrete wastes in sustainable high strength geopolymers. Journal of Cleaner Production, 338, 130650.

[71] Tan, J., Cai, J., & Li, J. (2022). Recycling of unseparated construction and demolition waste (UCDW) through geopolymer technology. Construction and Building Materials, 341, 127771.

[72] Zawrah, M. F., Gado, R. A., Feltin, N., Ducourtieux, S., & Devoille, L. J. P. S. (2016). Recycling and utilization assessment of waste fired clay bricks (Grog) with granulated blast-furnace slag for geopolymer production. Process Safety and Environmental Protection, 103, 237-251.

[73] Mahmoodi, O., Siad, H., Lachemi, M., Dadsetan, S., & Sahmaran, M. (2021). Development of normal and very high strength geopolymer binders based on concrete waste at ambient environment. Journal of Cleaner Production, 279, 123436.

[74] Rovnaník, P., Řezník, B., & Rovnaníková, P. (2016). Blended alkali-activated fly ash/brick powder materials. Procedia Engineering, 151, 108-113.

[75] Tchakouté, H. K., Rüscher, C. H., Kong, S., & Ranjbar, N. (2016). Synthesis of sodium waterglass from white rice husk ash as an activator to produce metakaolin-based geopolymer cements. Journal of Building Engineering, 6, 252-261.

[76] Firdous, R., & Stephan, D. (2021). Impact of the mineralogical composition of natural pozzolan on properties of resultant geopolymers. Journal of Sustainable Cement-Based Materials, 10(3), 149-164.

[77] Zhang, Z., Wang, H., Provis, J. L., & Reid, A. (2013, January). Efflorescence: a critical challenge for geopolymer applications?. In Concrete Institute of Australia's Biennial National Conference 2013. University of Southern Queensland.

[78] Yildirim, G., Ozcelikci, E., Alhawat, M., & Ashour, A. (2023, June). Development of Concrete Mixtures Based Entirely on Construction and Demolition Waste and Assessment of Parameters Influencing the Compressive Strength. In International

RILEM Conference on Synergising expertise towards sustainability and robustness of CBMs and concrete structures (pp. 510-520). Cham: Springer Nature Switzerland.

[79] Akbarnezhad, A., Ong, K. C. G., Zhang, M. H., Tam, C. T., & Foo, T. W. J. (2011). Microwave-assisted beneficiation of recycled concrete aggregates. Construction and Building Materials, 25(8), 3469-3479.

[80] Allujami, H. M., Abdulkareem, M., Jassam, T. M., Al-Mansob, R. A., Ng, J. L., & Ibrahim, A. (2022). Nanomaterials in recycled aggregates concrete applications: Mechanical properties and durability. A review. Cogent Engineering, 9(1), 2122885.

[81] Ozcelikci, E., Yildirim, G., Alhawat, M., Ashour, A., & Sahmaran, M. (2023, June). An Investigation into Durability Aspects of Geopolymer Concretes Based Fully on Construction and Demolition Waste. In International Symposium of the International Federation for Structural Concrete (pp. 377-386). Cham: Springer Nature Switzerland.

[82] Akduman, Ş., Kocaer, O., Aldemir, A., Şahmaran, M., Yıldırım, G., Almahmood, H., & Ashour, A. (2021). Experimental investigations on the structural behaviour of reinforced geopolymer beams produced from recycled construction materials. Journal of Building Engineering, 41, 102776.

[83] Aldemir, A., Akduman, S., Kocaer, O., Aktepe, R., Sahmaran, M., Yildirim, G., ... & Ashour, A. (2022). Shear behaviour of reinforced construction and demolition waste-based geopolymer concrete beams. Journal of Building Engineering, 47, 103861.

[84] Kocaer, O., & Aldemir, A. (2023). Compressive stress–strain model for the estimation of the flexural capacity of reinforced geopolymer concrete members. Structural Concrete, 24(4), 5102-5121.

[85] American Concrete Institute (ACI). Building code requirements, structural concrete and Commentary 318, ACI Committee; 2011.

[86] Energy Performance of Buildings Directive. Available online: https://ec.europa.eu/energy/topics/energy-efficiency/energy-efficient-buildings/energy-performance-buildings-directive_en, accessed on 7 October 2020.

[87] Kvočka, D., Lešek, A., Knez, F., Ducman, V., Panizza, M., Tsoutis, C., & Bernardi, A. (2020). Life cycle assessment of prefabricated geopolymeric façade cladding panels made from large fractions of recycled construction and demolition waste. Materials, 13(18), 3931.

[88] Wangler, T., Roussel, N., Bos, F. P., Salet, T. A., & Flatt, R. J. (2019). Digital concrete: a review. Cement and Concrete Research, 123, 105780.

[89] Buswell, R. A., De Silva, W. L., Jones, S. Z., & Dirrenberger, J. (2018). 3D printing using concrete extrusion: A roadmap for research. Cement and concrete research, 112, 37-49.

[90] Şahin, H. G., & Mardani-Aghabaglou, A. (2022). Assessment of materials, design parameters and some properties of 3D printing concrete mixtures; a state-of-the-art review. Construction and Building Materials, 316, 125865.

[91] Zhang, D. W., Wang, D. M., Lin, X. Q., & Zhang, T. (2018). The study of the structure rebuilding and yield stress of 3D printing geopolymer pastes. Construction and Building Materials, 184, 575-580.

[92] Panda, B., Unluer, C., & Tan, M. J. (2019). Extrusion and rheology characterization of geopolymer nanocomposites used in 3D printing. Composites Part B: Engineering, 176, 107290.

[93] Ishwarya, G. A., Singh, B., Deshwal, S., & Bhattacharyya, S. K. (2019). Effect of sodium carbonate/sodium silicate activator on the rheology, geopolymerization and strength of fly ash/slag geopolymer pastes. Cement and Concrete Composites, 97, 226-238.

[94] Chougan, M., Ghaffar, S. H., Jahanzat, M., Albar, A., Mujaddedi, N., & Swash, R. (2020). The influence of nano-additives in strengthening mechanical performance of 3D printed multi-binder geopolymer composites. Construction and Building Materials, 250, 118928.

[95] Chen, Y., Liu, C., Cao, R., Chen, C., Mechtcherine, V., & Zhang, Y. (2022). Systematical investigation of rheological performance regarding 3D printing process for alkali-activated materials: effect of precursor nature. Cement and Concrete Composites, 128, 104450.

[96] Şahin, O., İlcan, H., Ateşli, A. T., Kul, A., Yıldırım, G., & Şahmaran, M. (2021). Construction and demolition waste-based geopolymers suited for use in 3-dimensional additive manufacturing. Cement and Concrete Composites, 121, 104088.

[97] Ilcan, H., Sahin, O., Kul, A., Yildirim, G., & Sahmaran, M. (2022). Rheological properties and compressive strength of construction and demolition waste-based geopolymer mortars for 3D-Printing. Construction and Building Materials, 328, 127114.

[98] Pasupathy, K., Ramakrishnan, S., & Sanjayan, J. (2023). 3D concrete printing of eco-friendly geopolymer containing brick waste. Cement and Concrete Composites, 138, 104943.

[99] Li, V. C. (1993). From micromechanics to structural engineering the design of cementitious composites for civil engineering applications. Doboku Gakkai Ronbunshu, 1993(471), 1-12.

[100] Li, V. C. (2019). Engineered cementitious composites (ECC): bendable concrete for sustainable and resilient infrastructure. Springer.

[101] Li, V. C., Bos, F. P., Yu, K., McGee, W., Ng, T. Y., Figueiredo, S. C., ... & Kruger, P. J. (2020). On the emergence of 3D printable engineered, strain hardening cementitious composites (ECC/SHCC). Cement and Concrete Research, 132, 106038.

[102] Afroughsabet, V., Biolzi, L., & Ozbakkaloglu, T. (2016). High-performance fiber-reinforced concrete: a review. Journal of materials science, 51, 6517-6551.

[103] Provis, J. L. (2018). Alkali-activated materials. Cement and Concrete Research, 114, 40-48.

[104] Nematollahi, B., Sanjayan, J., Qiu, J., & Yang, E. H. (2017). Micromechanics-based investigation of a sustainable ambient temperature cured one-part strain hardening geopolymer composite. Construction and Building Materials, 131, 552-563.

[105] Cai, J., Pan, J., Han, J., Lin, Y., & Sheng, Z. (2021). Impact behaviours of engineered geopolymer composite exposed to elevated temperatures. Construction and Building Materials, 312, 125421.

[106] Ulugöl, H., Günal, M. F., Yaman, İ. Ö., Yıldırım, G., & Şahmaran, M. (2021). Effects of self-healing on the microstructure, transport, and electrical properties of 100% construction-and demolition-waste-based geopolymer composites. Cement and Concrete Composites, 121, 104081.

[107] US Geological Survey & Orienteering S (Ed.). (2007). Mineral Commodity Summaries 2007. Government Printing Office.

[108] Schorcht, F., Kourti, I., Scalet, B. M., Roudier, S., & Sancho, L. D. (2013). Best available techniques (BAT) reference document for the production of cement, lime and magnesium oxide. European Commission Joint Research Centre Institute for Prospective Technological Studies, Luxembourg, 506.

[109] Boesch, M. E., Koehler, A., & Hellweg, S. (2009). Model for cradle-to-gate life cycle assessment of clinker production. Environmental science & technology, 43(19), 7578-7583.

[110] Singh, G. B., & Subramaniam, K. V. (2019). Production and characterization of low-energy Portland composite cement from post-industrial waste. Journal of Cleaner Production, 239, 118024.

[111] Monteiro, P. J., Miller, S. A., & Horvath, A. (2017). Towards sustainable concrete. Nature materials, 16(7), 698-699.

[112] Davidovits, J. (1991). Geopolymers: inorganic polymeric new materials. Journal of Thermal Analysis and calorimetry, 37(8), 1633-1656.

[113] Juenger, M. C. G., Winnefeld, F., Provis, J. L., & Ideker, J. H. (2011). Advances in alternative cementitious binders. Cement and concrete research, 41(12), 1232-1243.

[114] Rangan, B. V. (2008). Fly ash-based geopolymer concrete.

[115] Ismail, I., Bernal, S. A., Provis, J. L., San Nicolas, R., Brice, D. G., Kilcullen, A. R., ... & van Deventer, J. S. (2013). Influence of fly ash on the water and chloride permeability of alkali-activated slag mortars and concretes. Construction and Building Materials, 48, 1187-1201.

[116] Nematollahi, B., & Sanjayan, J. (2014). Effect of different superplasticizers and activator combinations on workability and strength of fly ash based geopolymer. Materials & Design, 57, 667-672.

[117] Zhuang, X. Y., Chen, L., Komarneni, S., Zhou, C. H., Tong, D. S., Yang, H. M., ... & Wang, H. (2016). Fly ash-based geopolymer: clean production, properties and applications. Journal of Cleaner Production, 125, 253-267.

[118] Dadsetan, S., Siad, H., Lachemi, M., & Sahmaran, M. (2019). Construction and demolition waste in geopolymer concrete technology: a review. Magazine of Concrete Research, 71(23), 1232-1252.

[119] Dadsetan, S., Siad, H., Lachemi, M., & Sahmaran, M. (2021). Evaluation of the tridymite formation as a technique for enhancing geopolymer binders based on glass waste. Journal of Cleaner Production, 278, 123983.

[120] Brick Industry Association. (2006). Technical notes on brick construction: Manufacturing of Brick. Brick Ind. Assoc. 1–7.

[121] Komnitsas, K., Zaharaki, D., Vlachou, A., Bartzas, G., & Galetakis, M. (2015). Effect of synthesis parameters on the quality of construction and demolition wastes (CDW) geopolymers. Advanced Powder Technology, 26(2), 368-376.

[122] Zaharaki, D., Galetakis, M., & Komnitsas, K. (2016). Valorization of construction and demolition (C&D) and industrial wastes through alkali activation. Construction and Building Materials, 121, 686-693.

[123] Mahmoodi, O., Siad, H., Lachemi, M., & Sahmaran, M. (2021). Synthesis and optimization of binary systems of brick and concrete wastes geopolymers at ambient environment. Construction and Building Materials, 276, 122217.

[124] Xu, H., & Van Deventer, J. S. J. (2000). The geopolymerisation of alumino-silicate minerals. International Journal of Mineral Processing, 59(3), 247-266.

[125] Fletcher, R. A., MacKenzie, K. J., Nicholson, C. L., & Shimada, S. (2005). The composition range of aluminosilicate geopolymers. Journal of the European Ceramic Society, 25(9), 1471-1477.

[126] Steveson, M., & Sagoe-Crentsil, K. (2005). Relationships between composition, structure and strength of inorganic polymers: Part I Metakaolin-derived inorganic polymers. Journal of Materials Science, 40, 2023-2036.

[127] De Silva, P., Sagoe-Crenstil, K., & Sirivivatnanon, V. (2007). Kinetics of geopolymerization: Role of Al2O3 and SiO2. Cement and Concrete Research, 37(4), 512-518.

[128] Shao, J., Gao, J., Zhao, Y., & Chen, X. (2019). Study on the pozzolanic reaction of clay brick powder in blended cement pastes. Construction and Building Materials, 213, 209-215.

[129] Abdullah, M. M. A., Hussin, K., Bnhussain, M., Ismail, K. N., & Ibrahim, W. M. W. (2011). Mechanism and chemical reaction of fly ash geopolymer cement-a review. International Journal of Pure and Applied Sciences and Technology, 6(1), 35-44.

[130] Wong, C. L., Mo, K. H., Alengaram, U. J., & Yap, S. P. (2020). Mechanical strength and permeation properties of high calcium fly ash-based geopolymer containing recycled brick powder. Journal of Building Engineering, 32, 101655.

[131] Medina, C., Zhu, W., Howind, T., Frías, M., & De Rojas, M. S. (2015). Effect of the constituents (asphalt, clay materials, floating particles and fines) of construction and demolition waste on the properties of recycled concretes. Construction and Building Materials, 79, 22-33.

[132] Bui, N. K., Satomi, T., & Takahashi, H. (2018). Enhancement of recycled aggregate concrete properties by a new treatment method. GEOMATE Journal, 14(41), 68-76.

[133] Aquino, C., Inoue, M., Miura, H., Mizuta, M., & Okamoto, T. (2010). The effects of limestone aggregate on concrete properties. Construction and Building Materials, 24(12), 2363-2368.

[134] Kulisch, D., Katz, A., & Zhutovsky, S. (2022). Quantification of residual unhydrated cement content in cement pastes as a potential for recovery. Sustainability, 15(1), 263.

[135] Glass Sector Report, (2022). Republic Of Turkey Ministry of Industry and Technology. https://www.sanayi.gov.tr/plan-program-raporlar-ve-yayinlar/sektor-raporlari/mu2812011402

[136] Keawthun, M., Krachodnok, S., & Chaisena, A. (2014). Conversion of waste glasses into sodium silicate solutions. International Journal of Chemical Sciences, 12(1), 83-91.

[137] Vinai, R., & Soutsos, M. (2019). Production of sodium silicate powder from waste glass cullet for alkali activation of alternative binders. Cement and Concrete Research, 116, 45-56.

[138] Mir, N., Khan, S. A., Kul, A., Sahin, O., Sahmaran, M., & Koc, M. (2022). Life cycle assessment of construction and demolition waste-based geopolymers suited for use in 3-dimensional additive manufacturing. Cleaner Engineering and Technology, 10, 100553.

[139] Mir, N., Khan, S. A., Kul, A., Sahin, O., Ozcelikci, E., Sahmaran, M., & Koc, M. (2023). Construction and demolition waste-based self-healing geopolymer composites for the built environment: an environmental profile assessment and optimization. Construction and Building Materials, 369, 130520.

[140] Khan, S. A., Kul, A., Şahin, O., Şahmaran, M., Al-Ghamdi, S. G., & Koç, M. (2022). Energy-environmental performance assessment and cleaner energy solutions for a novel Construction and Demolition Waste-based geopolymer binder production process. Energy Reports, 8, 14464-14475.

[141] Zhang, Y., Xiao, R., Jiang, X., Li, W., Zhu, X., & Huang, B. (2020). Effect of particle size and curing temperature on mechanical and microstructural properties of waste glass-slag-based and waste glass-fly ash-based geopolymers. Journal of Cleaner Production, 273, 122970.

[142] Meghwal, M., & Goswami, T. K. (2013). Evaluation of size reduction and power requirement in ambient and cryogenically ground fenugreek powder. Advanced Powder Technology, 24(1), 427-435.

[143] Asensio, E., Medina, C., Frías, M., & de Rojas, M. I. S. (2016). Characterization of ceramic-based construction and demolition waste: use as pozzolan in cements. Journal of the American Ceramic Society, 99(12), 4121-4127.

[144] Pereira-de-Oliveira, L. A., Castro-Gomes, J. P., & Santos, P. M. (2012). The potential pozzolanic activity of glass and red-clay ceramic waste as cement mortars components. Construction and Building Materials, 31, 197-203.

[145] Ghiasvand, E., Ramezanianpour, A. A., & Ramezanianpour, A. M. (2015). Influence of grinding method and particle size distribution on the properties of Portland-limestone cements. Materials and Structures, 48, 1273-1283.

[146] Ayzenshtadt, A. M., Danilov, V. E., Drozdyuk, T. A., Frolova, M. A., & Garamov, G. A. (2021). Integral quality indicators of waste concrete for reuse. Nanotekhnologii v Stroitel'stve, 13(5), 276-281.

[147] Stekla, O. S. D. R. (2016). Evaluation of the grindability of recycled glass in the production of blended cements. Evaluation, 729, 734.

[148] Lee, W. K. W., & Van Deventer, J. S. J. (2003). Use of infrared spectroscopy to study geopolymerization of heterogeneous amorphous aluminosilicates. Langmuir, 19(21), 8726-8734.

[149] Tantawy, M. A. (2015). Characterization and pozzolanic properties of calcined alum sludge. Materials Research Bulletin, 61, 415-421.

[150] Cao, Z., Cao, Y., Dong, H., Zhang, J., & Sun, C. (2016). Effect of calcination condition on the microstructure and pozzolanic activity of calcined coal gangue. International Journal of Mineral Processing, 146, 23-28.

[151] Baronio, G., & Binda, L. (1997). Study of the pozzolanicity of some bricks and clays. Construction and Building Materials, 11(1), 41-46.

[152] Alujas, A., Fernández, R., Quintana, R., Scrivener, K. L., & Martirena, F. (2015). Pozzolanic reactivity of low grade kaolinitic clays: Influence of calcination temperature and impact of calcination products on OPC hydration. Applied Clay Science, 108, 94-101.

[153] Zhou, D., Wang, R., Tyrer, M., Wong, H., & Cheeseman, C. (2017). Sustainable infrastructure development through use of calcined excavated waste clay as a supplementary cementitious material. Journal of Cleaner Production, 168, 1180-1192.

[154] Ferone, C., Liguori, B., Capasso, I., Colangelo, F., Cioffi, R., Cappelletto, E., & Di Maggio, R. (2015). Thermally treated clay sediments as geopolymer source material. Applied Clay Science, 107, 195-204.

[155] Peyne, J., Joussein, E., Gautron, J., Doudeau, J., & Rossignol, S. (2017). Feasibility of producing geopolymer binder based on a brick clay mixture. Ceramics International, 43(13), 9860-9871.

[156] Moreno-Pérez, E., Hernández-Ávila, J., Rangel-Martínez, Y., Cerecedo-Sáenz, E., Arenas-Flores, A., Reyes-Valderrama, M. I., & Salinas-Rodríguez, E. (2018). Chemical and mineralogical characterization of recycled aggregates from construction and demolition waste from Mexico City. Minerals, 8(6), 237.

[157] Diliberto, C., Lecomte, A., Aissaoui, C., Mechling, J. M., & Izoret, L. (2021). The incorporation of fine recycled concrete aggregates as a main constituent of cement. Materials and Structures, 54, 1-14.

[158] Chen-Tan, N. W., Van Riessen, A., Ly, C. V., & Southam, D. C. (2009). Determining the reactivity of a fly ash for production of geopolymer. Journal of the American Ceramic Society, 92(4), 881-887.

[159] Nath, S. K., & Kumar, S. (2020). Role of particle fineness on engineering properties and microstructure of fly ash derived geopolymer. Construction and Building Materials, 233, 117294.

[160] Alhawat, M., Ashour, A., Yildirim, G., Aldemir, A., & Sahmaran, M. (2022). Properties of geopolymers sourced from construction and demolition waste: A review. Journal of Building Engineering, 50, 104104.

[161] Yaseri, S., Hajiaghaei, G., Mohammadi, F., Mahdikhani, M., & Farokhzad, R. (2017). The role of synthesis parameters on the workability, setting and strength properties of binary binder based geopolymer paste. Construction and Building Materials, 157, 534-545.

[162] Dadsetan, S., Siad, H., Lachemi, M., Mahmoodi, O., & Sahmaran, M. (2022). Optimization and characterization of geopolymer binders from ceramic waste, glass waste and sodium glass liquid. Journal of Cleaner Production, 342, 130931.

[163] Ren, X., & Zhang, L. (2019). Experimental study of geopolymer concrete produced from waste concrete. Journal of Materials in Civil Engineering, 31(7), 04019114.

[164] Abdila, S. R., Abdullah, M. M. A. B., Ahmad, R., Rahim, S. Z. A., Rychta, M., Wnuk, I., ... & Gucwa, M. (2021). Evaluation on the mechanical properties of ground granulated blast slag (GGBS) and fly ash stabilized soil via geopolymer process. Materials, 14(11), 2833.

[165] Phummiphan, I., Horpibulsuk, S., Rachan, R., Arulrajah, A., Shen, S. L., & Chindaprasirt, P. (2018). High calcium fly ash geopolymer stabilized lateritic soil and granulated blast furnace slag blends as a pavement base material. Journal of Hazardous Materials, 341, 257-267.

[166] Nergis, D. B., Vizureanu, P., Țopa, D., Minciuna, M. G., & Abdullah, M. M. A. B. (2020, June). Influence of Microparticles on Setting Time and Micromorphology of Coal Ash Geopolymers. In IOP Conference Series: Materials Science and Engineering (Vol. 877, No. 1, p. 012044). IOP Publishing.

[167] Dehghani, A., Aslani, F., & Panah, N. G. (2021). Effects of initial SiO2/Al2O3 molar ratio and slag on fly ash-based ambient cured geopolymer properties. Construction and Building Materials, 293, 123527.

[168] James, G., Witten, D., Hastie, T., & Tibshirani, R. (2013). An introduction to statistical learning (Vol. 112, p. 18). New York: Springer.

[169] Kutner, M. H., Nachtsheim, C. J., Neter, J., & Li, W. (2005). Applied linear statistical models. McGraw-hill.

[170] Montgomery, D. C., Peck, E. A., & Vining, G. G. (2021). Introduction to linear regression analysis. John Wiley & Sons.

[171] Fidell, L. S., & Tabachnick, B. G. (2014). Using multivariate statistics (new international edition ed.).

[172] Celik, F. E., Kim, T. J., & Bell, A. T. (2010). Effect of zeolite framework type and Si/Al ratio on dimethoxymethane carbonylation. Journal of Catalysis, 270(1), 185-195.

[173] García-Lodeiro, I., Palomo, A., Fernández-Jiménez, A., & Macphee, D. E. (2011). Compatibility studies between NASH and CASH gels. Study in the ternary diagram Na2O–CaO–Al2O3–SiO2–H2O. Cement and Concrete Research, 41(9), 923-931.

[174] Temuujin, J., Van Riessen, A., & Williams, R. (2009). Influence of calcium compounds on the mechanical properties of fly ash geopolymer pastes. Journal of Hazardous Materials, 167(1-3), 82-88.

[175] Al-Majidi, M. H., Lampropoulos, A., Cundy, A., & Meikle, S. (2016). Development of geopolymer mortar under ambient temperature for in situ applications. Construction and Building Materials, 120, 198-211.

[176] Ding, Y. C., Cheng, T. W., & Dai, Y. S. (2017). Application of geopolymer paste for concrete repair. Structural Concrete, 18(4), 561-570.

[177] Hajimohammadi, A., Ngo, T., & Vongsvivut, J. (2019). Interfacial chemistry of a fly ash geopolymer and aggregates. Journal of Cleaner Production, 231, 980-989.

[178] Xia, M., Muhammad, F., Zeng, L., Li, S., Huang, X., Jiao, B., ... & Li, D. (2019). Solidification/stabilization of lead-zinc smelting slag in composite based geopolymer. Journal of Cleaner Production, 209, 1206-1215.

[179] Tan, J., De Vlieger, J., Desomer, P., Cai, J., & Li, J. (2022). Co-disposal of construction and demolition waste (CDW) and municipal solid waste incineration fly ash (MSWI FA) through geopolymer technology. Journal of Cleaner Production, 362, 132502.

[180] Walkley, B., Ke, X., Hussein, O. H., Bernal, S. A., & Provis, J. L. (2020). Incorporation of strontium and calcium in geopolymer gels. Journal of Hazardous Materials, 382, 121015.

[181] Davidovits, J. (2015). False values on CO2 emission for geopolymer cement/concrete published in scientific papers. Technical paper, 24, 1-9.

[182] van Deventer, J. S., Provis, J. L., Duxson, P., & Brice, D. G. (2010). Chemical research and climate change as drivers in the commercial adoption of alkali activated materials. Waste and Biomass Valorization, 1, 145-155.

[183] Zakka, W. P., Lim, N. H. A. S., & Khun, M. C. (2021). A scientometric review of geopolymer concrete. Journal of Cleaner Production, 280, 124353.

[184] Zhang, P., Gao, Z., Wang, J., Guo, J., Hu, S., & Ling, Y. (2020). Properties of fresh and hardened fly ash/slag based geopolymer concrete: A review. Journal of Cleaner Production, 270, 122389.

[185] Shi, Y., & Xu, J. (2021). BIM-based information system for econo-enviro-friendly end-of-life disposal of construction and demolition waste. Automation in Construction, 125, 103611.

[186] Zhang, C., Hu, M., van der Meide, M., Di Maio, F., Yang, X., Gao, X., ... & Li, C. (2023). Life cycle assessment of material footprint in recycling: A case of concrete recycling. Waste Management, 155, 311-319.

[187] Gebremariam, A. T., Di Maio, F., Vahidi, A., & Rem, P. (2020). Innovative technologies for recycling End-of-Life concrete waste in the built environment. Resources, Conservation and Recycling, 163, 104911.

[188] Parthiban, K., & Mohan, K. S. R. (2017). Influence of recycled concrete aggregates on the engineering and durability properties of alkali activated slag concrete. Construction and Building Materials, 133, 65-72.

[189] Koushkbaghi, M., Alipour, P., Tahmouresi, B., Mohseni, E., Saradar, A., & Sarker, P. K. (2019). Influence of different monomer ratios and recycled concrete aggregate on mechanical properties and durability of geopolymer concretes. Construction and Building Materials, 205, 519-528.

[190] Rahman, S. S., & Khattak, M. J. (2021). Roller compacted geopolymer concrete using recycled concrete aggregate. Construction and Building Materials, 283, 122624.

[191] Rebitzer, G., Ekvall, T., Frischknecht, R., Hunkeler, D., Norris, G., Rydberg, T., ... & Pennington, D. W. (2004). Life cycle assessment: Part 1: Framework, goal and

scope definition, inventory analysis, and applications. Environment international, 30(5), 701-720.

[192] Salas, D. A., Ramirez, A. D., Ulloa, N., Baykara, H., & Boero, A. J. (2018). Life cycle assessment of geopolymer concrete. Construction and Building Materials, 190, 170-177.

[193] Dal Pozzo, A., Carabba, L., Bignozzi, M. C., & Tugnoli, A. (2019). Life cycle assessment of a geopolymer mixture for fireproofing applications. The International Journal of Life Cycle Assessment, 24, 1743-1757.

[194] Kastiukas, G., Ruan, S., Liang, S., & Zhou, X. (2020). Development of precast geopolymer concrete via oven and microwave radiation curing with an environmental assessment. Journal of Cleaner Production, 255, 120290.

[195] Marinković, S., Dragaš, J., Ignjatović, I., & Tošić, N. (2017). Environmental assessment of green concretes for structural use. Journal of Cleaner Production, 154, 633-649.

[196] Nguyen, L., Moseson, A. J., Farnam, Y., & Spatari, S. (2018). Effects of composition and transportation logistics on environmental, energy and cost metrics for the production of alternative cementitious binders. Journal of Cleaner Production, 185, 628-645.

[197] Turner, L. K., & Collins, F. G. (2013). Carbon dioxide equivalent (CO2-e) emissions: A comparison between geopolymer and OPC cement concrete. Construction and Building Materials, 43, 125-130.

[198] Fořt, J., Vejmelková, E., Koňáková, D., Alblová, N., Čáchová, M., Keppert, M., ... & Černý, R. (2018). Application of waste brick powder in alkali activated aluminosilicates: Functional and environmental aspects. Journal of Cleaner Production, 194, 714-725.

[199] Mir, N., Khan, S. A., Kul, A., Sahin, O., Lachemi, M., Sahmaran, M., & Koç, M. (2022). Life cycle assessment of binary recycled ceramic tile and recycled brick waste-based geopolymers. Cleaner Materials, 5, 100116.

[200] Burduhos Nergis, D. D., Abdullah, M. M. A. B., Sandu, A. V., & Vizureanu, P. (2020). XRD and TG-DTA study of new alkali activated materials based on fly ash with sand and glass powder. Materials, 13(2), 343.

[201] K.R. Iler. (1979). The chemistry of the Silica: solubility, polymerization, colloid and surface properties, and biochemistry.

[202] ASTM C109, Standard test method for compressive strength of hydraulic cement mortars (using 2-in. or [50-mm] cube specimens), ASTM International West Conshohocken, PA (2020).

[203] Cohen, I., Huang, Y., Chen, J., Benesty, J., Benesty, J., Chen, J., ... & Cohen, I. (2009). Pearson correlation coefficient. Noise reduction in speech processing, 1-4.

[204] Chen, X., Niu, Z., Wang, J., Zhu, G. R., & Zhou, M. (2018). Effect of sodium polyacrylate on mechanical properties and microstructure of metakaolin-based geopolymer with different SiO2/Al2O3 ratio. Ceramics International, 44(15), 18173-18180.

[205] Shi, C., Wu, Z., Cao, Z., Ling, T. C., & Zheng, J. (2018). Performance of mortar prepared with recycled concrete aggregate enhanced by CO2 and pozzolan slurry. Cement and Concrete Composites, 86, 130-138.

[206] Nedeljković, M., Visser, J., Šavija, B., Valcke, S., & Schlangen, E. (2021). Use of fine recycled concrete aggregates in concrete: A critical review. Journal of Building Engineering, 38, 102196.

[207] De Rossi, A., Ribeiro, M. J., Labrincha, J. A., Novais, R. M., Hotza, D., & Moreira, R. F. P. M. (2019). Effect of the particle size range of construction and demolition waste on the fresh and hardened-state properties of fly ash-based geopolymer mortars with total replacement of sand. Process Safety and Environmental Protection, 129, 130-137.

[208] Li, Y., Fu, T., Wang, R., & Li, Y. (2020). An assessment of microcracks in the interfacial transition zone of recycled concrete aggregates cured by CO2. Construction and Building Materials, 236, 117543.

[209] Hanjitsuwan, S., Hunpratub, S., Thongbai, P., Maensiri, S., Sata, V., & Chindaprasirt, P. (2014). Effects of NaOH concentrations on physical and electrical properties of high calcium fly ash geopolymer paste. Cement and Concrete Composites, 45, 9-14.

[210] Rovnaník, P. (2010). Effect of curing temperature on the development of hard structure of metakaolin-based geopolymer. Construction and Building Materials, 24(7), 1176-1183.

[211] Tuyan, M., Andiç-Çakir, Ö., & Ramyar, K. (2018). Effect of alkali activator concentration and curing condition on strength and microstructure of waste clay brick powder-based geopolymer. Composites Part B: Engineering, 135, 242-252.

[212] Biondi, L., Perry, M., Vlachakis, C., Wu, Z., Hamilton, A., & McAlorum, J. (2019). Ambient cured fly ash geopolymer coatings for concrete. Materials, 12(6), 923.

[213] Hassan, A., Arif, M., & Shariq, M. (2019). Use of geopolymer concrete for a cleaner and sustainable environment–A review of mechanical properties and microstructure. Journal of Cleaner Production, 223, 704-728.

[214] Silva, R. V., De Brito, J., & Dhir, R. K. (2015). Prediction of the shrinkage behavior of recycled aggregate concrete: A review. Construction and Building Materials, 77, 327-339.

[215] de Brito, J., & Kurda, R. (2021). The past and future of sustainable concrete: A critical review and new strategies on cement-based materials. Journal of Cleaner Production, 281, 123558.

[216] Poon, C. S., Shui, Z. H., & Lam, L. (2004). Effect of microstructure of ITZ on compressive strength of concrete prepared with recycled aggregates. Construction and Building Materials, 18(6), 461-468.

[217] Demie, S., Nuruddin, M. F., & Shafiq, N. (2013). Effects of micro-structure characteristics of interfacial transition zone on the compressive strength of self-compacting geopolymer concrete. Construction and Building Materials, 41, 91-98.

[218] Xuan, D., Zhan, B., & Poon, C. S. (2016). Assessment of mechanical properties of concrete incorporating carbonated recycled concrete aggregates. Cement and Concrete Composites, 65, 67-74.

[219] Ren, X., & Zhang, L. (2018). Experimental study of interfacial transition zones between geopolymer binder and recycled aggregate. Construction and Building Materials, 167, 749-756.

[220] Elsharief, A., Cohen, M. D., & Olek, J. (2003). Influence of aggregate size, water cement ratio and age on the microstructure of the interfacial transition zone. Cement and Concrete Research, 33(11), 1837-1849.

[221] Lyu, K., She, W., Chang, H., & Gu, Y. (2020). Effect of fine aggregate size on the overlapping of interfacial transition zone (ITZ) in mortars. Construction and Building Materials, 248, 118559.

[222] ISO Environmental Management-Life Cycle Assessment- Principles and Framework International Organisation for Standardisation, Geneva, Switzerland (2006)

[223] ISO Environmental Management-Life Cycle Assessment-Requirements and Guidelines International Organisation for Standardisation, Geneva, Switzerland (2006)

[224] U.S. Environmental Protection Agency (EPA). Life Cycle Assessment: Principles and Practice; EPA: Washington, DC, USA, (2006).

[225] LCA Measure - Global Warming Potential (GWP) – LCA Measure Details, (n.d.). https://calculatelca.com/static-content/software/impact-estimator/help-files/introduction/summary_measure_details_global_warming_potential.html (accessed November 8, 2021)

[226] Silla, E., Arnau, A., & TuñóN, I. (2001). Fundamental principles governing solvents use. Handbook of solvents, 7.

[227] Silvestre. J. D. (2012). Life Cycle Assessment 'from Cradle to Cradle' of Building Assemblies—Application to External Walls. Ph.D. Thesis, Instituto Superior Técnico, Lisbon, Portugal.

[228] Bicer, Y., & Dincer, I. (2018). Life cycle environmental impact assessments and comparisons of alternative fuels for clean vehicles. Resources, Conservation and Recycling, 132, 141-157.

[229] Kurda. R. (2017). Sustainable development of cement-based materials: Application to recycled aggregates concrete, Doctoral dissertation, Instituto Superior Técnico, Universidade de Lisboa.

[230] J.B. Guinée. (2002). Handbook on life cycle assessment: operational guide to the ISO standards (Vol. 7). Springer Science & Business Media.

[231] Bare, J., Young, D., Qam, S., Hopton, M., & Chief, S. (2012). Tool for the Reduction and Assessment of Chemical and other Environmental Impacts (TRACI). US Environmental Protection Agency: Washington, DC, USA.

[232] European Commission, Product Environmental Footprint Category Rules Guidance, (2018).

[233] Knudson, J. C., Crane, G. B., & Briggs, R. S. (1971). Atmospheric Emissions from Chlor-alkali Manufacture. Environmental Protection Agency, Air Pollution Control Office.

[234] Imtiaz, L., Kashif-ur-Rehman, S., Alaloul, W. S., Nazir, K., Javed, M. F., Aslam, F., & Musarat, M. A. (2021). Life cycle impact assessment of recycled aggregate concrete, geopolymer concrete, and recycled aggregate-based geopolymer concrete. Sustainability, 13(24), 13515.

[235] Hou, J., Zhang, P., Yuan, X., & Zheng, Y. (2011). Life cycle assessment of biodiesel from soybean, jatropha and microalgae in China conditions. Renewable and Sustainable Energy Reviews, 15(9), 5081-5091.

[236] Development of Green ECC for Sustainable Infrastructure Systems Multi-Physics and Multi-Scale Modelling of Next Generation Sustainable Civil Infrastructure View Project Concrete Materials

[237] United Nations. (2019). World Population Prospects 2019. Department of Economic and Social Affairs, Population Division

[238] Najafi, E., & Khanbilvardi, R. (2019). Evaluating global crop distribution in the 21st century to maximize food production. In AGU fall meeting abstracts (Vol. 2019, pp. B31F-2440).

[239] Eurostat. (2023). Eurostat Statistics for Waste Flow Generation 2020.

[240] Excell, J., & Nathan, S. (2010). The rise of additive manufacturing. The Engineer, 24.

[241] Zhang, J., Wang, J., Dong, S., Yu, X., & Han, B. (2019). A review of the current progress and application of 3D printed concrete. Composites Part A: Applied Science and Manufacturing, 125, 105533.

[242] Dey, D., Srinivas, D., Panda, B., Suraneni, P., & Sitharam, T. G. (2022). Use of industrial waste materials for 3D printing of sustainable concrete: A review. Journal of Cleaner Production, 340, 130749.

[243] Jianchao, Z., Zhang, T., Faried, M., & Wengang, C. (2017). 3D printing cement based ink, and it's application within the construction industry. In MATEC Web of Conferences (Vol. 120, p. 02003). EDP Sciences.

[244] Zhang, C., Nerella, V. N., Krishna, A., Wang, S., Zhang, Y., Mechtcherine, V., & Banthia, N. (2021). Mix design concepts for 3D printable concrete: A review. Cement and Concrete Composites, 122, 104155.

[245] Andrew, R. M. (2018). Global CO2 emissions from cement production. Earth System Science Data, 10(1), 195-217.

[246] Duxson, P., Provis, J. L., Lukey, G. C., & Van Deventer, J. S. (2007). The role of inorganic polymer technology in the development of 'green concrete'. Cement and Concrete Research, 37(12), 1590-1597.

[247] Kul, A., Ozel, B. F., Ozcelikci, E., Gunal, M. F., Ulugol, H., Yildirim, G., & Sahmaran, M. (2023). Characterization and life cycle assessment of geopolymer mortars with masonry units and recycled concrete aggregates assorted from construction and demolition waste. Journal of Building Engineering, 78, 107546.

[248] Guo, X., Yang, J., & Xiong, G. (2020). Influence of supplementary cementitious materials on rheological properties of 3D printed fly ash based geopolymer. Cement and Concrete Composites, 114, 103820.

[249] Panda, B., Paul, S. C., Hui, L. J., Tay, Y. W. D., & Tan, M. J. (2017). Additive manufacturing of geopolymer for sustainable built environment. Journal of Cleaner Production, 167, 281-288.

[250] Panda, B., Unluer, C., & Tan, M. J. (2018). Investigation of the rheology and strength of geopolymer mixtures for extrusion-based 3D printing. Cement and Concrete Composites, 94, 307-314.

[251] Alghamdi, H., Nair, S. A., & Neithalath, N. (2019). Insights into material design, extrusion rheology, and properties of 3D-printable alkali-activated fly ash-based binders. Materials & Design, 167, 107634.

[252] Souza, M. T., Simão, L., de Moraes, E. G., Senff, L., de Castro Pessôa, J. R., Ribeiro, M. J., & de Oliveira, A. P. N. (2021). Role of temperature in 3D printed geopolymers: Evaluating rheology and buildability. Materials Letters, 293, 129680.

[253] Nematollahi, B., Sanjayan, J., & Shaikh, F. U. A. (2015). Synthesis of heat and ambient cured one-part geopolymer mixes with different grades of sodium silicate. Ceramics International, 41(4), 5696-5704.

[254] Panda, B., Singh, G. B., Unluer, C., & Tan, M. J. (2019). Synthesis and characterization of one-part geopolymers for extrusion based 3D concrete printing. Journal of Cleaner Production, 220, 610-619.

[255] Bong, S. H., Xia, M., Nematollahi, B., & Shi, C. (2021). Ambient temperature cured 'just-add-water'geopolymer for 3D concrete printing applications. Cement and Concrete Composites, 121, 104060.

[256] Muthukrishnan, S., Ramakrishnan, S., & Sanjayan, J. (2021). Effect of alkali reactions on the rheology of one-part 3D printable geopolymer concrete. Cement and Concrete Composites, 116, 103899.

[257] Ng, T. S., & Foster, S. J. (2013). Development of a mix design methodology for high-performance geopolymer mortars. Structural Concrete, 14(2), 148-156.

[258] ASTM C1437-20; Standard Test Method for Flow of Hydraulic Cement Mortar. ASTM International: West Conshohocken, PA, USA, 2020. Available online: https://www.astm.org/c1437-15.html (accessed on 13 October 2022).

[259] ASTM ASTM C597-22; Standard test method for ultrasonic pulse velocity through concrete. 2022. West Conshohocken, PA: ASTM.

[260] Sun, Q., Yang, Z., Cheng, H., Peng, Y., Huang, Y., & Chen, M. (2018). Creation of three-dimensional structures by direct ink writing with kaolin suspensions. Journal of Materials Chemistry C, 6(42), 11392-11400.

[261] Murray, H. H. (2000). Traditional and new applications for kaolin, smectite, and palygorskite: a general overview. Applied clay science, 17(5-6), 207-221.

[262] Kanagaraj, B., Anand, N., Raj, R. S., & Lubloy, E. (2023). Techno-socio-economic aspects of Portland cement, geopolymer, and limestone calcined clay cement (LC3) composite systems: a-state-of-art-review. Construction and Building Materials, 398, 132484.

[263] Long, W. J., Lin, C., Tao, J. L., Ye, T. H., & Fang, Y. (2021). Printability and particle packing of 3D-printable limestone calcined clay cement composites. Construction and Building Materials, 282, 122647.

[264] Bayiha, B. N., Billong, N., Yamb, E., Kaze, R. C., & Nzengwa, R. (2019). Effect of limestone dosages on some properties of geopolymer from thermally activated halloysite. Construction and Building Materials, 217, 28-35.

[265] Kul, A., Ozcelikci, E., Ozel, B. F., Gunal, M. F., Yildirim, G., Bayer, I. R., & Demir, I. (2024). Evaluation of Mechanical and Microstructural Properties of Engineered Geopolymer Composites with Construction and Demolition Waste-Based Matrices. Journal of Materials in Civil Engineering, 36(1), 04023524.

[266] Phoo-ngernkham, T., Maegawa, A., Mishima, N., Hatanaka, S., & Chindaprasirt, P. (2015). Effects of sodium hydroxide and sodium silicate solutions on compressive and shear bond strengths of FA–GBFS geopolymer. Construction and Building Materials, 91, 1-8.

[267] Bong, S. H., Nematollahi, B., Nazari, A., Xia, M., & Sanjayan, J. (2019). Method of optimisation for ambient temperature cured sustainable geopolymers for 3D printing construction applications. Materials, 12(6), 902.

[268] Xu, H., & van Deventer, J. S. (2003). The effect of alkali metals on the formation of geopolymeric gels from alkali-feldspars. Colloids and Surfaces A: Physicochemical and Engineering Aspects, 216(1-3), 27-44.

[269] Chindaprasirt, P., Rattanasak, U., & Taebuanhuad, S. (2013). Role of microwave radiation in curing the fly ash geopolymer. Advanced Powder Technology, 24(3), 703-707.

[270] Reinhardt, H. W., & Grosse, C. U. (2004). Continuous monitoring of setting and hardening of mortar and concrete. Construction and Building Materials, 18(3), 145-154.

[271] Eurocode. NEN-EN 12504-4 - Testing concrete - Part 4: Determination of ultrasonic pulse velocity. 2005.

[272] Trtnik, G., & Gams, M. (2015). Ultrasonic assessment of initial compressive strength gain of cement based materials. Cement and Concrete Research, 67, 148-155.

[273] Feng, D., Provis, J. L., & van Deventer, J. S. (2012). Thermal activation of albite for the synthesis of one-part mix geopolymers. Journal of the American Ceramic Society, 95(2), 565-572.

[274] Chukanov, N. V., & Chervonnyi, A. D. (2016). Infrared spectroscopy of minerals and related compounds. Springer.

[275] Tan, J., Cizer, Ö., De Vlieger, J., Dan, H., & Li, J. (2022). Impacts of milling duration on construction and demolition waste (CDW) based precursor and resulting geopolymer: Reactivity, geopolymerization and sustainability. Resources, Conservation and Recycling, 184, 106433.

[276] Lee, W. K. W., & Van Deventer, J. S. J. (2002). Structural reorganisation of class F fly ash in alkaline silicate solutions. Colloids and Surfaces A: Physicochemical and Engineering Aspects, 211(1), 49-66.

[277] Chindaprasirt, P., Jaturapitakkul, C., Chalee, W., & Rattanasak, U. (2009). Comparative study on the characteristics of fly ash and bottom ash geopolymers. Waste Management, 29(2), 539-543.

[278] Balachandra, A. M., Abdol, N., Darsanasiri, A. G. N. D., Zhu, K., Soroushian, P., & Mason, H. E. (2021). Landfilled coal ash for carbon dioxide capture and its potential as a geopolymer binder for hazardous waste remediation. Journal of Environmental Chemical Engineering, 9(4), 105385.

[279] Pu, S., Zhu, Z., Song, W., Huo, W., & Zhang, J. (2021). Mechanical and microscopic properties of fly ash phosphoric acid-based geopolymer paste: A comprehensive study. Construction and Building Materials, 299, 123947.

[280] Ismail, I., Bernal, S. A., Provis, J. L., San Nicolas, R., Hamdan, S., & van Deventer, J. S. (2014). Modification of phase evolution in alkali-activated blast furnace slag by the incorporation of fly ash. Cement and Concrete Composites, 45, 125-135.

[281] Zhang, S., Li, Z., Ghiassi, B., Yin, S., & Ye, G. (2021). Fracture properties and microstructure formation of hardened alkali-activated slag/fly ash pastes. Cement and Concrete Research, 144, 106447.

[282] Thiery, M., Villain, G., Dangla, P., & Platret, G. (2007). Investigation of the carbonation front shape on cementitious materials: Effects of the chemical kinetics. Cement and concrete research, 37(7), 1047-1058.

[283] Bernal, S. A., De Gutierrez, R. M., Provis, J. L., & Rose, V. (2010). Effect of silicate modulus and metakaolin incorporation on the carbonation of alkali silicate-activated slags. Cement and Concrete Research, 40(6), 898-907.

[284] Fabbri, B., Gualtieri, S., & Leonardi, C. J. A. C. S. (2013). Modifications induced by the thermal treatment of kaolin and determination of reactivity of metakaolin. Applied Clay Science, 73, 2-10.

[285] Ingraham, T. R., & Marier, P. (1963). Kinetic studies on the thermal decomposition of calcium carbonate. The Canadian Journal of Chemical Engineering, 41(4), 170-173.

[286] Criado, J., González, M., Málek, J., & Ortega, A. (1995). The effect of the CO2 pressure on the thermal decomposition kinetics of calcium carbonate. Thermochimica acta, 254, 121-127.

[287] Ariffin, M. A. M., Bhutta, M. A. R., Hussin, M. W., Tahir, M. M., & Aziah, N. (2013). Sulfuric acid resistance of blended ash geopolymer concrete. Construction and Building Materials, 43, 80-86.

[288] Abdalqader, A. F., Jin, F., & Al-Tabbaa, A. (2015). Characterisation of reactive magnesia and sodium carbonate-activated fly ash/slag paste blends. Construction and Building Materials, 93, 506-513.

[289] Wagh, A. S., Singh, J. P., & Poeppel, R. B. (1993). Dependence of ceramic fracture properties on porosity. Journal of Materials Science, 28, 3589-3593.

[290] Birchall, J. D., Howard, A. J., & Kendall, K. (1981). Flexural strength and porosity of cements. Nature, 289(5796), 388-390.

[291] Ding, T., Xiao, J., Zou, S., & Zhou, X. (2020). Anisotropic behavior in bending of 3D printed concrete reinforced with fibers. Composite Structures, 254, 112808.

[292] Ma, G., Li, Z., Wang, L., Wang, F., & Sanjayan, J. (2019). Mechanical anisotropy of aligned fiber reinforced composite for extrusion-based 3D printing. Construction and Building Materials, 202, 770-783.

[293] Xiao, J., Liu, H., & Ding, T. (2021). Finite element analysis on the anisotropic behavior of 3D printed concrete under compression and flexure. Additive Manufacturing, 39, 101712.

[294] Hou, D., Li, D., Hua, P., Jiang, J., & Zhang, G. (2019). Statistical modelling of compressive strength controlled by porosity and pore size distribution for cementitious materials. Cement and Concrete Composites, 96, 11-20.

APPENDIX

APPENDIX 1 – Publications Derived from Thesis

Kul, A., Ozel, B. F., Ozcelikci, E., Gunal, M. F., Ulugol, H., Yildirim, G., & Sahmaran, M. (2023). Characterization and life cycle assessment of geopolymer mortars with masonry units and recycled concrete aggregates assorted from construction and demolition waste. Journal of Building Engineering, 78, 107546.